Steel Sheet Pile Walls in Soft Soil

Steel Sheet Pile Walls in Soft Soil

Proefschrift

ter verkrijging van de graad van doctor
aan de Technische Universiteit Delft,
op gezag van de Rector Magnificus prof.dr.ir. J.T. Fokkema,
voorzitter van het College voor Promoties,
in het openbaar te verdedigen op maandag 25 februari 2002 om 16.00 uur

door Dick Arjen KORT

civiel ingenieur
geboren te Haarlem

Engineering is the art of modelling materials we do not wholely understand, into shapes we cannot precisely analyse so as to withstand forces we cannot entirely assess, in such a way that the public has no reason to suspect the extent of our ignorance.

A.R. Dykes, 1976

Acknowledgements

In his 'Habilitationsschrift' Von Wollfersdorff [88] wrote that he had the luck that he could design and carry out *two* full-scale field test. I feel already very lucky that I got the opportunity to design, construct and carry out only *one* full-scale field test. After all, how many geotechnical engineers are given the possibility to design and construct a building pit according to their own views and let it fail on purpose?

I would like to thank everybody who was involved in carrying out the Rotterdam Sheet Pile Wall Field Test. In the first place, I am very grateful to my first promotor, Prof. Frits van Tol, with who I closely worked for the past 7 years, for his trust and guidance and for giving me the opportunity to carry out this research. In the second place I am most grateful to Dr. Alex Schmitt for the many details he taught me in the field of sheet piling and for the many interesting and enjoyable discussions we had.

I gratefully thank Fred Jonker of the CUR, supported by Yvonne Versluis, for the pleasant collaboration and for his enthusiasm in co-ordinating the field test. This support was indispensable for carrying out this research.

I am obliged to all the members of CUR Committee C119, under whose auspices the field test was carried out. In particular I wish to thank the mentor Wim Heijnen whose consults were of great support for me.

I am also very grateful to Ad Baldée for his support and guidance, and the many discussions we had on the technical and practical parts of the field test.

I wish to thank Henk van de Graaf for conducting the soil investigation, Ad Amesz, Aaltjo Kuiper and Henk Spek for conducting the preparation of the field test, and Gareth Reece, David Rowbottom, Dr. Alex Schmitt, Henk Vonhoff, and Andreas von Wurmb for the practical consults they gave me during the many 'Schiphol meetings'. I thank Nico Goedhart for his design of the special interface pile and COFRA for delivering the strong, sealing VLDPE-foils for these piles.

During the construction and execution of the test, I could work together with many different people at the construction site. I have experienced this as a pleasant time and therefore I would like to thank all the people who I worked with for their enthusiasm, the fun and the terrific job they have done at the job site, and in particular Dick Verbaas for his guidance and support during the pile driving, all the pile drivers, Ruud van Zanten for all the necessary construction preparations, Arie Dubbeld for all the necessary practical works he carried out for the testing (very important!) and for his practical consults, Jan Remmits, Mijndert Kramer, Koos Klooster and Rein Nieuwboer for the patience they had with me when I needed them or their equipment 'right now', Mark de Groot from VERVAT for his help in excavating the pit, all the time without complaints, and Arjaan for driving the shovel.

I also would like to thank Herman van der Velde for the permission to carry out the field test on 'his' job site.

Carrying out a field test makes no sense, unless the monitoring and instrumentation is successful, and for that I wish to thank Paul Dekker, Remco van der Ham, Flip Hoefsloot, André Opstal, and Ton Peters for the effort they committed during day's, nights and weekends, and Arnold Buis and his colleagues for carrying out the many inclinometer measurements, Cees den Hollander for conducting the land surveying, and the security and their dogs for guarding the instrumentation.

The Rotterdam Sheet Pile Wall Field Test costed money and in this respect I am most grateful to the more than 30 sponsors for the financial and material support. In particular I would like to thank the sheet pile producers ARBED, HOESCH and CORUS (formerly BRITISH STEEL) and the contractors of the Beneluxlijn COMBINATIE BENELUXLIJN and the subcontractors BALLAST NEDAM FUNDERINGSTECHNIEK, DIRK VERSTOEP, NEDERHORST GRONDTECHNIEK and VAN SPLUNDER FUNDERINGSTECHNIEK for propagating the field test, because I am convinced that this test could never be carried out without this support.

I am indebted to the Technology Foundation STW, and in particular to Mrs. Margriet Jansz, for the financial support that was provided to me for the past almost four years.

I am most grateful to the 20 predictors who were willing to make a prediction for their effort and for the amount of data they provided me to write Chapter 5.

I wish to thank the members of the International Advisory Committee for their guidance and consults, and for their confidence in the field test.

Apart from the Rotterdam Sheet Pile Wall Field Test I have also done other research and I would like to thank all the people who supported me in this. In the first place, I have pleasant memories of the work I did together with Dr. Ralf Hartmann-Linden. I have learnt a lot from the many discussions we had and I would like to thank him for that.

I am most grateful to Evert Aukema, Arnoud Joling, Johan Hockx and Noud Kelleners. Their graduation works were of great value for this thesis and therefore I am happy that they permitted me to borrow their work.

I also wish to thank Dr. Ronald Brinkgreve and Nol Gresnigt for his guidance and the many interesting discussions we had during this research.

I like to express my gratitude to Dr. Wout Broere, who was my room mate for more than six year of my stay at the University. Together we had a lot of interesting discussions both about geotechnical topics, such as the Haarajoki test embankment, and about other 'personal' matters. The many hours we worked together during days and evenings were of great stimulation to complete this research.

I would like to thank all my other colleagues and former colleagues at the Geotechnical Laboratory for the pleasant time and the useful discussions we had about a large variety of topics.

I gratefully thank Jaap Boelens for his help in designing the cover. I am confident that everybody has already noticed the many realistic details in the strutting and the special interface piles.

I am most grateful to David Rowbottom for his outstanding job and patience of checking my English and I feel sorry for his red pen.

I would like to thank my parents for their patience in listening to my uninteresting and tedious problems.

I thank my friends and former colleagues Edwin Dado, Dr. Eddie Koenders, and Dr. Roeland Ris for the practical and less useful discussions we had, taking many pizza's and beers.

I thank all my friends at VEW for keeping me sharp and letting me realise that life is much easier than research, and playing football is much more difficult.

Last but certainly not least I express my deepest gratitude to my second promotor Prof. Arnold Verruijt, in whose group I could work for more than 7 years. During the few technical discussions we had, I admired his ability to turn my unbridgeable problems into ridiculously simple solutions. Maybe these discussions have been of the greatest value for this research.

Arjen Kort

Summary

Steel sheet pile walls in soft soil

The research described in this thesis, is focused on two recent developments in the design of steel sheet piling: *Plastic Design* and *Oblique Bending*. In the first part of this thesis the theoretical background to these topics are treated. In the second part of this thesis plastic design and oblique bending are investigated in a full-scale field test on two steel sheet pile walls carried out in Pernis, near Rotterdam in 1999.

In 1953 Brinch Hansen developed a method for the plastic design of steel sheet pile walls, which has been used to design many walls but mainly in Denmark. Plastic design may result in material savings of about 35%, subdivided into 15% to 20% from adoption of the full-plastic section modulus instead of the elastic section modulus, and about 20% when rotation at a plastic hinge is allowed.

Three classical methods for plastic design of steel sheet pile walls are presented: the methods of Brinch Hansen, Windels and Weißenbach. These three methods focus on the geotechnical aspects of plastic design and assume an unlimited rotation capacity for the steel sheet piles. However, in reality the rotation capacity of steel sheet piles is limited because of the particular cross-section.

Within the framework of this research, a large number of geotechnical calculations were carried out to investigate how the limited rotation capacity of the sheet piling can taken into account in plastic design. Therefore, the subgrade reaction model PLASWALL has been developed that is able to generate a plastic hinge when the yield moment is reached and to calculate the rotation requirement of the plastic hinge.

It follows from this research that the rotation requirement of the sheet piling depends on the geometrical dimensions and the soil properties. A verification of the rotation capacity should therefore be a part of plastic design. Most state-of-the-art geotechnical tools that are suitable for plastic design, are not able to determine the rotation in a plastic hinge. In this thesis two simplified methods to determine the rotation requirement are presented and are verified by a large number of calculations, using both the subgrade reaction and the finite element methods.

Oblique bending is relevant for double-U piles, i.e., pairs of U-piles connected with a crimped or welded interlock. The particular cross-section of the double-U pile means that the principal axes of inertia are rotated, which involves a decrease of the effective height of the cross-section. In other words, oblique bending involves a significant loss of the effective moment of inertia and effective section modulus of a sheet pile wall. When the effects of

oblique bending are not taken into account in a design, the safety level of excavations with respect to strength and stiffness of the sheet piling may be overestimated.

In practice, oblique bending can be influenced by other effects, such as shear resistance in the interlocks, detailing of the structural supports, and the method of sheet pile driving. Therefore, the loss of strength and stiffness may not so be drastic as derived from the structural geometry. In Europe oblique bending is not always recognised: most countries do not even have a directive.

To derive a new design rule for oblique bending, the subgrade reaction model SKEW-WALL has been developed. The applicability of SKEWWALL is investigated by means of a comparison with fully 3D analyses using DIANA. It was found that SKEWWALL is a useful tool to investigate oblique bending and to determine suitable reduction factors to account for the loss of strength and stiffness.

Some factors that influence oblique bending, are quantified. The effects of structural supports have been investigated. Good countermeasures to reduce the effects of oblique bending are welding of the free interlocks during excavation, and to a lesser extent a capping beam. Furthermore, it is concluded that the driving method plays an important role on oblique bending, but the effects could not be quantified within the framework of this research.

On the basis of these findings a new design method is presented to take oblique bending into account. Finally, the workability of this method has been illustrated with two examples.

The recent developments regarding the design of steel sheet pile walls generated the desire to carry out a full-scale field test. This field test was focused on the investigation of the following three phenomena:

- the performance of a sheet pile wall with a plastic hinge

- the performance of a sheet pile wall composed of double U-sections (oblique bending)

- the short-term and long-term performance of both sheet pile walls in very soft soil

A prediction exercise was also organised to investigate the quality of state-of-the-art calculation models for steel sheet pile walls in soft soil, including short-term and long-term behaviour.

From evaluation of the full-scale field test results, it could be concluded that the behaviour of the plastic hinge was as expected, meaning that the assumptions on which the design rules in ENV 1993-5 are based, are valid for a real sheet pile wall. Further, the rotation in the plastic hinge can be back-calculated with the simplified verification methods, which means that these methods are applicable to a design.

The evaluation of the Larssen 607K-wall proved that oblique bending occurred. The reduction factors differed for each pile and were in the order of $\beta_I = 0.70$ and $\beta_W = 0.75$. These factors are in the same order as recommended by the directives of CUR 166 and the design rule proposed in this thesis.

The evaluation of the field test is concluded with some back-analyses with PLASWALL and PLAXIS, from which the influence of consolidation and creep on the long-term soil behaviour could be investigated. It could be shown from the calculations that the influence of soil creep on the behaviour of the sheet piling was very important.

Contents

Symbols

Latin upper case letters

A	cross-sectional area
A_{web}	area of the web
δA	virtual work
C	concentrated force accounting for fixation of the sheet pile in the ground (in Blum)
C_C	compression index
C_S	swelling index
D	constant reflecting dilatancy
E	effect of an action
E	Young's modulus (steel: $E = 2.1 \cdot 10^5$ N/mm^2)
E, F	horizontal and vertical component of earth pressure resultant
E_a, F_a	anchor or strut force
E_d	design value of effect of actions
E_{oed}	Oedometric stiffness
E^{ref}	reference stiffness in PLAXIS
E_u^{50}	undrained Young's modulus at 50% of the failure load
E_{ur}	unloading-reloading stiffness
δE	dissipated energy
EA	axial stiffness
EI	bending stiffness
F	load or action
F_d	design value of an action
F_{el}	load to attain the elastic bending moment resistance
F_{pl}	load to attain the full-plastic bending moment resistance
F_{rep}	representative value of an action
ΔF	$F_{pl} - F_{el}$
$\mathbf{F}$	transfer field matrix
G	shear modulus
I	moment of inertia
$I_{1,2}$	principal moments of inertia
I_{xx}	moment of inertia around y-axis
I_{yy}	moment of inertia around x-axis
I_{xy}	product of inertia

K	bulk modulus
K_a and K_p	active and passive earth pressure coefficient
K_n or K_0	neutral earth pressure coefficient
K_0^u	neutral earth pressure coefficient in terms of total stresses
L	span length
M	bending moment
M_{el}	elastic bending moment resistance ($M_{el} = f_y W_{el}$)
M_f	ultimate bending moment between contraflexural point and pile toe
M_{pl}	full-plastic bending moment resistance ($M_{pl} = f_y W_{pl}$)
M_s	ultimate bending moment between prop and contraflexural point
M_{Sd}	design value of the bending moment
$\mathcal{M}$	number of measured points of bending moment
N	normal force
$\mathcal{N}$	number of measured points of displacement
$\mathbf{P}$	transfer point matrix
Q	number of measured points of earth pressure difference
$\mathcal{R}$	resistance
R_d	design value of the resistance
R_e	relative density
R_f	friction ratio in CPT
S	degree of saturation
$\mathcal{S}$	internal forces and moments (sollicitation)
T	temperature
T	torque
T	wall friction
$\mathbf{T}$	transfer matrix
V	shear force
W	weight
W	section modulus
W_{el}	elastic section modulus
W_{pl}	full-plastic section modulus
X_d	design value of a material property
X_k	characteristic value of a material property

Latin lower case letters

a_d	design value of geometrical data
b	width of a steel sheet pile
b_f	width of the flange of a steel sheet pile
b_s	width of a single U-section
c	cohesion
c'	cohesion in terms of effective stress
c_d	design value of cohesion
c_s	distance between the central bending axis of a continuous wall and the neutral axis of a single U-profile
c_u	undrained shear strength

c_v	coefficient of consolidation
d	embedment depth of a retaining wall
d_i	thickness of layer
e	void ratio
f_y	yield strength
h	retaining height
h	height of a steel sheet pile
i	hydraulic gradient
k	permeability
k_{oed}	permeability from the oedometer test using Taylor
k	subgrade reaction modulus or spring stiffness
k_i	spring stiffness in interlock
k_u	undrained subgrade reaction modulus
k_x	spring stiffness in x-direction
k_y	spring stiffness in y-direction
ℓ	length
m_v	coefficient of volume compressibility
n	porosity
n	ratio between plastic bending moment and cantilever bending moment
p'	isotropic stress, in terms of effective stress
p_c	preconsolidation pressure
p^{ref}	reference pressure in PLAXIS
q	deviatoric stress
q	distributed load
q_c	cone resistance
s	surface settlement
t	thickness of a steel specimen
t_f	thickness of the flange of a steel sheet pile
u	water pressure
w	wall displacement or deflection (at a certain depth)
$x,\ y$	distance
z	application point of earth pressure resultant
z_a	depth of maximum bending moment
$\mathbf{z}$	state vector

Greek upper case letters

Φ	plastic contribution of the rotation in a plastic hinge
Φ_C	rotation capacity
Φ_{Cd}	design value of the rotation capacity
Φ_R	rotation requirement
Φ_{Rd}	design value of the rotation requirement

Greek lower case letters

α	rotation angle of the principal axes of inertia
α	temperature coefficient
β	compressibility of water
β_I	reduction factor for I accounting for oblique bending
$\beta_{I,0}$	eigen value of β_I determined from the cross-sectional geometry
β_W	reduction factor for W accounting for oblique bending
$\beta_{W,0}$	eigen value of β_W determined from the cross-sectional geometry
γ	rotation angle of the neutral axis
γ	unit weight
γ_{dry}	unit weight of dry ground
γ_F	partial load factor
γ_m	partial material factor
γ_M	partial material factor accounting for model uncertainties and dimensional variations
γ_{sat}	unit weight of saturated ground
γ_{Sd}	partial factor associated with the uncertainty of the action and/or action effect model
δ	angle of friction between ground and structure
ε	steel grade
ε	strain
ε_y	strain at the onset of yielding
κ	curvature
κ^*	modified swelling index
λ	parameter defined by (C.3)
λ^*	modified compression index
μ^*	modified creep index
ν	Poisson ratio
σ	normal stress
$\sigma_{1,2,3}$	principal stresses
σ_h	horizontal stress
σ_v	vertical stress
σ'	effective stress
σ'_a	effective stress for active earth pressure
σ'_p	effective stress for passive earth pressure
τ	shear stress
φ	rotation angle
φ	angle of internal friction
φ'	angle of internal friction in terms of effective stress
φ_d	design value of angle of internal friction
φ, φ_{pl}, φ_{rot}	sum of the angle of a beam at the points of inflection
φ_{pl}	rotation when reaching M_{pl} if a linear elastic model would have been used
φ_{rot}	total rotation at the onset of moment decrease
$\Delta\varphi$	rotation in a plastic hinge
ψ'	dilatancy angle

Miscellaneous

stroke   required movement to bring the soil from an active state to a passive
               state

Definitions

lateral direction   direction perpendicular to the plane of the wall (the known
                         direction)
transverse direction   direction in plane of the wall

Chapter 1

Introduction

1.1 European standardisation

Within the framework of the European harmonisation process European technical standards (*Structural Eurocodes*) for the structural design and execution of buildings and civil engineering works are being developed. For example, Eurocode 1 (EN 1990) covers the basis of design, Eurocode 3 (EN 1993) concerns design of steel structures, and geotechnical design is dealt with in Eurocode 7 (EN 1997). It is expected that in the first decade of the 21st century all national building codes will have been replaced by unified European standards.

The first step in the achievement of unified European standards is the formulation of pre-standards, the ENV's. The specific ENV's are written under the auspices of the CEN[1] by specialists from the different member states. ENV's are established as prospective standards and are intended for experimental application and for the submission of comments. For certain safety elements in the ENV's indicative values are assigned which are identified by ☐ or [ ], the so-called *boxed values*.

Each ENV Eurocode is provided with a *National Application Document* (NAD). The NAD's, which are drawn up by the national standardisation institutes of the specific members, cover the discrepancies between the Eurocodes and the national codes. The authorities in each member country are expected to review the *boxed values* and may substitute alternative values for these safety elements in their NAD's. During a trial period of at least 3 years the ENV's together with the NAD of the specific country may be used next to or instead of the corresponding national building codes.

After the trial period in which practical experience with the ENV's is gained, the ENV together with the NAD's of all the member states and the gathered comments are processed to a unified European Standard, the EN. The EN's are established as a general rule, because it is important that member's national standards are harmonised as far as possible. The member states are obliged to implement the European Standards by giving them the status of national standards. In this way the current national standards will be replaced by one unified European code, the Eurocode.

---

[1] European Committee for Standardization

1.2 Limit state design

An important principle of the Eurocode system is the requirement of design verification for all possible limit states, which can be achieved by *Limit State Design*. ENV 1991-1 [21] distinguishes between the *Serviceability Limit State* (SLS) and the *Ultimate Limit State* (ULS). Guidance on the geotechnical aspects of steel sheet piling design is provided by ENV 1997-1 [22] and guidance for the structural aspects by ENV 1993-5 [24]. The limit state design process can be summarised according to Figure 1.1.

	γ_F			γ_m			γ_{Sd}
	Actions			Ground properties			Action effects
Case	Permanent		Variable	$\tan\varphi$	c'	c_u	
	Unfavou-rable	Favou-rable	Unfavou-rable				
Case B	[1.35]	[1.00]	[1.50]	[1.0]	[1.0]	[1.0]	[1.00]
	[1.00]	[1.00]	[1.11]	[1.0]	[1.0]	[1.0]	[1.35]
Case C	[1.00]	[1.00]	[1.30]	[1.25]	[1.6]	[1.4]	[1.00]
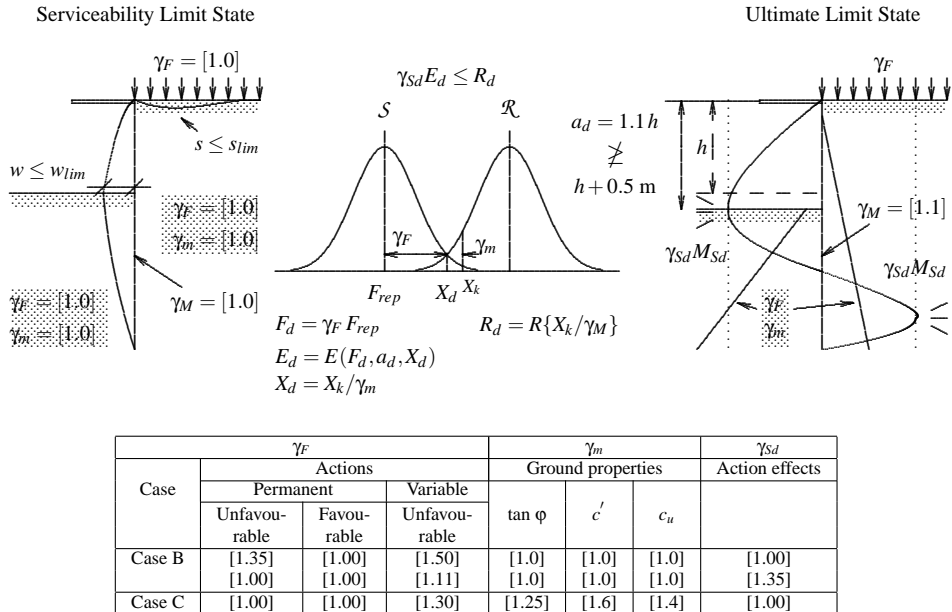
Figure 1.1: *Limit State Design for steel sheet pile walls*

Verification of the Serviceability Limit State is carried out using deformation limits for the wall displacement w_{lim} and for the surface settlement s_{lim}, if required. Loading, soil parameters, and resistance of the sheet pile are considered as conservative characteristic values in the design: $\gamma_F = \gamma_m = 1$. In addition, it is necessary to verify that yielding does not occur in any cross-section or that, if yielding occurs, it can be shown that this will not lead to an Ultimate Limit State. In most cases a sheet pile wall will behave elastic in the Serviceability Limit State.

Ultimate Limit State design is carried out using partial safety factors for the actions and the resistances. The resistance of the sheet piling is reduced using a safety factor of $\gamma_M = \boxed{1.1}$ in accordance with Eurocode 3, part 5. The actions F_{rep}, which include the characteristic earth pressures, should be increased using a safety factor of γ_F or γ_m according to case B or case C of ENV 1997-1, see the table in Figure 1.1. In addition, the excavation depth has to be increased by 10% of the retained height of a cantilever wall or the distance between the lowest anchor or strut level and the nominal excavation level for a propped wall, up to a maximum of 0.5 m.

However, Clause 2.4.2.(17) of ENV 1997-1 states that when calculating the design earth pressures for Case B, the application of partial factors γ_F to characteristic earth pressures may lead to unrealistic or physically impossible design values. For these situations the partial factors given in the table in Figure 1.1 may be treated as model factor γ_{Sd}. This model factor is then directly applied to the action effects E, i.e., internal structural forces and bending moments, derived from the characteristic earth pressures.

When calculating design earth pressures for Case C, the partial factors γ_m and γ_F are applied to the characteristic strength of the ground and to the characteristic surface loads; for Case C the model factor γ_{Sd} is unity.

Plastic design

For Ultimate Limit State design the retaining structure shall be verified against all possible failure modes. Examples of limit modes for structural failure presented in part 1 of Eurocode 7, are listed in Figure 1.2.
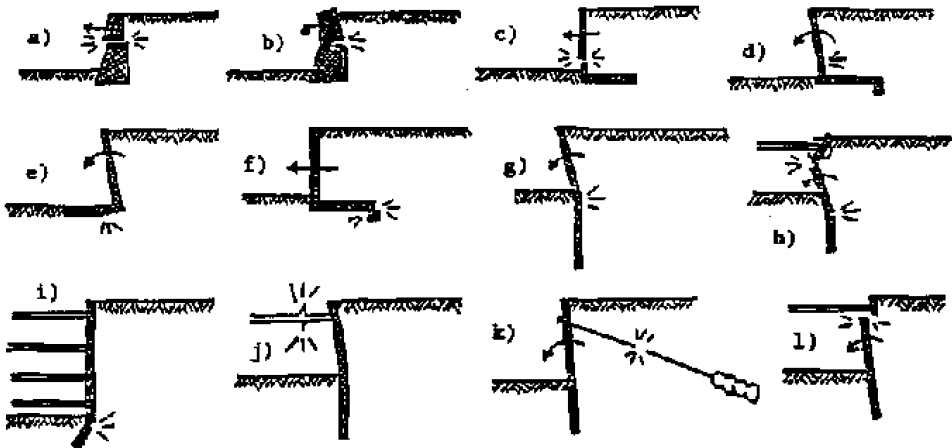
Figure 1.2: *Examples of limit modes for structural failure of retaining structures (after Eurocode 7, part 1 [22])*

Limit state *h)* is based on *plastic collapse* of the structure, and is similar to the classical theory of plasticity for framework structures (see e.g., Neal [60]). A collapse mechanism with plastic hinges is determined by which the sheet pile wall can fail and according to which the sheet pile wall shall be designed. Clause 8.6.6 of ENV 1997-1 states the following about the design.

(3)P *For each ultimate limit state it shall be demonstrated that the required strengths can be mobilised in the ground and the structure with compatible deformations.*

(4) *In structural elements, reduction in strength with deformation, due to effects such as cracking of unreinforced sections, large rotations of plastic hinges or*

> *local buckling of steel sections should be considered with the material-related Eurocodes. . . .*

In the case of steel sheet piling the material related Eurocode 3, part 5 applies. In contrast to plastic design for frame structures, plastic design of sheet piling is not common in geotechnical engineering. Although in 1953 Brinch Hansen [13] presented a method for plastic design of sheet pile walls, this method never had a much wider acceptance than Denmark and the north of Germany.

When ENV 1993-5 was being developed, little knowledge existed on which the basic application rules for the structural resistance of steel sheet piles could be based. This was particularly the case in respect of the full-plastic cross-sectional resistance and the plastic deformation capabilities of steel sheet piles. The Technical European Sheet Piling Association (TESPA), a technical forum involving PROFIL ARBED (L), KRUPP HOESCH (D) and CORUS (UK), thought that the competitiveness of steel sheet piles against other construction materials could be improved, and initiated in 1993 research into the plastic structural behaviour of steel sheet piles [68]. On the basis of the success of this first project PROFIL ARBED, KRUPP HOESCH and CORUS initiated an ECSC multipartner research project with the title *Development of Unified European Design Rules for Steel Sheet Piles and Introduction into Part 5 of Eurocode 3* [39]. The framework of this ECSC research project can be subdivided in two main parts.

In the first part, design and application rules were formulated on the basis of more than 20 large scale experimental tests and more than 80 numerical simulations on various types of steel sheet piles. These design and application rules form the basis of the regulation in ENV 1993-5.

In the second part, investigation of the soil-structure interaction was carried out to develop a suitable method for determination of the rotation requirement for typical design cases. A parametric study of the rotation requirement for simplified single and double propped sheet pile walls was carried out in order to investigate economic measures to optimise the design. Based on these insights, four suitable methods to determine the rotation requirement are presented in ENV 1993-5.

The majority of the results of the ECSC project regarding the structural design resistance of steel sheet piles are described in the thesis of Hartmann-Linden [38]. The part concerning the geotechnical aspects of plastic design, especially that covering the generation of plastic hinges, is the first subject of this thesis.

Oblique bending

Another important topic of the ECSC research was the structural resistance of U-shaped sections. In steel sheet pile walls built up of U-sections the interlocks of the individual U-piles are on the central bending axis of the sheet pile wall, see Figure 1.3. If sufficient shear friction capacity of the interlocks is present, the central bending axis is the neutral axis and the maximum cross-sectional resistance is obtained. Sheet pile producers often provide the cross-sectional data of a U-section for the maximum cross-sectional resistance.

In European practice, sheet pile walls composed of U-sections are generally built either with *single piles*, where the interlocks are threaded together *during pile installation*, or with *double piles*, in which two piles are threaded together and crimped or welded *before pile installation*, and occasionally use is made of *triple piles*.

Continuous wall (highest cross-sectional resistance)

Single U-piles

Double U-piles

Triple U-piles
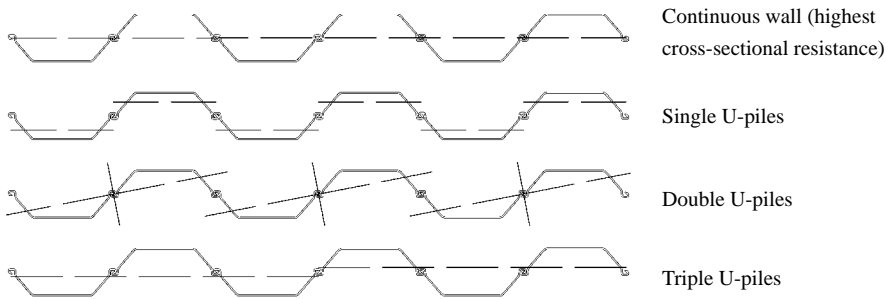
Figure 1.3: *Axes of inertia for different systems of U-sections*

The shear force transmission in the interlocks may not always be sufficient to assume the maximum cross-sectional resistance. In extreme cases, if the shear capacity of the interlocks is absent, single, double, and triple U-piles behave as follows, see also Figure 1.3:

- Single U-piles bend about the principal axis of inertia of an individual pile. This causes a reduction of the moment of inertia to approximately 30% and a reduction of the section modulus to 50% of the maximum cross-sectional resistance values

- Double U-piles bend about the inclined principal axis of inertia, which causes a deflection both perpendicular to the wall and in plane of the wall. The moment of inertia reduces to approximately 50% and the section modulus to about 60% of the maximum cross-sectional resistance values

- Triple U-piles bend about the principal axis which causes a reduction to approximately 90% for the moment of inertia and to about 80% for the section modulus of the maximum cross-sectional resistance values

During the formulation of ENV 1993-5 a lack of knowledge was apparent. Most countries in Europe do not recognise the *oblique bending* phenomenon and the possible loss of stiffness and strength for double U-sheet piles. Some countries do not recognise the possible loss of stiffness and strength for single U-sheet piles. On the other hand, in the Netherlands a rather strict regulation for reduction factors on the strength and stiffness of single and double U-piles is proposed in the *CUR Handboek Damwandconstructies* [27]. The rules in the CUR handbook account for possible advantageous effects, such as the number of anchor or strut levels, the conditions of the free interlocks, and the soil type in front of and behind the sheet pile wall, but sufficient scientific evidence was lacking for the introduction of this regulation in ENV 1993-5.

It was not clear whether sheet piling design in the Netherlands with U-sections is too safe and therefore too expensive, or unsafe in most other countries. ENV 1993-5 does not define reduction factors for the strength and stiffness of sheet pile walls composed of single and double U-sections but instead the foreword states:

(20) *Certain reduction factors concerning possible slip in the interlocks of U-shaped sheet piles have been left open and can be supplied in NADs at the discretion of national competent authorities.*

The phenomenon of oblique bending in the design of steel sheet piling is the second subject of this thesis.

1.3 Rotterdam sheet pile wall field test

The development of Structural Eurocodes and the expected role in the design practice of steel sheet piling together with the knowledge of plastic design and oblique bending gained in the ECSC research project, gave the inspiration for the Geotechnical Laboratory of Delft University and the Dutch Centre for Civil Engineering Research and Codes (CUR) to carry out a full-scale sheet pile wall field test at a site near Rotterdam with typical Western Dutch soil conditions, where the soil consists of very weak clay and peat and where the groundwater level is just below groundsurface [49, 54, 75]. In this field test the research was focused on:

- the performance of a sheet pile wall in real soil conditions in which a plastic hinge is generated

- the performance of a sheet pile wall constructed of double U-sections in real soil conditions

- the short-term and the long-term performance of both sheet pile walls in soft soil

For this field test an excavation approximately 12 metres square was constructed in which two test walls were included, see Figure 1.4. One test wall consisted of *AZ13-piles* and the second test wall was built using *double U-piles Larssen 607K*. The two side walls were single U-pile walls built up with *single LX32-piles*. Special measures were taken to obtain, as far as possible, a plane strain behaviour of both test walls.
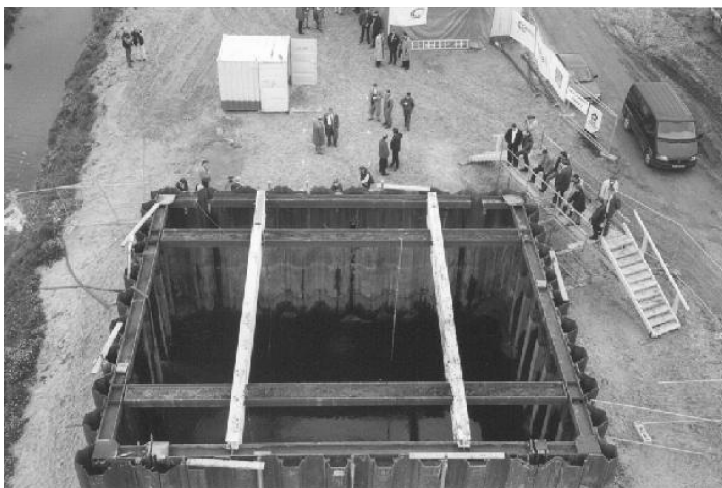
Figure 1.4: *Rotterdam sheet pile wall field test (May 11 1999)*

Within the framework of the field test a prediction exercise was organised. The aim of this exercise was to make designers aware of recent developments in steel sheet piling and to provoke discussion. Twenty-three predictions were submitted, from which an interesting overview of the state-of-the-art calculation models could be made [50, 53].

A major part of the activities carried out for this field test form the third subject of this thesis: the design and execution of the field test, the organisation and evaluation of the prediction exercise, the interpretation of the measurement results, and evaluation of the test results with the emphasis on plastic design and oblique bending.

1.4   Aim of this research

The introduction of limit state design of steel sheet pile walls in Eurocode 3, part 5 has exposed a number of design aspects for which insufficient knowledge was available to formulate uniform European design rules. This thesis focuses on two of these aspects:

- Plastic design

- Oblique bending

The first aim of this research is to develop design rules for steel sheet pile walls that take plastic design and oblique bending into account and the second aim is to validate these design rules to data from a full-scale field test.

As there were no field data available for such a validation, a full-scale field test was designed and carried out within the framework of this research, to generate suitable field data that can also be used for validation of design models for sheet pile walls in soft soil with time-dependent behaviour.

1.5   Benefits to be gained from the research

Plastic design

The available national and international design rules for steel sheet pile walls are mainly based on elastic design (permissible stress method). Only a few countries (e.g., Denmark) apply plastic design. The results from plastic design sometimes differ considerably from elastic designs: *important material savings may be expected when applying plastic design.*

In 1988 Steenfelt [69] presented a numerical experiment conducted by Krebs Ovesen of the design of a sheet pile wall for a 6 metre deep excavation according to the Norwegian, Swedish, Finnish and Danish design codes (Figure 1.5). The Danish design code is based on plastic design, the other design codes on the permissible stress method. The outcome of the experiment was that the design results of the other countries showed minor differences but that *the amount of steel required by the Danish code was 40% less.* The major part of this difference results from allowance of a plastic hinge in the design.

A second comparison between the Danish and the British design practice carried out by Steenfelt and Haahr [70] showed a similar 'conservatism' for British designs. In addition, both Hartmann-Linden [38], and Van Tol and Kort [74] mention possibilities for *material saving of more than 35%.* According to them, 15% to 20% can be gained from moving the

SF — Classical earth pressure theory:
E^A : +25%
E^P : −20%
Computer programme

S — Free earth support
+ Rowe's moment reduction

N — Free earth support
+ Rowe's moment reduction
+ vertical equilibrium cond.

DK — Brinch Hansen's method
rotation abt. prop
+ yield hinge

SF — $d \approx 1.9$ m; $M_{max} = 77$ kN m/m; $W = 456 \times 220/260 = 386$ cm³/m; $A \approx 55$ kN/m — Steel required: $G \approx 640$ kg/m

S — $d \approx 1.8$ m; $M_{red} = 0.7 \cdot 88 = 62$ kN m/m; $W = 344$ cm³/m; $A \approx 44$ kN/m — $G = 505$ kg/m

N — $d = 2.1$ m; $M_{red} = 0.7 \cdot 117 = 82$ kN m/m; $W = 455 \times 240/260 = 420$ cm³/m; $A = 85.5$ kN/m — $G = 675$ kg/m

DK — $d = 0.62$ m; $M_{max} = 17.5$ kN m/m; $W = 92$ cm³/m; $A = 68.8$ kN/m — $G \approx 380$ kg/m

Figure 1.5: *Numerical experiment of a sheet pile wall design according to the Norwegian, Swedish, Finnish and Danish design codes (after Steenfelt [69])*

definition of structural failure from yielding of the outermost fibre to yielding of the full cross-section and about 20% from the redistribution of earth pressures after the generation of the plastic hinge.

Oblique bending

Research of the oblique bending phenomenon may contribute to the filling-in of Table E.5 in ENV 1993-5, the table which includes factors to take the loss of strength and stiffness into account when using single or double U-sections. *An underestimation of oblique bending* may result in an underestimation of the deformation and in an overestimation of the strength of the sheet pile wall, and consequently to *an underestimation of the influence of an excavation on adjacent structures*. This may lead to serious problems in respect of settlements of adjacent structures, especially in built-up areas where nowadays more and more underground construction activities take place. *An overestimation of oblique bending* will lead to uneconomical reduction factors and therefore to *unnecessarily expensive sheet piling*.

Full-scale field test

The sheet pile wall field test in soft soil contributes to a *better validation* of the behaviour of steel sheet pile walls in which a plastic hinge is generated or which is subjected to oblique bending, and of soil-structure interaction problems for retaining structures in general. Today, for the design of a steel sheet pile wall the engineer generally makes use of a numerical calculation model, such as a limit earth pressure model, a subgrade reaction model or a finite element model. More complicated design models are rapidly developed and therefore the need for validation of these models to real behaviour of steel sheet piling increases.

A well monitored full-scale field test may also serve as a *benchmark* for validation of numerical or centrifuge models. When the behaviour of the full-scale field test can be

successfully simulated with a numerical model or with a centrifuge model, a calibrated model has been obtained which can be used as a basis for further investigation.

Evaluation

When the new developments of plastic design and oblique bending are accepted in geotechnical design practice, it may lead to more economical solutions for steel sheet piling with respect to both costs and safety.

1.6 Arrangement of the thesis

This thesis is set up of 7 chapters including this introduction. Chapter 2 covers plastic design, and focuses on verification of the rotation in the plastic hinge and on the practical application of plastic design to steel sheet pile walls. Chapter 3 covers oblique bending and new developments for oblique bending in the design of steel sheet pile walls, and proposes design rules which account for these new developments. The research carried out for the Rotterdam Sheet Pile Wall Field Test is presented in Chapters 4, 5 and 6. The test and the test results are presented in Chapter 4, the evaluation of the submitted predictions in Chapter 5, and the evaluation of the field measurements and back-analyses with the subgrade reaction and the finite element methods in Chapter 6. Conclusions and recommendations are presented in Chapter 7.

Chapter 2

Plastic design

2.1 Introduction

Plastic design of steel sheet pile walls is not a new development in geotechnical engineering. In 1953 Brinch Hansen [13] developed a design method with plastic hinges for sheet pile walls and ever since this method has formed the basis for the current Danish design practice. Later Windels [92, 93, 94, 95] and Weißenbach [89, 90, 91] developed verification methods for plastic design of steel sheet pile walls, which were applied to quay walls in the port area of Hamburg. Different competitive studies of Brinch Hansen's plastic design method and conventional elastic design methods proved the possibility for very interesting savings of material and costs [38, 39, 69, 70, 74], see also Figure 1.5. But although plastic design has been successfully applied to the construction of many sheet pile walls in Denmark and all over the world, the acceptance for practical application has never grown much farther than Denmark and the Northern part of Germany.

In most other countries steel sheet pile walls are traditionally designed according to an *elastic design method*, in which *elastic* refers to the structural behaviour. The structural verification is based on an ultimate bending moment capacity which generates *yielding of the outermost fibre*:

$$M_{Sd} \leq f_y W_{el} / \gamma_M \tag{2.1}$$

where M_{Sd} is the design value of the bending moment (action effect), f_y is the yield stress of steel, W_{el} is the elastic section modulus of the sheet pile, traditionally provided by most producers of steel sheet piles, and γ_M is the partial material factor.

To illustrate the fundamental differences between elastic and plastic design, a single anchored sheet pile wall is presented in Figure 2.1, and subjected to an increasing excavation: $D_3 > D_2 > D_1$. As a result of the excavation the differential earth pressure on the wall increases until a plastic hinge is generated and finally the limit state is obtained. Three main stress states can be distinguished for the sheet pile wall.

a) When the excavation D_1 is small, the wall behaves elastically. Structural verification of the bending moment should include:

$$M_{Sd} \leq f_y W_{el} / \gamma_M \tag{2.1}$$

Displacement	Moment	State of cross-section
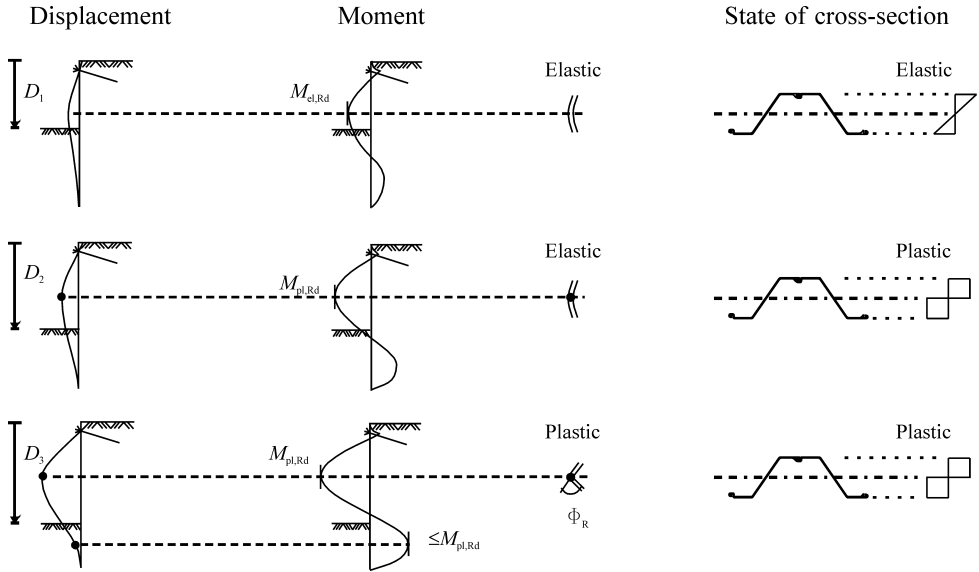
Figure 2.1: *States of stress in a sheet pile wall during an excavation [38]*

b) When the excavation is increased to D_2, the cross-section of the sheet pile at the level of the maximum moment becomes fully plastic, but there is still some reserve in the soil that prevents the system from collapsing: the first plastic hinge is about to be formed. Structural verification of the bending moment should include:

$$M_{Sd} \leq f_y W_{pl} / \gamma_M \tag{2.2}$$

where W_{pl} is the plastic section modulus.

c) When the excavation is gradually increased to D_3, rotation in the plastic hinge is generated and earth pressure is redistributed. Excavation depth D_3 can only be achieved if the first plastic hinge has sufficient rotation capacity, either to mobilise more resistance from the 'passive' earth pressure, or to allow other plastic hinges to develop in the sheet pile. Therefore the available rotation capacity of the sheet pile, Φ_C, should be checked to ensure that it is larger than or equal to the rotation required by the first plastic hinge in the sheet pile, Φ_R. Structural verification of the bending moment should include:

$$M_{Sd} \leq f_y W_{pl} / \gamma_M \tag{2.2}$$

$$\Phi_C \geq \Phi_R \tag{2.3}$$

In comparison to traditional elastic design given by stress state **a)**, the stress states **b)** and **c)** involve a more effective material use, which can also be reflected in material saving. A design using the full-plastic section modulus without allowance of a plastic hinge, state **b)**, may result in a material saving of about 15% to 20%. Allowing rotation of the plastic hinge, state **c)**, provides an additional material saving with a maximum of about 20%.

Consequently the material saving that can be obtained from plastic design can be more than 35%.

The equations (2.1) and (2.2) imply sufficient geometrical stability of the cross-section in respect of local buckling. However, because of the particular cross-sectional shape, both the ultimate resistance and the rotation capacity of the steel sheet pile may be predominated by loss of geometrical stability of the cross-section due to local buckling of the compression flange. Hartmann-Linden [38] proposed design rules to determine the ultimate moment resistance and rotation capacity of a steel sheet pile, taking into account the possible loss of strength due to geometrical instability.

The structural models in most available geotechnical tools, such as SPOOKS [37] and PLAXIS [79], are based on perfectly plastic material behaviour and can not be used to predict any hardening or softening behaviour of the steel sheet pile. Nevertheless, the geotechnical capabilities of these models are so strong that application of these models to the design of steel sheet pile walls is obvious. Furthermore, these existing geotechnical models can be applied to design when it can be shown that the rotation capacity of the steel sheet pile wall is not overestimated.

The aim of this chapter is to provide a practical guidance for plastic design, focussing on the geotechnical aspects. Emphasis is put on the investigation of the rotation in plastic hinges and on the various important aspects governing this rotation. Existing classical design methods are discussed, with respect to plastic design, followed by an explanation of the structural behaviour of steel sheet piles. Next, four methods for the determination of the rotation requirement are presented which have been introduced in Appendix E.4.4. of ENV 1993-5, and the subgrade reaction model with an elasto-plastic beam PLASWALL is developed. The sensitivity of the rotation requirement to structural and geometrical properties is investigated, and finally the rotation check is applied to two design examples.

2.2 Classical methods for plastic design

2.2.1 Blum

Blum's method [8] is often used as an introduction to sheet pile walls in many textbooks about soil mechanics, see e.g. [11, 26, 55, 84], and here this method is also used as an introduction to plastic design.

The basis of the method is the assumption of limit earth pressures acting on the sheet pile wall. Blum introduced the concept of an extra concentrated force C to account for fixity of the sheet pile in the ground, see Figure 2.2. This force is the result of the passive earth pressure increase generated by the fixity of the sheet pile in the ground. To generate this extra force C, the embedment depth, d, needs to be increased by 20%.

The earth pressure distribution in Blum's method is based on Rankine's earth pressure theory and does not account for earth pressure redistribution due to arching in the soil behind the sheet pile wall. According to clause R 77 of EAU [25], earth pressure redistribution may be taken into account by correcting the calculation results according to Blum as follows: the part of the bending moment resulting from the active effective earth pressure may be reduced by 33% but the strut force must then be increased by 15%.
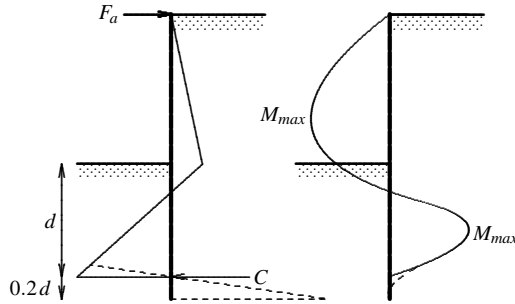
Figure 2.2: *Anchored sheet pile wall according to Blum [8]*

Plastic design with Blum's method

Although Blum's method for sheet pile walls has never been presented as a method for *plastic* design, it is interesting to explain this method from the point of view of plastic design. In fact, in the context of this thesis it is intended to present Blum's method as an *introduction* of Brinch Hansen's method [13].

For this explanation, the example in Figure 2.3 is considered, in which a single propped, smooth, sheet pile wall retains a 5 metre deep excavation ($h = 5$ m) in dry sand ($c' = 0$ kPa and $\varphi' = 30^o$). The wall is assumed as infinitely stiff and can be designed with 0, 1 or 2 plastic hinges. The soil is characterised as a plastic material: unless the wall movement is zero, the soil is in an active or a passive state, depending on the direction of the wall movement. Further it is assumed that the earth pressure distribution can be described using Rankine's active and passive earth pressure coefficients K_a, and K_p, depending upon the direction of the wall movement.

It should be noted that in this example Blum's concept of replacement of the earth pressure jump by a concentrated force is not adopted.
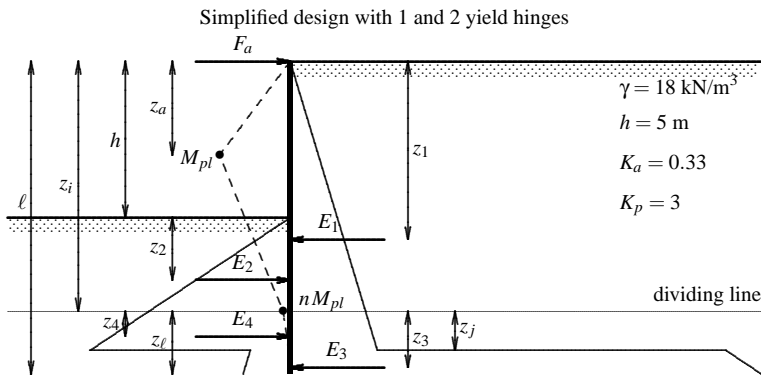
Figure 2.3: *Design with plastic hinges*

Example of a wall with a fixed earth support

In Figure 2.3 a sheet pile wall retaining a 5 metre deep excavation is designed with a fixed earth support. The wall is designed in such a way that a plastic hinge is generated at z_a. As a result of plastic rotation in the hinge, the lower part of the wall will be clamped in the soil involving a fixed moment nM_{pl}, with $0 \leq n \leq 1$. If $n = 0$, the wall has a free earth support, and if $n = 1$, the wall is fully fixed in the sand and a second plastic hinge is about to be generated.

The design starts with a choice of the wall movement. The wall movement, indicated with the dashed line in Figure 2.3, is chosen in such a way, that one plastic hinge can be formed at z_a and a fixed moment can be generated at z_i. The fixed moment, however, can only be developed when the wall is longer than z_i, because the bending moment at the toe of the wall must be zero. This involves an *earth pressure jump* which can be obtained when the toe of the wall is pushed towards the retained side.

On the basis of the selected wall movement, a compatible earth pressure distribution can be chosen as follows, see Figure 2.3: active earth pressure when the wall moves away from the soil, and passive earth pressure when the wall moves towards the soil. As the shear force in the plastic hinges must be zero, the earth pressure jump must be beneath the location of the second plastic hinge.

Moment equilibrium and horizontal equilibrium are obtained if the following equations are satisfied.

$$M_{pl} = \frac{2}{3} F_a z_a \tag{2.4}$$

$$nM_{pl} = -E_1 z_1 + E_2 (h + z_2) \tag{2.5}$$

$$E_1 - E_2 = F_a = \frac{1}{2} K_a \gamma z_a^2 \tag{2.6}$$

$$nM_{pl} = E_3 z_3 - E_4 z_4 \tag{2.7}$$

$$E_3 - E_4 = 0 \tag{2.8}$$

The forces E_1 to E_4 are the resultants of the active and passive earth pressure distributions above and below the dividing line. Their points of application are given by z_1 to z_4. Equations (2.4), (2.5) and (2.6) describe equilibrium above the dividing line and equations (2.7) and (2.8) equilibrium below the dividing line. Vertical equilibrium is of no importance for the perfectly smooth wall.

Case 1: $n = 0$
For the case $n = 0$ it follows from equation (2.7) and (2.8) that $z_3 - z_4 = 0$, which is only possible when $z_3 = z_4 = 0$, see Figure 2.3. The case is reduced to the solution of equations (2.4), (2.5) and (2.6). After some elaboration one obtains $\ell = 6.99$ m, $z_a = 3.59$ m, $F_a = 38.22$ kN/m and $M = 91.42$ kNm/m.

Case 2: $0 < n \leq 1$
For the case $0 < n \leq 1$ the derivation process of wall length ℓ and plastic moment M_{pl} is a very laborious and tedious process and is therefore not treated in detail. Trial and error, or a computer program are suitable tools to solve the equations (2.4) to (2.8). The calculation results are presented in Table 2.1.

n	ℓ (m)	z_a (m)	M_{pl} (kNm/m)	F_a (kN/m)
0	6.99	3.59	91.42	38.22
0.5	8.06	3.33	73.35	33.01
1	8.37	3.15	61.85	29.56

Table 2.1: *Calculation results*

Wall displacement

The wall displacement can be derived from four successive integrations of the earth pressure distribution. For the boundary conditions of the displacement curve, the geometry and the chosen wall movement require zero wall displacement at strut level and at the level of the pressure jump. In Figure 2.4 the solid line represents the displacement of the sheet pile wall without a plastic hinge. Just above the pressure jump the displacement curve clearly shows a wall displacement towards the retaining side whereas the wall was assumed to move to the opposite direction. Obviously the chosen earth pressure distribution can not be in agreement with the wall movement for the case of a non-plastic wall behaviour.

Displacements with and without a plastic hinge for the case $n = 1$
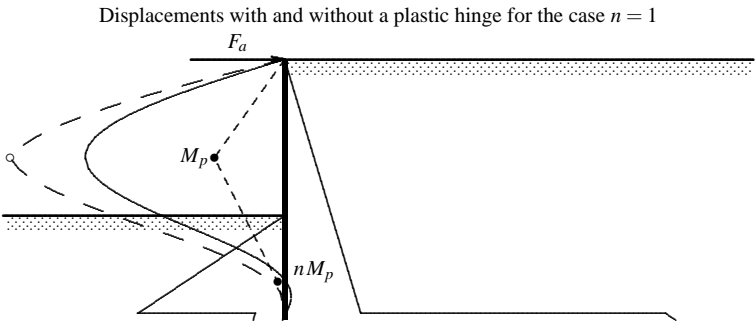
Figure 2.4: *Wall displacements for the case $n = 1$, without a plastic hinge (solid line) and with a plastic hinge (large-dashed line). The small-dashed line indicates the chosen wall movement.*

In order to correct the wall displacement, one or more hinges must be introduced to the sheet pile wall in such a way that the calculated wall displacement is in the same direction as the chosen wall movement. The only possible location for such a hinge to satisfy both the kinematical and equilibrium conditions, appears to be at the location of the maximum span moment. The large-dashed line in Figure 2.4 represents the displacement line that is corrected from a plastic hinge at $z = z_a$ and works at every depth giving displacements in the same direction as the chosen wall movement.

Step by step procedure

On the basis of the example a general step by step procedure for the design of this sheet pile wall can be formulated as follows:

1. Determine the geometry of the construction, i.e., the excavation depth and the number and position of the struts

2. Choose a failure mechanism according to which the wall should fail

   This failure mechanism may be determined by the number of plastic hinges, by the degree of fixity in the ground, or, for example, by the maximum pull-out anchor force.

3. Express the failure mechanism as a possible profile of wall movement

   This profile is based on the assumption of a *rigid-plastic* wall behaviour, i.e., all deformation of the sheet pile wall is concentrated in one or more plastic hinges.

4. Choose an earth pressure distribution that is *compatible* with the wall movement

   In the example the earth pressure distribution was based on the assumption of rigid-plastic soil with limits described by Rankine's earth pressure theory. Brinch Hansen developed an earth pressure theory based on compatibility with wall movement, see Section 2.2.2.

5. Determine the resultant earth pressure forces E_1, E_2, etc. and appropriate points of application z_1, z_2, etc from the chosen earth pressure distribution

6. Determine the wall length, maximum moment and anchor or strut forces under the condition of moment equilibrium and horizontal equilibrium. In the case of rough walls, $(\delta \neq 0^o)$ vertical equilibrium should also be satisfied

7. Determine the wall displacement and verify for every depth that the direction corresponds with the chosen shape of wall movement

8. Check if other ultimate limit states or overall stability failure are more critical

   The calculation procedure is based on a failure mechanism chosen by the designer. The designer should be aware that other failure mechanisms or other construction stages can be more critical for the design.

Evaluation of Blum's method

By means of the example, Blum's method for design of sheet pile walls has been used to provide an introduction of the basic requirements of Brinch Hansen's method for plastic design. When using limit earth pressure models it is important to realise that the designer is responsible for the choice of wall movement and the corresponding earth pressure distribution. This choice is the basis of Brinch Hansen's earth pressure theory.

2.2.2 Brinch Hansen

The background to Brinch Hansen's design method for sheet pile walls is basically explained with the example of *Plastic design with Blum's method* in the previous section. The step by step procedure is, in principal, the same procedure as described by Brinch Hansen [13, pp.49-51]. However, the main difference between the so-called Blum model and Brinch

Hansen's earth pressure model is expressed by step 4 and 5. In the Blum model the earth pressure distribution was based on Rankine's earth pressure theory, which is acceptable for the special case of a smooth wall in sand, with $c' = 0$ kPa and $\varphi' = 30^o$. In Brinch Hansen's earth pressure theory the resultant earth pressure force, E, is calculated from a failure mechanism of the soil which is statically and kinematically compatible with the chosen wall movement.

Rupture figures

Brinch Hansen represented failure mechanisms in the soil by *line ruptures*, *zone ruptures* or combinations of those, *composite ruptures*, which he coded in a clever way. A line rupture is characterised by failure in a very thin plastic, possibly dilating zone and in a zone rupture the whole area above the lowest rupture line is in a state of failure. Well-known examples of zone ruptures are the **R**ankine and the **P**randtl ruptures. The type of rupture figure is determined from the movement and the roughness of a rigid-plastic wall. Examples of possible rupture figures as function of wall movement are presented in Figure 2.5.
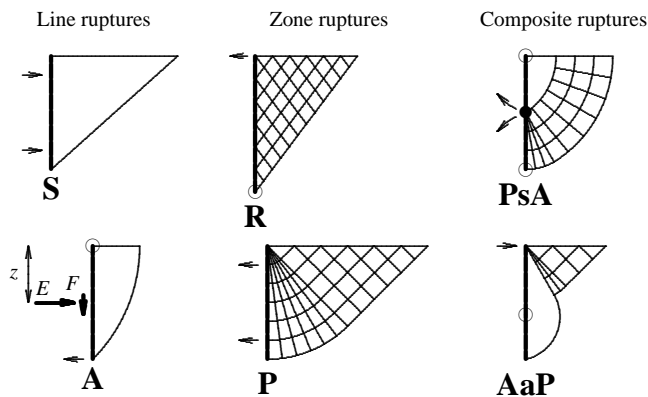
Figure 2.5: *Schematic representation of rupture figures related to different wall movements.* → *indicates the wall movement,* ○ *a rotation axis and* • *a hinge.*

In Brinch Hansen's earth pressure theory the horizontal and vertical component of the earth pressure force, E and F, and their point of application z are determined from the rupture figure. Essentially, in a sheet pile wall design the rupture figure is chosen by the designer, who can only determine the correct earth pressure resultant if the rupture figure is statically and kinematically compatible with the chosen wall movement. It is equally possible, however, that the imposed wall movement can be described by more than one rupture figure. In that case the critical rupture figure is determined from the failure mechanism with the least dissipation of potential energy.

The choice of the proper rupture figure is part of step 4 of the step by step procedure and the calculation of the resultant earth pressure forces and their points of application is part of step 5. For calculation of the resultant earth pressure forces and the accompanying points of application from a rupture figure, reference is made to one of the works of Brinch Hansen [13, 14, 15].

Choice of wall movement and rupture figures

Possible choices of wall movements for a propped sheet pile wall are presented in Figure 2.6. Each wall movement is accompanied by a rupture figure, representing a critical failure mechanism of the soil:
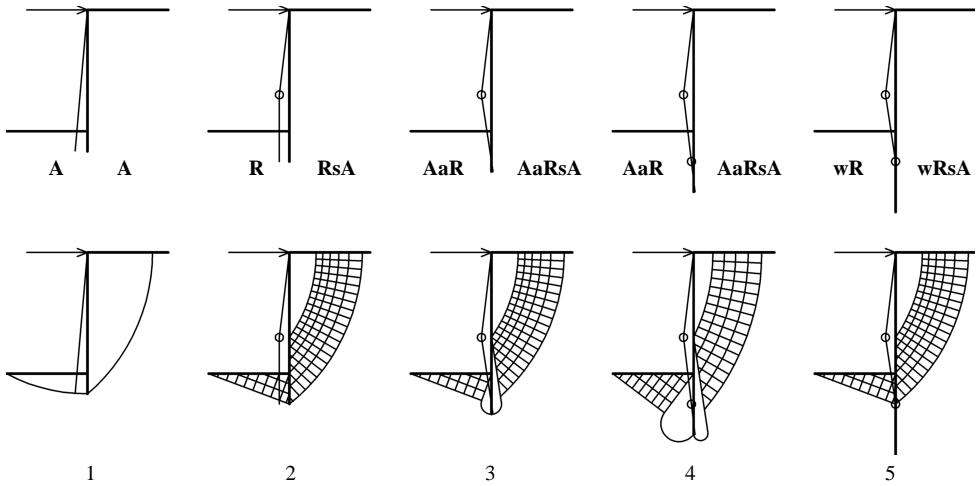
Figure 2.6: *States of failure of a propped sheet pile wall and schematic representations of rupture figures, drawn for a perfectly smooth wall (based on [13])*

1. In the first wall movement the wall rotates about the anchor. This type of wall movement involves a free earth support and results in the shortest wall with the highest ultimate moment. The soil fails by two circular rupture lines

2. In the second wall movement, a plastic hinge has been generated. The wall is only slightly longer but due to the ability of the earth pressures to redistribute, the ultimate bending moment is considerably lower. The redistribution of the soil load is expressed by a combination of a circular rupture line and an active Rankine pressure zone on the retained side and a passive Rankine zone on the excavated side

3. When the wall is made longer again, the third type of wall movement is obtained. The lower end of the wall is partially fixed in the ground, involving a fixed moment $M_c < M_{pl}$. M_{pl} decreases again as a result of the earth pressure redistribution. The failure mode in the soil is extended with two circular rupture lines

4. In the fourth type of wall movement, a second plastic hinge is about to be generated by the fixed moment. The wall has now 2 plastic hinges and, together with the hinged connection at prop level, the wall movement is kinematically indeterminate. The lowest plastic moment M_{pl} is obtained

5. Although the wall can be made even longer, the failure mode in the soil or the plastic moment will not change significantly. The fifth type of wall movement is in fact not different to the fourth type

The states of failure in Figure 2.6 are far from complete. Other failures such as prop failure possibly in combination with a plastic hinge, or global failure are also relevant for this propped sheet pile wall.

SPOOKS

The determination of a compatible rupture figure and the resultant earth pressure forces E and F are perfectly suited to analysis by a computer program. The computer program SPOOKS, developed at the Danish Geotechnical Institute, is able to determine the critical rupture figure on the basis of a prescribed wall movement, and to calculate the critical wall length ℓ, plastic bending moment M_{pl} and strut force F_a [37].

The example from Section 2.2.1 was calculated with SPOOKS; the results are given in Table 2.2.

n	ℓ (m)	z_a (m)	M_{pl} (kNm/m)	F_a (kN/m)
0	6.89	3.53	72.78	39.71
0.5	7.96	3.28	58.44	34.31
1	8.27	3.10	49.32	30.63

Table 2.2: *Calculation results with* SPOOKS

Comment

The bending moment calculated with SPOOKS (Table 2.2) appears to be 20% lower than the bending moment in the so-called Blum model, see Table 2.1 and the strut force is practically equal. These differences are the result of of redistribution of earth pressures in front of and behind the sheet pile wall. In SPOOKS, the limit earth pressures are determined from compatible rupture figures whereas in the example, the Rankine earth pressure distribution has been assumed without consideration of arching of the soil behind the wall. For a more detailed explanation, reference is made to Craig [26], Rowe [66] or clause R 77 of the EAU [25].

2.2.3 Windels

Almost 30 years after Blum developed his design method for sheet pile walls [8], Windels developed a method combining the wide experience of Blum's method with Brinch Hansen's development of plastic design and with the structural theory of plasticity [92, 93, 94, 95].

Windels considered a soldier pile wall propped at different levels, see Figure 2.7, *left*. The strut levels are designed in such a way that ultimate bending moments occur at both strut levels and in the span between two struts. In a span subjected to an average earth pressure σ, the ultimate bending moment follows from the theory of plasticity,

$$M_{pl} = \frac{1}{16} \sigma \ell^2 \tag{2.9}$$

The lower part of the wall is analysed according to Blum's method, see Figure 2.7, *right*.
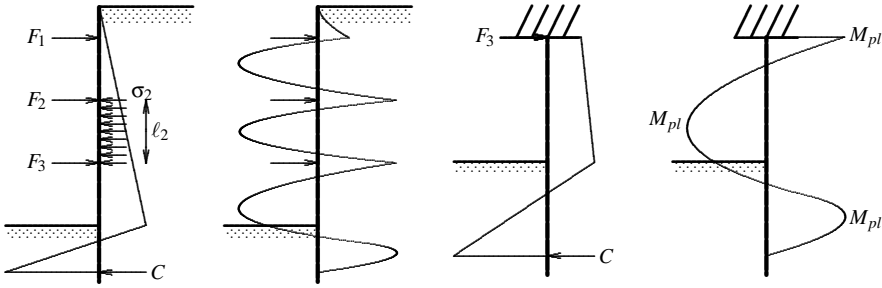
Figure 2.7: *Braced sheet pile wall (according to Windels [94])*

Windels recognises that the earth pressure distribution is heavily dependent upon the wall displacement, which is the basis of Brinch Hansen's method, but nevertheless he prefers a design method that meets the wide experience gained with Blum's method. To account for the advantageous effects of earth pressure redistribution, the bending moment may be reduced and the strut force increased according to clause R 77 of EAU [25].

The structural resistance of the soldier piles is taken into account by available design rules for I-sections that consider interaction between bending moment, normal force and shear force, see Figure 2.8.
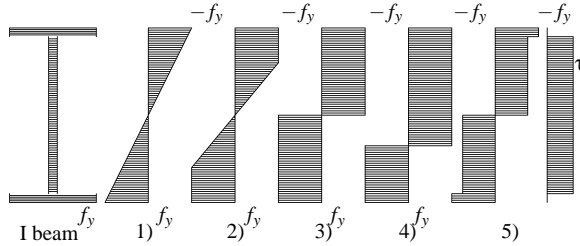
Figure 2.8: *Behaviour of I-sections: 1) elastic bending, 2) partially plastic bending, 3) full-plastic bending, 4) full-plastic bending with normal force interaction, 5) full-plastic bending with shear force interaction (according to Windels [95])*

Basically these design rules are based on the following three common checks for steel structures [95]:

$$\sigma = \frac{N}{A} + \frac{M}{W_{pl}} \tag{2.10}$$

$$\tau = \frac{V_{max}}{A_{web}} \tag{2.11}$$

$$\sqrt{\sigma^2 + 3\tau^2} \leq f_y \tag{2.12}$$

These design rules, however, do not account for geometric instability of the cross-section.

2.2.4 Weißenbach

Weißenbach [89, 90, 91] modified Windels' method for plastic design of braced walls in two parts. Firstly, Weißenbach proposes a trapezium-shaped distribution that accounts for earth pressure redistribution indicated in Figure 2.9, and gives various design graphs and tables for a practical application of the method in his book [91].
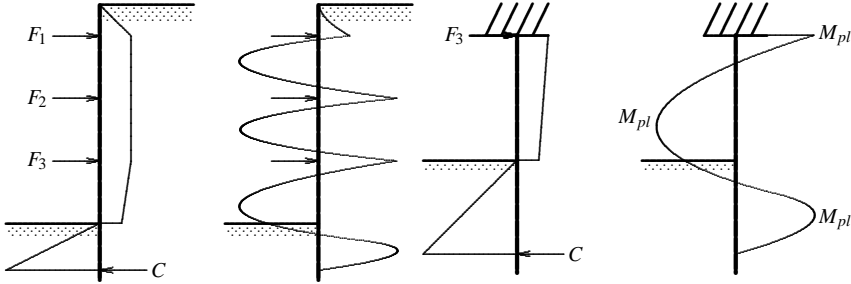
Figure 2.9: *Braced sheet pile wall according to Weißenbach*

Secondly Weißenbach gives $\frac{b_f}{t_f}$ ratio's for I-sections which should be satisfied to prevent the compression flange from buckling.

For St 37: $f_y = 370$ N/mm² $\qquad\qquad\qquad\qquad t_f \geq \dfrac{b_f}{34}$ (2.13)

For St 52: $f_y = 520$ N/mm² $\qquad\qquad\qquad\qquad t_f \geq \dfrac{b_f}{28}$ (2.14)

According to Weißenbach [91] these ratio's are applicable to steel sheet piles when half the flange width is substituted for b_f, see Figure 2.10. Only a number of the available sheet pile sections satisfy these requirements.
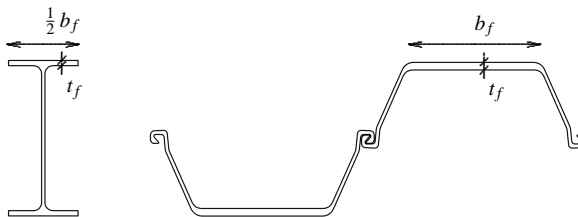
Figure 2.10: *Structural requirements for I-sections and for steel sheet piles according to Weißenbach*

2.3 Structural resistance of steel sheet piles

2.3.1 General

The structural $\frac{b_f}{t_f}$ rules proposed by Weißenbach are aimed at verifying the performance of the steel sheet piles with respect to geometrical stability of the compression flange. When this relation is satisfied, an *unlimited* rotation capacity of the sheet pile is assumed but in reality, the rotational behaviour of a steel sheet pile is limited. For the ECSC multipartner research project *Development of Unified European Design Rules for Steel Sheet Piles and Introduction into Part 5 of Eurocode 3* [39] an elaborate investigation of the structural resistance of steel sheet piles was carried out, particularly with respect to rotation capacity. An important part of this research formed the basis of the thesis of Hartmann-Linden [38] concerning the structural resistance of steel sheet piles.

2.3.2 Plastic behaviour of a steel sheet pile

The generation of a plastic hinge for a steel sheet pile in bending can be explained using a four-point bending test, where a simply supported steel sheet pile is loaded by two steadily increasing concentrated forces, each of $\frac{1}{2}F$, see Figure 2.11. It is assumed that the steel will behave in accordance with the $\sigma - \varepsilon$ diagram from a tensile test, shown in the figure, which is typically found for hot rolled sheet piling: the relation is linear until the upper yield stress is reached, next, the stress drops abruptly to the lower yield stress, f_y, and the strain then increases at constant stress, until strain hardening starts. At the onset of strain hardening, the strain is of the order of $10\varepsilon_y$, where ε_y is the strain at the onset of yielding.

Furthermore, it will be assumed that the cross-section will not be deformed by the deflections of the sheet pile and that the deflections due to shear force are negligible by comparison with those due to bending, until the decrease of the moment resistance, starting at *rc*.
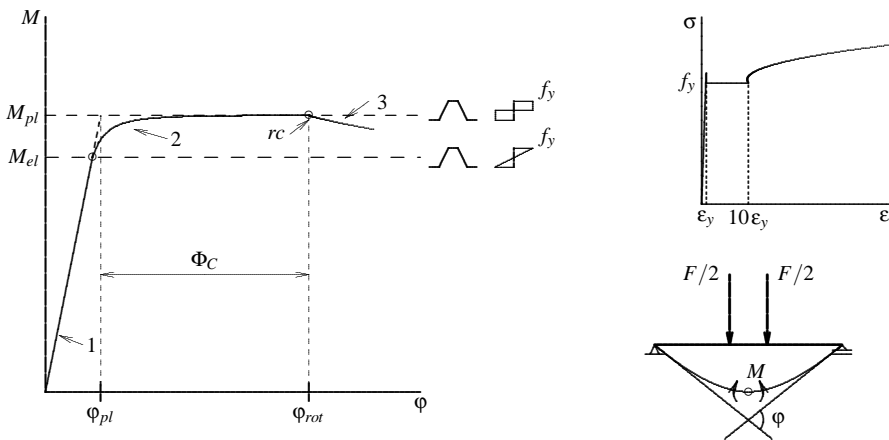
Figure 2.11: *Structural resistance of a steel sheet pile in a four-point bending test*

For this four-point bending test, a typical moment-rotation curve ($M - \varphi$ curve) is observed which can be subdivided in 3 branches:

1. When the beam is gradually loaded with load F, it will behave elastically until yield stress f_y is obtained in the ultimate fibre of the midspan section; the elastic bending moment capacity $M_{el} = f_y W_{el}$ is reached

2. The load is subsequently increased: between the point loads, the fibres closer to the bending axis start yielding until finally a full-plastic cross-section is obtained. At the same time the outermost fibres at the opposite sides of the loads will start yielding. In this way a plastic zone is obtained which has the ability to rotate as a hinge. The rotation will rapidly increase and the full-plastic cross-section will be obtained when a significant plastic rotation has occurred. The amount of plastic rotation depends on the distance between the loads and increases for larger distances. The onset of strain hardening is typically at more than 99% of the full-plastic moment resistance, $M_{pl} = f_y W_{pl}$, which is generally at a significant amount of plastic rotation

3. Due to the increasing load and deflection, the force in the compression flange will increase to a level that will cause the flange to deform out-of-plane and buckle; the nett height of the cross-section will decrease and therefore the moment resistance will also decrease

In the moment-rotation curve in Figure 2.11, it is shown that the sheet pile is able to undergo a certain irreversible rotation, before the moment resistance decreases. This irreversible rotation is defined as the *rotation capacity* of the sheet pile, and is denoted by Φ_C.

The amount of rotation capacity is determined by the rotation at the onset of the buckling branch, rc, and differs for every sheet pile profile.

2.3.3   Classification of cross-sections

The rotation capacity is dependent on the geometrical stability of the cross-section of the sheet pile, and in particular on the slenderness and steel grade of the compression flange and web. As these parameters differ for every sheet pile profile, the cross-sectional behaviour of the sheet pile can be subdivided into four classes which are in accordance with Eurocode 3, part 1-1 [20], see Figure 2.12:

Class 1 cross-sections are those which can form a plastic hinge with a rotation capacity required for plastic analysis

Class 2 cross-sections are those which can develop their plastic moment resistance, but have a negligible rotation capacity

Class 3 cross-sections are those in which the calculated stress in the extreme compression fibre of the steel member can reach its yield strength, but development of the plastic moment resistance is prevented by local buckling

Class 4 cross-sections are those in which the effects of local buckling determine the moment resistance or compression resistance instead of the section modulus
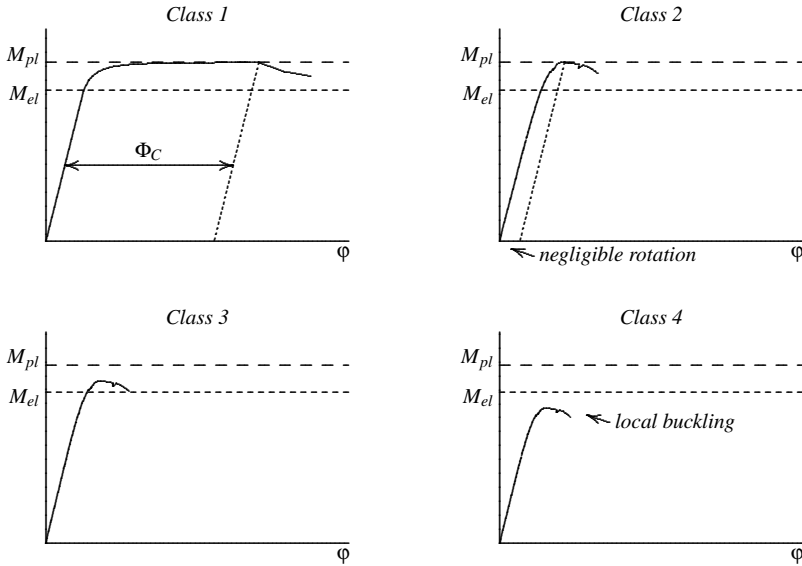
Figure 2.12: *Classification of cross-sections*

2.3.4 Determination of rotation capacity

According to Hartmann-Linden [38] the rotation capacity of steel sheet piles in bending can be described by the slenderness and the steel grade of the compression flange, using the $\frac{b_f}{t_f \varepsilon}$ ratio, where b_f and t_f are the width and thickness of the compression flange and ε is a function of the steel grade, defined by

$$\varepsilon = \sqrt{\frac{235 \text{ N/mm}^2}{f_y}} \quad \text{with } f_y \text{ in N/mm}^2 \tag{2.15}$$

Differentiation must be made between U- and Z-profiles when determining their moment resistance and rotation capacity. The interlock of a Z-profile has a stiffening effect on the buckling resistance of the compression flange, which leads to a higher moment resistance. U-sections, on the other hand, have a higher rotation capacity than Z-sections for a low slenderness ratio, because the web of U-sections is stiffened by the interlock, which favours the rotation capacity. The boundaries for $\frac{b_f}{t_f \varepsilon}$ ratio's between the different cross-sectional classes of Z-profiles and U-profiles given by ENV 1993-5 [24] are presented in Table 2.3. The rules for U-sections are derived from sections with welded interlocks but the formulae are conservative for cases with a limited interlock friction capacity.

The $\frac{b_f}{t_f \varepsilon}$ ratios are related to a maximum moment level of $M_{max} = M_{pl} = f_y W_{pl}$. Howe-ver, on the basis of the typical $M - \varphi$ behaviour observed in many four-point bending tests and finite element calculations, Hartmann-Linden concluded that the 'effective' rotation capacity can be increased by reducing the maximum moment level to 95% M_{pl}, 90% M_{pl} or 85% M_{pl}, and developed practical design charts for the determination of the rotation capa-
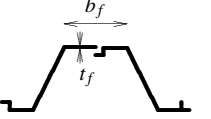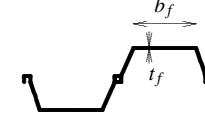
	Z-profile			U-profile		
$\varepsilon = \sqrt{\dfrac{235 \text{ N/mm}^2}{f_y}}$						
Class 1	a rotation check has to be carried out					
Class 2	$\dfrac{b_f}{t_f \varepsilon} \leq [45]$			$\dfrac{b_f}{t_f \varepsilon} \leq [37]$		
Class 3	$\dfrac{b_f}{t_f \varepsilon} \leq [66]$			$\dfrac{b_f}{t_f \varepsilon} \leq [49]$		
f_y (N/mm^2)	240	270	320	355	390	430
ε	0.99	0.93	0.86	0.81	0.78	0.74

Table 2.3: *Design rules for classification of cross-sections (according to ENV 1993-5 [24])*

city on the basis of the plastic moment M_{pl} and the slenderness of the compression flange $\dfrac{b_f}{t_f \varepsilon}$, see Figure 2.13, which have been introduced in ENV 1993-5.
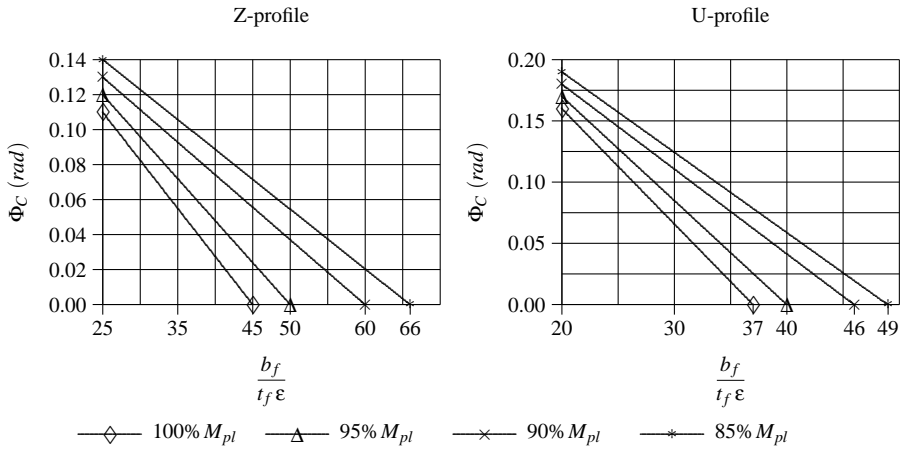
Figure 2.13: *Plastic rotation angle Φ_C provided by the cross-section at different levels of $M_{pl,Rd}$ (according to Hartmann-Linden [38])*

2.4 Rotation requirement for steel sheet pile walls

2.4.1 General

In a sheet pile wall where a plastic hinge is generated, the hinge must undergo a certain rotation in order to allow the earth pressures to redistribute, before a new equilibrium in the soil is obtained. This necessary plastic rotation is defined as the *rotation requirement* of the sheet pile wall.

In accordance with Clause 8.6.6.(3) and (4) of ENV 1997-1, see page 3, it is necessary to demonstrate for the sheet pile wall design that the rotation requirement from the geotechnical calculation does not exceed the rotation capacity of the sheet pile, see Figure 2.14.
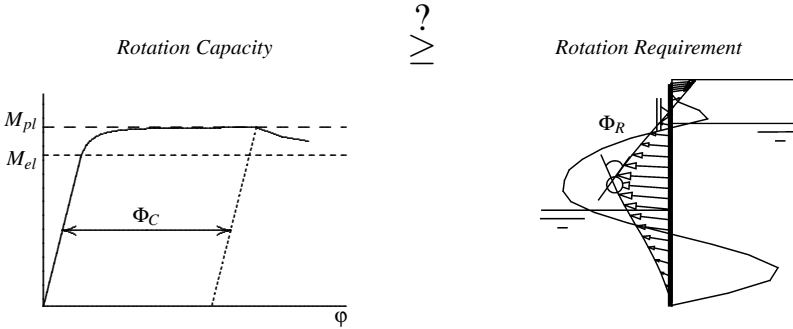
Figure 2.14: *Rotation check*

2.4.2 Failure modes and rotation check

Figure 2.15 shows examples of failure modes for steel sheet piling. In the upper seven modes an ultimate limit state is generated either by soil or prop failure. In these modes, rotation at a plastic hinge will not lead to moment redistribution in the sheet pile wall. Full plasticity of the cross-section, however, can be allowed in the upper seven failure modes. On the other hand, in the lower seven modes, rotation at a plastic hinge can lead to moment redistribution in the sheet pile wall. In these modes, a certain minimum rotation in the plastic hinge must be generated before the ultimate limit state is obtained.

Systems without rotation requirement ($\Phi_R = 0$ rad)

Systems with rotation requirement ($\Phi_R > 0$ rad)
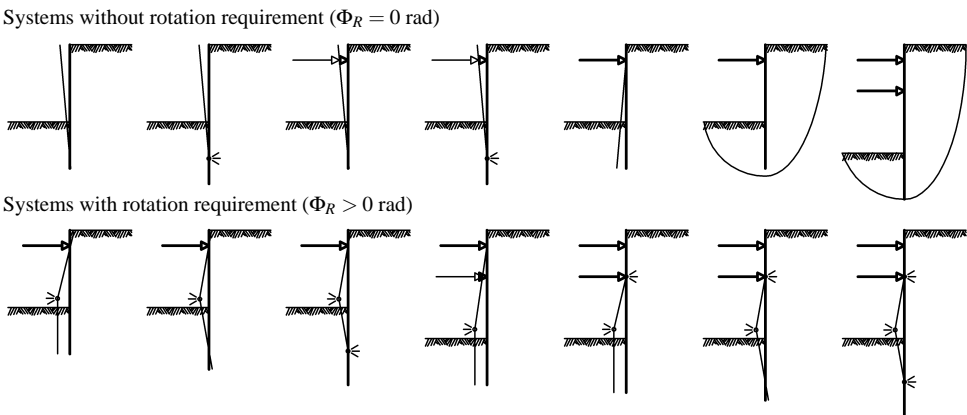
Figure 2.15: *Failure modes without and with rotation requirement*

2.4.3 Rotation requirement in structural analysis

The calculation of the amount of rotation in a plastic hinge has never been considered in plastic design of steel sheet pile walls. However, the effects of ultimate limit state design and rotation requirement of plastic hinges are well-known in theory of structural analysis and are commonly considered in structural engineering, see e.g., Neal [60].

Plastic design methods for beams are based on the plastic hinge hypothesis: all plasticity, that in reality is spread out in a plastic zone, is concentrated in a plastic hinge. Use is made of an idealised beam with $M_{pl} = M_{el}$ so that the beam behaves elastically until the plastic moment is attained, and then deforms plastically without losing strength. Neal discusses two calculation methods which are based on this principle. One method is based on virtual work and results in an upper bound solution of the failure load, the other method is based on a continuous load increase until a mechanism is formed, and results in a lower bound solution.

The calculation of rotation requirement in structural analysis is illustrated with an example of a statically indeterminate beam loaded with a concentrated force.

> **Example of a statically indeterminate beam loaded with a concentrated force**
>
> When a statically indeterminate beam is subjected to a steadily increasing load, the formation of the first plastic hinge does not generally cause plastic collapse. Further increases of the load can usually be carried and other plastic hinges are generated successively until finally there are enough hinges to form a mechanism. Plastic collapse then occurs. This process is illustrated in Figure 2.16, where a beam with span length l is loaded with a steadily increasing concentrated load F at $\frac{3}{4}l$ until plastic collapse is obtained.
>
> In the left part of Figure 2.16 two elastic bending formulae are presented as well as the upper bound virtual work solution. The virtual work solution results in a maximum load of $F_{pl} = \frac{20}{3}M_{pl}l^{-1}$ but is not suitable to give results for the *rotation requirement* of the plastic hinge. In the right part of Figure 2.16 the lower bound solution for the failure load is presented. A steadily increasing load F is applied up to F_{el}, which results in a plastic moment M_{pl} directly under the concentrated load. The moment at the fixed support is $\frac{20}{27}M_{pl}$. When the load F is further increased, a plastic hinge is generated in the span and the beam *kinks* at the plastic hinge until the moment at the support reaches the plastic moment too. The load increase is ΔF, the total applied load is $F_{pl} = F_{el} + \Delta F = \frac{20}{3}M_{pl}l^{-1}$, which is the same as in the virtual work solution, and the rotation requirement of the supports is expressed in the moment capacity of the beam: $\Delta \varphi = \frac{7}{24}\frac{M_{pl}l}{EI}$.
>
> In this method the *rotation requirement* is expressed in the plastic rotation:
>
> $$\Phi_R = \Delta \varphi \qquad (2.16)$$

From this example two conclusions can be drawn. Firstly, for a specific geometry and loading procedure the rotation requirement Φ_R depends on the span length l, the plastic moment resistance of the beam M_{pl} and the stiffness EI. Secondly, in structural analysis the rotation requirement can only be determined when using the lower bound solution taking into account the loading sequence. The importance of these two conclusions for steel sheet piling is discussed in the next section.

Theory of elasticity *Theory of plasticity*

$$M_1 = -\frac{15}{128} Fl$$

$$M_2 = \frac{81}{512} Fl$$

$$w_2 = \frac{117}{16384} \frac{Fl^3}{EI}$$

$$\phi_3 = \frac{9}{256} \frac{Fl^2}{EI}$$

$$F_e = \frac{512 M_p}{81\, l}$$

$$\Delta F = \frac{28 M_p}{81\, l}$$

$$M_1 = -\frac{3}{4} Fl$$

$$w_2 = \frac{9}{64} \frac{Fl^3}{EI}$$

$$\phi_2 = -\frac{9}{32} \frac{Fl^2}{EI} - \phi_3$$

$$\phi_3 = \frac{9}{16} \frac{Fl^2}{EI}$$

$$F_p = F_e + \Delta F \qquad F_p = \frac{20}{3} \frac{M_p}{l}$$

Theory of plasticity

Virtual work

$$\delta A = \delta E$$

$$\delta A = F_p \frac{3}{4} l\theta$$

$$\delta E = 5 M_p \theta$$

$$F_p = \frac{20 M_p}{3\, l}$$

$$\Delta\phi = \frac{27}{32} \frac{\Delta Fl^2}{EI} = \frac{7}{24} \frac{M_p l}{EI} = \frac{7}{160} \frac{Fl^2}{EI}$$
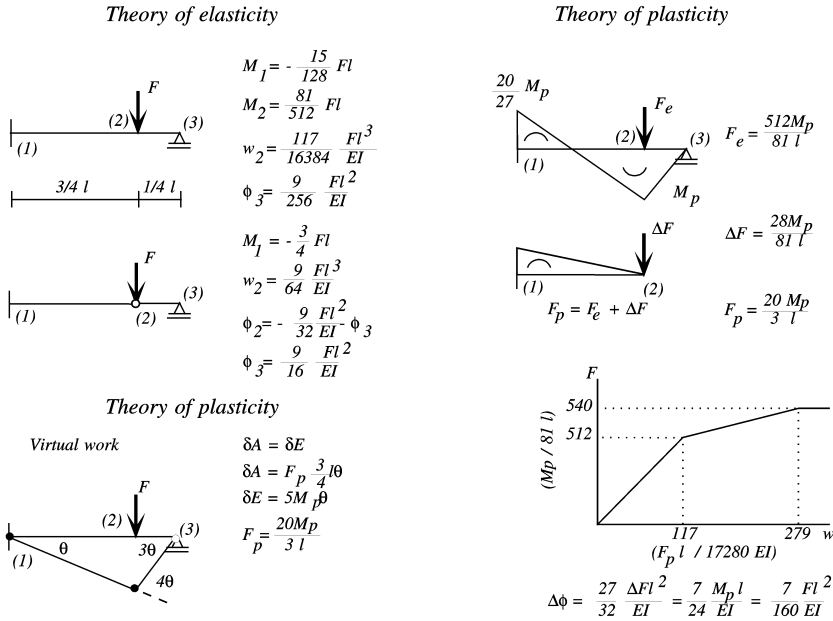
Figure 2.16: *Rotation requirement in an elasto-plastic beam (based on Neal [60])*

2.4.4 Rotation requirement in steel sheet piling

In Figure 2.16 it has been demonstrated that in structural analysis the rotation requirement Φ_R depends on the span length l, the plastic moment resistance of the beam M_{pl} and the stiffness EI. The equivalent variables in steel sheet piling include:

- geometry of the construction, i.e., wall length, excavation level, and number and level of struts

- soil properties and soil stratification

- plastic moment resistance and bending stiffness of the wall

The effects of these variables on the rotation requirement are investigated by means of a parametric study in Section 2.6.

Further, in the former section, it has been shown that in structural analysis the rotation requirement can only be determined when taking into account the loading sequence. For steel sheet piling this means that the rotation requirement can only be determined properly when taking into account construction stages. To illustrate the importance of construction stages on the calculation of the rotation requirement, Figure 2.17 is considered. In this figure, the calculation result of two displacement and moment curves are given for a double propped wall; the solid lines have been calculated considering construction stages whereas, for the dashed lines, the construction stages have been omitted. The limit earth pressure distribution was equal for both cases.
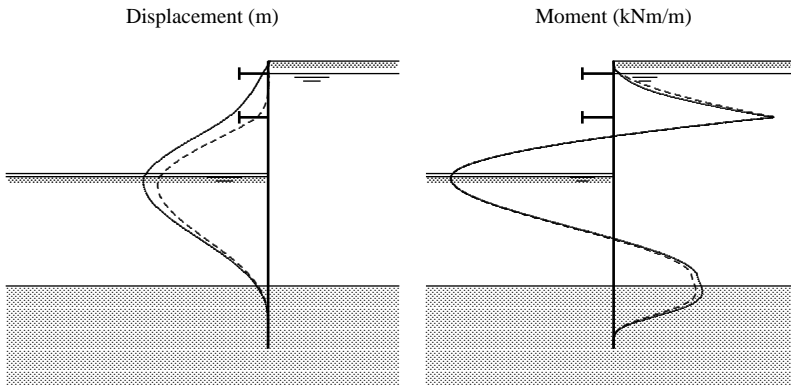
Figure 2.17: *Displacement and bending moment of a double propped wall taking into account (solid lines) and omitting (dashed lines) construction stages*

The effect of the omission of construction stages on the moment distribution is negligible, which may be expected because the earth pressure distribution in the ultimate limit state of both cases is equal. However, it should be realised that, in reality, the earth pressure distribution in the ultimate limit state is determined by the wall displacement.

On the other hand, the calculated wall displacement is strongly influenced by the construction stages. In the case where intermediate stages were omitted, a first plastic hinge was developed at the level of the deepest strut and the second close to the excavation depth. In the real situation, the wall has already displaced at the location of the deepest strut before this strut was installed. Therefore, in the final excavation stage the first plastic moment was generated close to the excavation depth and the second plastic moment was about to be generated at strut level.

2.4.5 Ground and structural models

The determination of the rotation requirement in sheet piling is a process in which ground-structure interaction plays a dominant role. Different soil-structure interaction models require a different approach for design. Therefore the rotation requirement of the sheet piling should always be determined taking into account the possibilities and restrictions of the different interaction models. Basically a soil-structure interaction model is composed of a ground model and a structural model. Examples of ground models are:

- limit earth pressure models (Blum, Brinch Hansen)

- subgrade reaction models (Winker spring)

- fully numerical (finite element) models

Examples of structural models are:

- beam models:

    - with elastic behaviour
    - with plastic hinges
    - with plastic zones

- general finite elements:

    - with elasto-plastic behaviour (discretisation of the cross-section in elements)

Not every combination of ground and structural model can form an appropriate soil-structure interaction model. In Table 2.4 a matrix is given with possible and recommended combinations of ground and structural models.

Structural model	Ground model		
	Limit earth pressures	Subgrade reaction	Fully numerical
Beam: elastic	$\sqrt{}$	$\sqrt{}$	$\sqrt{}$
Beam: plastic hinges	$\sqrt{}\sqrt{}$	$\sqrt{}\sqrt{}+$	$-$
Beam: plastic zones	$(\sqrt{}\sqrt{})$	$\sqrt{}\sqrt{}+$	$\sqrt{}\sqrt{}+$
FE: elasto-plastic	$-$	$-$	$(\sqrt{}\sqrt{})$
Key:			
$\sqrt{}$ Possible combination for elastic design			
$\sqrt{}\sqrt{}$ Possible combination for plastic design			
$\sqrt{}\sqrt{}+$ Possible combination for the determination of the rotation requirement			
$(\sqrt{}\sqrt{})$ Possible combination for plastic design but rarely used			
$-$ Combination not recommended or not possible			

Table 2.4: *Possible combinations of ground and structural models for design of steel sheet pile walls*

For the determination of the rotation requirement only the models with a $\sqrt{}\sqrt{}+$ are suitable for the following reasons:

- It is evident that the rotation requirement of the sheet pile wall can not be determined with an elastic beam model

- In a finite element elasto-plastic model the exact shape of the sheet pile is taken into account by shell elements. This way of modelling leads to three-dimensional analysis including local buckling phenomena. The stress-strain curve to model the elasto-plastic behaviour can be elastic-perfectly plastic or elasto-plastic with strain hardening. The $M - \varphi$ curve resulting from such a model can be considered as a 'true' $M - \varphi$ curve. Rotation requirement is then not relevant, because it is implicitly covered in the design model. However, this type of analysis is very time-consuming and therefore often too expensive for engineering practice

- The problem of rotation requirement is only important for beam models with plastic hinges and plastic zones. Hartmann-Linden [38] has demonstrated that the fundamental differences between a plastic hinge and a plastic zone structural model have a negligible result on the calculation results

- Although limit earth pressure ground models in combination with a plastic hinge or a plastic zone beam model are appropriate to determine the plastic rotation in a hinge, this combination cannot be used to determine the wall deflections for multi-staged cases in a proper manner. Limit earth pressure models cannot take the stress-strain theory of soil and structure into account and may therefore give an erroneous result for the rotation requirement, as is demonstrated in Section 2.4.4

2.4.6   Methods to determine the rotation requirement

Determination of the rotation requirement is not difficult when the rotation in the plastic hinge Φ_R is a direct result of the calculation. This is generally the case for plastic hinge models where all plastic rotation is concentrated at a node. However, in a plastic zone model the plasticity is spread over a certain zone along the beam and the angle of the plastic *kink* is therefore not a direct result of the calculation; the rotation requirement for the plastic hinge cannot be determined directly but must be determined with an implicit method.

The following four possible methods to determine the rotation requirement are presented [38, 74]:

- Method I: Determination of Φ_R by direct calculation

- Method II: Determination of Φ_R by unloading of the sheet pile

- Method III: Determination of Φ_R with a simplified assumption based on rotations

- Method IV: Determination of Φ_R with a simplified assumption based on displacements

Application examples are given in Section 2.7.

Method I: direct calculation

The most simple method to determine the rotation requirement is by direct calculation of the plastic rotation in the hinge, Φ_R. However, this is only possible for models that are based on plastic hinge theory with a bi-linear $M - \varphi$ relation. When a realistic $M - \varphi$ relationship with a softening branch is implemented in the sheet pile model, a rotation check becomes unnecessary.

Method II: unloading of the construction

In method II the sheet pile is unloaded after analysis of the final stage. By taking away all the load from the sheet pile, the residual (plastic) deformation and the plastic rotation angle can be derived directly from the output. This method is applicable for both plastic hinge models and plastic zone models that have the option to calculate residual deformations. This method takes into account the effects of all construction stages.

Method III: simplified assumption based on rotations

In method III the required plastic rotation angle Φ_R is determined according to:

$$\Phi_R = \varphi_{rot} - \varphi_{pl} \tag{2.17}$$

where φ_{rot} is the elastic + plastic rotation angle at the critical construction stage (which is not necessarily the final stage) and is determined from the sum of the rotations at the points of zero moments, see Figure 2.18. The rotation angle at first yielding, φ_{pl}, is determined from a simplified load distribution according to

$$\varphi_{pl} = \frac{2}{3} \frac{M_{pl}L}{EI} \tag{2.18}$$

where span length L is the distance between the points of zero moment and EI and M_{pl} are the design values of the sheet pile properties.
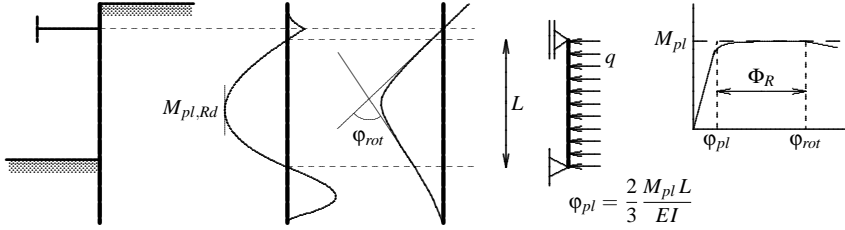
Figure 2.18: *Method III: simplified assumption of Φ_R based on rotations*

Although the assumed load distribution is an extremely simplified version of the realistic earth pressure distribution, it appears from various FE calculations that the results are in accordance with method II [39, 74]. This method is applicable for both plastic hinge models and plastic zone models.

The starting-point in this procedure is that the action effects M_{Sd} and Φ_R are determined for a realistic sheet pile profile (e.g. AZ 18 S 390).

Method IV: simplified assumption based on displacements

In method IV the rotation requirement Φ_R is also determined according to:

$$\Phi_R = \varphi_{rot} - \varphi_{pl} \tag{2.17}$$

In this method φ_{rot} and φ_{pl} are assessed from the wall displacements as shown in Figure 2.19. This method can be used for both plastic hinge and plastic zone models that don't give the rotation as an output. The elastic + plastic rotation φ_{rot} is determined according to

$$\varphi_{rot} = \frac{w_2 - w_1}{L_1} + \frac{w_2 - w_3}{L_2} \tag{2.19}$$

$$\varphi_{rot} = \frac{w_2 - w_1}{L_1} + \frac{w_2 - w_3}{L_2}$$
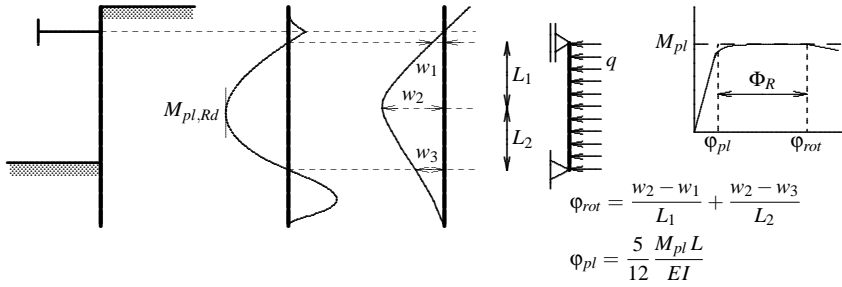
$$\varphi_{pl} = \frac{5}{12} \frac{M_{pl} L}{EI}$$

Figure 2.19: *Method IV: simplified assumption of Φ_R based on displacements*

The elastic rotation φ_{pl} is determined according to

$$\varphi_{pl} = \frac{5}{12} \frac{M_{pl} L}{EI} \tag{2.20}$$

Although the assumed load distribution is an extremely simplified version of the realistic earth pressure distribution, it appears from various FE calculations the results are in accordance with method II [39, 74]. Method IV is applicable for both plastic hinge models and plastic zone models.

Starting-point in this procedure is that the action effects M_{Sd} and Φ_R are determined for a realistic sheet pile profile (e.g. AZ 18 S 390).

2.5   Development of a subgrade reaction model for plastic design

2.5.1   General

Over the past 25 years, many advanced computer programs for the design of earth retaining structures have been developed based on the subgrade reaction method [4, 5, 11, 30, 82, 85]. The subgrade reaction method is recognised as a popular tool in the daily practice of sheet pile wall design, as it gives the designer insight in the soil-structure interaction, has a short calculation time and offers the possibility to account for rather complicated construction stages in multi-layered soil. Nevertheless, a subgrade reaction model that accounts for plastic hinges is not available as a common tool for plastic design. Therefore the development of a subgrade reaction model for plastic design is described in this section. The model is based on the transfer matrix method as described in Appendix B. The choice of the transfer matrix method is not obvious because it is a numerically unstable method when compared with other numerical methods [65] but the method is insightful and good for model extrapolations.

2.5.2   Modelling an elasto-plastic beam

The case presented in Figure 2.16 is considered again in Figure 2.20. The maximum moment capacity of the beam is $M_{pl} = \frac{20}{3}F_{pl}l$. A load $F = F_{pl}$ is applied to the beam in 50 equal steps. From Figure 2.16 it can be derived that the first plastic hinge is generated after application of the 48th load step and that a kinematically indeterminate mechanism is obtained after the 50th load step.
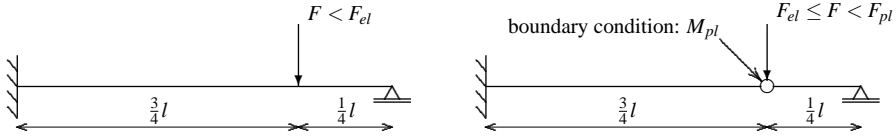
Figure 2.20: *Splitting the problem into parts*

To model this structure using the transfer matrix method, the problem is split into two parts. One part is used when the load $F < F_{el}$, the other part is used when $F_{el} \leq F < F_{pl}$. When, as a result of a load increment, the moment capacity is reached ($F = F_{el}$), an intermediate boundary condition is added to the beam. The intermediate boundary condition consists of an imposed moment with boundary condition M_{pl} and is placed at the location where the maximum moment would have occurred if the beam had been elastic. Both parts can be solved with the techniques treated in Appendix B.

Next the case where the beam is unloaded after the 49th load increment is considered. In the 49th load increment a plastic hinge *and rotation* is generated. When subsequently the beam is unloaded, a residual kink $\Delta\Phi$ remains in the beam until a new load of $F = -F_{el}$ is obtained. The kink is then $-\Delta\Phi$. Finally, when the beam is unloaded to $F = 0$ a small bending moment remains due to the residual kink. This process is illustrated with a sketch of the load-rotation and the moment-rotation diagram in Figure 2.21.
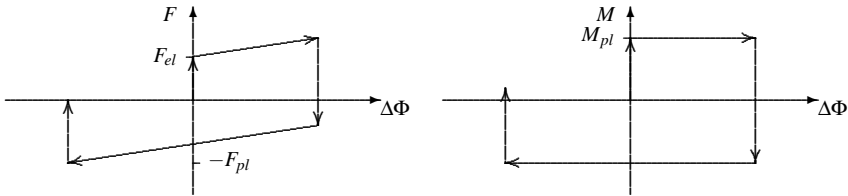
Figure 2.21: *Load-rotation and moment-rotation diagram for $x = \frac{3}{4}l$*

If a hinge is introduced at a node, the *procedure hinge* has been developed, the flow chart being presented in Figure 2.22. In the *procedure hinge* it is determined which boundary condition is to be assumed at each node. Possible boundary conditions are:

- $+M_{pl}$

- none

- $-M_{pl}$
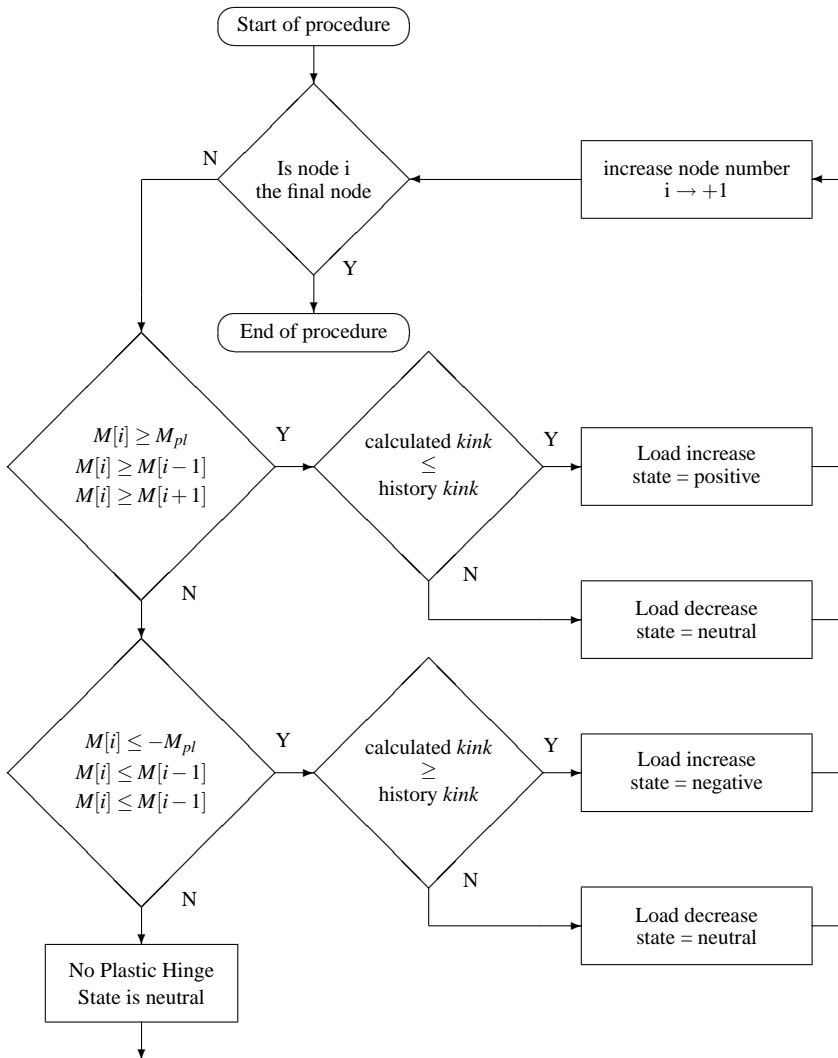
Figure 2.22: *Flow chart of* procedure hinge

A plastic hinge is assumed when the following conditions are fulfilled (all signs are considered positive):

- $M_i = M_{max}$

- $M_i \geq M_{pl}$

- $\Delta\Phi_{i;calculated} \geq \Delta\Phi_{i;existing}$

2.5.3 Modelling soil with discrete springs

In the subgrade reaction method, soil is modelled with a large number of discrete springs, each with the characteristic shown by Figure 2.23. These springs do not interact with one another and therefore arching of the soil behind the sheet pile wall is not properly accounted for.
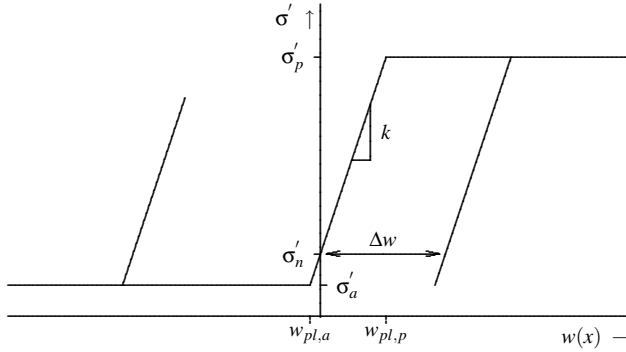
Figure 2.23: *Elasto-plastic spring model*

To model active and passive earth pressures the springs are composed of an active, a neutral and a passive branch. The levels of these branches are derived from the vertical (effective) soil stress $\sigma_v - u$ and the earth pressure coefficients K_a, K_n and K_p. Unloading and reloading is taken into account with the plastic parameter Δw. The stiffness of the spring may be either expressed as the subgrade reaction modulus k or by the *stroke* which is the required movement to bring the soil from an active state to a passive state or vice versa. The relationship between the subgrade reaction modulus k and the *stroke* is

$$k = \frac{\sigma_p' - \sigma_a'}{stroke} = \frac{\sigma_p' - \sigma_a'}{w_{pl,p} - w_{pl,a}} \tag{2.21}$$

The active and passive states are obtained if wall movement $w(x)$ is

$$w(x) < \Delta w + w_{pl,a} \qquad \text{active state} \tag{2.22}$$
$$w(x) > \Delta w + w_{pl,p} \qquad \text{passive state} \tag{2.23}$$

Similar to the *procedure hinge* in Section 2.5.2 a *procedure springs* is introduced in which the state of a nodal spring is determined, i.e., if the soil response is active, neutral or passive earth pressure. In *procedure springs* a correction force F_c is used to account for the unloading-reloading branch and the parameter n_{error} is used to check the necessary assumptions. It is remarked that the flow chart given in Figure 2.24 has been developed for the transfer matrix method, see Appendix B, and is somewhat different from the procedure Verruijt developed for the finite difference method [85].

2.5.4 Assembly into a subgrade reaction model

The final step needed to create a subgrade reaction model requires the assembly of the elasto-plastic beam model and the elasto-plastic spring model into a subgrade reaction model which is suitable for the analysis of sheet pile walls.

The flow chart in Figure 2.25 gives a possible algorithm for the analysis of a construction stage with a subgrade reaction model. First the material properties are assigned to the beam and springs. Next anchors, struts and other imposed loads are defined. Subsequently in the *procedure springs* the load on the sheet pile is determined and the state of each spring (active, neutral or passive) is assumed. The *procedure hinge* then determines whether a hinge is assumed at a node.

Based on the assumed states of the springs and hinges, equilibrium of the structure is calculated (*procedure sweeps*) using the transfer matrix method (Appendix B). The states of the springs and hinges are determined again and checked to ensure that they fulfil the assumptions. If not, new assumptions for the springs and hinges are made based on the last iteration, until all assumptions are correct. The final step that has to be performed is to assign the plastic properties Δw and $\Delta \Phi$ to the relevant nodes.

2.5.5 Testing

The presented theory has been implemented in the computer program PLASWALL [48]. The program consists of a conventional subgrade reaction model in which a plastic hinge is generated when the ultimate moment in the retaining structure is exceeded. The program calculates the redistribution of the earth pressures until new equilibrium is found.

The capabilities of PLASWALL are tested on the basis of two problems:

- infinite elasto-plastic beam on elastic foundation
- staged excavation in multi-layered soil compared with SPW99 [87]

Infinite elastic-plastic beam on elastic foundation

The first test concerns an infinitely long (20 m) elasto-plastic beam on elastic foundations, loaded with a concentrated force. The beam is gradually loaded until the plastic moment is obtained, see Figure 2.26. Next the load on the beam is increased until the second and third plastic hinges are formed and subsequently decreased to 50% of the original load. The analytical solutions are derived from Hetényi [41] and are presented in Appendix C.

In Figure 2.27 the calculation results of PLASWALL are compared with analytical solutions for the situation after the 50% unloading. The entire beam has been modelled in PLASWALL (201 springs) but the results are only plotted for the right half of the structure.
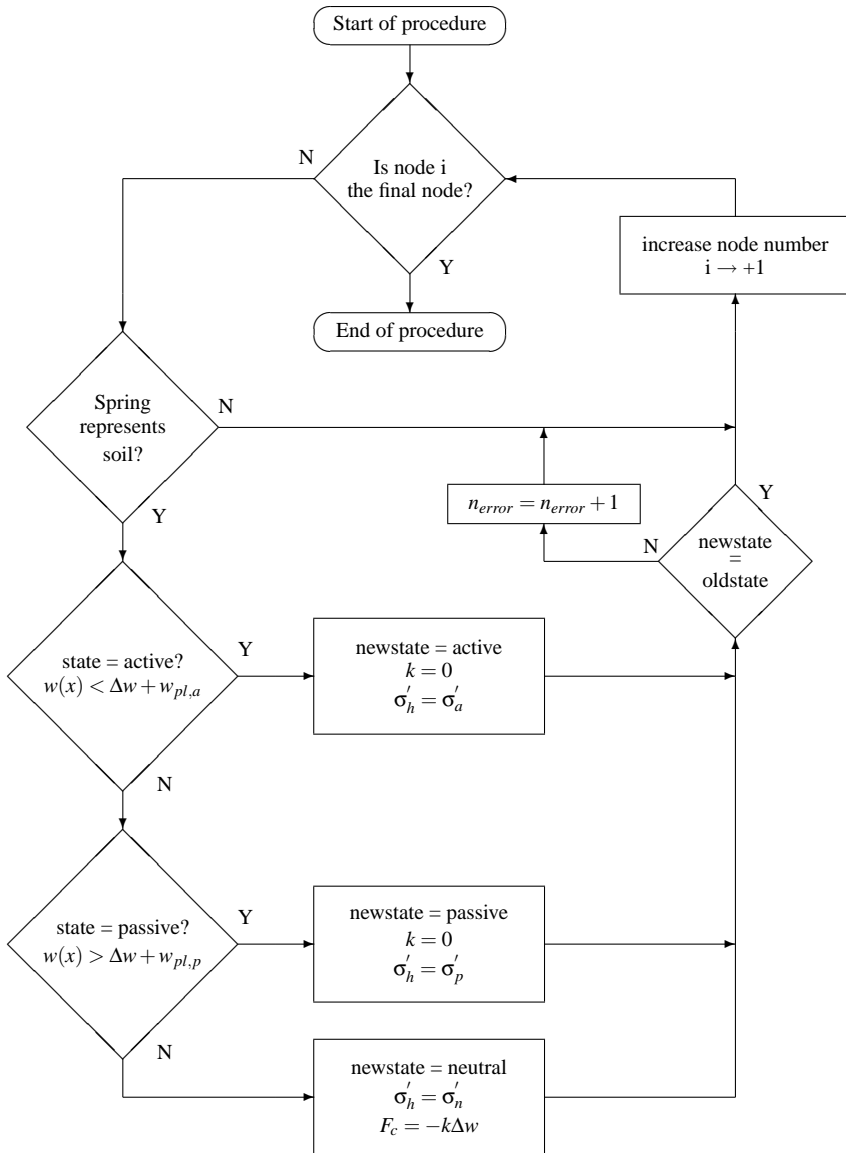
Figure 2.24: *Flow chart of* procedure spring
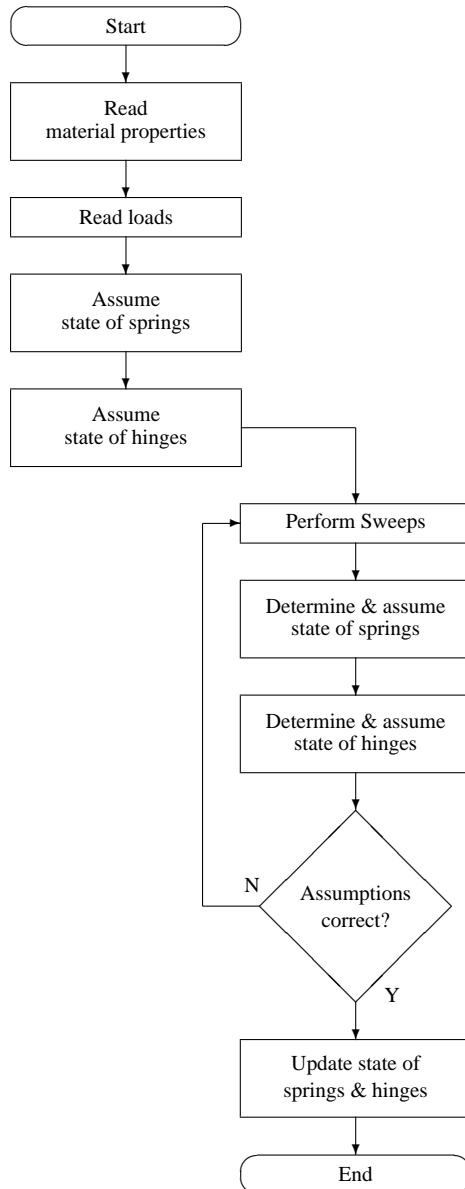
Figure 2.25: *Flow chart for the analysis of a construction stage*
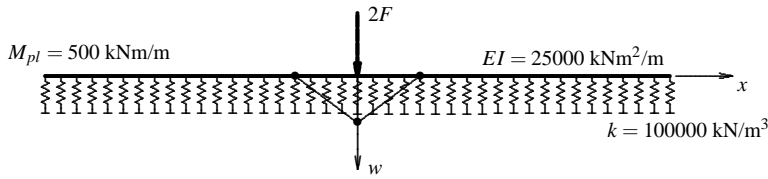
Figure 2.26: *Elasto-plastic beam on elastic foundation*
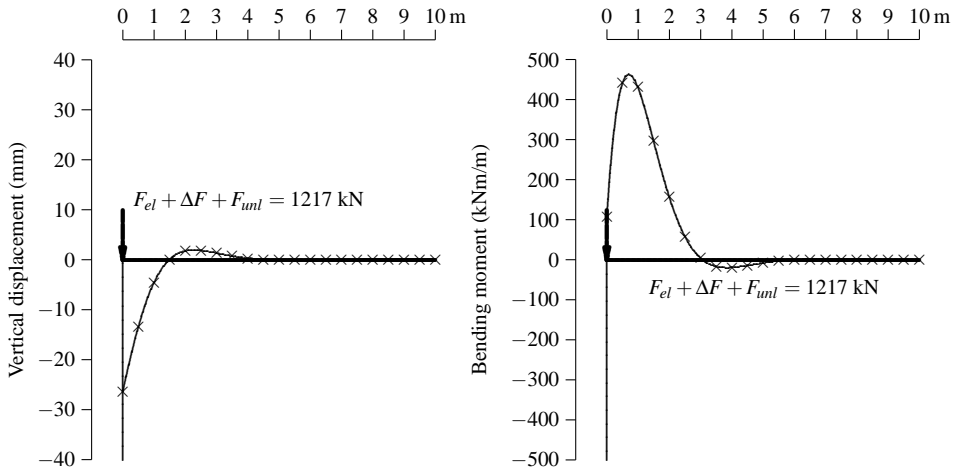
Figure 2.27: *Vertical displacement after 100% loading and subsequently 50% unloading. The solid line is calculated with* PLASWALL, *the ×-marks indicate the analytical solution*

The figure shows a good agreement between PLASWALL and the analytical solution for both the displacement and the bending moment. The analytical rotation requirement is $\Phi_{R;analytical} = 0.05736$ rad and the rotation requirement calculated with PLASWALL deviates by less than 1%: $\Phi_{R;Plaswall} = 0.05701$ rad. It can therefore be concluded that the inplementation of the *procedure hinge* has been carried out successfully.

Multi-staged excavation in multi-layered soil compared with SPW99

The second test concerns a multi-staged excavation in multi-layered soil, the analysis results being compared to those from SPW99. SPW99 is a subgrade reaction computer model, developed by Verruijt [87], which is able to calculate the displacements and bending moments of a sheet pile wall in multi-layered soil and for multi-staged constructions. SPW99 makes use of the finite difference method to solve the system of equations [85].

The tests considers a 23 metre long steel sheet pile and the soil consists of 17 metres of soft clay overlaying a sand layer. The groundwater level in the clay layer is 1 metre below the soil surface and the head in the sand layer is 4 metres below the original surface. Excavation is carried out in three construction stages. In the first stage the excavation depth is 1 metre. Next, the first horizontal restraint is placed at 0.75 metre depth and dry excavation

is carried out to 7 metres. In the third construction stage, the second strut is placed at a depth of 6.50 metres and excavation is carried out to 9.25 metres. The water level in the excavation is not lowered beyond a depth of 9.00 metre. At this stage, the soil behind the sheet pile wall is unloaded. Values of relevant soil and sheet pile properties are given in Figure 2.28.
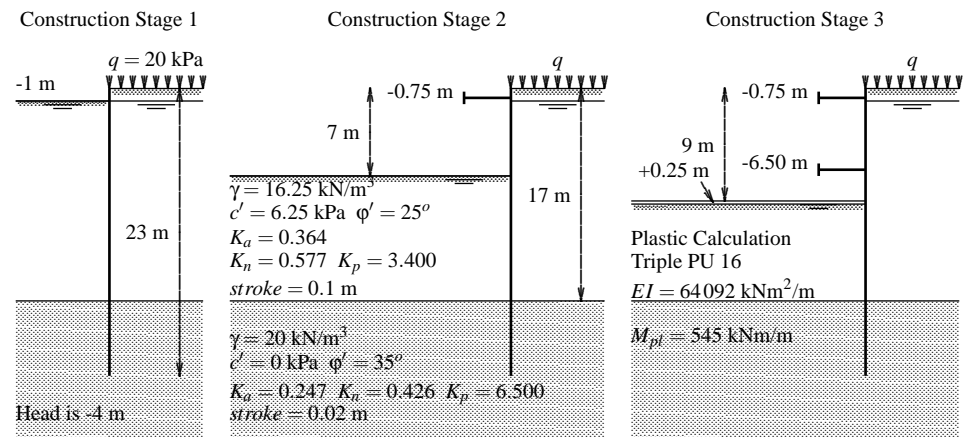
Figure 2.28: *Comparison between* PLASWALL *and* SPW99

The calculation results of the second and third construction stage are presented in Figure 2.29. Both an elastic and a plastic calculation have been made: the elastic calculation is indicated with solid lines and the plastic calculation with dashed lines. The results from SPW99 are indicated with the ×-marks. The calculation results are summarised in Table 2.5.
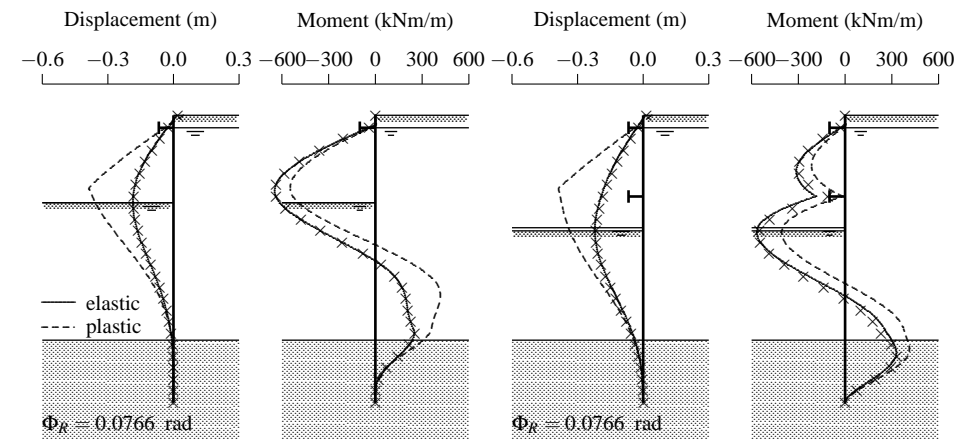
Figure 2.29: *Elastic calculation with* PLASWALL *compared with* SPW99 *and plastic calculation with* PLASWALL. *Solid lines are calculated by* PLASWALL *and* ×-*marks by* SPW99

	w_{max}(mm)	$z_{w_{max}}$(m)	M_{max}(kNm/m)	$z_{M_{max}}$(m)
PLASWALL Elastic[2]	185	-7.00	-645.2	-6.13
SPW99[2]	183	-7.00	-644.2	-6.04
PLASWALL Plastic[2]	387	-5.83	-545.0	-5.83
PLASWALL Elastic[3]	220	-9.25	-565.4	-9.35
SPW99[3]	217	-9.48	-535.4	-9.71
PLASWALL Plastic[3]	387	-5.52	-405.9	-9.35

Table 2.5: *Calculation results of* PLASWALL *and SPW99 for stage 2 and 3*

The differences between the calculated results for the displacement and bending moment in Stage 2 and for the displacement in Stage 3 using PLASWALL and SPW99, are about 1%. These differences may be caused by a different number and locations of the springs, by differences in the assumptions of one or two springs, and by different numerical solvers. It can therefore be concluded that the implementation of multi-staged calculations in stratified soil in PLASWALL has been carried out successfully.

2.6   Parametric study

2.6.1   General

The aim of this parametric study is to provide insight into the way in which rotation requirement is influenced by design parameters. Generally, soil data is obtained from soil investigation and, in this study, is therefore considered as imposed data. However, other design parameters can be cleverly chosen by the designer, such as the length, section and steel grade of the sheet pile, and the position of struts.

When sufficient insight into the rotation requirement is obtained, it will be possible to decide whether standard design cases can be defined from which it may be stated that the rotation requirement remains below a certain limit. For example, when it can be proven that the rotation requirement will not exceed a certain value for walls with a free earth support, a general design rule can be defined for the rotation requirement that can be used as a simple and practical rotation check.

The parametric studies are subdivided into a case with one strut, a case with two struts and a case calculated using different earth pressure theories.

2.6.2   Parametric study for a case with one strut

For the case with one strut, the following parameters and their effects on rotation of the plastic hinge are investigated:

- development of plastic rotation as a result of excavation

- the steel grade of the wall or the level of M_{pl}

- the length of the wall

Development of plastic rotation as a result of excavation

The development of rotation in the plastic hinge is analysed using the example of an 8.8 metre long sheet pile wall propped at ground level retaining 5 metres of water and sand. The toe of the wall stands in a impermeable layer, so that hydrostatic water pressure may be assumed on both sides of the wall. The plastic moment in the wall is $M_{pl} = 270$ kNm/m. The calculations have been made with PLAXIS 6.31 [79]. Other relevant data is presented in Figure 2.30.
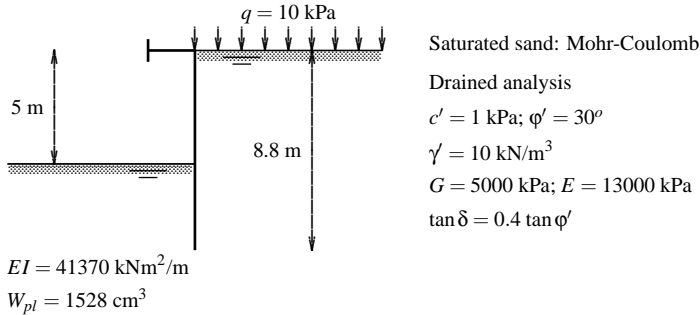
Figure 2.30: *Example of a single propped wall*

An ultimate limit state is obtained for an excavation of 5 metre. At 4.8 metre, which is 96% of the excavation, the first plastic hinge is about to be developed, see Figure 2.31. When the plastic hinge is formed, the rotation increases progressively with the excavation depth.
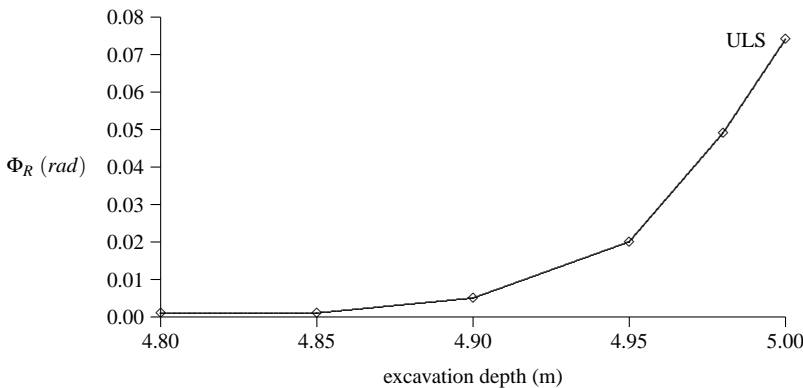
Figure 2.31: *Development of rotation requirement due to increasing excavation*

In more extensive parametric studies [52], it has been typically found that rotation of the plastic hinge is developed during the last 5% to 8% of the excavation. Reference is made to clause 8.3.2.1.(2) of ENV 1997-1 [22], which requires an additional allowance of $\Delta_a = 10\%$ of the excavation depth below the lowest prop to a maximum of 0.5 metre for

ultimate limit state conditions to apply. This additional excavation depth alone would in most cases provide all the safety against rotation of the plastic hinge in the Serviceability Limit State.

Influence of the steel grade or the plastic moment

The influence of the steel grade on the rotation requirement, or the plastic moment, is investigated with the example from Figure 2.30. In all these cases, use is made of a constant bending stiffness. The structure is in an ultimate limit state for $f_y = 177$ N/mm^2 or $M_{pl} = 270$ kNm/m. Starting from this construction, new calculations are carried out with higher yield stresses, or plastic moments. These calculations are further away from the ultimate limit state.
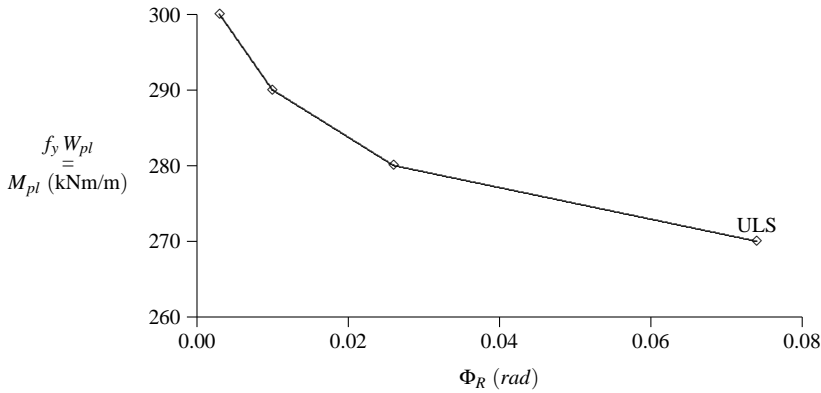
Figure 2.32: *Rotation requirement as function of M_{pl}*

Figure 2.32 shows the effect of an increase of yield stress or plastic moment on the rotation requirement. The rotation in the plastic hinge decreases progressively if a higher yield stress or plastic moment is applied. Therefore, an increase in steel grade will result in a considerable reduction of the rotation requirement. However, it should be realised that when a higher yield stress is chosen, the rotation capacity of the sheet pile decreases.

Influence of the length of the wall

The influence of the wall length on the rotation requirement is investigated using the example from Figure 2.30. The length of the wall is varied between 8.8 metre and 15 metre, these lengths being the extremes between the wall with free earth support and fixed earth support.

All the cases were brought to an ultimate limit state by progressively reducing the plastic moment resistance M_{pl}. In this study the yield stress was kept constant: $f_y = 430$ N/mm^2. To ignore the influence of discrete sheet pile sections but maintain a realistic section, the bending stiffness was approximated by the relation $EI = 110M_{pl} - 18657$ [52]. The result of this parametric study is presented in Figure 2.33.

When the wall has free earth support, the rotation requirement is small but when the length of the wall is increased, the rotation in the plastic hinge and the bending moment
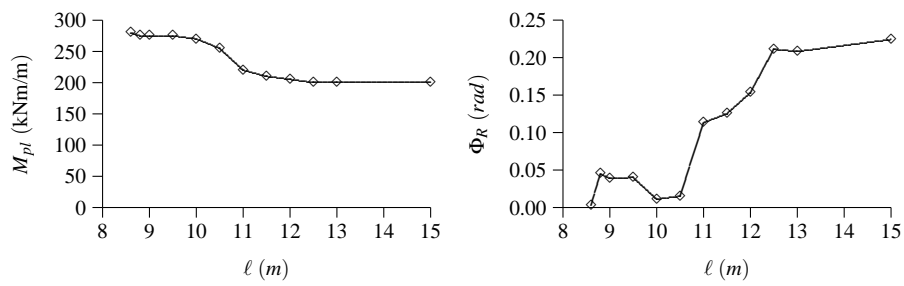
Figure 2.33: *Required M_{pl} and Φ_R as function of the wall length for constant f_y*

hardly decrease, until the length of the wall is about 11 metres. Then the failure mode in the soil changes, end-fixity starts to be developed which involves an increase in rotation at the plastic hinge and a decrease of the bending moment until the wall length is 12.5 metres, when the major part of the fixed moment has been developed. When the wall is made longer, the ultimate bending moment will not decrease, and the rotation requirement will not increase.

Alteration of the rotation requirement for shorter or longer walls can be related to the different failure modes that occur in the soil due to different wall movements, which is explained in Brinch Hansen's method in Section 2.2.2. As a result of the change of failure mode in the soil, the capacity of earth pressure redistribution changes: the more redistribution capacity the soil has, the greater the rotation can be developed at the plastic hinge.

2.6.3 Parametric study for a case with two struts

The effect of a change of strut level on the rotation requirement for a sheet pile wall at ultimate limit state is demonstrated with the example of a double propped sheet pile wall in sand overlain by 17 metres of soft clay. The basic configuration of this example, including other relevant data, is presented in Figure 2.34.

The rotation requirements of the basic configuration and variations of the deeper strut level are presented in Table 2.6. For the cases with strut levels at 5.5 m and 6.5 m the second construction stage is critical for the design. For the case with strut level at 7.5 m the third construction stage appears to be critical.

	M_{pl} (kNm/m)	Φ_R (rad)
elastic configuration	1207	0
basic configuration	900	0.0356
strut level 1 m lower [1]	1110	0.007
strut level 1 m higher	950	0.0732
[1] third excavation stage is critical		

Table 2.6: *Variation of strut level*

Figure 2.35 shows the effect of the strut level variation on the displacements and bending moments. The second strut level appears to have an enormous influence on the plastic mo-

Construction Stage 1

-1.5 m

-2 m

23 m

Construction Stage 2

20 kPa

-0.90 m

6.5 m

$\gamma = 15$ kN/m³
$c = 5$ kPa $\varphi = 22.5^o$
$\tan\delta = 0.5\tan\varphi$
$G = 550$ kPa $E = 1520$ kPa

17 m

$\gamma = 21$ kN/m³
$c = 1$ kPa $\varphi = 40^o$
$\tan\delta = 0.67\tan\varphi$
$G = 40000$ kPa $E = 101000$ kPa

Construction Stage 3

-0.90 m

12 m   -6.50 m   -5.50 m
-7.50 m

$EI = 151746$ kNm²/m
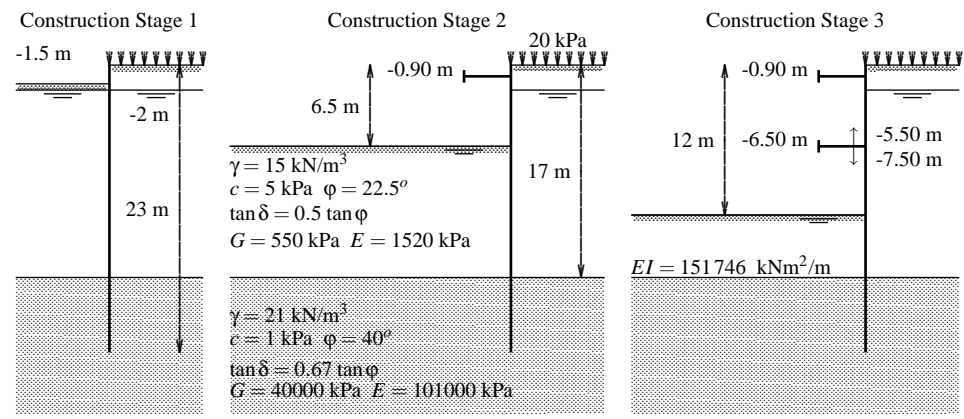
Figure 2.34: *Variation of strut levels for a double propped wall*

ment and the plastic rotation of the sheet pile at ultimate limit state. The main cause for this difference can also be ascribed to the capacity to redistribute earth pressures. Furthermore, when the strut levels are changed the failure mode in the soil changes and the resultant earth pressure forces will move upwards or downwards. Therefore the effective span length, i.e., the span length between the points of zero moment will alter, which directly influences the bending moment distribution and rotation in the plastic hinge.

Displacement (m)

−0.6   −0.3   0.0   0.3

Moment (kNm/m)

−1200   −600   0   600   1200

-7.5 m

-5.5 m
-6.5 m
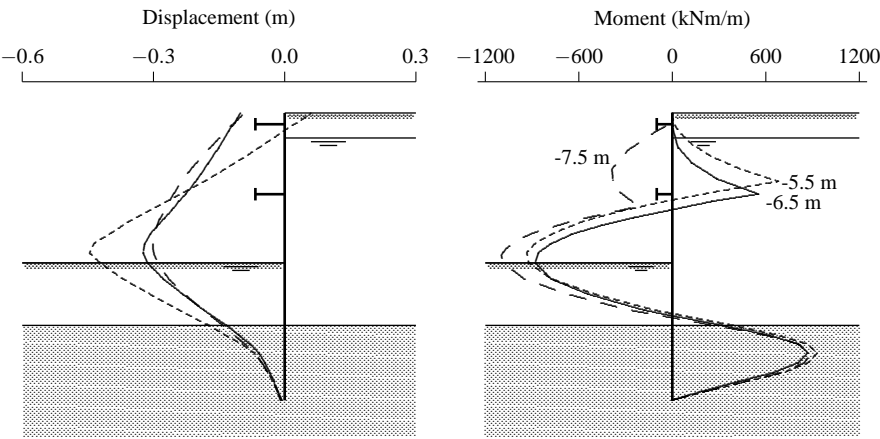
Figure 2.35: *Displacement and bending moment influenced by strut levels*

From the parametric study it can be concluded that the rotation in a plastic hinge is mainly determined by two factors:

- the plastic moment, which determines the size and location of the earth pressure resultants when the first plastic hinge is developed

- the reserve resistance in the soil that can be used for earth pressure redistribution, which is determined by the geometry and the soil conditions

2.6.4 Parametric study for a case calculated with different earth pressure theories

In this section the effects of different earth pressure theories on a calculation with plastic hinges is investigated. Therefore a 17.5 m long continuous PU 16 sheet pile wall in dry sand is considered retaining a 12.5 m deep excavation and propped 2 m below the original ground level. Relevant soil and sheet pile parameters are given in Figure 2.36. This case is the same case as that presented by Hartmann-Linden in his thesis [38].

Soil conditions:
$\gamma = 19$ kN/m^3
$c'_d = 0$ kPa $\varphi'_d = 30^o$ $\delta = 2/3\,\varphi'$

FE: Advanced Mohr Coulomb
$c'_d = 1$ kPa $E = 25000$ kPa$(p'/100)^{0.6}$

SRM
$k = 20000$ kN/m^3
Kerisel and Absi:
$K_a = 0.30$ $K_n = 0.5$ $K_p = 5.30$

Kötter:
$K_a = 0.29$ $K_n = 0.5$ $K_p = 4.63$

Müller-Breslau:
$K_a = 0.28$ $K_n = 0.5$ $K_p = 5.74$

Brinch Hansen: Spooks failure 0,1,1
$z > -11.88$ m $K_a = 0.22$ $K_n = 0.5$ $K_p = 4.92$
-11.88 m $> z > -16.63$ m $K_a = 0.28$ $K_n = 0.5$ $K_p = 4.94$
-16.63 m $> z > -17.5$ m $K_a = 0.28$ $K_n = 0.5$ $K_p = 0.69$ (left) and $K_p = 3$ (right)

PU 16: $EI = 64092$ kNm^2/m
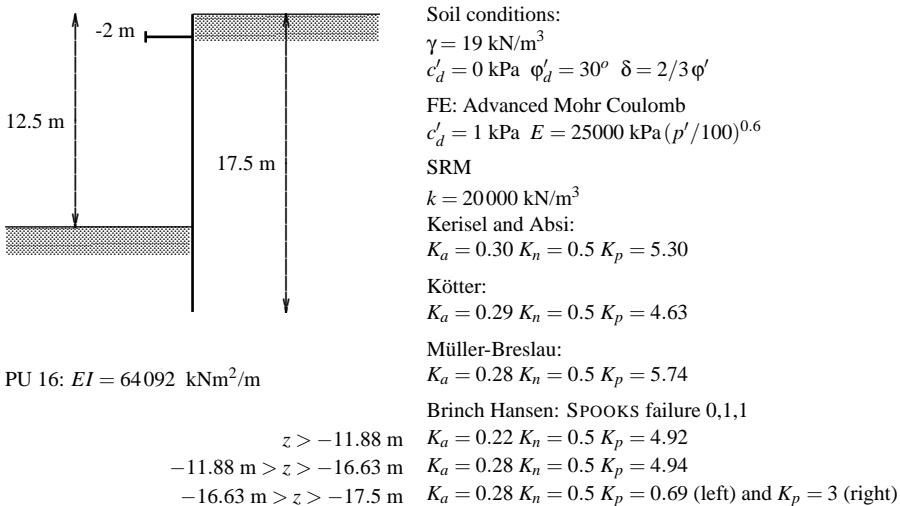
Figure 2.36: *Comparison between a subgrade reaction model and a finite element model*

The PLASWALL calculations were carried out using the earth pressure theories of Kerisel and Absi [47], Kötter [30], Müller-Breslau [59] and Brinch Hansen [13], and were compared to the finite element model PLAXIS 6.31 [79] using the Advanced Mohr-Coulomb soil model that is based on a stress-dependent elastic soil response and the Mohr-Coulomb failure criterion. These four earth pressure theories are explained in Appendix D. For the Brinch Hansen calculation, the limit earth pressure distribution was derived from a calculation with SPOOKS 7.1.5 [37] with failure mode 0,1,1. This SPOOKS calculation gave a wall length of 17.8 m and a plastic moment $M_{pl} = 421$ kNm/m.

The calculation results are presented in Figure 2.37 and 2.38. The wall displacements were mutually adjusted and therefore the bending moments should be compared. For this
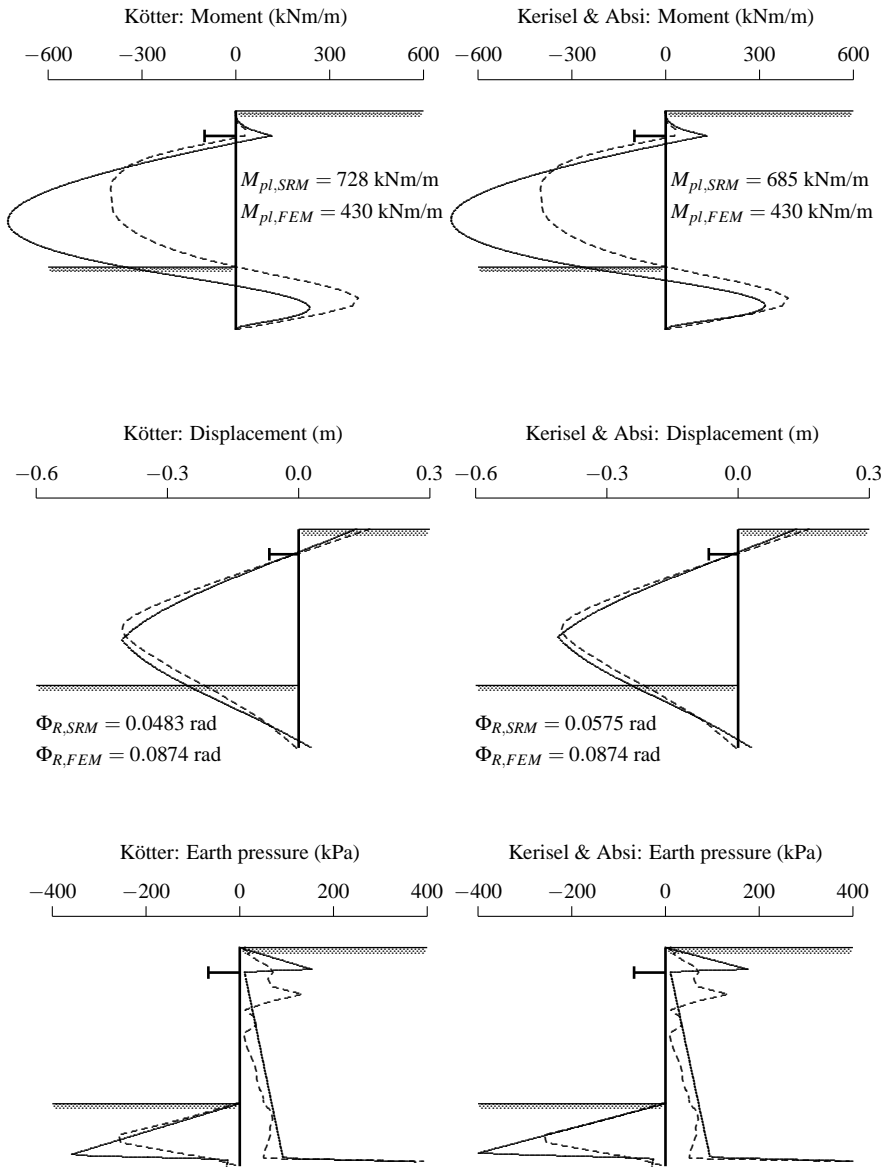
Figure 2.37: *Distribution of moment, wall displacement and earth pressure in the ultimate limit state. Solid lines indicate the subgrade reaction model and dashed lines the finite element model.*
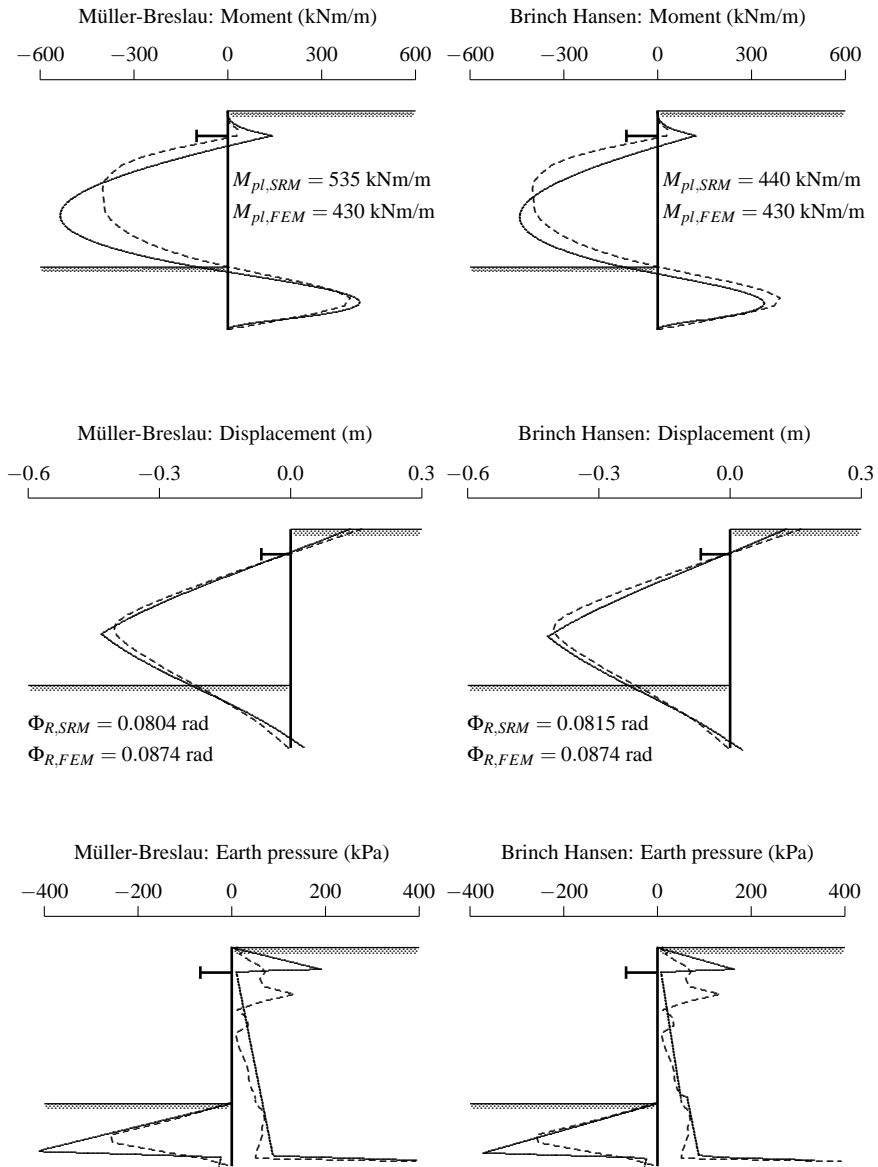
Figure 2.38: *Distribution of moment, wall displacement and earth pressure in the ultimate limit state. Solid lines indicate the subgrade reaction model and dashed lines the finite element model.*

case one may consider the bending moment as the design parameter on the basis of which an appropriate sheet pile section is chosen.

The moment calculated with Brinch Hansen's earth pressure theory is in close agreement with the PLAXIS result. This may prove the practicality of applying Brinch Hansen's earth pressure theory to the limit earth pressure distribution in a subgrade reaction model.

The moment calculated with Müller-Breslau's earth pressure theory is about 20% higher than with Brinch-Hansen, because earth pressure redistribution due to arching is not taken into account. However, a rule of thumb given in recommendation R 77 of EAU [25] is that for this situation the bending moment may be reduced by 33% to account for arching in the soil on the retained side, which gives: $M_{pl} = 357$ kNm/m. This value is lower than calculated with PLAXIS but is in accordance with the experience expressed in CUR 166 [27, p.108] that the Müller-Breslau's earth pressure theory may overpredict the passive earth pressure resistance.

The moment calculated according to the earth pressure theory of Kerisel and Absi is $M_{pl} = 685$ kNm/m. However, when this moment is reduced according to EAU R77, the plastic moment of $M_{pl} = 457$ kNm/m is obtained, and this value is only 4% higher than that calculated with Brinch Hansen and 6% higher than the PLAXIS result.

The moment from Kötter's earth pressure theory is $M_{pl} = 728$ kNm/m. By reduction according to EAU R77, the plastic moment is $M_{pl} = 485$ kNm/m, which is 10% higher than that calculated with Brinch Hansen and 13% higher than the PLAXIS result.

It can be concluded that implementation of Brinch-Hansen's earth pressure theory would be a logical progress in the development of a subgrade reaction model for plastic design, because the Brinch-Hansen earth pressure theory accounts for a redistribution of earth pressure that corresponds to the calculated wall movement. In the example, this procedure has been carried out by hand, because suitable formulae for implementation in a subgrade reaction model are lacking.

2.7   Design examples

2.7.1   General

The application of plastic design to steel sheet pile walls is demonstrated with two design examples. One example is made with (PLASWALL), the other with (PLAXIS). The examples concern:

- a single propped wall: subgrade reaction model

- a single propped wall: finite element model

Verification of the bending moment, $\dfrac{b_f}{t_f \varepsilon}$ and the rotation requirement are carried out. The verifications of shear force, transverse bending, load introduction, etc., are not considered, nor are the issues of interlock friction and oblique bending. The differences between plastic and elastic design are demonstrated.

2.7.2   Design example for a single propped wall: PLASWALL

The first example deals with a 20 metre long sheet pile wall composed of triple PU 16 profiles, retaining a 7 metre deep excavation and propped 1 metre below ground level. The ground consists of an 18 metre thick clay layer overlaying a sand layer. The clay has characteristics of $\gamma_{dry,k} = \gamma_{sat,k} = 16$ kN/m^3, $c'_k = 10$ kPa and $\varphi'_k = 30.2^o$. Using the partial factors from Table 2.1 case C of ENV 1997-1:1994 (see also Figure 1.2) the design values are:

$$\gamma_{dry,d} = \gamma_{sat,d} = 1.0 \cdot 16 \text{ kN/m}^3$$
$$c'_d = c'_k/1.6 = 6.25 \text{ kPa}$$
$$\varphi'_d = \arctan\left(\tan\varphi'_k/1.25\right) = 25^o$$
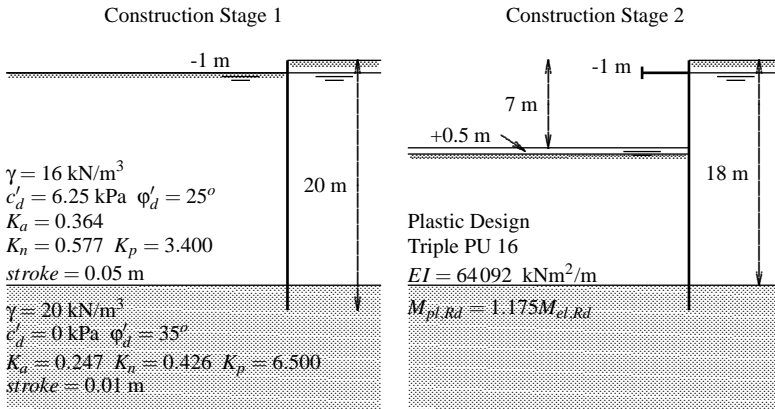
Figure 2.39: *Design example of a single propped wall using a subgrade reaction model*

In accordance with Clause 8.3.2.1.(2) of ENV 1997-1:1994 an additional allowance of 0.5 metre is applied to the retained height; hence the design retained height is 7.5 metre. It is accepted that the properties for the continuous PU 16 are used. Active, neutral and passive earth pressure coefficients are determined according to Kerisel and Absi [47], with $\delta = +\frac{2}{3}\varphi'$ for the active side and $\delta = -\frac{1}{2}\varphi'$ for the passive side. The example with the design values is summarised in Figure 2.39 and the results of the elastic and plastic calculation are given in Figure 2.40.

Elastic design

The elastic calculation gives a span moment of $M_{Sd} = 556$ kNm/m. For the sheet pile wall a steel grade of S 390 ($f_y = 390$ N/mm^2) is sufficient when the following two checks are satisfied:

- $M_{Sd} = 556$ kNm/m $\leq M_{el,Rd} = 1600$ cm^3/m $\cdot$ 390 N/mm^2/1.1 = 567 kNm/m

- As $M_{Sd} \leq M_{el,Rd}$, a Class 3 cross-section is sufficient. It can be shown using Figure 2.13, Table 5.1 of ENV 1993-5 [24] or the manufacturer's catalogue that the
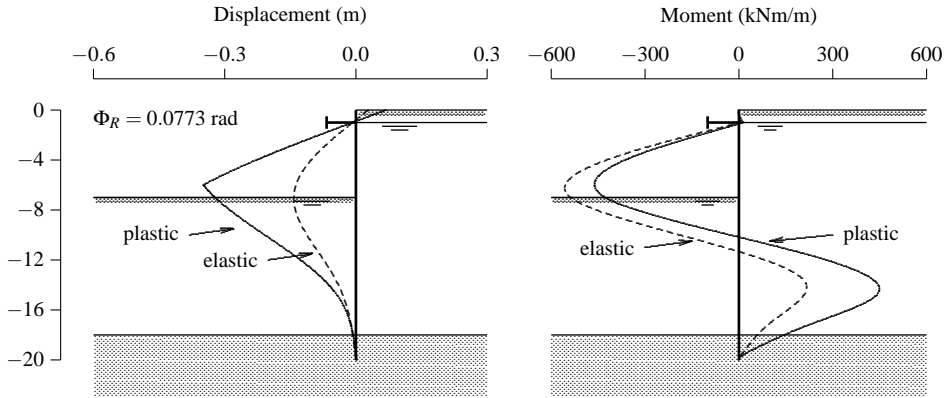
Figure 2.40: *Calculation results of the single propped wall using a subgrade reaction model*

cross-sectional class is adequate if

$$\frac{b_f}{t_f \varepsilon} = \frac{303}{12 \cdot 0.78} = 32.4 \leq 49 \tag{2.24}$$

Plastic design without rotation requirement

The calculation without a plastic hinge gives a span moment of $M_{Sd} = 556$ kNm/m. For the sheet pile wall a steel grade of S 355 ($f_y = 355$ N/mm^2) is sufficient when the following two checks are satisfied:

- $M_{Sd} = 556$ kNm/m $\leq M_{pl,Rd} = 1.175 \cdot 1600$ cm^3/m $\cdot 355$ N/mm^2/1.1 $= 607$ kNm/m

- Because of $M_{Sd} \leq M_{pl,Rd}$ and because $\Phi_R = 0$ rad, a Class 2 cross-section is sufficient. It can be shown using Figure 2.13, Table 5.1 of ENV 1993-5 [24] and the manufacturer's catalogue that the cross-sectional class is adequate if

$$\frac{b_f}{t_f \varepsilon} = \frac{303}{12 \cdot 0.81} = 31.2 \leq 37 \tag{2.25}$$

Plastic design with rotation requirement

The design with one plastic hinge results in a limit design moment of $M_{Sd} = 461$ kNm/m with a rotation requirement of the plastic hinge of $\Phi_{Rd} = 0.0773$ rad. For the sheet pile wall a steel grade of S 270 ($f_y = 270$ N/mm^2) is sufficient when the following three checks are satisfied:

- $M_{Sd} = 461$ kNm/m $\leq M_{pl,Rd} = 1.175 \cdot 1600$ cm^3/m $\cdot 270$ N/mm^2/1.1 $= 461$ kNm/m

- As $M_{Sd} \leq M_{pl,Rd}$ and because $\Phi_R > 0$ rad, a Class 1 cross-section is required. It can be shown using Table 5.1 of ENV 1993-5 [24], Figure 2.13 and the manufacturer's catalogue that the cross-sectional class is adequate if

$$\frac{b_f}{t_f \varepsilon} = \frac{303}{12 \cdot 0.93} = 27.2 \leq 37 \tag{2.26}$$

- It is derived from Figure 2.13 that for 100% M_{pl} and $\dfrac{b_f}{t_f \varepsilon} = 27.2$ the rotation capacity is $\Phi_{Cd} = 0.092$ rad. The rotation check is fulfilled if

$$\Phi_{Rd}, \text{ determined hereafter} \leq \Phi_{Cd} = 0.092 \text{ rad} \tag{2.27}$$

Method I: Direct calculation

The rotation requirement can be directly calculated by the plastic hinge model. It was found that $\Phi_{Rd} = 0.0773$ rad $\leq \Phi_{Cd} = 0.092$ rad.

Method II: Unloading of the construction

After analysis of the final construction stage, the residual deformations can be determined by adding a second boundary condition and removing all the load on the sheet pile. However, the numerical solver in PLASWALL has not been optimised to calculate this load step without numerical problems.

Method III: Simplified assumption based on rotations

The rotation requirement is determined using equation (2.17):

$$\Phi_R = \varphi_{max} - \varphi_{pl} \tag{2.17}$$

The calculation model gave as output $\varphi_{max} = 0.0761 + 0.0421 = 0.1182$ rad and $L = 9.1$ m (see Figure 2.18). The elastic rotation is calculated from equation (2.18):

$$\varphi_{pl} = \frac{2}{3} \frac{M_{pl}L}{EI} = \frac{2}{3} \frac{461 \cdot 9.1}{64092} = 0.0436 \text{ rad} \tag{2.28}$$

Hence the rotation requirement is

$$\Phi_{Rd} = \varphi_{max} - \varphi_{pl} = 0.1182 - 0.0436 = 0.0746 \text{ rad} \leq \Phi_{Cd} = 0.092 \text{ rad} \tag{2.29}$$

Method IV: Simplified assumption based on displacements

The rotation requirement is determined using equation (2.17):

$$\Phi_R = \varphi_{max} - \varphi_{pl} \tag{2.17}$$

The elastic+plastic rotation angle is determined according to equation (2.19):

$$\varphi_{max} = \frac{w_2 - w_1}{L_1} + \frac{w_2 - w_3}{L_2} \tag{2.19}$$

It is found that (see Figure 2.19):

$$\varphi_{max} = \frac{0.349 - 0.015}{4.9} + \frac{0.349 - 0.200}{4.2} = 0.104 \text{ rad} \tag{2.30}$$

The elastic rotation φ_{pl} is determined with equation (2.20):

$$\varphi_{pl} = \frac{5}{12} \frac{M_{pl}L}{EI} = \frac{5}{12} \frac{461 \cdot 9.1}{64092} = 0.027 \text{ rad} \tag{2.31}$$

Hence the rotation requirement is

$$\Phi_{Rd} = \varphi_{max} - \varphi_{pl} = 0.104 - 0.027 = 0.077 \text{ rad} \leq \Phi_{Cd} = 0.092 \text{ rad} \tag{2.32}$$

2.7.3   Design example for a single propped wall: PLAXIS

The second design example involves a 19 metre long, propped sheet pile wall retaining 7.5 metre of homogeneous sand with a characteristic angle of internal friction of $\varphi'_k = 35.8^o, c'_k = 1.6$ kPa and $\tan \delta_k = \frac{2}{3} \tan \varphi'_k$. Behind the wall a variable surcharge acts of $q_k = 7.7$ kN/m^2. According to Table 2.1 case C of ENV 1997-1 [22] the design values are:

$$\gamma'_d = 1.0 \gamma'_k = 10 \text{ kN/m}^3$$
$$c_d = c_k/1.6 = 1 \text{ kPa}$$
$$\varphi_d = \arctan (\tan \varphi_k/1.25) = 30^o$$
$$\tan \delta_k = \frac{2}{3} \tan \varphi'_k$$
$$q_d = 1.3 q_k = 10 \text{ kN/m}^2$$

In accordance with 8.3.2.1.(2) of ENV 1997-1:1994 an additional allowance of 0.5 metres is applied to the retaining height: the design retained height is 8.0 metres. The wall is formed with its toe in an impermeable layer, so that hydrostatic water pressures act on both sides of the wall. The wall is composed of triple U-profiles and may be treated as a continuous wall. The section is determined from the calculation. The example with the design values is summarised in Figure 2.41.

Design example with finite element method

$q_d = 10$ kPa

8 m

19 m

Soil conditions:
Drained Mohr Coulomb
$\gamma = 20$ kN/m^3
$c'_d = 1$ kPa $\varphi'_d = 30^o$
$\tan \delta = 0.4 \tan \varphi'$
$E' = 52\,000$ kPa $G = 20\,000$ kPa
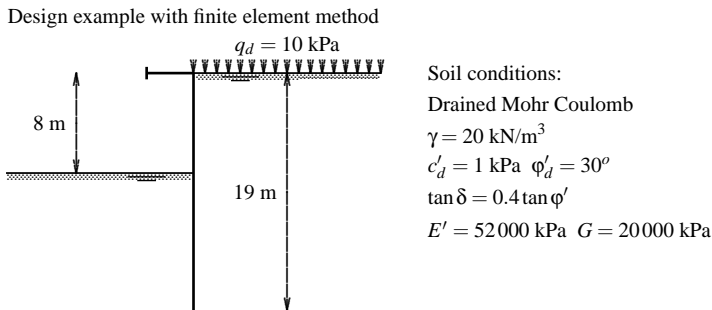
Figure 2.41: *Design example of a single propped wall using a finite element model*

Elastic design

The elastic calculation results in a span moment of $M_{Sd} = 1050$ kNm/m. When only the elastic moment resistance is taken into account, a triple U-profile composed of PU 32 with a steel grade of S 390 ($f_y = 390$ N/mm^2) is sufficient when the following two checks are satisfied:

- $M_{Sd} = 1050$ kNm/m $\leq M_{el;Rd} = 3200$ cm^3/m $\cdot$ 390 N/mm^2/1.1 = 1135 kNm/m

- As $M_{Sd} \leq M_{el;Rd}$, a Class 3 cross-section is sufficient. It can be shown using Table 5.1 of ENV 1993-5 [24], Figure 2.13 and the manufacturer's catalogue that verification of the cross-sectional class is adequate if

$$\frac{b_f}{t_f \varepsilon} = \frac{341}{19.5 \cdot 0.78} = 22.4 \leq 49 \tag{2.33}$$

Plastic design without rotation requirement

When the plastic moment resistance is taken into account, a triple U-profile composed of PU 25 with a steel grade of S 430 ($f_y = 430$ N/mm^2) is sufficient when the following two checks are satisfied:

- $M_{Sd} = 1050$ kNm/m $\leq M_{pl,Rd} = 1.16 \cdot 2500$ cm^3/m $\cdot$ 430 N/mm^2/1.1 = 1133 kNm/m

- As $M_{Sd} \leq M_{pl,Rd}$ and because $\Phi_{Rd} = 0$ rad, a Class 2 cross-section is sufficient. It can be shown using Table 5.1 of ENV 1993-5 [24], igure 2.13 and the manufacturer's catalogue that verification of the cross-sectional class is adequate if

$$\frac{b_f}{t_f \varepsilon} = \frac{339}{14.2 \cdot 0.74} = 32.2 \leq 37 \tag{2.34}$$

This example shows that a smaller profile can be adopted if the full plastic moment resistance is taken into account instead of the elastic moment resistance. A saving of 18% on the weight of the steel is obtained.

Plastic design with rotation requirement

Ultimate limit state design with one plastic hinge results in a design moment of $M_{Sd} = 862$ kNm/m. For the sheet pile wall either a triple PU 25 with steel grade S 355 ($f_y = 355$ N/mm^2) or a triple PU 20 with steel grade S 430 ($f_y = 430$ N/mm^2) are sufficient when the following three checks are satisfied:

PU 25 S 355

- $M_{Sd} = 862$ kNm/m $\leq M_{pl,Rd} = 1.16 \cdot 2500$ cm^3/m $\cdot$ 355 N/mm^2/1.1 = 935 kNm/m

- $\dfrac{b_f}{t_f \varepsilon} = \dfrac{339}{14.2 \cdot 0.81} = 29.5 < 37$ (Class 1 or 2)

- It can be derived from Figure 2.13 that for 100% M_{pl} and $\dfrac{b_f}{t_f \varepsilon} = 29.5$ the rotation capacity is $\Phi_{Cd} = 0.071$ rad. The rotation check is fulfilled if

$$\Phi_{Rd}, \text{ determined hereafter} \leq \Phi_{Cd} = 0.071 \text{ rad} \tag{2.35}$$

PU 20 S 430

- either $M_{Sd} = 862$ kNm/m $\leq M_{pl,Rd} = 1.18 \cdot 2000 \text{ cm}^3/\text{m} \cdot 430 \text{ N/mm}^2/1.1 = 923$ kN

- or $M_{Sd} = 862$ kNm/m $\leq M_{pl,Rd} = 0.95 \cdot 1.18 \cdot 2000 \text{ cm}^3/\text{m} \cdot 430 \text{ N/mm}^2/1.1 = 876$ kN

- $\dfrac{b_f}{t_f \varepsilon} = \dfrac{307}{12.4 \cdot 0.74} = 33.5 < 37$ (Class 1 or 2)

- It is derived from Figure 2.13 that for 100% M_{pl} and $\dfrac{b_f}{t_f \varepsilon} = 33.5$ the rotation capacity is $\Phi_{Cd} = 0.033$ rad and for 95% M_{pl} and $\dfrac{b_f}{t_f \varepsilon} = 33.5$ the rotation capacity is $\Phi_{Cd} = 0.0792$ rad. The rotation check is fulfilled if

$$\Phi_{Rd}, \text{ determined hereafter} \leq \Phi_{Cd} = 0.033 \text{ rad} \tag{2.36}$$

Method I: Direct calculation

It is not possible to determine the rotation requirement of the sheet pile with a plastic zone model, unless a $M - \varphi$ relation is implemented that is representative for steel sheet piling.

Method II: Unloading of the construction

After analysis of the final construction stage, the residual deformations can be determined. A free support at the pile toe is added and the weight of the ground and water is switched off. The following results are found:

- PU 25: $\Phi_{Rd} = 0.030$ rad $\leq \Phi_{Cd} = 0.071$ rad

- either PU 20 with 100% $M_{pl,Rd}$: $\Phi_{Rd} = 0.064$ rad $\nleq \Phi_{Cd} = 0.033$ rad

- or PU 20 with 95% $M_{pl,Rd}$: $\Phi_{Rd} = 0.064$ rad $\leq \Phi_{Cd} = 0.0792$ rad

The PU 20 S 430 with 100% $M_{pl,Rd}$ seems to be insufficient for this design case. However, the rotation requirement may be increased by arithmetical reduction of the structural resistance to 95% $M_{pl,Rd}$, see also Section 2.3.4.

It will be demonstrated that an increase of M_{Sd} to $M_{Sd} = M_{pl;Rd}$ will lead to a decrease of the rotation requirement. Therefore a new calculation, which is now no longer an ultimate limit state calculation, is carried out with $M_{Sd} = M_{pl,Rd} = 923$ kNm/m. This calculation gives the following result:

PU 20: $\Phi_{Rd} = 0.026$ rad $< \Phi_{Cd} = 0.033$ rad

It can be concluded that the PU 20 S 430 is a suitable profile for this design case. This result can either be obtained if the structural resistance is arithmetically reduced in accordance with Figure 2.13 or if a calculation is made using the properties of the *specific section*.

Method III: Simplified assumption based on rotations

Method III is applied to the calculation with a real sheet pile. The rotation requirement is determined using equation (2.17):

$$\Phi_R = \varphi_{max} - \varphi_{pl} \tag{2.17}$$

For the PU 20 S 430 the model gave $\varphi_{max} = 0.099$ rad and $L = 10.88$ m (see Figure 2.18). The elastic rotation is calculated with equation (2.18):

$$\varphi_{pl} = \frac{2}{3} \frac{M_{pl}L}{EI} = \frac{2}{3} \frac{923 \cdot 10.88}{90300} = 0.074 \text{ rad} \tag{2.37}$$

Hence the rotation requirement is

$$\Phi_{Rd} = \varphi_{max} - \varphi_{pl} = 0.099 - 0.074 = 0.025 \text{ rad} \leq \Phi_{Cd} = 0.033 \text{ rad} \tag{2.38}$$

For the PU 25 S 355 the model gave $\varphi_{max} = 0.079$ rad and $L = 10.88$ m (see Figure 2.18). The elastic rotation is calculated with equation (2.18):

$$\varphi_{pl} = \frac{2}{3} \frac{M_{pl}L}{EI} = \frac{2}{3} \frac{935 \cdot 10.88}{118650} = 0.057 \text{ rad} \tag{2.39}$$

Hence the rotation requirement is

$$\Phi_{Rd} = \varphi_{max} - \varphi_{pl} = 0.079 - 0.057 = 0.022 \text{ rad} \leq \Phi_{Cd} = 0.033 \text{ rad} \tag{2.40}$$

Method IV: Simplified assumption based on displacements

Similar to Method III, Method IV is applied to the calculation with a real sheet pile. The rotation requirement is determined using equation (2.17):

$$\Phi_R = \varphi_{max} - \varphi_{pl} \tag{2.17}$$

The elastic+plastic rotation angle is determined according to equation (2.19):

$$\varphi_{max} = \frac{w_2 - w_1}{L_1} + \frac{w_2 - w_3}{L_2} \tag{2.19}$$

For the PU 20 S 430 it was found that (see Figure 2.19):

$$\varphi_{max} = \frac{0.285 - 0.042}{5.25} + \frac{0.285 - 0.148}{5.63} = 0.074 \text{ rad} \tag{2.41}$$

The elastic rotation φ_{pl} is determined with equation (2.20):

$$\varphi_{pl} = \frac{5}{12} \frac{M_{pl}L}{EI} = \frac{5}{12} \frac{923 \cdot 10.88}{90300} = 0.046 \text{ rad} \tag{2.42}$$

Hence the rotation requirement is

$$\Phi_{Rd} = \varphi_{max} - \varphi_{pl} = 0.074 - 0.046 = 0.028 \text{ rad} \leq \Phi_{Cd} = 0.033 \text{ rad} \tag{2.43}$$

For the PU 25 S 355 it was found that (see Figure 2.19):

$$\varphi_{max} = \frac{0.237 - 0.036}{5.25} + \frac{0.237 - 0.128}{5.63} = 0.058 \text{ rad} \tag{2.44}$$

The elastic rotation φ_{pl} is determined with equation (2.20):

$$\varphi_{pl} = \frac{5}{12} \frac{M_{pl}L}{EI} = \frac{5}{12} \frac{935 \cdot 10.88}{118650} = 0.036 \text{ rad} \tag{2.45}$$

Hence the rotation requirement is

$$\Phi_{Rd} = \varphi_{max} - \varphi_{pl} = 0.058 - 0.036 = 0.022 \text{ rad} \leq \Phi_{Cd} = 0.071 \text{ rad} \tag{2.46}$$

Summary of chosen sections with regard to material saving

Table 2.7 shows an overview of the chosen sections and the material saving that can be obtained in this example, expressed by kilo's of steel. The material savings obtained when the full-plastic section modulus is utilised instead of the elastic section modulus, amounts in this case to 18%. If a rotation at the plastic hinge of about $\Delta\varphi = 0.022$ rad is acceptable, an other 8% is saved.

Design	Section	Steel grade	Mass (kg/m²) [57]	Material saving
Elastic	PU 32	S 390	191	
Plastic without rotation	PU 25	S 430	157	18%
Plastic with rotation	PU 20	S 430	141	26%

Table 2.7: *Possible material saving compared to the elastic design*

Chapter 3

Oblique bending

3.1 Introduction

In steel sheet piling *oblique bending* is synonym for the more common term, *bending in two directions*. Bending in two directions is relevant for beams with an asymmetrical cross-section where the product of inertia has a value $I_{xy} \neq 0$. For bending theory of beams with asymmetrical cross-section in general, see e.g., Timoshenko and Young [71].

Oblique bending is relevant for U-shaped sheet piles when they are driven in pairs with a fixed central interlock, the so-called double U-piles. To illustrate the phenomenon of oblique bending, the cross-section of a double PU 8 pile is considered in Figure 3.1. Axes (1) and (2) are the principal axes of inertia which are inclined with $\alpha = 10.95^o$. I_{xx} denotes the moment of inertia about the *y*-axis and I_{yy} about the *x*-axis (see Appendix A). The indices s and d denote *single* and *double* piles.

PU 8 [57]	b (cm)	h (cm)	A (cm^2)	I_{xx} (cm^4)	I_{xy} (cm^4)	I_{yy} (cm^4)	α (^{o})
Single	60	14	69.5	29000		2360	
Double	120	28	139	183100	-33986	13953	10.95
Brochure	120	28	139			13940	
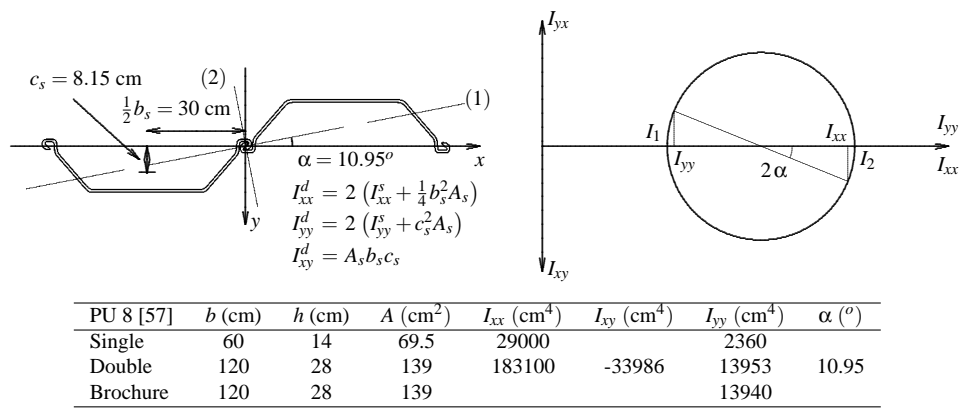
Figure 3.1: *Double PU 8 profile*

In engineering beam theory, the neutral axis is defined as the axis with zero axial strain and is the axis about which the sheet pile bends. When the resulting load on the sheet pile

is perpendicular to the plane of the wall (in the *y*- or *lateral direction*) and absent in the *x*-direction (*transverse direction*), the neutral axis coincides with the minor principal axis of inertia (1). As the direction of the displacement is perpendicular to the neutral axis, it follows that a *lateral load* generates both a *lateral* and a *transverse displacement*.

However, of more importance is the fact that due to the rotated neutral axis, the effective height of the double-U profile, i.e., the distance between neutral axis and outermost fibre, decreases, which results in a loss of strength and stiffness of the double-U sheet pile.

Traditionally in steel sheet piling, the moment of inertia and section modulus are provided for a continuous wall and are therefore related to a neutral axis that coincides with the *x*-axis. In Figure 3.1 this moment of inertia is denoted by I_{yy}.

Hence, if oblique bending occurs whereas the design is based on the structural properties of the continuous wall, the real structural behaviour of the sheet pile wall will be overestimated. This overestimation, however, is in practice also determined by other than only geometrical factors.

Firstly, it should be realised that a sheet pile wall is composed of a series of U-piles threaded together, driven into the soil. Oblique bending can only occur when these pile can slide along each other in the free interlocks. The sheet piles, however, are not always installed perfectly straight, see Figure 3.2: rotation at the clutches, tolerances of the geometrical cross-section, or slightly bent piles, mean that high contact forces can be generated between the clutches of individual piles, causing high resistance to slipping interlocks. In addition, other forms of imperfect driving, sand intrusion into the interlocks during installation, and structural detailing of anchors, struts and walings, may lead to a significant increase of resistance against interlock slippage.
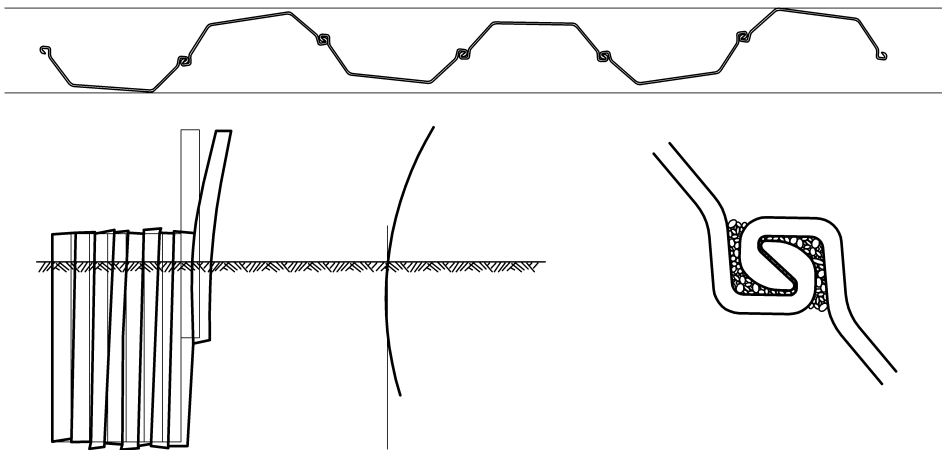
Figure 3.2: *A series of U-piles threaded together in practice*

When slipping in the interlocks is impeded, oblique bending is impeded and the structural resistance of the double U-pile increases. Resistance of the ground to transverse displacement may also allow the structural resistance to increase. As steel sheet pile walls can never be installed perfectly straight, the amount of loss of structural resistance is not so

dreastic as geometric consideration alone may imply.

Consequently, when steel sheet pile walls composed of double U-piles are designed with the traditionally provided properties W and I, the effective bending stiffness and section modulus may be overestimated. This will lead to a real wall displacement which is larger than designed for and to a real structural resistance smaller than designed for, and therefore to a structure that is less safe.

The aim of this chapter is to provide a practical guidance to take oblique bending into account, which can be used in combination with plane strain calculation models. Therefore the approach of reduction factors is followed: the effective moment of inertia I_{eff} and section modulus W_{eff} are derived from the traditionally provided properties by means of the reduction factors β_I and β_W:

$$I_{eff} = \beta_I \, I_{continuous\ wall} \tag{3.1}$$
$$W_{eff} = \beta_W \, W_{continuous\ wall} \tag{3.2}$$

where the values of β_I and β_W are determined by geometrical and practical factors that influence oblique bending. To be able to quantify these factors, the subgrade reaction model SKEWWALL is developed and validated to 3D finite element calculations in DIANA. SKEWWALL is then used in a parametric study to investigate the influence of structural supports and the shear resistance of soil on oblique bending. Finally, a new design method for oblique bending is proposed and applied to two design examples.

3.2 Theory of elasticity of oblique bending

3.2.1 General remark

In engineering mechanics the bending behaviour of a beam with symmetrical cross-section is described with the following differential equation:

$$\frac{d^4w}{dx^4} = \frac{q(x)}{EI} \tag{3.3}$$

It can be derived that the displacement at midspan of a simply supported beam loaded with a uniformly distributed load is given by

$$w = \frac{5}{384} \frac{q\ell^4}{EI} \tag{3.4}$$

It should be noticed that the general equations for oblique bending and the derivation show a fundamental similarity with the well-known bending formulae in engineering mechanics, which results from a substitution of $I_{xy} = I_{yx} = 0$. The specific term for the simply supported beam loaded with a uniformly distributed load, $\frac{5}{384}q\ell^4$, may be replaced with another term belonging to its loading condition.

3.2.2 General equations

The behaviour of a beam with an asymmetric cross-section subjected to bending in two directions, see Figure 3.3, can be described with the general differential equations in (3.5). The sign convention is presented in Appendix A.
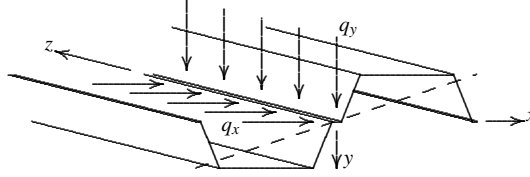
Figure 3.3: *Beam with an asymmetrical cross-section loaded in two directions*

$$
\begin{bmatrix} -\dfrac{d^2 w_x(z)}{dz^2} \\[2mm] -\dfrac{d^2 w_y(z)}{dz^2} \end{bmatrix} = \frac{1}{EI_{xx}EI_{yy} - EI_{xy}EI_{yx}} \begin{bmatrix} EI_{yy} & -EI_{xy} \\ -EI_{yx} & EI_{xx} \end{bmatrix} \begin{bmatrix} M_x(z) \\ M_y(z) \end{bmatrix} \tag{3.5}
$$

where

$$
\frac{d^2 M_x(z)}{dz^2} = -q_x(z) \quad \text{and} \quad \frac{d^2 M_y(z)}{dz^2} = -q_y(z) \tag{3.6}
$$

In the same way as for the beam with symmetrical cross-section, it can be derived that the deflection formulae for a simply supported beam loaded with a uniform distributed load are:

$$
w_x = \frac{5}{384} q_x \ell^4 \frac{I_{yy}}{E(I_{xx}I_{yy} - I_{xy}I_{yx})} - \frac{5}{384} q_y \ell^4 \frac{I_{xy}}{E(I_{xx}I_{yy} - I_{xy}I_{yx})} \tag{3.7}
$$

$$
w_y = \frac{5}{384} q_x \ell^4 \frac{I_{yx}}{E(I_{xx}I_{yy} - I_{xy}I_{yx})} - \frac{5}{384} q_y \ell^4 \frac{I_{xx}}{E(I_{xx}I_{yy} - I_{xy}I_{yx})} \tag{3.8}
$$

The stress distribution in the cross-section can be written as

$$
\sigma_{zz}(x,y) = E\varepsilon_{zz}(x,y) = E\left(\varepsilon_{zz}(0,0) + \kappa_x x + \kappa_y y\right) \tag{3.9}
$$

where

$$
\kappa_x = -\frac{d^2 w_x}{dz^2} \quad \text{and} \quad \kappa_y = -\frac{d^2 w_y}{dz^2} \tag{3.10}
$$

3.2.3   Basic example of oblique bending

In Figure 3.4 two 6 metre long simply supported beams loaded with two point loads are considered. One beam is composed of two threaded double PU 8 piles, the other beam is a quadruple PU 8 pile. Reduction factors are derived for two special cases:

- Transversely restrained bending

- Transversely unrestrained bending

PU 8 [57]	b (cm)	h (cm)	A (cm^2)	I_{xx} (cm^4)	I_{xy} (cm^4)	I_{yy} (cm^4)	α (^{o})
1 Double	120	28	139	183100	-33986	13953	10.95
Quadruple	240	28	278	1367000	-67971	27905	2.90
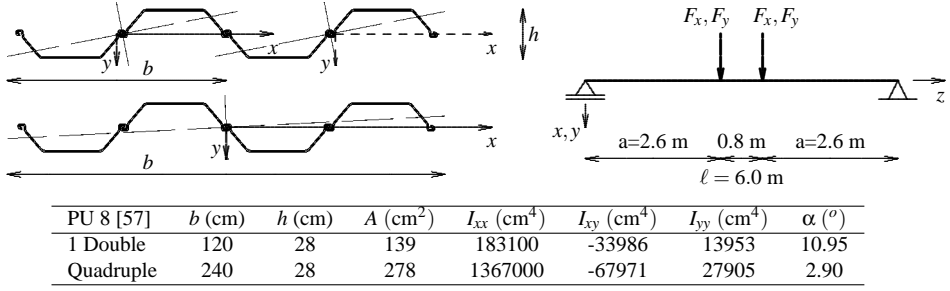
Figure 3.4: *Four point bending of two double U-piles compared with a quadruple U-pile*

In the transversely restrained case, the boundary conditions are $w_x(z) = 0$ and therefore $\kappa_x(z) = 0$. The bending formulae at $z = \frac{1}{2}\ell$ are reduced to the formulae for plane bending:

$$w_y = \frac{F_y \ell^2 a}{8EI_{yy}} - \frac{F_y a^3}{6EI_{yy}} \tag{3.11}$$

$$\sigma_{zz}(x,y) = \frac{M_y y}{I_{yy}} \tag{3.12}$$

$$M_y = F_y a \tag{3.13}$$

$$F_x = \frac{I_{xy}}{I_{yy}} F_y \tag{3.14}$$

In the transversely unrestrained case the boundary conditions are $F_x = 0$ and therefore $M_x = 0$. The following bending formulae apply at $z = \frac{1}{2}\ell$:

$$w_x = -\frac{1}{8} F_y \ell^2 a \frac{I_{xy}}{E(I_{xx}I_{yy} - I_{xy}I_{yx})} + \frac{1}{6} F_y a^3 \frac{I_{xy}}{E(I_{xx}I_{yy} - I_{xy}I_{yx})} \tag{3.15}$$

$$w_y = \frac{1}{8} F_y \ell^2 a \frac{I_{xx}}{E(I_{xx}I_{yy} - I_{xy}I_{yx})} - \frac{1}{6} F_y a^3 \frac{I_{xx}}{E(I_{xx}I_{yy} - I_{xy}I_{yx})} \tag{3.16}$$

$$\sigma_{zz}(x,y) = \frac{1}{I_{xx}I_{yy} - I_{xy}I_{yx}} (-I_{xy} M_y x + I_{xx} M_y y) \tag{3.17}$$

$$M_y = F_y a \tag{3.18}$$

$$w_x = \frac{-I_{xy}}{I_{xx}} w_y \tag{3.19}$$

The maximum moment $M_{y,max}$ at $z = \frac{1}{2}\ell$ follows from:

$$M_{y,max} = -f_y \frac{I_{xx}I_{yy} - I_{xy}I_{yx}}{I_{xy}x - I_{xx}y} \tag{3.20}$$

where f_y is the yield stress of the steel.

Double PU 8 pile

In the case of transversely restrained bending, the neutral axis coincides with the x-axis, see Figure 3.4, and the maximum stress will occur in the flange of the cross-section: $y = \frac{1}{2}h$. Using a maximum allowable stress of $f_y = 360$ N/mm^2 and the parameters from Figure 3.4, and subsequently substituting in equations (3.11) to (3.14), it is found that $F_{y;max} = 138$ kN, $F_{x;max} = -336$ kN and $w_{y;max} = 41.3$ mm.

In the case of transversely unrestrained bending, the sheet pile will yield first at the free clutch at $(x,y) = (0.60$ m$, 0.016$ m$)$ when the maximum force is

$$F_{y,max} = -\frac{f_y}{a} \frac{I_{xx}I_{yy} - I_{xy}I_{yx}}{I_{xy}x - I_{xx}y} \tag{3.21}$$

Using $f_y = 360$ N/mm^2, it follows from substitution of the parameters from Figure 3.4 in equations (3.15) to (3.20) that $F_{y,max} = 83.0$ kN, $w_{x,max} = 8.4$ mm and $w_{y,max} = 45.3$ mm.

Quadruple PU 8 pile

The transversely restrained bending case can be solved in the same way as for the double PU 8 pile. It is found that $F_{y;max} = 138$ kN, $F_{x;max} = -336$ kN and $w_{y;max} = 41.3$ mm, twice the values of the double PU 8 pile.

In the case of transversely unrestrained bending, the sheet pile will yield first at the second corner point, $(x,y) = (0.46$ m$, 0.14$ m$)$. Using $f_y = 360$ N/mm^2, it follows that $F_{y,max} = 208.3$ kN, $w_{x,max} = 1.8$ mm and $w_{y,max} = 35.5$ mm.

Calculation results

Table 3.1 gives a summary of the calculation results for one double U-pile, two double U-piles and the quadruple U-pile. The forces are related to a maximum allowable yield stress of $f_y = 360$ N/mm^2.

Restrained	F_x (kN)	F_y (kN)	M_x (kN)	M_y (kN)	w_x (mm)	w_y (mm)
1 Double PU 8	-336	138	-874	359	0	41.35
2 Double PU 8	-673	276	-1750	718	0	41.35
Quadruple PU 8	-673	276	-1750	718	0	41.35

Unrestrained	F_x (kN)	F_y (kN)	M_x (kN)	M_y (kN)	w_x (mm)	w_y (mm)
1 Double PU 8	0	83	0	216	8.41	45.32
2 Double PU 8	0	166	0	432	8.41	45.32
Quadruple PU 8	0	208	0	542	1.76	35.47

Table 3.1: *Calculation results of the double and quadruple PU 8 pile*

3.2.4 Determination of reduction factors

Two double PU 8 piles threaded together can be compared to the quadruple PU 8, because these two profiles form the two extreme cases for two double U-piles with steel on steel friction in the middle interlock, see Figure 3.4. The calculation results in Table 3.1 show

that when bending in the transverse direction is impeded, double U-piles and quadruple U-piles behave identically to the continuous wall. However, when bending in the transverse direction is permitted, the ultimate bending moment capacity of the double U-pile is lower than that of the quadruple U-pile and of the continuous wall. Furthermore, the lateral displacement of the double pile has increased as a result of the transversely unrestrained bending but the lateral displacement of the quadruple pile has decreased because the maximum load to obtain f_y is smaller.

The differences between transversely unrestrained and transversely restrained bending for the lateral displacements and ultimate bending moments can be expressed in the reduction factors β_I and β_W as defined in equations (3.1) and (3.2). As for equal yield stress the lateral bending moment M_y is equivalent to the section modulus W and for equal applied load the lateral displacement w_y is equivalent to the inverse of moment of inertia I^{-1}, it follows that

$$\beta_I = \frac{I_{y,unrestrained}}{I_{y,restrained}} \equiv \frac{F_{y,unrestrained} \cdot w_{y,restrained}}{F_{y,restrained} \cdot w_{y,unrestrained}} \tag{3.22}$$

$$\beta_W = \frac{W_{y,unrestrained}}{W_{y,restrained}} \equiv \frac{M_{y,unrestrained}}{M_{y,restrained}} \tag{3.23}$$

In the case where transverse restraint is absent, the reduction factors can be writtten as function of the cross-sectional properties:

$$\beta_{I,0} = 1 - \frac{I_{xy} I_{yx}}{I_{xx} I_{yy}} \tag{3.24}$$

$$\beta_{W,0} = \frac{I_{xx} I_{yy} - I_{xy} I_{yx}}{-I_{xy} x + I_{xx} y} \frac{h}{2 I_{yy}} \tag{3.25}$$

where for $\beta_{W,0}$ the minimum value is determined from any position (x,y) on the cross-section.

On the basis of the analytical results in Table 3.1 the reduction factors for the four-point bending case with two double and a quadruple PU 8 pile are presented in Table 3.2.

	β_I	β_W
2 Double PU 8	0.55	0.60
1 Quadruple PU 8	0.88	0.76

Table 3.2: *Reduction factors for four-point bending on a double and quadruple PU 8 pile*

3.2.5   Comparison to large scale bending tests

In 1996 two bending tests on two double PU 8 piles threaded together were carried out at the University of Liège [51, 67]. The configuration and the test setup are given in Figure 3.4, and both transversely restrained and transversely unrestrained bending were investigated.

In these tests the following results were measured (see also Table 3.5):

- In the transversely unrestrained bending test a lateral load $F_y = 166$ kN gave a lateral displacement of $w_y = 45$ mm and a transverse displacement of $w_x = 7$ mm. These measurement results are close to the analytical results for the double U-pile, see Table 3.1

- In the experiment the condition $w_x = 0$ could not be realised. A lateral load $F_y = 166$ kN gave a lateral displacement of $w_y = 33$ mm and a horizontal reaction force of $F_x = 250$ kN. The same results were obtained with the analytical solution for the double U-pile. The calculated horizontal displacement was $w_x = 3$ mm

The experimental results from the transversely restrained bending tests corresponded to the analytical solution for two double piles without friction in the middle interlock. Further, it was observed in the bending tests that shift of a threaded interlock was not blocked by oblique bending, not even for large or plastic deformations. These results support the premise that the theory of elasticity, presented in this section, is applicable to the investigation of oblique bending of real double-U steel sheet piles.

3.3 Reduction factors for oblique bending

3.3.1 Factors that influence oblique bending

The theory of elasticity of oblique bending shows that the reduction factors β_I and β_W depend only on the amount of transverse bending. If transverse bending is completely impeded, then $\kappa_x = 0$ and the differential equations in (3.5) and (3.6) are reduced to the differential equation for plane bending (3.3). However, if transverse bending is not impeded, the loss of structural resistance can be significant, see e.g., Table 3.2. Transverse bending is influenced either by resistance in transverse direction, such as earth pressure resistance, or by interlock friction. In practice the following factors may influence oblique bending:

- Shear resistance of the soil against the sheet pile

    When the sheet pile wall deflects in transverse direction, the retaining soil has to move in transverse direction as well. The shear resistance of the soil may hamper the transverse bending. Sand and stiff clays may give more resistance than soft clays, peat or water.

- Lateral supports

    Firstly, as a result of a lateral support, the shear force in the sheet pile wall is locally increased, which may lead to an increase of the normal stress in the interlocks and to a local increase of the friction capacity in the interlocks. Secondly, due to the addition of a lateral support, the lateral curvature is decreased and therefore the transverse curvature as well. It is not obvious that these decreases are proportional.

- Transverse supports or a capping beam

    A transverse support can have a direct influence on transverse bending.

- Soil particles in the interlock

   When sheet piles are driven into the ground and threaded to the adjacent pile(s), soil particles may intrude into the free space between both interlocks. Dilating sand grains may have a more positive effect on the interlock friction capacity than non-dilating clay particles and water without soil has no significant influence on the interlock friction.

- (Local) fixation of interlocking during excavation

   Fixation of the interlocks during excavation hampers transverse bending.

- Lubrication of interlocks

   Lubrication of the interlocks for sealing or for diminishing the driving resistance may reduce the friction capacity of the interlocks.

- Straightness of piles and the sequence of installation

   The shear resistance of the interlocks may be influenced by the deviations during installation. Pitch and drive may lead to more deviations than staggered driving. Slender piles or (re-used) bent piles may also result in more shear resistance in the interlocks, but run also the risk of declutching.

In Section 3.6 an elaborate study of the influence of these factors is presented.

3.3.2   Reduction factors according to CUR 166

CUR 166 [27] gives design rules which are based partly on local experience gained with U-piles in the Netherlands [29] and partly on engineering judgement. CUR 166 mentions the following factors that may influence oblique bending:

- Type of soil in which the sheet piles are driven

- Lubrication of free interlocks

- Number of anchors or struts (local increase of shear force)

- Local fixation of free interlocks or a capping beam

- Installation method

The reduction factors β_I and β_W are covered by the design rule given by Table 3.3.

3.3.3   Reduction factors according to ENV 1993-5

ENV 1993-5 [24] gives global directives for oblique bending. The traditional sheet pile properties W_{el}, W_{pl} and I should be determined for a continuous wall and the effective sheet pile parameters should be determined according to equations (3.1) and (3.2)

$$I_{eff} = \beta_I\,I_{continous\ wall} \tag{3.1}$$
$$W_{eff} = \beta_W\,W_{continuous\ wall} \tag{3.2}$$

Number of piles	Number of supports	Interlock fixity	Ground top	Ground bottom	Reduction factors β_I	Reduction factors β_W
1	irrelevant	irrelevant	all	all	0.35	0.6
2	0	no	sand	sand	0.7	0.8
			no sand	sand	0.6	0.7
			no sand	no sand	0.6	0.7
		yes	sand	sand	0.8	0.9
			no sand	sand	0.7	0.8
			no sand	no sand	0.6	0.7
	1	no	sand	sand	0.8	0.9
			no sand	sand	0.7	0.8
			no sand	no sand	0.7	0.8
		yes	sand	sand	0.9	1.0
			no sand	sand	0.8	0.9
			no sand	no sand	0.7	0.8
	≥ 2	no	sand	sand	0.9	1.0
			no sand	sand	0.8	0.9
			no sand	no sand	0.8	0.9
		yes	sand	sand	1.0	1.0
			no sand	sand	1.0	1.0
			no sand	no sand	0.8	0.9
3	irrelevant	irrelevant	all	all	1.0	1.0
4	irrelevant	irrelevant	all	all	1.0	1.0

- *Supports* are anchors, struts or or other concentrated lateral restraints: fixity near the pile toe is not a *support*
- *Interlock fixity* concerns only additional treatment after driving
- *Sand* includes sand, silt and unsaturated soil but not a fill
- *No sand* includes saturated clay, peat, gravel, (open) water and also a sand fill
- *Bottom* is where the cantilever moment is generated (from point of zero moment to pile toe), but below excavation level
- *Top* is above *bottom*
- For slender sections ($h/2b < 0.2$) β_D and β_B are reduced with 0.1 in case of *sand* and with 0.05 in case of *no sand*
- For *sand* above groundwater level β_D and β_B may be increased with 0.1
- Between two points of fixity of the free interlocks $\beta_D = 0.85$ and $\beta_B = 0.85$. For the part between a point of interlock fixity and a pile end, *interlock fixity* applies
- $\beta_I \leq 1$ and $\beta_W \leq 1$

Table 3.3: *Reduction factors* β_I *and* β_W *according to CUR 166 [27]*

Row	Effect	Criterion	Single pile $\Delta\beta_{I,i}$	Single pile $\Delta\beta_{W,i}$	Double pile $\Delta\beta_{I,i}$	Double pile $\Delta\beta_{W,i}$
1	Soil in the interlock	≥ medium dense sand grain size distribution and density	[ ]	[ ]	[ ]	[ ]
		≥ stiff clay	[ ]	[ ]	[ ]	[ ]
2	Soil shear resistance (oblique bending)	≥ medium dense sand soil stiffness and shear strength	0.0	0.0	[ ]	[ ]
		≥ stiff clay	0.0	0.0	[ ]	[ ]
3	Support levels	0	[ ]	[ ]	[ ]	[ ]
		1	[ ]	[ ]	[ ]	[ ]
		≥ 2	[ ]	[ ]	[ ]	[ ]
4	Fixing of interlocks	Welded	0.0	0.0	[ ]	[ ]
		Crimped	0.0	0.0	0.0	0.0
5	Interlock threaded on jobsite	Lubricated	[ ]	[ ]	[ ]	[ ]
		Weld or capping on top and fixed toe	[ ]	[ ]	[ ]	[ ]
6	Installation	[ ]	[ ]	[ ]	[ ]	[ ]

- The factors β_I and β_W are determined from

$$\beta_I = \beta_{I,0} + \sum_{i=1}^{6} \Delta\beta_{I,i} \leq [1.0] \qquad \beta_W = \beta_{W,0} + \sum_{i=1}^{6} \Delta\beta_{W,i} \leq [1.0]$$

applying the summation only over those of the six effects for which the criteria are fulfilled

- The basic values $\beta_{I,0}$ and $\beta_{W,0}$ should be determined for bare steel piles used as cantilevers, retaining water only, without the presence of any soil

- Row 1 accounts for the effect of the soil particles pressed into the void of the interlocks, thus increasing the friction. Initially the piles should be installed fully embedded into these soil layers

- Row 2 accounts for the shear resistance of the ground behind the wall, hindering the occurrence of oblique bending of double piles

- Row 3 accounts for the restraint provided by the waling

- Row 4 accounts for the higher stiffness of the welding (even if it is intermittent) compared to the crimps

- Row 5 accounts for the various possible effects on the interlock to be treated on site, that can be influenced by human intervention, such as lubrication to reduce friction and hindering of relative displacement in the interlock by fixing the top by welding or by using a capping beam, or the toe, by driving into a very stiff soil layer

- Row 6 takes into account the effect of the driving system used to install the sheet piling. Depending upon local experience, it might be useful to add to this row the driving method: panel driving, pitch and drive, *etc.*

Table 3.4: *Reduction factors* β_I *and* β_W *according to ENV 1993-5 [24]*

in which the factors β_I and β_W account for the possible loss of stiffness and strength. For Z-piles these factors are $\beta_I = [1.0]$ and $\beta_W = [1.0]$.

For U-piles in oblique bending, these factors are $\beta_I \leq [1.0]$ and $\beta_W \leq [1.0]$. According to ENV 1993-5 the factors β_I and β_W should be determined from:

$$\beta_I = \beta_{I,0} + \sum_{i=1}^{6} \Delta\beta_{I,i} \leq [1.0] \tag{3.26}$$

$$\beta_W = \beta_{W,0} + \sum_{i=1}^{6} \Delta\beta_{W,i} \leq [1.0] \tag{3.27}$$

The eigen values $\beta_{I,0}$ and $\beta_{W,0}$ are determined from the cross-sectional properties by equations (3.28) and (3.29).

$$\beta_{I,0} = 1 - \frac{I_{xy} I_{yx}}{I_{xx} I_{yy}} \tag{3.28}$$

$$\beta_{W,0} = \frac{I_{xx} I_{yy} - I_{xy} I_{yx}}{-I_{xy} x + I_{xx} y} \frac{h}{2 I_{yy}} \tag{3.29}$$

in which for $\beta_{W,0}$ the minimum value of any position (x,y) on the cross-section should be taken.

The different influences that may reduce oblique bending, are taken into account by increments $\Delta\beta_{I,i}$ and $\Delta\beta_{W,i}$. ENV 1993-5 distinguishes 6 influences, which are indicated in Table 3.4 for both single and double U-piles.

3.3.4   Discussion

Considering the cross-sectional shape of a double U-pile, oblique bending in steel sheet piling may not be neglected. The possible loss of stiffness and strength of the wall can be taken into account by the reduction factors β_I and β_W. The question is not *if* the traditionally provided stiffness and strength properties should be reduced, but *by how much*. In the Netherlands, the CUR 166 regulation is often experienced as conservative, which means that sheet pile walls become more expensive than necessary.

On the other hand the German and British regulations allow $\beta_I = 1.0$ and $\beta_W = 1.0$ for double U-piles, and it may be questioned if these regulations are too optimistic. In the British and French design practice even reduction factors $\beta_I = 1.0$ and $\beta_W = 1.0$ are often applied to single U-piles.

In spite of the strict Dutch regulation, oblique bending is hardly ever observed in practice in steel sheet piling. However, loss of stiffness for walls composed of single U-piles has been reported in literature, for example by Hebert *et al.* [40] where $\beta_I = 0.36$ to 0.42 and $\beta_W = 0.52$ to 0.68, and Gigan [35] where $\beta_I \approx 0.6$.

The different regulations in the various countries, the mutual differences between regulations and observations in most countries, and a lack of scientific evidence, were the main reasons why ENV 1993-5 gives indicative influences rather than figures in Table 3.4.

3.4 Development of a subgrade reaction model for oblique bending

3.4.1 General

The need for a proper set of reduction factors to account for oblique bending demands the development of a tool based on bending in two directions. The bending tests carried out in Liège proved that such a tool may be based on the elastic constitutive equations of (3.5). The transverse matrix method which was used for the development of PLASWALL in Chapter 2, can easily be extended for oblique bending. In this section the extension of the subgrade reaction model for oblique bending is described.

3.4.2 Analogy with a subgrade reaction model for a conventional beam

The transfer matrix method for a beam subjected to oblique bending can be solved in an analogous way to a conventional beam. The transfer point matrices for loads and springs can similarly be derived and on the basis of this analogy, a beam on a lateral and transverse elastic foundation can be analysed, see Figure 3.5.
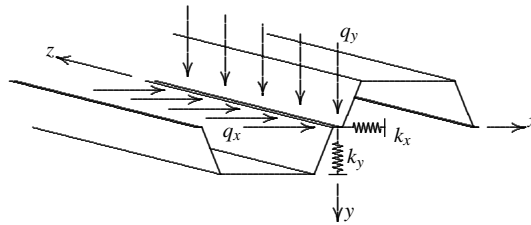
Figure 3.5: *Beam on a lateral and transverse elastic foundation*

The beam in Figure 3.5 serves as the basis for a subgrade reaction model to analyse the phenomenon of *oblique bending* in sheet piling. Such a model can be solved using the flow chart presented in Figure 2.25. However, in the *procedure springs* not only the lateral springs but also the transverse springs need to be considered.

3.4.3 Soil model for oblique bending

In Section 2.5.3 a soil model for lateral springs is described. However, as a consequence of the asymmetrical profile and the rotated neutral axis, lateral earth pressure on the wall results in a lateral and a transverse wall deflection. Oblique bending will be partially impeded if the retained material is able to bear load arising from the transverse displacement. If the sheet pile bends transversely (in plane), a shear mechanism in the soil may be developed. This shear mechanism can be taken into account with the transverse springs as follows.

In Figure 3.6 a top view of the sheet pile with both the lateral and the transverse springs is shown. The lateral spring k_y is used to model the soil which is compressed (or unloaded) and the transverse spring k_x is used to model the soil which is subjected to shear. The
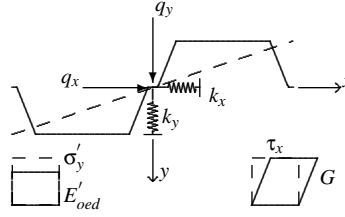
Figure 3.6: *Soil-sheet pile element used to model oblique bending*

ratio between the lateral and the transverse spring stiffnesses may be assessed from the ratio between the oedometer stiffness E'_{oed} and the shear stiffness G as follows:

$$\frac{k_x}{k_y} \equiv \frac{G}{E'_{oed}} = \frac{1 - 2\nu'}{2 - 2\nu'} \tag{3.30}$$

The maximum shear stress $\tau_{x;max}$ is dependent on the lateral effective earth pressure σ'_y and is assumed to be

$$\pm\tau_{x;max} = c' + \sigma'_y \tan \varphi' \tag{3.31}$$

The complete elasto-plastic spring model for lateral and transverse wall movement is presented in Figure 3.7.
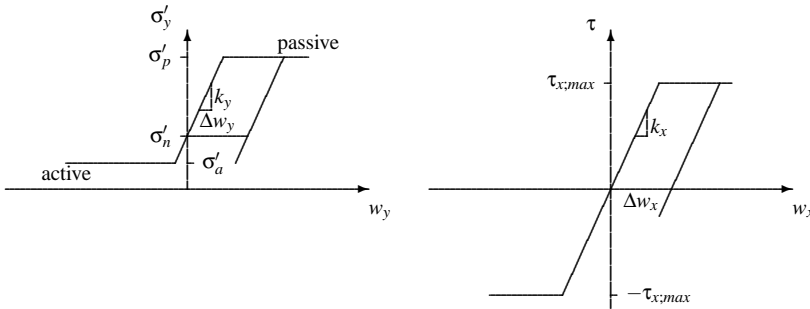
Figure 3.7: *Elasto-plastic spring model for the lateral and transverse spring*

It is noted that this soil model is a gross simplification of the real soil behaviour close to the soil-sheet pile interface. For discussion about this soil model in SKEWWALL, reference is made to Section 3.4.7.

3.4.4   Interlock friction

A second factor that may partially impede oblique bending, is *interlock friction* in the free interlocks. Interlock friction hinders transverse bending and prevents therefore weakening of the cross-sectional resistance. Interlock friction can be taken into account by interlock springs as shown in Figure 3.8.
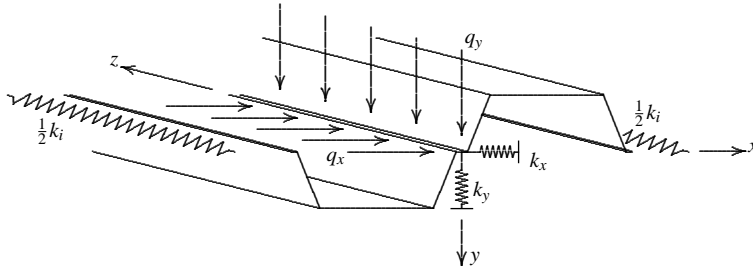
Figure 3.8: *Sheet pile with an asymmetrical cross-section restrained by springs at the interlock (see also Figure B.11)*

The transfer point matrix for the nodal interlock spring is derived in Appendix B.6.2. For realistic spring values, see Section 3.6.3.

3.4.5 Testing

On the basis of the information presented, the computer program SKEWWALL has been developed. The program consists of a conventional subgrade reaction model as described in Section 2.5, which has been extended for bending in two directions. The program calculates both lateral and transverse action effects of a sheet pile with an asymmetrical cross-section, usually a sheet pile wall composed of double U-piles. The program can calculate the maximum bending stress on the basis of

$$\sigma_{zz}(x,y) = E\left(\kappa_x x + \kappa_y y\right) \tag{3.32}$$

in which (x,y) is the most remote point from the neutral axis; this will be either the corner point between the flange and web closest to the central fixed interlock, or the outer free interlock of one double pile.

The capabilities of SKEWWALL have been tested with three cases:

- Four-point bending test from Liège

- Loss of interlock friction

- Staged excavation in multi-layered soil compared with SPW99 [87]

Four-point bending test from Liège

In the first test a comparison is made with bending tests A3 and A4, carried out for the ECSC research project at the University of Liège on two double PU 8 piles threaded together [67]. The bending tests concern a 6 metre long span loaded by two symmetrical concentrated forces at a spacing of 0.8 metre. The boundary conditions at both supports and in both directions can be considered as simply supported. The central interlock has not been treated. Both a transversely restrained and a transversely unrestrained bending test have been carried out. The test setup is presented in Figure 3.9.

PU 8 [57]	b (cm)	h (cm)	A (cm^2)	E (kN/m^2)	I_{xx} (cm^4)	I_{xy} (cm^4)	I_{yy} (cm^4)	α (^{o})
1 Double	120	28	139	2.1 10^8	183100	-33986	13953	10.95
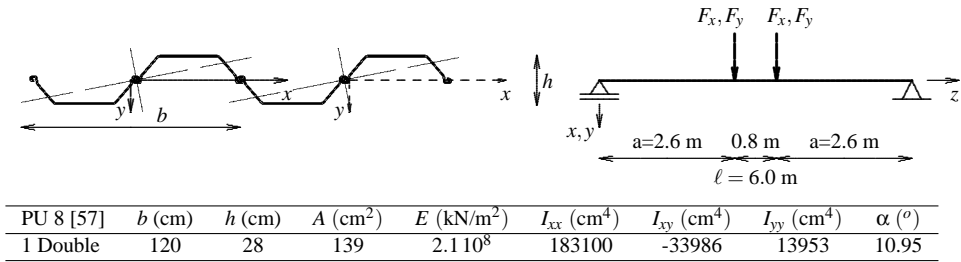
Figure 3.9: *Four point bending of two double U-piles carried out in Liège*

Both cases have been analysed using SKEWWALL and are compared to the analytical solutions from Section 3.2.3. Transversely restrained bending is modelled with concentrated forces. The calculation results are presented in Table 3.5 and show that the calculation results of SKEWWALL are compare well with the analytical solutions for both the transversely restrained and the transversely unrestrained cases.

Method	Support	F_x (kN)	F_y (kN)	w_x (mm)	w_y (mm)	k_i (kN/m^2)	f_y (MPa)
Analytical	restr.	-673	276	0	41.35	0	360
Analytical	unrestr.	0	166	8.41	45.33	0	360
Measured A3	restr.	-250	166	—	33	—	—
Measured A4	unrestr.	0	166	7	45	—	—
SKEWWALL	restr.	-250	166	3.22	32.72	0	257
SKEWWALL	restr.	-673	276	0.00	41.34	0	361
SKEWWALL	unrestr.	0	166	8.43	45.42	0	360

Table 3.5: *Validation to the four-point bending tests in Liège*

Loss of interlock friction

In the second test the same configuration of the four-point bending test from Liège is used to investigate the effects of loss of interlock friction. Infinite interlock friction represents transversely restrained bending and an interlock friction stiffness of $k_i = 0$ kN/m^2 transversely unrestrained bending. Table 3.6 shows the calculation results of a gradual loss of the interlock spring stiffness.

The calculation results show that interlock friction is significant for an interlock spring stiffness of $k_i = 100\,000$ kN/m^2 and that the interlock spring stiffness must be in the range of $k_i = 10^7$ kN/m^2 to obtain an impediment of transverse bending. These results are in the same range as the values reported by Juaristi [45], see Section 3.6.3. In this section the implementation of interlock springs is merely treated.

Furthermore, the transversely restrained case and the case with an interlock spring stiffness $k_i = 10^7$ kN/m^2 are in agreement with the analytical solution for transversely restrained bending.

On the basis of the comparison with the Liège bending test and of the analysis of interlock friction, it can be concluded that the implementation of the equations for oblique

Method	Support	F_x (kN)	F_y (kN)	w_x (mm)	w_y (mm)	k_i (kN/m^2)	f_y (MPa)
SKEWWALL	restr.	-404	166	0.01	24.90	0	217
SKEWWALL	interlock	0	166	0.14	25.21	10 000 000	222
SKEWWALL	interlock	0	166	1.21	27.81	1 000 000	238
SKEWWALL	interlock	0	166	5.22	37.60	100 000	286
SKEWWALL	interlock	0	166	7.30	42.68	25 000	319
SKEWWALL	interlock	0	166	7.94	44.23	10 000	342
SKEWWALL	interlock	0	166	8.38	45.38	1000	358
SKEWWALL	unrestr.	0	166	8.43	45.42	0	360

Table 3.6: *Loss of interlock friction*

bending in SKEWWALL and the implementation of an elastic interlock spring have been carried out successfully.

Staged excavation in multi-layered soil compared with SPW99

In the third test, a multi-staged excavation in multi-layered soil is compared with SPW99. The case is the same as treated in Section 2.5.5 for PLASWALL, see page 42. The sheet pile wall is 23 metre long. The soil consists of 17 metre of soft clay overlaying a sand layer. The groundwater level in the clay layer is 1 metre below the ground surface and the head in the sand layer is 4 metres below the original surface. Excavation takes place in three stages. In the first stage the excavation is 1 metre. Next, the first horizontal restraint is placed at 0.75 metre depth and dry excavation is carried out to 7 metres. In the third construction stage, the second strut is placed at 6.50 metres and excavation is carried out to 9.25 metres. The water level in the excavation is not lowered beyond 9.00 metres. In this stage the soil behind the sheet pile wall is unloaded. Values of relevant soil and sheet pile properties are given in Figure 3.10.
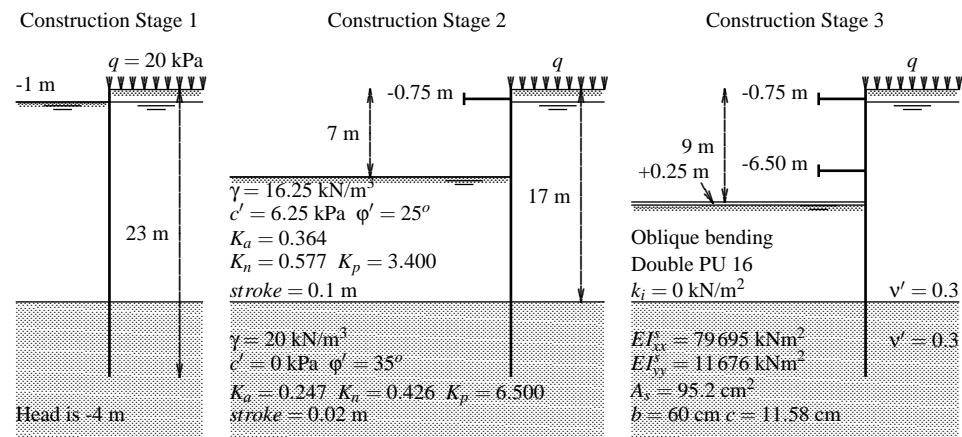
Figure 3.10: *Comparison between* SKEWWALL *and* SPW99

Calculations are made for normal bending ($EI_{xy} = 0$) and oblique bending. In the

	$w_{y,max}$(mm)	$z_{w_{y,max}}$(m)	$M_{y,max}$(kNm/m)	$z_{M_{y,max}}$(m)	f_y (MPa)
SKEWWALL[2] $EI_{xy} = 0$	184	-7.00	-645.4	-6.13	402
SPW99[2]	183	-7.00	-644.2	-6.04	—
SKEWWALL[2] $EI_{xy} \neq 0$	263	-6.75	-642.2	-6.13	544
SKEWWALL[3] $EI_{xy} = 0$	215	-9.25	-557.7	-9.35	402
SPW99[3]	217	-9.48	-535.4	-9.71	—
SKEWWALL[3] $EI_{xy} \neq 0$	303	-9.05	-551.0	-9.35	544

Table 3.7: *Calculation results of* SKEWWALL *and* SPW99 *for stage 2 and 3*

oblique bending calculation the struts support both the lateral and the transverse direction. The normal bending calculation can be compared with the SPW99 calculation. The calculated values are presented in Table 3.7.

The differences between SKEWWALL and SPW99 are less than 1% for the second construction stage and for the displacement in the third construction stage. It is noted that the results of PLASWALL (see Table 2.5) and SKEWWALL differ slightly although both programs use the same algorithm. This difference is caused by different strut stiffnesses, which appeared to be a very sensitive parameter for the calculation results of the third construction stage.
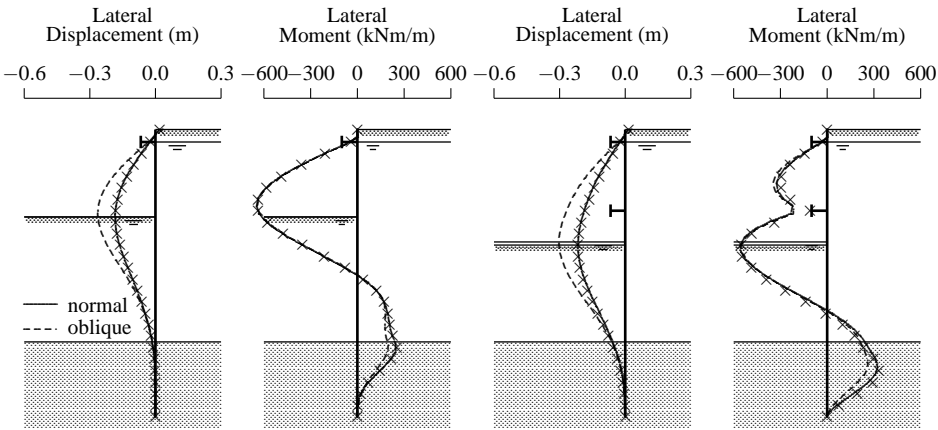
Figure 3.11: *Normal bending calculation with* SKEWWALL *compared with* SPW99 *and oblique bending calculation with* SKEWWALL. *The* ×*-marks were calculated with* SPW99

In Figure 3.11 the lateral displacements and bending moments for the second and third construction stage are presented. The results show increasing lateral displacement due to oblique bending. The lateral bending moment, however, remains practically the same, as in the calculation the lateral earth pressure distribution is hardly influenced. The increasing lateral displacement without significant change of bending moment satisfy the expectations of oblique bending.

Transverse Displacement (m) | Transverse Moment (kNm/m) | Effective Earth Pressure (kN/m²) | Transverse soil shear Resistance (kN/m²)

−0.1 0.0 0.1 −600 −300 0 300 600 −200 −100 0 100 200 −50 −25 0 25 50

Stg.2
Stg.3
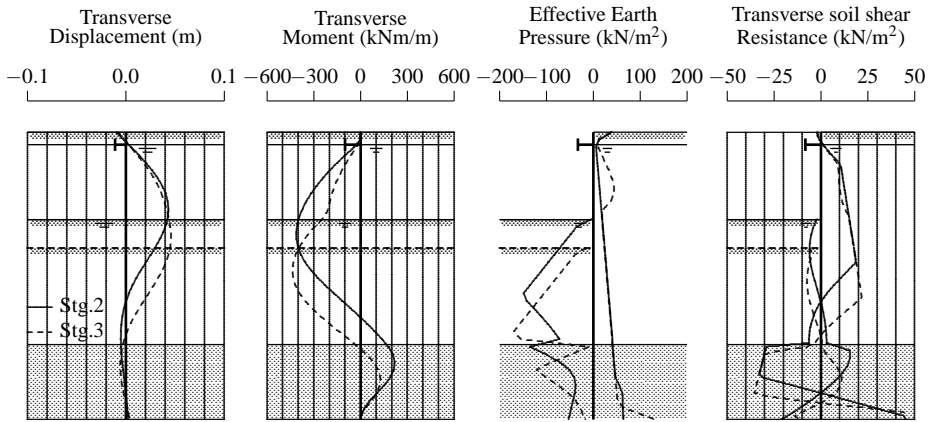
Figure 3.12: *Transverse displacements, transverse bending moments, lateral effective earth pressure and transverse soil shear resistance for the oblique bending calculation with* SKEW-WALL. *Solid lines represent Stage 2 and dashed lines Stage 3. Transverse actions are viewed from the excavation towards the retaining structure.*

Figure 3.12 shows the lateral effective earth pressure and the action effects in the transverse direction. The ultimate transverse displacement in this example is about 15% of the ultimate lateral displacement and the ratio between the ultimate transverse and lateral bending moment is about $2/3$. In Figure 3.13 the shear resistance of the soil in the transverse direction is investigated. Two calculations were carried out:

- One case in which the shear resistance in the upper layer was taken into account with equation (3.30) using $\nu' = 0.3$, denoted with *soil*

- One case in which the shear resistance in the upper layer was taken into account using $\nu' = 0.499$, denoted with *no soil*

For the lower layer $\nu' = 0.3$ was applied. In the case of *no soil*, a lower resistance to oblique bending was calculated. Further increase of lateral and transverse displacement, absence of transverse moment and of transverse shear resistance in front of and behind the wall are results which were expected.

On the basis of these calculated results, it can be concluded that the implementation of multi-staged calculations in stratified soil in SKEWWALL has been carried out successfully.
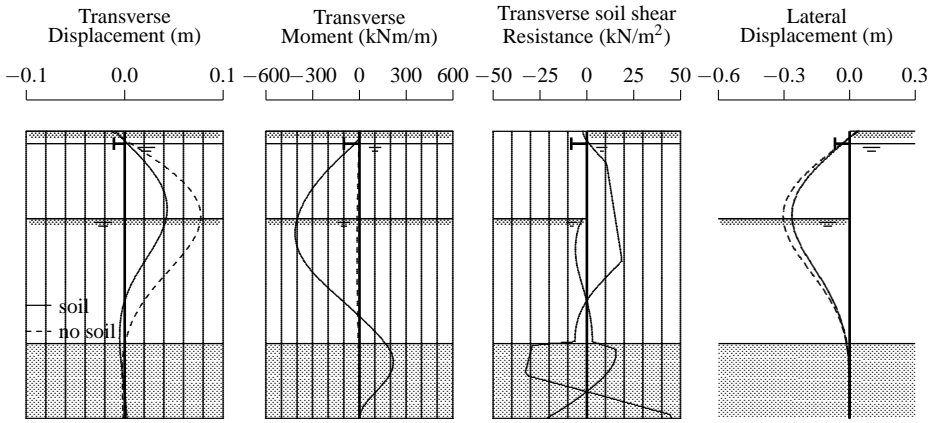
Figure 3.13: *Oblique bending with and without transverse soil restraint. Transverse actions are viewed from the excavation towards the retaining structure*

3.4.6 Method to determine the reduction factors

In this section a simplified method is proposed to derive the reduction factors β_I and β_W from a SKEWWALL calculation. When the load on the sheet pile wall is more or less equal to the normal bending case and the oblique bending case, the reduction factors β_I and β_W follow from the calculated displacements and maximum stresses for the normal bending (restrained) and the oblique bending (unrestrained) cases as follows.

$$\beta_I = \frac{w_{y,max,normal}}{w_{y,max,oblique}} \tag{3.33}$$

$$\beta_W = \frac{f_{y,normal}}{f_{y,oblique}} \tag{3.34}$$

As an example, the example in Figure 3.10 is reconsidered. The calculation results are given in Table 3.7. From equations (3.33) and (3.34) it follows that:

$$\beta_I = \frac{w_{y,max,normal}}{w_{y,max,oblique}} = \frac{184 \text{ mm}}{263 \text{ mm}} = 0.70 \tag{3.35}$$

$$\beta_W = \frac{f_{y,normal}}{f_{y,oblique}} = \frac{402 \text{ N/mm}^2}{544 \text{ N/mm}^2} = 0.74 \tag{3.36}$$

Figure 3.14 shows a comparison between a calculation in which oblique bending is taken into account by bending in two directions, and one in which oblique bending is taken into account by adopting $\beta_I = 0.7$. The results of both calculations correspond very well.

Therefore it can be concluded that equations (3.33) and (3.34) provide a good and practical method to determine the reduction factors β_I and β_W.
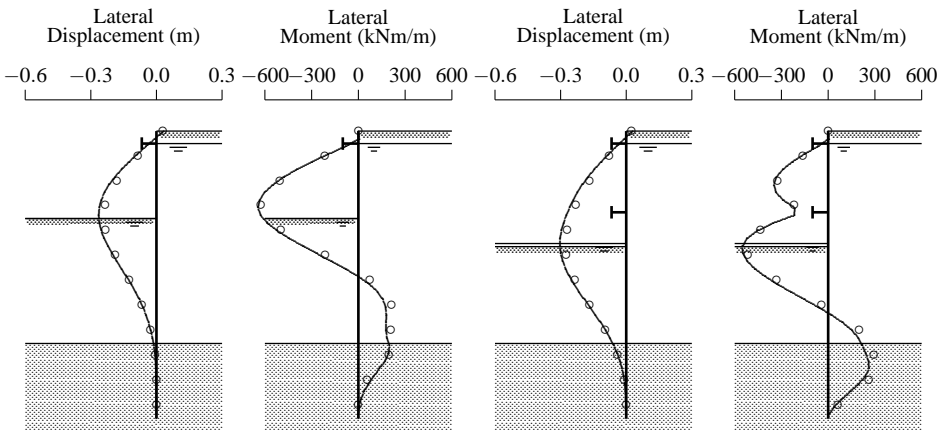
Figure 3.14: *Oblique bending calculation compared with normal bending calculation using* $\beta_I = 0.70$. *Solid lines represent the oblique bending calculation and* ∘-*marks the reduced normal bending calculation*

3.4.7 Discussion about SKEWWALL

The 3-dimensional subgrade reaction model described in this section appears to be a powerful tool to obtain insight into the oblique bending phenomenon. The calculation time is only a few minutes and therefore different configurations, such as the influence of fixity near the struts, capping beams, etc., can be quickly and easily investigated. However, the soil model in the 3-dimensional subgrade reaction model described in Section 3.4.3, is only a gross simplification of real soil behaviour; real soil behaviour at the interface with a sheet pile which deflects both in lateral and transverse directions, is a complex 3-dimensional stress- and strain dependent problem. A serious attempt to model this complex behaviour with simple elasto-plastic springs to account for the various failure modes in the soil, friction between soil and the sheet pile in both transverse and vertical directions, arching effects in the soil, etc., would be inappropriate.

A better option to validate the soil model of SKEWWALL would be to verify it against a 3-dimensional finite element calculation using a soil model that is able to model the complex 3-dimensional soil behaviour. Such a verification is made in the next section.

3.5 Validation of SKEWWALL to 3D FE calculations

3.5.1 General

In this section the soil model in SKEWWALL is validated against 3-dimensional finite element calculations made with DIANA 7.0 [96]. The reference case is an academic case developed by Aukema and Joling [2] to study the phenomenon of oblique bending. Hockx [42] used this case to investigate the effect of various structural measures to reduce the

effect of oblique bending [1]. The robustness of this case has been proven by Groen [36].

3.5.2 The reference case in DIANA

The reference case used for the DIANA calculations considers an infinite wall composed of double PU 8 sections [57] of 9 m length, retaining an excavation in sand. The soil body is initially loaded with a surcharge of $q = 10$ kPa, which is in later stages maintained only on the retaining side. Excavation is taken into account by gradual removal of soil elements in layers of 0.9 m thick, to a maximum excavation depth of 4.5 m. The sand is modelled with the Modified Mohr-Coulomb model. Relevant dimensions and soil properties are given in Figure 3.15.
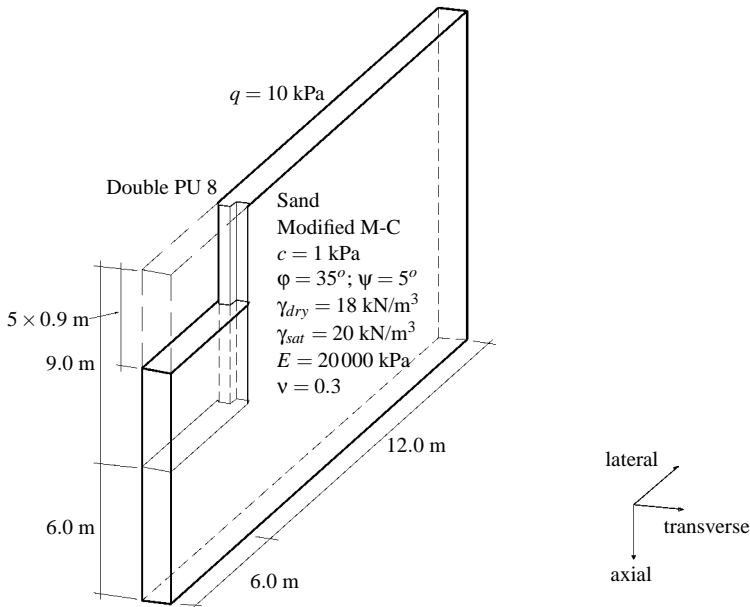
Figure 3.15: *Reference case for the* DIANA *calculations*

The finite element mesh for the soil body and the sheet pile is presented in Figure 3.16. The soil is modelled with 20-noded brick elements of type CHX60. The boundary conditions are chosen such that an infinite sheet pile wall is modelled, by applying *tyings* between the two transverse planes of the mesh. The sheet pile is modelled with 8-noded curved Mindlin shell elements, type CQ40S. The geometry of the sheet pile is close to the properties of a PU 8. Relevant properties of the sheet pile compared to the PU 8 are given in Table 3.8.

The interface between soil and structure is modelled with tyings. To avoid singularities, the soil and sheet pile are tied in lateral and transverse directions. In the axial direction the soil and sheet pile are also tied to model a perfectly rough wall. Groundwater is taken

---

[1]The contributions from the graduation works of Aukema & Joling and Hockx are gratefully appreciated.
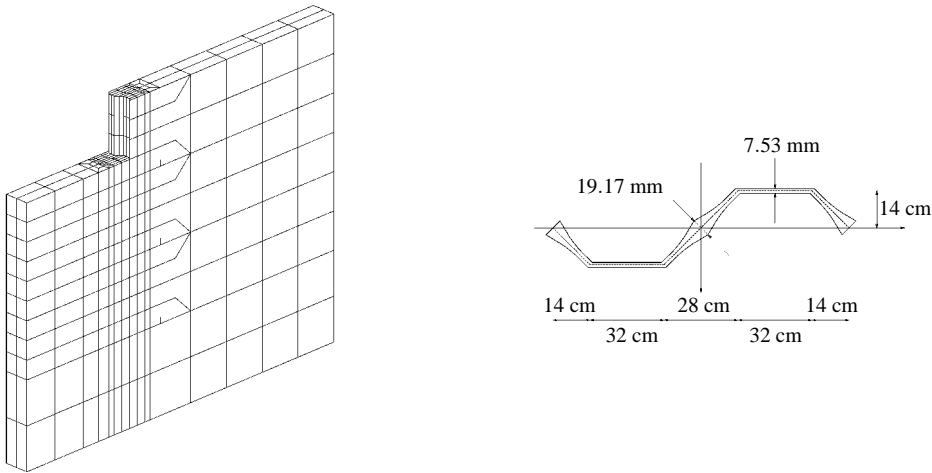
Figure 3.16: *Finite element mesh for soil and sheet pile*

	$A_s(\text{cm}^2)$	c (cm)	$I_{xx}(\text{cm}^4)$	$I_{xy}(\text{cm}^4)$	$I_{yy}(\text{cm}^4)$	$I_1(\text{cm}^4)$	$I_2(\text{cm}^4)$	$\alpha(^o)$
PU 8	69.5	8.15	183100	-33986	13953	7367	189673	10.95
Model pile	69.3	8.66	183143	-35990	13953	6615	190481	11.52
$E = 2.1\ 10^8\ \text{kN/m}^2$								

Table 3.8: *Properties of model pile compared with the PU 8*

into account by effective volume weight and by a water pressure difference acting as a face load in lateral direction. Slippage between the interlocks is also modelled with tyings. Each interlock can be modelled either as perfectly free (no tyings in the axial direction), or as perfectly fixed (tyings in the axial direction). The influence of a restraint on top of the wall is modelled with additional *supports* (boundary conditions).

This reference model can be easily adapted to investigate the behaviour of a double pile or a continuous wall or to investigate the effects of different boundary conditions, such as lateral and transverse supports and a capping beam [2]. The following configurations are compared:

- Cantilever wall without groundwater

  - Double PU 8 transversely unrestrained
  - Double PU 8 with capping beam on top
  - Double PU 8 with horizontal restraint on top
  - Double PU 8 blocking the shifted interlock displacements above the excavation level after each excavation step
  - Continuous PU 8

---

[2]A capping beam is modelled by boundary conditions $\varphi_x = 0$ and $V_x = 0$.

- Propped wall with groundwater

    - Double PU 8 transversely unrestrained

    - Double PU 8 with horizontal restraint on top

    - Continuous PU 8

The basic reduction factors $\beta_{I,0}$ and $\beta_{W,0}$ are derived from the cross-sectional properties by equations (3.28) and (3.29). It follows that $\beta_{I,0} = 0.49$ and $\beta_{W,0} = 0.61$. The reduction factors β_I and β_W have been determined using the method explained in Section 3.4.6.

3.5.3 Validation for the cantilever wall

The calculations with SKEWWALL were fitted to the results of the continuous wall from DIANA. The earth pressure coefficients were determined using the earth pressure theory of Müller-Breslau. Comparable results for the cantilever wall could be obtained with a subgrade reaction modulus of $k = 30,000$ kN/m^3.

DIANA Cantilever wall	w_x(mm)	w_y(mm)	M_y(kNm/m)	f_y (N/mm^2)	β_I	β_W
Transversely unrestrained	12.89	-88.80	82.27	175	0.59	0.61
Capping beam	4.50	-71.33	82.02	144	0.73	0.74
Horizontally restrained	0.00	-69.47	81.49	142	0.75	0.75
Welding	-1.21	-62.05	81.48	128	0.84	0.84
Continuous	0.00	-52.09	82.03	107	1.00	1.00
SKEWWALL Cantilever wall	w_x(mm)	w_y(mm)	M_y(kNm/m)	f_y (N/mm^2)	β_I	β_W
Transversely unrestrained	5.67	-72.93	84.60	152	0.65	0.67
Capping beam	1.67	-62.41	84.60	142	0.75	0.72
Horizontally restrained	1.35	-61.13	84.70	139	0.77	0.73
Continuous		-47.06	84.90	102	1.00	1.00

Table 3.9: *Calculation results of* DIANA *and* SKEWWALL *for the cantilever wall retaining the excavation without groundwater*

Figure 3.17 shows the lateral and transverse displacements and the lateral bending moment of the cantilever wall calculated with DIANAand with SKEWWALL. A tabular overview with calculation results of DIANA and SKEWWALL is presented in Table 3.9. In this table w_x and w_y represents the displacements of the top of the wall in the transverse and lateral directions, M_y, the maximum lateral bending moment and f_y, the minimum required yield stress.

The DIANA and SKEWWALL calculations give comparable results. The bending moments in lateral direction are in close agreement, as are the lateral displacements, when the global wall translation in DIANA is disregarded. With regard to the reduction factors β_I and β_W, almost the same values are found.

Both calculations indicate that structural measures, such as provision of a capping beam, horizontal restraint, or welding of the shifted interlocks during the excavation let increase the structural resistance of the sheet pile. In this case, both calculations indicate that horizontal restraint is hardly any better than a capping beam.
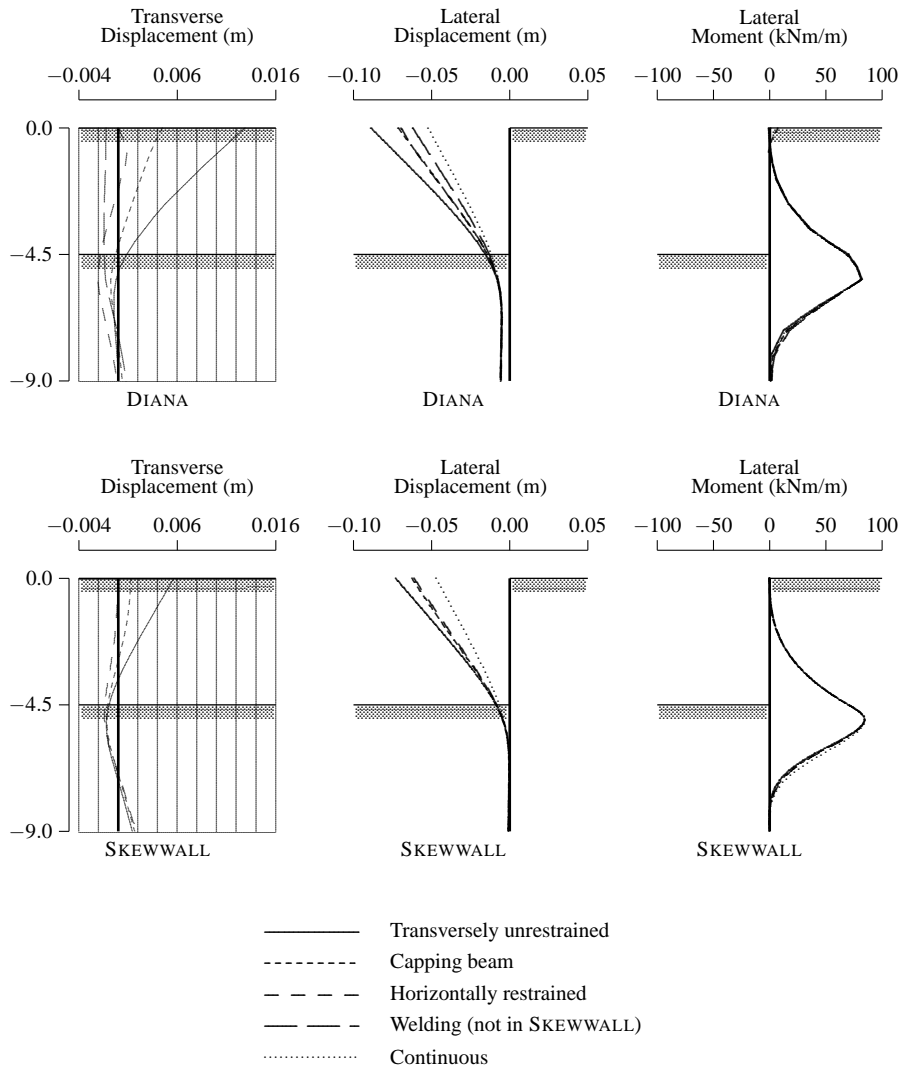
Figure 3.17: *Calculation results of* DIANA *and* SKEWWALL *for the cantilever wall in dry sand. Transverse results are viewed from the excavation towards the sheet pile wall.*

In the case of the transversely unrestrained cantilever wall, the reduction factor on the bending stiffness increases from $\beta_{I,0} = 0.49$ to $\beta_I = 0.59$ according to DIANA and from $\beta_{I,0} = 0.49$ to $\beta_I = 0.65$ according to SKEWWALL. The increase itself can be explained by the soil-structure interaction in general, which has an influence on oblique bending, and the difference in increase between DIANA and SKEWWALL by the different methods of modelling that soil-structure interaction.

From this comparison between the SKEWWALL and the DIANA calculations it can be concluded that SKEWWALL gives reliable results for the calculation of cantilever walls.

3.5.4 Validation of the propped wall

The calculations for the propped wall using SKEWWALL were fitted to the results of the continuous wall from DIANA in the same way as for the cantilever wall. A subgrade reaction modulus of $k = 2500$ kN/m^3 was required.

Figure 3.18 shows the lateral and transverse displacements and the lateral bending moment of the propped wall calculated with DIANA and with SKEWWALL. A summary of the calculation results of DIANA and SKEWWALL is presented in Table 3.10.

DIANA						
Propped wall	w_x(mm)	w_y(mm)	M_y(kNm/m)	f_y (N/mm^2)	β_I	β_W
Transversely unrestrained	2.43	-51.61	-134.28	291	0.69	0.62
Horizontally restrained	7.24	-50.60	-130.77	278	0.70	0.65
Continuous	0.00	-35.60	-143.85	181	1.00	1.00
SKEWWALL						
Propped wall	w_x(mm)	w_y(mm)	M_y(kNm/m)	f_y (N/mm^2)	β_I	β_W
Transversely unrestrained	2.88	-51.36	-114.8	261	0.74	0.61
Horizontally restrained	6.48	-50.51	-116.4	247	0.75	0.65
Continuous	0.00	-38.08	-132.8	160	1.00	1.00

Table 3.10: *Calculation results of* DIANA *and* SKEWWALL *for the propped wall retaining the excavation with groundwater*

As for the cantilever wall, the DIANA and SKEWWALL calculations give comparable results for the propped wall, with both bending moments and lateral displacements in close agreement.

The shape of the transverse displacement line is also comparable, apart from the displacement of the wall toe. This difference can be explained from the modelling of the boundary conditions near the toe of the sheet pile wall. In DIANA the wall toe is tied to the underlying soil elements, and because the bottom of the mesh is supported in all directions, the toe of the wall is hardly able to move in transverse direction. In SKEWWALL, on the other hand, the toe of the wall is modelled with a free boundary condition, in both lateral and transverse directions. It has been verified that the shape of the transverse wall movement was in close agreement with the DIANA calculation when the pile toe was modelled in SKEWWALL by a hinged support. The effects of this support on the action effects in the lateral direction, however, were negligible.

The reduction factors calculated with SKEWWALL are in a quite good agreement with the factors from DIANA. Both calculations indicate that the effect of a transverse support is negligible for the effective wall stiffness but has a slight influence on the minimum required yield stress. In the case of the transversely unrestrained propped wall, the loss of stiffness seems to be not so drastic as for the cantilever wall. However, the simple structural measure to restrain the top of the propped sheet pile also in the transverse direction has a negligible effect on the action effects in the lateral direction.

From this comparison between the SKEWWALL and the DIANA calculations it can be concluded that SKEWWALL gives reliable results for the calculation of propped walls.
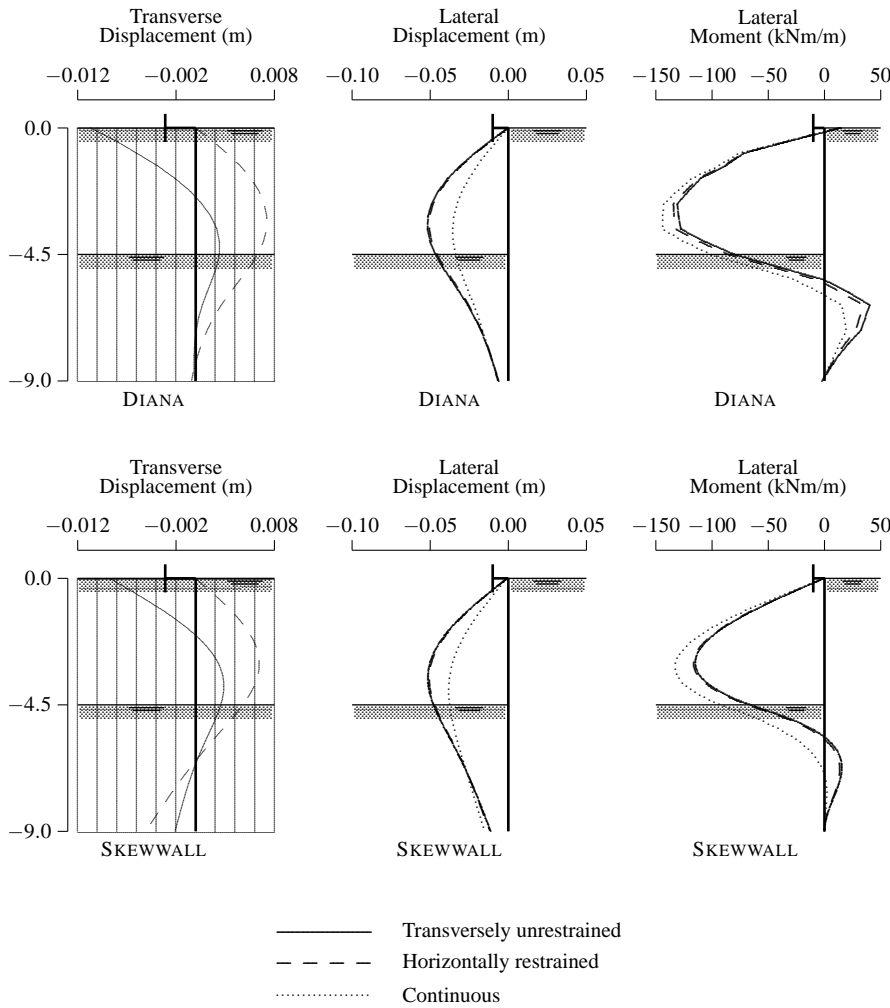
Figure 3.18: *Calculation results of* DIANA *for the propped wall in saturated sand. Transverse results are viewed from the excavation towards the sheet pile wall.*

3.5.5 Evaluation of the comparison

In the preceding sections the calculation results of SKEWWALL have been tested against two 3D cases calculated with DIANA. The tests show that both the β_I and the β_W factors determined with DIANA and SKEWWALL correspond quite well.

SKEWWALL is proven to be a useful tool to investigate oblique bending and to determine suitable reduction factors that can be applied in design to account for the loss of strength and stiffness due to oblique bending.

3.6 Quantification of factors influencing oblique bending

3.6.1 General

In Section 3.3.1 some important factors were discussed that may influence oblique bending, such as soil particles in free interlocks, structural detailing of struts, walings or welding of interlocks, and pile installation.

In this section these factors are quantified. SKEWWALL is used as a tool to investigate the influence of different kind of soils and of different structural detailing. For other factors, where the influence could not be determined with SKEWWALL, use is made of full-scale experiments available from literature.

3.6.2 Influence of structural supports and shear resistance of soil

The influence of lateral and transverse supports and a capping beam has been investigated with more than 100 SKEWWALL calculations, and the DIANA calculations from Section 3.5.

The configurations are subdivided into cantilever walls and propped walls, which are either retaining, or not retaining, soil, see Figure 3.19. Two different soil types were used: one representing a soft clay and one a medium dense sand. The stratification was either one or two layers and the boundary was chosen such that in the lower layer a cantilever moment could be generated whenever possible.

| Cantilever wall without soil | Cantilever wall with soil | Propped wall without soil | Propped wall with soil |

	γ_{dry} (kN/m^3)	γ_{sat} (kN/m^3)	c' (kPa)	φ' (^{o})	δ (^{o})	ν' -	k (kN/m^3)	K_a -	K_0 -	K_p -
clay	15	15	5	20	13.3	0.3	5000	0.442	0.66	2.75
sand	18	20	1	30	20	0.2	20000	0.3	0.5	5.3
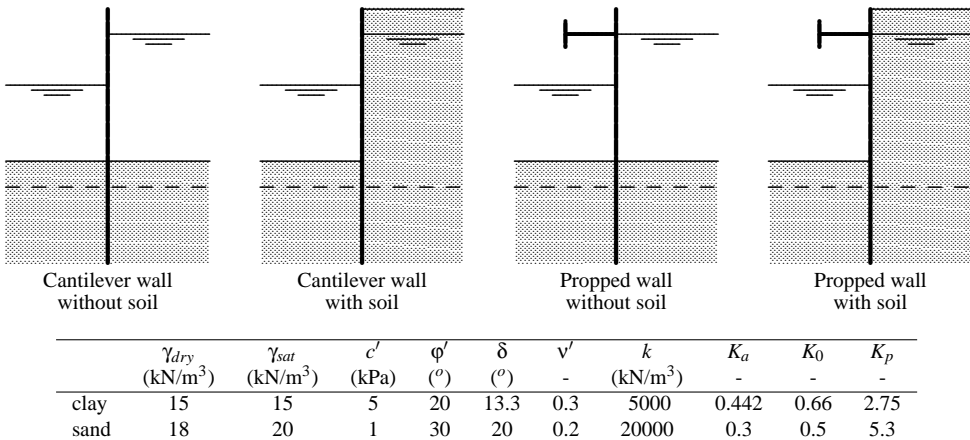
Figure 3.19: *Definition of configurations*

The calculations with SKEWWALL indicated that the shear resistance of the soil in the transverse direction gives a positive contribution to the impediment of oblique bending. However, it could not be concluded that the soil type (i.e., sandy or clayey soil) was an important factor in the impediment of oblique bending. Therefore distinguish is only made between *with soil* and *without soil*. Figure 3.20 shows a categorised set of reduction factors β_I and β_W. From this figure the following observations are made:

- There is no clear relationship between the loss of strength of a cantilever wall or a propped wall, and the $\beta_{I,0}$ of a sheet pile section
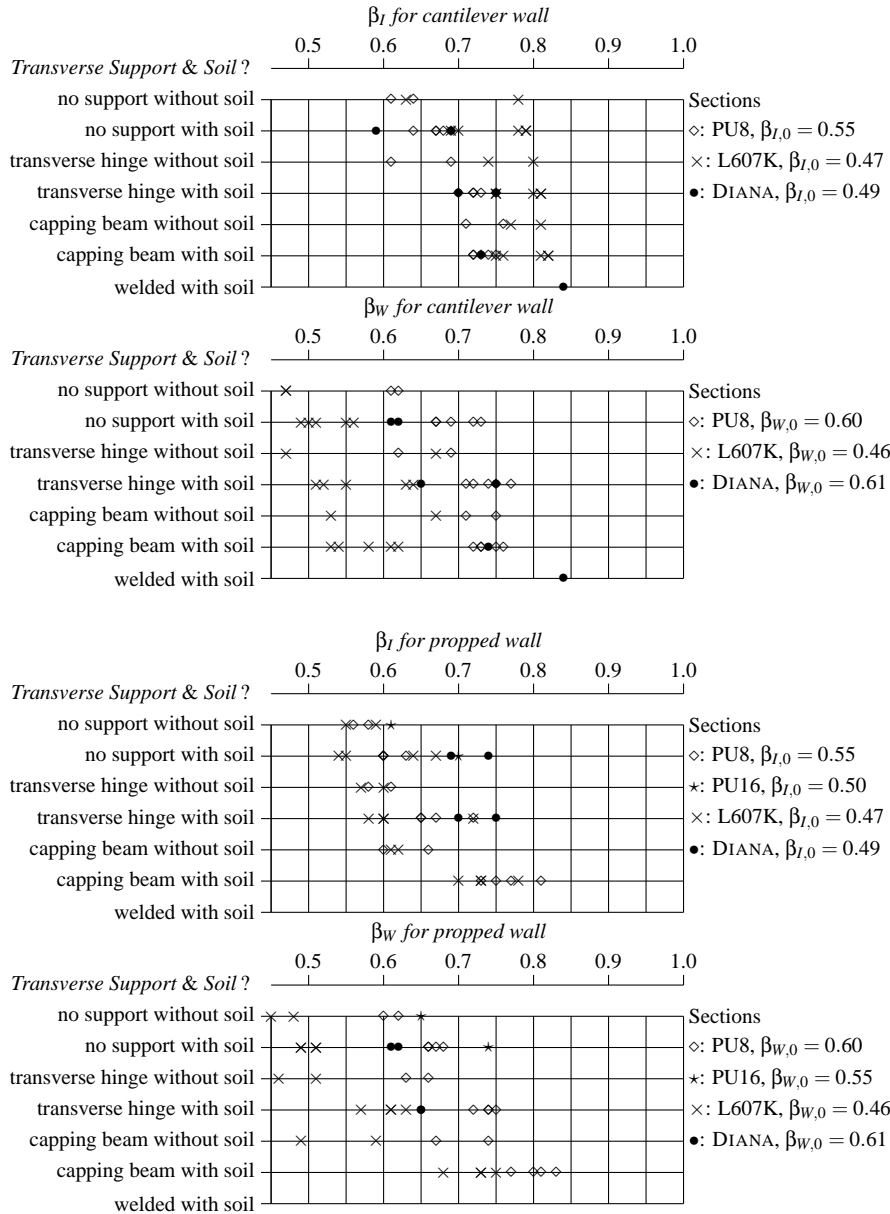
Figure 3.20: *Reduction factors for cantilever and propped walls*

- There can be a constant difference recognised between the $\beta_{W,0}$ of a sheet pile section and the β_W resulting from the calculations

- Both soil resistance behind the sheet pile and transverse supports contribute to the reduction of oblique bending

- In the case of a cantilever wall, a transverse restraint and a capping beam may be treated equally

- In the case of a propped wall, a transverse restraint at the prop does not give additional resistance against oblique bending

Based on these observations it is proposed to apply incremental factors for β_I and β_W to take the effects due to structural supports and shear resistance of the soil into account, as proposed by ENV 1993-5.

The following conclusions can be made as a basis of design, with respect to β_I:

- For a cantilever wall, a minimum value of $\beta_{I,0} = 0.60$ and for a propped wall a minimum value of $\beta_{I,0} = 0.55$ may be applied, provided that the sheet pile wall can be defined as a geotechnical construction

- In the case of a cantilever wall, β_I may be increased with $\Delta\beta_{I,support} = 0.10$ when a transverse restraint or a capping beam is applied to the top

- In the case of a propped wall, $\beta_{I,0}$ may be increased with $\Delta\beta_{I,support} = 0.05$ when a capping beam is applied to the top

- For all sheet pile walls embedded in soil β_I may be increased with $\Delta\beta_{I,soil} = 0.05$, unless the sheet pile wall is retaining just water (no soil) or a backfill

With respect to β_W the following conclusions are made:

- For both a cantilever and a propped wall a minimum value of $\beta_{W,0}$ should be applied in accordance with the structural properties

- For a cantilever wall, β_W may be increased with $\Delta\beta_{W,support} = 0.05$ when a transverse restraint or a capping beam is applied to the top

- For a propped wall $\beta_{W,0}$ may be increased with $\Delta\beta_{W,support} = 0.10$ when a capping beam is applied to the top

- For all sheet pile walls embedded in soil β_W may be increased with $\Delta\beta_{W,soil} = 0.10$, unless the sheet pile wall is retaining just water (no soil) or a backfill

3.6.3 Influence of interlock friction

Juaristi [45] and Vanden Berghe *et al.* [77, 78] conducted a series of experiments to determine the influence of intruded soil particles on friction in the free interlocks. A cylindrical tank with two clutches ($d = 0.625$ m, $h = 1.5$ m) was filled with sand of a known density and subsequently a test specimen, consisting of two clutches welded together, was driven

Soil	Yellow med. dense	Yellow loose	Grey
k_i (kN/m^2)	26,300	2,600	12,600
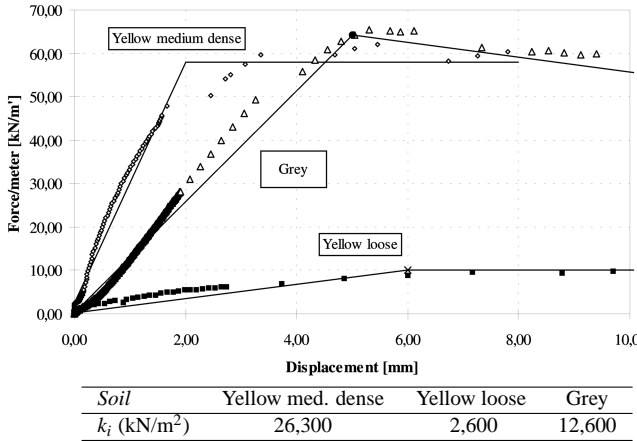
Figure 3.21: *Experimental determination of interlock spring laws, conducted by Juaristi [45]*

in the two receptive clutches using a small vibrator. Next the pile was extracted and at the same time the load displacement curve was measured, see Figure 3.21.

The load-displacement curve can be approximated by a simplified bi-linear spring law, from which the interlock spring stiffness parameter k_i can be derived. Two different kinds of sands were used: *Yellow* or *Fine Sand* ($d_{50} = 0.18$ mm, $d_{60}/d_{10} = 2.22$) and *Grey* or *Coarse Sand* ($d_{50} = 0.63$ mm, $d_{60}/d_{10} = 2.65$). The maximum interlock spring stiffness observed in the tests was order of magnitude $k_i = 25,000$ kN/m^2.

The calculation in Figure 3.22 was used to compare the order of magnitude of measured interlock spring stiffness to that required to impede oblique bending. A simply supported double PU 8 sheet pile loaded with a concentrated load is subjected to different levels of interlock friction. The presented calculations show that an interlock spring stiffness in the order of $k_i = 100,000$ kN/m^2 to $k_i = 10,000,000$ kN/m^2 is required to obtain a significant reduction of the vertical displacement. In the case of an interlock spring stiffness of $k_i = 25,000$ kN/m^2 the reduction factors increase with $\Delta\beta_I = 0.03$ and $\Delta\beta_W = 0.07$.
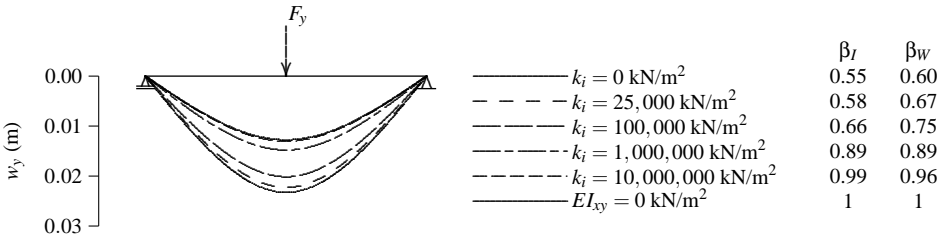
Figure 3.22: *Vertical displacement w_y of a beam in three-point bending as function of different levels of interlock friction*

Comparing $k_i = 25,000$ kN/m^2 observed in the experiments to the minimum value of $k_i = 100,000$ kN/m^2 to obtain a significant reduction of the vertical displacement, the fol-

lowing recommendations are proposed:

- In loosely packed sand ($q_c \leq 20$ N/mm^2) intrusion of soil particles in the free space within the free interlocks will not lead to a significant reduction in oblique bending

- In densely packed sand ($q_c \geq 20$ N/mm^2) intrusion of soil particles in the free space between the driving interlocks may lead to a small reduction of oblique bending. For this case $\beta_{I,0}$ may be increased with $\Delta\beta_{I,interlock} = 0.05$ and $\beta_{W,0}$ with $\Delta\beta_{W,interlock} = 0.05$

Vanden Berghe *et al.* [77] reported two additional tests in saturated sand. For each test series the CPT cone resistance and duration of vibrodriving were comparable. The interlock resistance was reduced to about 20% of the original value when the pile was installed in the saturated sand. Vanden Berghe *et al.* suggest that the loss is the result of liquefaction induced during the vibrodriving; the liquefaction of the sand increases mobility of sand in the interlock and it can escape, reducing the interlock resistance.

It is, however, questionable whether the mechanism described by Vanden Berghe *et al.*is still valid for pile driving in deeper densely packed sand layers, as typically found in the Netherlands. Therefore the presented proposals do not distinguish dry or saturated soil.

3.6.4 Influence of welding during excavation

The influence of welding during excavation is investigated for the cantilever wall using the DIANA calculations, see Table 3.9. These calculations show that for the cantilever wall considerably more resistance against oblique bending may be expected than when a short weld is made near the pile top immediately after installation (capping beam). Therefore the following directives are proposed:

- In all cases β_I may be increased with $\Delta\beta_{I,weld} = 0.20$

- In all cases β_W may be increased with $\Delta\beta_{W,weld} = 0.20$

3.6.5 Influence of pile installation

The shear resistance of the interlocks may be influenced by deviations during installation. There are several different methods available to install the sheet piles in the ground. The most common methods are *pitch and drive*, in which the (double) piles are installed one by one to the full depth, *panel driving* in which a panel of piles is installed in one or more stages to the full depth, and *staggered driving* in which piles are installed in turn as follows: first pile 1, 3 and 5, then pile 2 and 4, etc. Piles can be installed in the ground either by pushing, vibrating or driving.

With regard to reduction of oblique bending, the greater the interlock friction that is developed, the more the oblique bending is reduced. Slender piles or (re-used) bent piles may also generate more shear resistance in the interlocks. In practice, steel sheet piles are never installed perfectly straight and are never installed with the same installation imperfections.

> *A general rule of thumb is that the driving techniques with the greatest risk of declutching give the highest resistance against oblique bending.*

The effect of pile installation on oblique bending is illustrated with two cases.
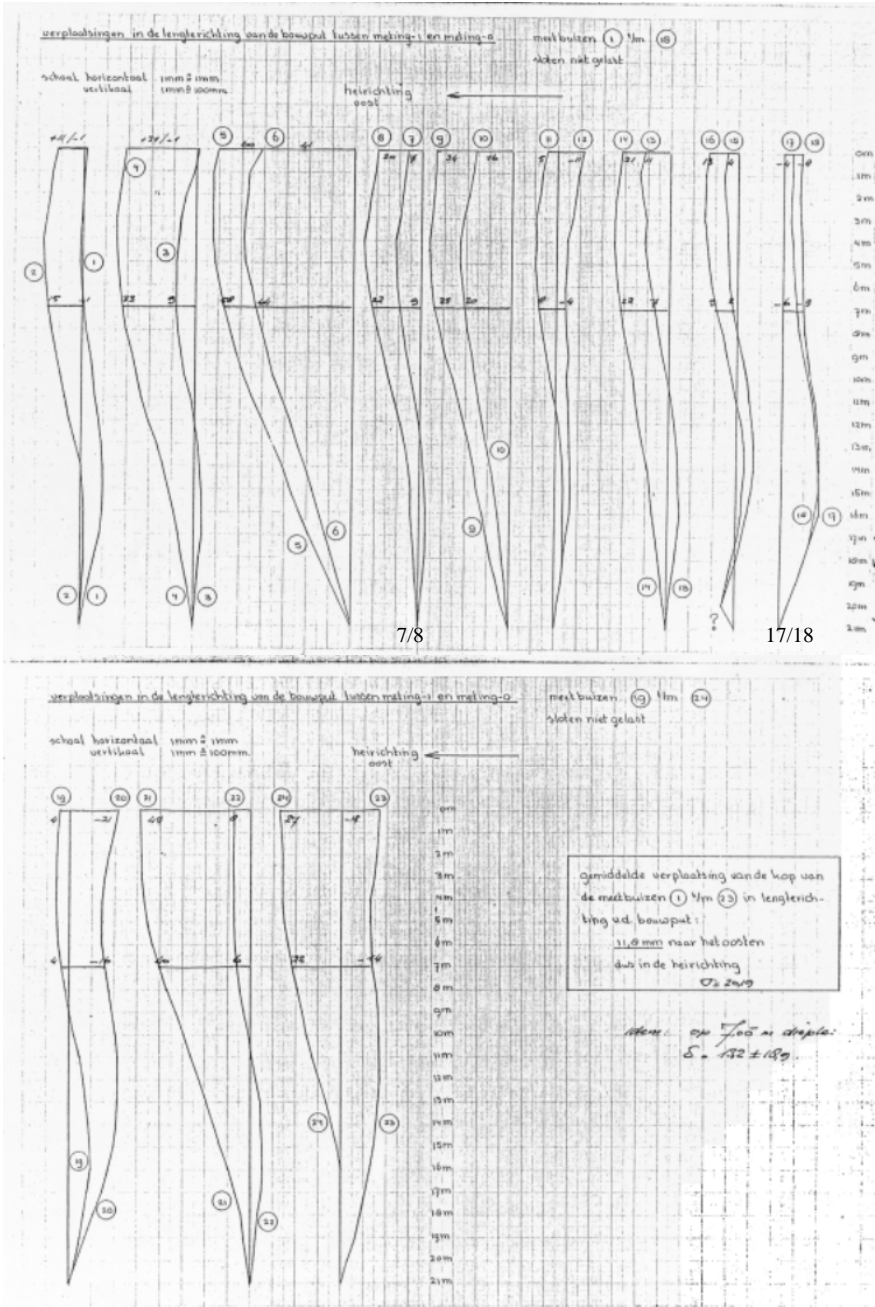
Figure 3.23: *Transverse bending of a series of double U-piles, measured in Schiedam [6]*

Case 1

The first case concerns a full-scale field test carried out by Bats and Smit in 1985 [6] for the construction of a metro in Rotterdam. 12 Pairs of Larssen V sections, 21 m long, retained an 8 m deep excavation and were laterally restrained at the top. The central interlocks of the pile pairs were crimped and the piles were driven into the ground by the pitch and drive method. Bats and Smit reported the occurrence of both lateral and transverse lean of 0.25 m at 8 m depth and 0.8 m at 21 m depth, and an average rotation around the driving interlocks of 22° due to pile driving.

Figure 3.23 shows the transverse displacement of the 12 pile pairs after excavation. The transverse curvature is an indication of oblique bending. Each pair of piles shows different transverse bending behaviour; some piles, e.g., pair 7/8 show transverse curvature, other piles, e.g., pair 17/18 show no transverse curvature at all.

This case illustrates the importance of pile driving to oblique bending. The large twist between the individual piles due to imperfect pile driving, causes high contact forces between the threaded driving interlocks. Obviously these contact forces were in some pile pairs, e.g., pair 17/18, higher than in other pile pairs, e.g., pair 7/8.

It is evident that a designer may not rely on *imperfect pile driving*. Imperfect pile driving implies a high risk of declutching and can even lead to a loss of the complete structure.

Case 2

The second case concerns the Rotterdam sheet pile wall field test, for which reference is made to Chapter 4. Figure 3.24 shows the transverse displacement of three non-adjacent pile pairs. These piles were vibrated to the required depth using the pitch and drive method; the rig was equipped with a leader. Both the design team and the installation team strived for as perfect a pile installation as possible.
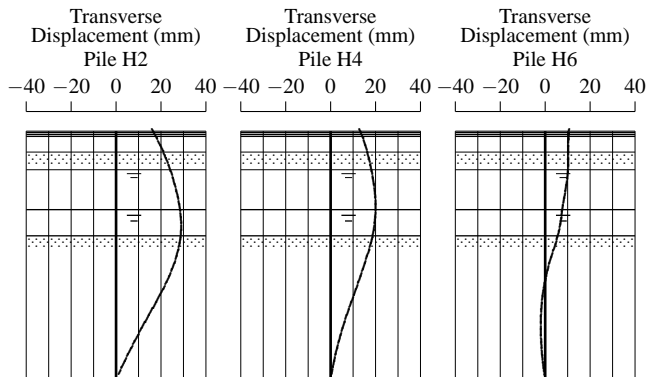
Figure 3.24: *May 11 1999: results in transverse direction for a ±5.5 m deep excavation*

The piles H2 and H4 clearly show the occurrence of oblique bending, pile H2 more than H4. In H6, the amount of oblique bending is even smaller. The reduction factors for the stiffness were $\beta_I = 0.57$ in H2, $\beta_I = 0.68$ in H4 and $\beta_I = 0.76$ in H6, see also Section 6.3.

The explanation for this global wall behaviour is most probably that the closing pile of the excavation was close to pile H6, which was installed with much more effort than the other piles, see Section 4.3.1. As pile installation was the only variable for these three piles, it can be stated that the contribution of pile installation was $\Delta\beta_{I,installation} = 0.1$ for pile H4 and $\Delta\beta_{I,installation} = 0.2$ for pile H6.

This case illustrates that even when perfect pile driving is strived for, there will always be some driving imperfections that cause high contact forces between the driving interlocks.

Evaluation on pile installation

It is evident that the designer should not rely on *imperfect pile installation*. However, the practice of pile installation obviously shows that there will be some imperfections and that some friction in the free interlocks may be taken into account. An exception should be made for installation by pushing. This technique is often chosen to install the sheet piles in the ground in a more controlled way. Therefore it may be expected that the contact forces between the driving interlocks are significantly smaller than in cases of pile vibrating or pile driving.

Information about the magnitude of $\Delta\beta_{I,installation}$ and $\Delta\beta_{W,installation}$ is scarce. In the three piles from the Rotterdam Sheet Pile Wall Field Test an average of $\beta_I = 0.7$ was found with a deviation of ± 0.1. This 0.1 may be regarded as an average value that accounts for pile installation: $\Delta\beta_{I,installation} = 0.10$. According to Figure 3.22 an appropriate increment for $\Delta\beta_W$ would be $\Delta\beta_{W,installation} = 0.15$.

In order to prevent the designer from specifying bad driving techniques, the following proposal is made to account for pile driving:

- When piles are installed by pushing:

    - $\Delta\beta_{I,installation} = 0.00$ and $\Delta\beta_{W,installation} = 0.00$

- For the other pile installation techniques:

    - $\Delta\beta_{I,installation} = 0.10$ and $\Delta\beta_{W,installation} = 0.15$

This proposal does not include techniques that are aimed at decreasing the driving resistance, such as making use of friction reducers, water jetting and boring at the free interlocks.

3.7   A new design method for oblique bending

On the basis of the analyses made in the preceding sections, a new design rule is proposed to take oblique bending into account. This method assumes that the traditional sheet pile properties W_{el}, W_{pl} and I are determined for a continuous wall.

The effective sheet pile parameters should be determined according to equations (3.1) and (3.2)

$$I_{eff} = \beta_I\, I_{continous\ wall} \tag{3.1}$$
$$W_{eff} = \beta_W\, W_{continuous\ wall} \tag{3.2}$$

The factors β_I and β_W should be determined from:

$$\beta_I = \beta_{I,0} + \sum_{i=1}^{3} \Delta\beta_{I,i} + \max\left(\Delta\beta_{I,A}, \Delta\beta_{I,B}, \Delta\beta_{I,C}\right) \leq 1.00 \tag{3.37}$$

$$\beta_W = \beta_{W,0} + \sum_{i=1}^{3} \Delta\beta_{W,i} + \max\left(\Delta\beta_{W,A}, \Delta\beta_{W,B}, \Delta\beta_{W,C}\right) \leq 1.00 \tag{3.38}$$

where the eigen values $\beta_{I,0}$ and $\beta_{W,0}$ are determined from the cross-sectional properties by equations (3.39) and (3.40).

$$\beta_{I,0} = 1 - \frac{I_{xy}\,I_{yx}}{I_{xx}\,I_{yy}} \tag{3.39}$$

$$\beta_{W,0} = \frac{I_{xx}\,I_{yy} - I_{xy}\,I_{yx}}{-I_{xy}\,x + I_{xx}\,y} \frac{h}{2\,I_{yy}} \tag{3.40}$$

where for $\beta_{W,0}$ the minimum value of any point (x,y) on the cross-section should be taken and a minimum value for the stiffness may be applied of

- $\beta_{I,0} \geq 0.60$ in the case of a cantilever wall

- $\beta_{I,0} \geq 0.55$ in the case of a propped wall

and where the different influences that may reduce oblique bending, are taken into account by increments $\Delta\beta_{I,i}$ and $\Delta\beta_{W,i}$ in accordance with Table 3.11.

The increments in Row 1 to 3 may be added to $\beta_{I,0}$ and $\beta_{W,0}$ and for those in Row A to C, only the maximum value may be taken, because these rows are all related to interlock friction.

It is noted that as a result of the scatter in the calculation results in Figure 3.20, the factors are chosen such that rather conservative factors might be obtained.

Row	Effect	Criterion	Double pile	
			$\Delta\beta_{I,i}$	$\Delta\beta_{W,i}$
The following influences may be added				
1	Soil shear resistance (due to transverse bending)	Cohesive or frictional soil	0.05	0.10
		Water or a backfill	0.00	0.00
2	Transverse supports in case of 0 lateral supports	No support	0.00	0.00
		Simply supported	0.10	0.05
		Weld or capping beam at top	0.10	0.05
3	Transverse supports in case of ≥ 1 lateral supports	No support	0.00	0.00
		Simply supported	0.00	0.00
		Weld or capping beam at top	0.05	0.10
For the following influences, the maximum value may be taken				
A	Soil in the interlock	$q_c \geq 20$ N/mm^2 or $R_e \geq 0.75$	0.05	0.05
		$q_c < 20$ N/mm^2 or $R_e < 0.75$ or lubricated interlocks	0.00	0.00
B	Treatment of driving interlocks	Lubricated	0.00	0.00
		Welded during excavation	0.20	0.20
C	Driving into the soil	Pushed or lubricated interlocks	0.00	0.00
		Other installation methods	0.10	0.15

- The factors β_I and β_W are determined from

$$\beta_I = \beta_{I,0} + \sum_{i=1}^{3} \Delta\beta_{I,i} + \max\left(\Delta\beta_{I,A}, \Delta\beta_{I,B}, \Delta\beta_{I,C}\right) \leq 1.00$$

$$\beta_W = \beta_{W,0} + \sum_{i=1}^{3} \Delta\beta_{W,i} + \max\left(\Delta\beta_{W,A}, \Delta\beta_{W,B}, \Delta\beta_{W,C}\right) \leq 1.00$$

  applying the operation only over those of the six effects for which the criteria are fulfilled

- The eigen values $\beta_{I,0}$ and $\beta_{W,0}$ should be determined from the structural properties of the cross-section of the double-U pile. For a cantilever wall a minimum value of $\beta_{I,0} = 0.60$ may be taken and for a propped wall a minimum value of $\beta_{I,0} = 0.55$

- Row 1 accounts for the shear resistance of the ground behind the wall, hindering the occurrence of oblique bending of double piles

- Row 2 accounts for the transverse restraint provided by the waling of a cantilever wall. The transverse support must be installed prior to excavation

- Row 3 accounts for the transverse restraint provided by the waling of a propped wall. The transverse support must be installed prior to excavation

- Row A accounts for the effect of the soil particles pressed into the void of the interlocks, thus increasing the friction. Initially the piles should be installed fully embedded into these soil layers. When the piles are only partly installed in the soil layer, $\Delta\beta_I$ and $\Delta\beta_W$ should be reduced proportionally

- Row B accounts for the various possible effects on the interlock to be treated on site, that can be influenced by human intervention, such as lubrication to reduce friction and welding of the free interlocks during excavation to prevent the interlocks from slipping

- Row C takes into account the effect of the driving system used to install the sheet piling into the ground. Row C excludes techniques that are aimed at decreasing the driving resistance, such as making use of friction reducers, water jetting and boring at the free interlocks.

Table 3.11: *Reduction factors β_I and β_W for double-U sheet pile walls*

3.8   Design examples

3.8.1   Cantilever wall

In Figure 3.25 the case of a cantilever wall in sand is considered. A double PU 8 [57]
($I = 13940$ cm^4/m, $W = 830$ cm^3/m) sheet pile wall of 12 m length retains a 4 m deep exca-
vation. The wall is not supported laterally and simply supported at the top in the transverse
direction. The sheet pile wall is vibrated into sand with a relative density of $R_e = 0.75$. The
driving interlocks are not treated. The design values of the other relevant parameters are
given in the figure.
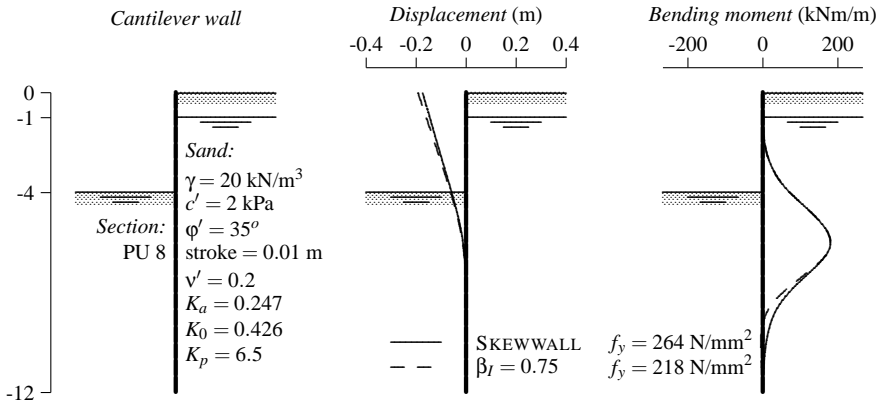
Figure 3.25: *Design example and calculation results of a cantilever wall*

According to Table 3.11 the following reduction factors should be applied:

$$\beta_I = \beta_{I,0} + \sum_{i=1}^{3} \Delta\beta_{I,i} + \max\left(\Delta\beta_{I,A}, \Delta\beta_{I,B}, \Delta\beta_{I,C}\right) \leq 1.00 \tag{3.37}$$

$$\beta_W = \beta_{W,0} + \sum_{i=1}^{3} \Delta\beta_{W,i} + \max\left(\Delta\beta_{W,A}, \Delta\beta_{W,B}, \Delta\beta_{W,C}\right) \leq 1.00 \tag{3.38}$$

Zero values: A PU 8 section has $\beta_{I,0} = 0.55$ and $\beta_{W,0} = 0.60 \rightarrow \beta_{I,0} = 0.60$ and $\beta_{W,0} = 0.60$

Row 1: The advantageous effects of shear resistance of the soil may be taken into account
→ $\Delta\beta_{I,1} = 0.05$ and $\Delta\beta_{W,1} = 0.10$

Row 2: No support in the lateral direction and simply supported in the transverse direction
→ $\Delta\beta_{I,2} = 0.10$ and $\Delta\beta_{W,2} = 0.05$

Row 3: Not applicable

Row A: The advantageous effects of intrusion of soil particles into the free interlocks may
be fully taken into account → $\Delta\beta_{I,A} = 0.05$ and $\Delta\beta_{W,A} = 0.05$

Row B: Not applicable

Row C: The sheet pile wall is installed by vibrating $\rightarrow \Delta\beta_{I,C} = 0.10$ and $\Delta\beta_{W,C} = 0.15$

It follows that

$$\beta_I = \beta_{I,0} + \sum_{i=1}^{3} \Delta\beta_{I,i} + \max\left(\Delta\beta_{I,A}, \Delta\beta_{I,B}, \Delta\beta_{I,C}\right) = 0.85 \tag{3.41}$$

$$\beta_W = \beta_{W,0} + \sum_{i=1}^{3} \Delta\beta_{W,i} + \max\left(\Delta\beta_{W,A}, \Delta\beta_{W,B}, \Delta\beta_{W,C}\right) = 0.90 \tag{3.42}$$

When the practical influences of row A and C are not taken into account, a reduction factor would have been found of $\beta_I = 0.75$ and $\beta_W = 0.75$. These factors are required for a comparison with SKEWWALL. Figure 3.25 shows the lateral displacements and lateral bending moments calculated with SKEWWALL, compared to a conventional calculation using a reduction factor of $\beta_I = 0.75$. The maximum displacement with $\beta_I = 0.75$ is 11% larger than that calculated with SKEWWALL. The factor β_W following from SKEWWALL, is derived from the calculated maximum steel stresses f_y, such that

$$\beta_W = \frac{218}{264} = 0.83 \tag{3.43}$$

This factor is less conservative than $\beta_W = 0.75$ determined with Table 3.11 without practical influences. The calculations show that in this example the theoretical result for both β_I and β_W is rather conservative. However, when the installation effects are taken into account, the results according to Table 3.11 are quite acceptable.

CUR 166 [27] recommends the following reduction factors for this case: $\beta_I = 0.80$ and $\beta_W = 0.90$.

3.8.2 Propped wall

The second case concerns a propped wall retaining sand. The sheet pile wall is composed of double U Larssen 606 sections [44] ($I = 54370 \text{ cm}^4/\text{m}$, $W = 2500 \text{ cm}^3/\text{m}$) and the excavation is 7 m deep. The wall is supported at the top in both lateral and transverse direction. Although the soil properties above and below excavation level are assumed to be identical, the relative density of the sand is $R_e = 0.70$ above excavation level and $R_e = 0.80$ below excavation level. The piles are installed by driving. The driving interlocks are not lubricated. The design values of the other relevant parameters are given in Figure 3.26.
According to Table 3.11 the following reduction factors should be applied:

$$\beta_I = \beta_{I,0} + \sum_{i=1}^{3} \Delta\beta_{I,i} + \max\left(\Delta\beta_{I,A}, \Delta\beta_{I,B}, \Delta\beta_{I,C}\right) \leq 1.00 \tag{3.37}$$

$$\beta_W = \beta_{W,0} + \sum_{i=1}^{3} \Delta\beta_{W,i} + \max\left(\Delta\beta_{W,A}, \Delta\beta_{W,B}, \Delta\beta_{W,C}\right) \leq 1.00 \tag{3.38}$$

Zero values: A Larssen 606 section has $\beta_{I,0} = 0.51$ and $\beta_{W,0} = 0.54 \rightarrow \Delta\beta_{I,0} = 0.55$ and $\Delta\beta_{W,0} = 0.54$
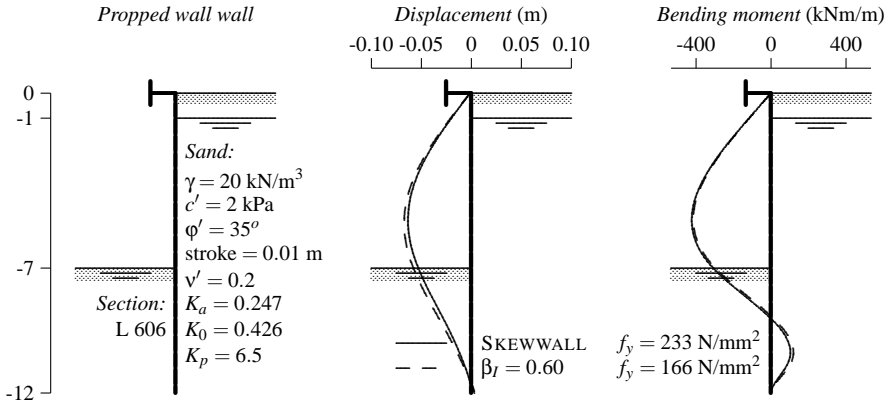
Figure 3.26: *Design example and calculation results of a propped wall*

Row 1: The advantageous effects of shear resistance of the soil are not dependent on R_e and may be taken into account $\rightarrow \Delta\beta_{I,1} = 0.05$ and $\Delta\beta_{W,1} = 0.10$

Row 2: Not applicable

Row 3: Simply supported in the lateral direction and simply supported in transverse direction $\rightarrow \Delta\beta_{I,3} = 0.00$ and $\Delta\beta_{W,3} = 0.00$

Row A: As a result of the relative density of the soil layers, the advantageous effects of intrusion of soil particles into the free interlocks may be taken into account from a depth of 7 m and below. Therefore $\Delta\beta_{I,A} = 7/12 \times 0.05 = 0.03$ and $\Delta\beta_{W,A} = 7/12 \times 0.05 = 0.03 \rightarrow \Delta\beta_{I,A} = 0.03$ and $\Delta\beta_{W,A} = 0.03$

Row B: Not applicable

Row C: The sheet pile wall is installed by vibrating $\rightarrow \Delta\beta_{I,C} = 0.10$ and $\Delta\beta_{W,C} = 0.15$

It follows that

$$\beta_I = \beta_{I,0} + \sum_{i=1}^{3} \Delta\beta_{I,i} + \max\left(\Delta\beta_{I,A}, \Delta\beta_{I,B}, \Delta\beta_{I,C}\right) = 0.70 \qquad (3.44)$$

$$\beta_W = \beta_{W,0} + \sum_{i=1}^{3} \Delta\beta_{W,i} + \max\left(\Delta\beta_{W,A}, \Delta\beta_{W,B}, \Delta\beta_{W,C}\right) = 0.79 \qquad (3.45)$$

When the practical influences of row A and C are not taken into account, a reduction factor would have been found of $\beta_I = 0.60$ and $\beta_W = 0.64$. These factors are required for a comparison with SKEWWALL. Figure 3.26 shows the lateral displacements and the lateral bending moments calculated with SKEWWALL, compared to a conventional calculation using a reduction factor of $\beta_I = 0.60$. The maximum displacement with $\beta_I = 0.60$ is only 6% larger than that calculated with SKEWWALL. The real factor β_W required for this case is derived from the calculated maximum stresses f_y, such that

$$\beta_W = \frac{168}{233} = 0.72 \qquad (3.46)$$

This factor is less conservative than $\beta_W = 0.64$ determined with Table 3.11 without practical influences.

The calculations show that for this example Table 3.11 gives an good result for β_I but a rather conservative result for β_W.

CUR 166 [27] recommends the following reduction factors for this case: $\beta_I = 0.80$ and $\beta_W = 0.90$.

Chapter 4

Sheet pile wall field test in Rotterdam

4.1   Introduction

4.1.1   Motivation and aims

The development of Structural Eurocodes described in Chapter 1 together with the developed knowledge about plastic design and oblique bending presented in Chapters 2 and 3 were the inspiration behind a full-scale field test in which plastic design and oblique bending were topics of research.

In 1993 a full-scale sheet pile wall field test was carried out in Karlsruhe by the Institute of Soil Mechanics and Rock Mechanics of the University of Karlsruhe (D) in close cooperation with the Dutch Centre for Civil Engineering Research and Codes (CUR). This test involved a 5 metre deep excavation retained by a 6 metre long single supported sheet pile wall composed of lightweight trench sheeting sections KD VI of HOESCH (D) ($W = 242$ cm^3). The subsoil consisted of dry sand and the groundwater level was 0.5 m below the excavation. Motivation for the Karlsruhe field test was to 'investigate the possibilities and limitations of calculation tools with respect to the prediction of wall displacements'. For this test, 43 predictions were made as well as a number of recalculations based on the field measurements. For a detailed report of this field test, see Von Wolffersdorff [88].

Also in 1993 drafting of ENV 1993-5 started. It was intended to include design rules that would account for plastic design and oblique bending, and therefore the ECSC research project mentioned in Chapter 1 was initiated.

For drafting of ENV 1993-5, missing knowledge concerning the structural behaviour of the sheet pile could be provided but several questions concerning the soil structure interaction in practical situations remained.

Two of the remaining problems that justify a full-scale field test are the following:

- The effects of moment redistribution due to a plastic hinge can be demonstrated numerically with various soil-structure interaction models but have never been validated in an actual practical case

- Oblique bending is hardly ever observed in practice, but the reason could not be explained from an extensive programme of laboratory tests. Therefore it is not known whether oblique bending can occur in practice and what loss of structural resistance it involves

These issues regarding the design of steel sheet pile walls inspired the Geotechnical Laboratory of Delft University of Technology and the Dutch Centre for Civil Engineering Research and Codes (CUR) to initiate a full-scale sheet pile wall field test in very weak clay and peat and with a high groundwater level. In this sheet pile wall field test research was focused on:

- the performance of a sheet pile wall with a plastic hinge

- the performance of a sheet pile wall composed of double U-sections (oblique bending)

- the short-term and the long-term performance of both sheet pile walls in very soft soil

For this field test an excavation of approximately 12 metres square was constructed in which two test walls were included. One test wall consisted of *AZ13-sections* and the second test wall comprised *double U-piles Larssen 607K*. The two side walls were composed of *single U-piles LX32*. Four slurry walls and four special interface piles which are cut along almost their full length, had to ensure that both the test wall and the active soil wedge behave more or less independently from the surrounding soil, so that a situation as close as possible to a plane strain behaviour was obtained. An overview of all the technical drawings is given in Appendix E.

A prediction exercise also formed part of this field test. The aims of the prediction exercise were to determine the state-of-the-art of the available models for analysis of steel sheet pile walls in soft soil and to introduce the new phenoma of plastic design and oblique bending to practising design engineers. The prediction exercise and the results of the predictions submitted, are presented in Chapter 5.

In this chapter the test setup is described and the measured results are reported. In Chapter 6 the test results are evaluated in more detail and several back-analyses with the subgrade reaction and the finite element methods are presented.

4.1.2 Location

The test site was situated near Pernis, which is a suburb west of Rotterdam, and formed part of the construction site for the Benelux metro line in Rotterdam. In the Pernisserpark a small area of land was available, about 20×50 metre, where the field test could be carried out.

4.1.3   Project organisation

The project organisation is illustrated by the chart in Figure 4.1 and was supervised by CUR committee C119. Partners in C119 were all national and international parties who were involved in the test. An international scientific advisory committee was founded, who had the task of advising on the design and progress of the field test.
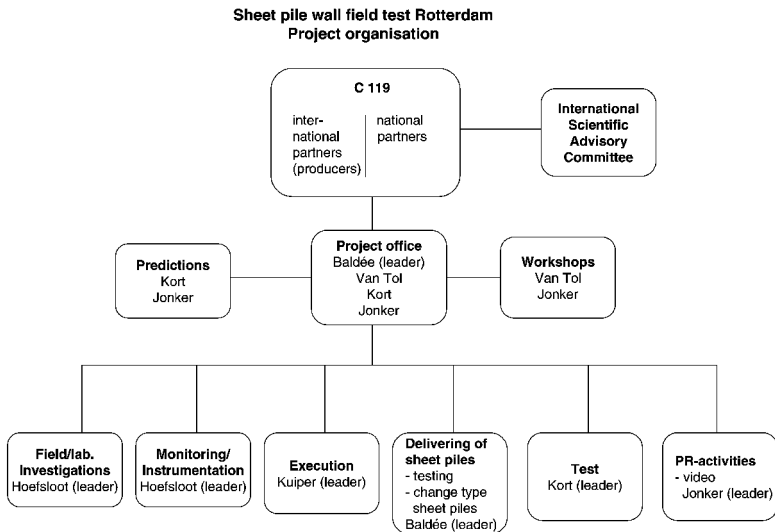
Figure 4.1: *Project organisation of the Rotterdam sheet pile wall field test*

Daily management was provided by a *project office*, consisting of four members of committee C119. The *project office* was also required to advise Committee C119, to organise the prediction exercise and workshops, and to manage the progress of several parts of the test: soil investigation, monitoring, execution aspects, delivering of sheet piles, the actual test and PR-activities. For each specific part of the test small workgroups were created, supervised by a member of committee C119 and by at least one member of *project office*.

4.2   Pretesting

The structural behaviour of the AZ13-wall was investigated with three four-point bending tests. One bending test was carried out prior to the field test on a specimen which was fabricated using a pile from the same rolling as most of the AZ13 piles used in the field test. The other two bending tests were carried out after the field test on the piles A3 and A4 which actually were used in the field test. The aims of the bending tests were:

- To determine the moment-rotation curve ($M - \varphi$ curve), the moment-curvature curve ($M - \kappa$ curve) and the ultimate bending resistance M_u of the AZ13-test pile

- To verify the measurement procedure of the bending moment from strain gauges

- To verify the instrumentation plan for the strain gauges as was foreseen for the field test, including positioning and protection of gauges and lead wires

In the first bending test it was noted that the structural behaviour was less stiff than expected. A clear explanation for this loss of stiffness was not found, and therefore the structural behaviour of this first bending test is not considered in this thesis.

The instrumentation plan was verified by forming an epoxy strip covering the strain gauges and lead wires. In the field test such a strip is necessary to protect the strain gauges and lead wires from damage during transport, handling and driving of the piles. The influence of the epoxy strip on the stiffness of the pile appeared to be negligible. Furthermore, the instrumentation continued functioning even after the sheet pile had buckled. Figure 4.2 shows the ductile behaviour of the epoxy strip when the sheet pile was subjected to large deformations.
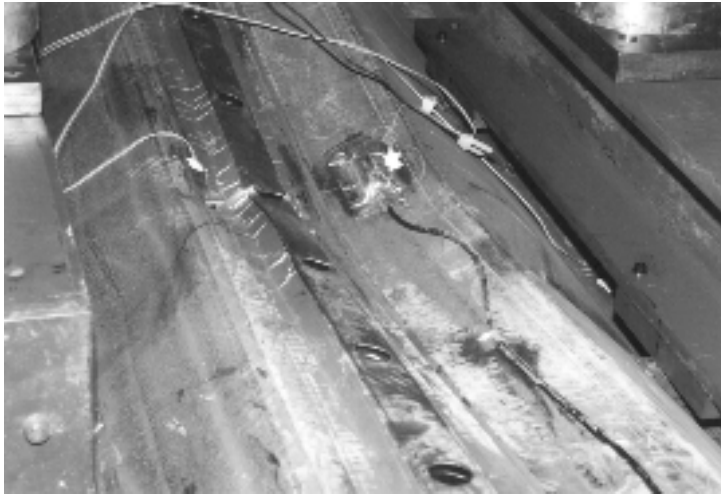
Figure 4.2: *Epoxy protection strip subjected to large deformatons*

After the field test, two tests on piles A3 and A4 were carried out. The aim of these tests was to determine a representative $M - \kappa$ curve which could be used to determine the bending moment from the strain measured in the field test. The test setup is presented in Figure 4.3 and the measured $M - \varphi$ curves and $M - \kappa$ curves of piles A3 and A4 in Figures 4.4 and 4.5. The elastic behaviour of the two additional bending tests is in agreement with the theoretical behaviour. The moment capacity of the piles decreased with increasing plastic curvature because of the loss of stability of the cross-section due to yielding and buckling of the compression flange; this mechanism is explained in Section 2.3.2.

An overview of the test results is given in Table 4.1 and the test specimens are close to the boundary of a Class 1 and a Class 2 section, see Table 2.3. It is noted that this cross-section is suitable for the purpose of the field test, as plastic design using Class 2 cross-sections is allowed; see also the design examples in Section 2.7.

After the field test, when the test piles had been extracted, six coupons 0.5 m long were cut from the toe of the six AZ13 test piles A1 to A6 for tensile testing. The numbering
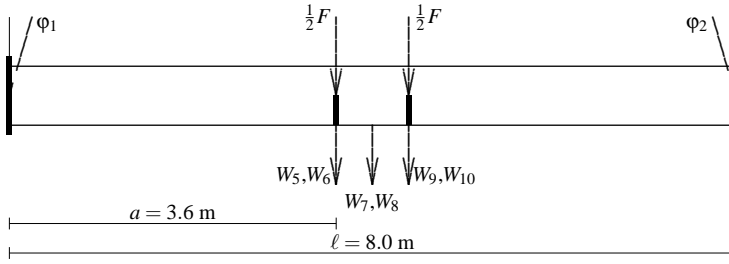
Figure 4.3: *Setup of the four point bending tests on Piles A3 and A4*
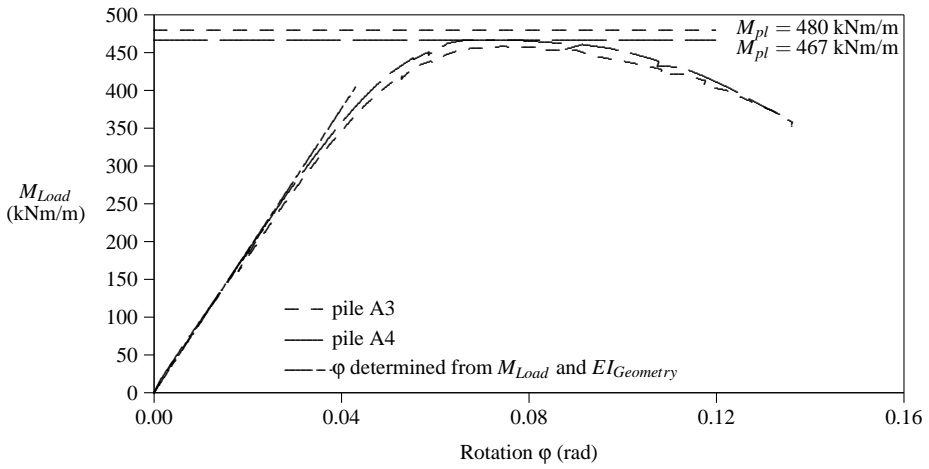
Figure 4.4: *Moment-rotation curve determined from the bending tests at TNO [12]*
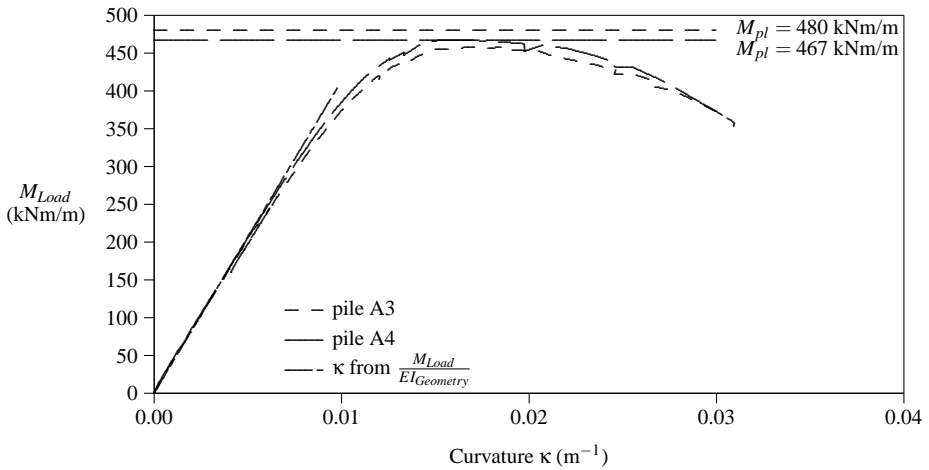
Figure 4.5: *Moment-curvature curve, determined from the bending tests at TNO [12]*

pile	b	A	I	W	b_f	t_f	f_y	$\frac{b_f}{t_f\varepsilon}$	W_{pl}	M_{pl}	M_u
	mm	cm^2	cm^4	cm^3	mm	mm	MPa		cm^3	kNm/m	kNm/m
A3	1354	184	26851	1752	383	9.6	314	46.1	2050	480	458
A4	1356	182	25636	1697	387	9.7	315	46.1	1985	467	467
catalogue	1340	183	26400	1740	360	9.5					

Table 4.1: *Structural properties of pile A3 and pile A4, determined with a four-point bending test, compared with characteristics from the catalogue [57]*

of the tested flanges and webs is indicated in Figure 4.6 and is in accordance with Annex A of prEN 10248-1:1993 [23]. The tensile tests were carried out in accordance with EN 10002-1:1991 [19].
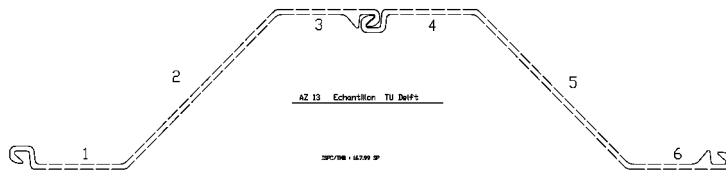
Figure 4.6: *Position of the specimen in the cross-section*

The results of the tensile tests are presented in Table 4.2. It is clearly shown from the test results that the test piles have been manufactured in two rolling processes. In one process the average yield stress was about $f_{y;L} = 300$ N/mm^2 and in the other, $f_{y;L} = 330$ N/mm^2. The piles A1 and A6 have a higher yield stress because these piles were not part of the original two rolling processes.

Pile	Position	A mm^2	t mm	$f_{y;L}$ N/mm^2	$f_{y;M}$ N/mm^2
A1	3	283.1	9.42	363.9	482.2
	5	277.5	9.25	364.0	488.3
A2	1	276.9	9.20	330.4	429.7
	2	279.0	9.30	342.3	433.7
	6	268.5	8.95	301.7	413.4
A3	3	263.1	8.80	311.6	425.7
	5	280.5	9.35	308.4	424.2
	6	268.8	8.96	316.2	427.8
A4	1	276.0	9.20	333.3	431.2
	2	278.1	9.27	330.8	438.7
	4	273.9	9.10	295.7	416.2
A5	2	280.5	9.35	328.0	433.2
	3	266.8	8.88	303.5	416.0
	6	263.5	8.77	299.8	413.8
A6	2	296.1	9.87	378.3	493.1
	4	283.8	9.46	373.5	403.5

Table 4.2: *Results of the tensile tests on the piles from the field test [12]*

4.3 Test setup and test procedure

4.3.1 Layout of the test site

Figures 4.7 and 4.8 show the layout of the sheet pile walls. The four walls were installed in an almost square form, with sides of about 12 metres. The top of the sheet piles was at NAP+1.0 m and the greenfield at NAP−0.6 m. The north and the south walls were test walls of 19 metres length, and the east and west walls were 2 metre longer.
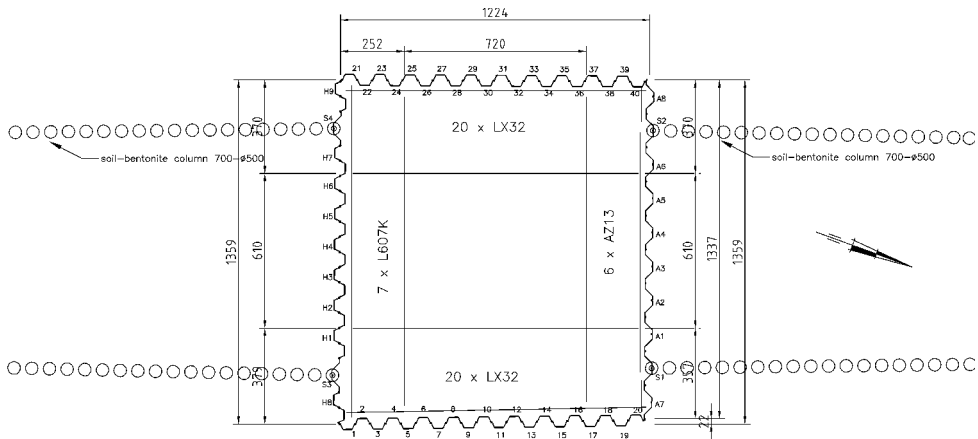
Figure 4.7: *Topview of the Rotterdam Sheet Pile Wall Field Test*
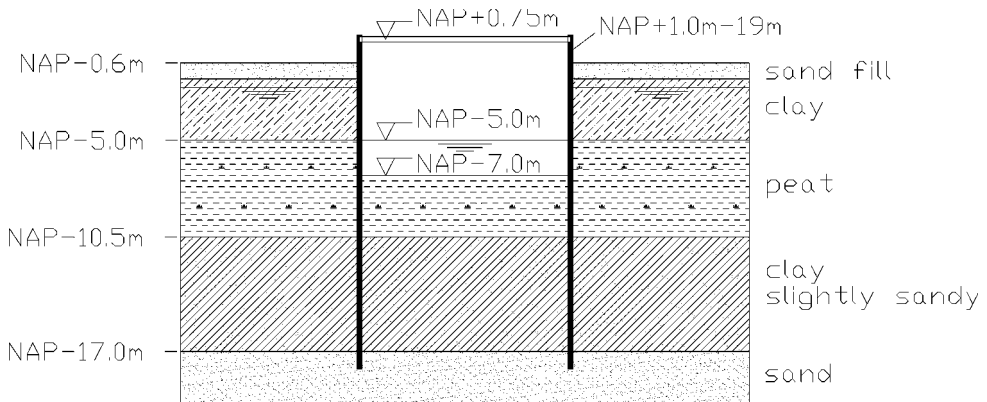
Figure 4.8: *Sideview of the Rotterdam Sheet Pile Wall Field Test*

Enabling works

The enabling works for the test site started in May 1998. To make the test site accessible for the necessary soil investigation equipment, a sand fill about 0.4 m thick was put over the entire test area. In addition to the soil testing, 9 piezometers were installed to measure the initial pore pressure distribution over their depth, and the pore pressure increase as a result of placing the sand fill. In September 1998 the sand fill was completed to a total thickness of 1 metre and as a result, the site settled approximately 2 cm before sheet pile driving started.

In February 1999 the sheet piles were installed using a rig type *Hitachi KH 150 PD* and a high-frequency continuously adjustable impact-vibration hammer, type *ICE 23 RF*. The impact-vibration hammer was connected to a leader in order to drive the sheet piles as straight as possible.

Piles S1 and S4 experienced a very high driving resistance, as these were the closing piles in the specific corners. For pile S1 and the last few meters of pile S4 a heavier vibrator was required. Therefore high interlock friction may be expected in these piles, and possibly in the neighbouring one or two piles. Further, piles A1 and A6 were new piles with higher yield stresses ($f_y \approx 370$ N/mm^2).

Test walls

The north wall consisted of 10 ARBED AZ13 double piles of length 19 metres. Of these, 6 formed the test wall, 2 the interfacing piles, AZ13S, and 2 the corner piles. The interconnecting interlocks of the double piles were welded over the full length but for the free interlocks no special measures were taken. The sheet piles were vibrated to NAP$-$18 m. Inclinometer tubes were welded onto piles A2, A4 and A5, pile A3 was equipped with 12 earth pressure cells of which 4 on the excavated side and 8 on the retaining side, and test pile A4 was fitted with 40 vibrating wire (VW) strain gauges.

The south wall was formed by 7 Larssen 607K double U-piles from HOESCH, H1 to H7, of length 19 metres. The interlocks of the double piles were welded but no special measures were taken for the free interlocks. The toe of the sheet piles was installed at NAP$-$18 m. Inclinometer tubes were welded onto piles H2, H4 and H6, pile H3 was equipped with 12 earth pressure cells of which 4 on the excavated side and 8 on the retaining side, and test pile H5 was fitted with 40 vibrating wire strain gauges. The south wall was completed by 2 interface piles, AZ13S, and two corner piles H8 and H9.

The east and the west walls were each formed by 20 LX32 single U-piles from BRITISH STEEL, of length 21 metres. These piles were installed to NAP$-$20 m in order to reduce the disturbance to the passive zones developed by both test walls. Piles BS6, BS14, BS26 and BS34 were equipped with inclinometer tubes.

Strutting

The plan of the struts and walings is given in Figure 4.9 and the centre line of the frame work was at NAP$+$0.75 m. The struts for the north and south test walls were designed in a such way that both test walls could act as independently as possible and that influence from other sheet piles was minimised. Any difference between the strut forces was carried by to the stiff HE 600B struts between the east and west walls. The struts and the walings were constructed as hinged connections with sufficient rotation capacity between the sheet pile

walls and the frames. The strut system included 6 pressure cells, 4 to measure the lateral strut force by the north and south test walls and 2 to measure the axial force in the waling of the double U test wall on the south side. To minimise the effect of the air temperature and direct sunlight on the strut force, the two 2×HE 300A beams were painted white.
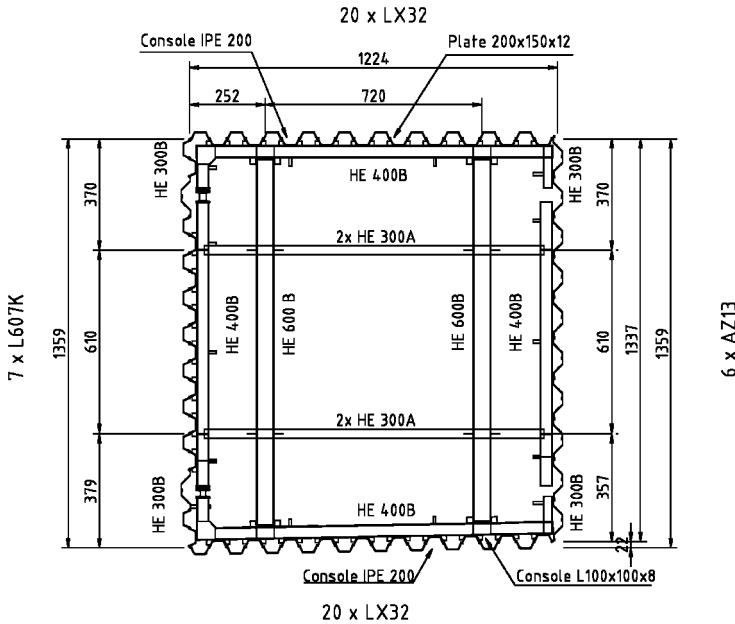
Figure 4.9: *Strutting plan*

Corner effects

As the corners of the excavation would have a large effect on the test walls, four special interface piles were developed, see Figure 4.10. These piles, consisting of AZ13 sections, were cut over a length of 16 metre. In order to prevent water leakage into the excavation, the gap was covered with a 2 mm thick VLDPE foil clamped against the sheet pile. For better drivability of these special piles, 2 metres at the pile toe and 1 metre at the top of the pile was not cut through and to protect the foil, the special piles were placed in a bentonite column extending to NAP$-$15.5 m. After driving, the pile was also cut at the top.

In order to obtain plane strain behaviour of the active soil wedge, two separation walls were installed behind each test wall. The separation walls comprised bentonite-soil columns ø500-700 which were mixed-in-place with a hollow auger rig. The toe of the columns varied from NAP$-$13.5 m close to the test wall to NAP$-$3.5 m at 13 metres behind the test walls. Inside the excavation the bentonite screens were omitted because of the risk of seepage during excavation and pumping.
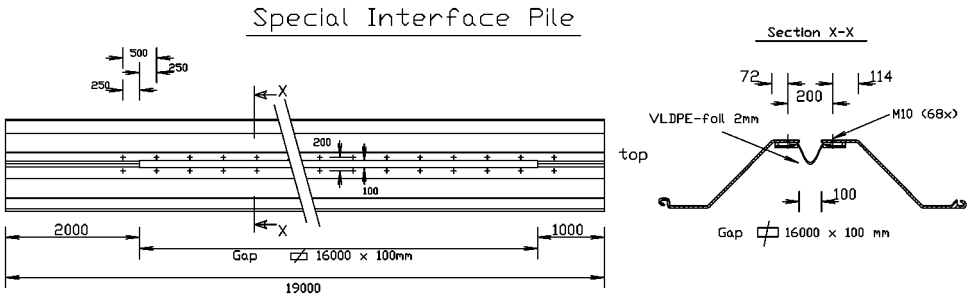
Figure 4.10: *Special interface pile*

4.3.2 Material parameters

Structural data

In Table 4.3 the characteristics of the AZ13 and the L607K sheet piles are given. These characteristics are conform the specifications given by PROFIL ARBED [57] and KRUPP HOESCH [44].

pile	A cm^2/m	I cm^4/m	W cm^3/m	b_f mm	t_f mm	I_{xx}^s cm^4	I_{yy}^s cm^4	c mm	EI_{yy} kNm^2/m	$\beta_{I,0}$	$\beta_{W,0}$
AZ13	137	19700	1300	360	9.5	-	-	-	41370	-	-
L607K	244	70030	3220	-	-	52980	10740	146	147260	0.47	0.46

Table 4.3: *Structural properties of the AZ13-pile and the L607K-pile*

Soil data

Prior to the installation of the sheet pile walls, site investigation and laboratory testing were carried out by FUGRO, GEODELFT, MOS GRONDMECHANICA RHOON and ROTTERDAM PUBLIC WORKS. An overview of the site investigation and laboratory testing is presented in Figure 4.11.

The subsoil consists of a 16.5 metre thick normally consolidated soft clay-peat-clay stratification. Underneath, the top of the Pleistocene sand layer is found which is in connection with the river Maas 2 km away and the ground water level is about 1 metre below the ground surface. In Figure 4.12 a representative boring and CPT are presented together with the initial water pressures.

A comprehensive summary of the soil investigation is given in Appendix F. For the complete report of the site investigation and laboratory testing see Reference [32].
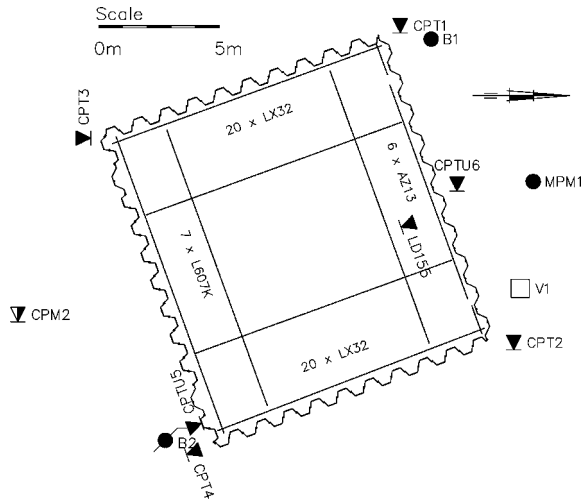
Site investigation

Number	Code	Soil test	Depth
4	CPT1-CPT4	static cone penetration tests	NAP−20 m
2	CPTU5 & CPTU6	CPT's with measurement of pore water pressure during penetration, including 8 dissipation tests	NAP−20 m
1	V1	in-situ vane test on 16 levels	NAP−16.5 m
1	CPM2	cone pressuremeter test on 11 levels	NAP−19.2 m
1	MPM1	Ménard-pressuremeter test on 20 levels	NAP−21 m
2	B1 & B2	borings incl. continuous undisturbed sampling	NAP−22.1 m & −20.2 m

Laboratory testing

Soil description
  Description of the two borings and full colour photography of one boring
Classification tests
19 Determinations of bulk density, dry density and water content
17 torvane tests
17 pocket penetrometer tests
17 determinations of the organic content
12 grain size analyses
11 determinations of the Atterberg Limits (Plastic Limit, Liquid Limit and Plasticity Index)
Triaxial tests
12 triaxial compression tests
 2 triaxial extension tests
Oedometer tests
14 oedometer tests, including 2 horizontally
Dutch cell tests
 3 Dutch cell tests

Figure 4.11: *Site investigation and laboratory testing*
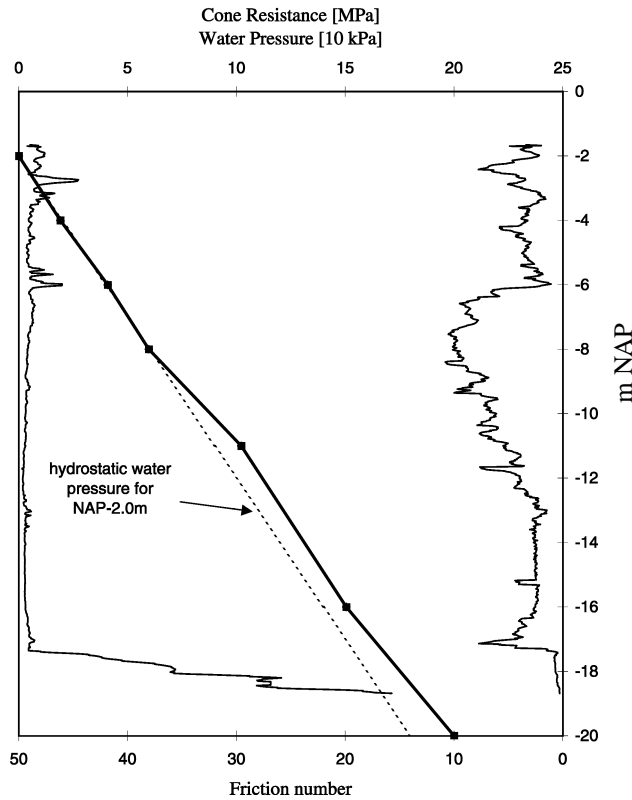
Figure 4.12: *CPT and piezometric head (after Kort et al. [54])*

4.3.3 Monitoring and instrumentation

Figure 4.13 shows the layout of the instrumentation in the field: 10 inclinometer casings on the four sheet pile walls, 2 inclinometer casings behind each test wall, 3 open standpipes, 9 electrical piezometers at 1.5 m behind the test walls and 19 settlement pawns at 1.0, 2.5, 4.5, 7.0 and 10.0 m behind the test walls.

Other manual instrumentation consisted of heave rods to measure the heave of the excavation base, and 4 pairs of rulers to measure relative displacement of the free interlocks of L607K-piles H3/H4 and H4/H5 and LX32-piles BS10/BS11 and BS30/BS31.

Other electrical instrumentation consisted of 80 VW strain gauges, 20 VW earth pressure cells, 20 VW piezometers and 2 tiltmeters on the sheet pile walls, 6 load cells and 2 temperature sensors on the strut frame, 1 piezometer to monitor the water level in the excavation and 1 temperature sensor and 1 barometer located in the measuring container. During the test readings of every sensor (272) were taken, varying from 1 per minute when construction activities were carried out on the job site, to 1 per 10 minutes during long-term testing. The data were stored in a CR10X datalogger [64].

The inclinometer casings were regularly measured by GEODELFT, for a schedule see
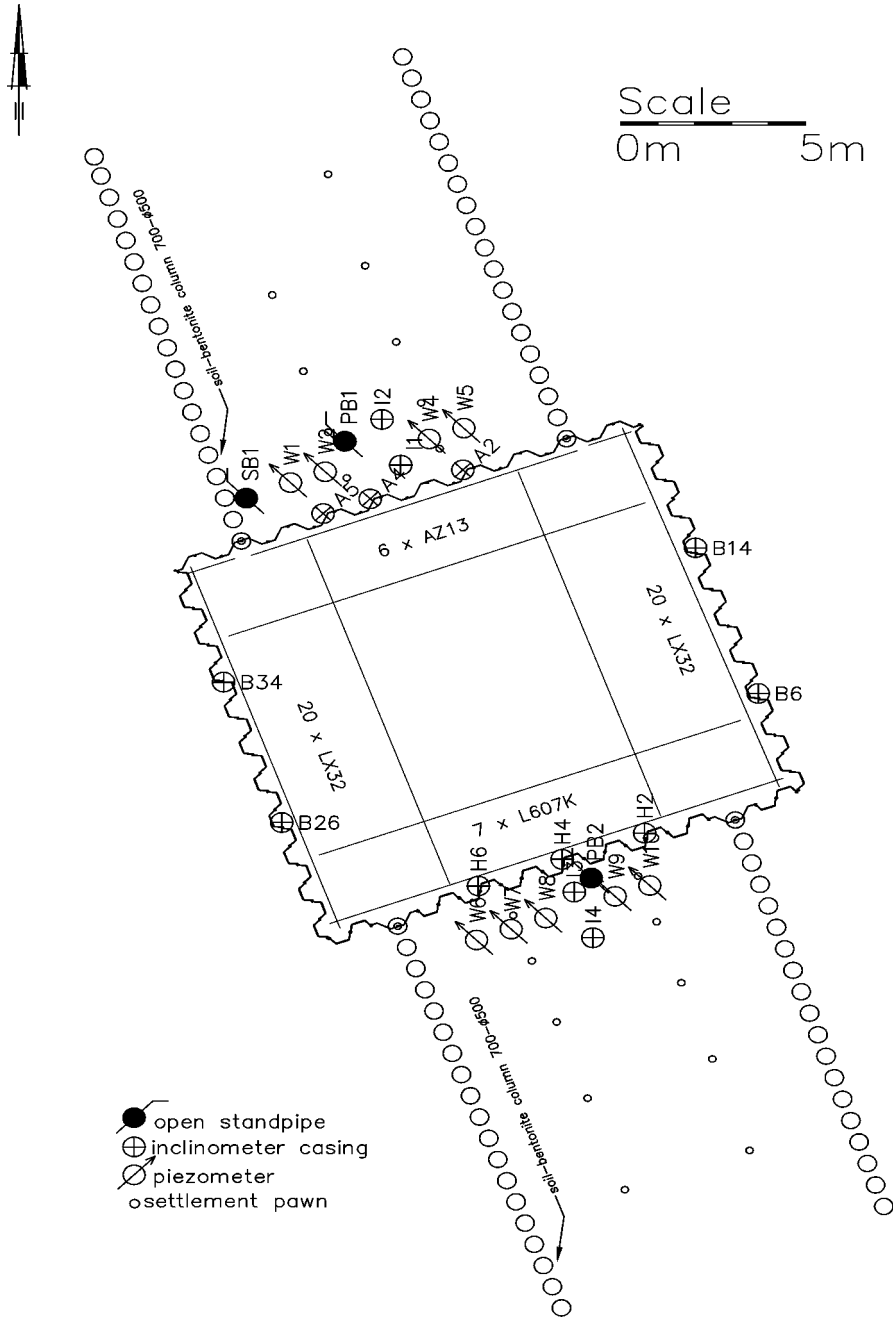
Figure 4.13: *Layout of the Rotterdam Sheet Pile Wall Field Test including all the measurement devices*

Appendix G. At the same time a survey team of the MINISTRY OF TRANSPORT AND PUBLIC WORKS carried out geodetic X-Y measurements on 18 points of the structure: the top of 14 inclinometer casings and the 4 corners of the excavation. The X-Y measurements of the inclinometer casings were ment for the geodetic location of the inclinometer measurements and the global behaviour of the excavation has been monitored with the corner measurements. For the interpretation of the inclinometer measurements, see Section 4.4.2.

The same team from the MINISTRY OF TRANSPORT AND PUBLIC WORKS levelled the settlement pawns behind the two test walls 14 times.

For details of the monitoring and instrumentation plan, see Peters [64] or Kort [49].

4.3.4 Test procedure

A condensed overview of the test procedure is given in Table 4.4; for a complete overview, see Appendix G.

Stage	Activity	Start Date	End Date
Enabling works			
	sand fill to NAP−1.25 m		May 15 1998
	sand fill to NAP−0.65 m	September 17 1998	September 18 1998
	test set up	February 15 1999	March 8 1999
Stage 1: short-term field test			
1.1	dry excavation to NAP−4.0 m	April 13 1999	April 14 1999
1.2	fill with water to NAP−1.5 m		April 16 1999
1.3	excavation under water to NAP−7.0 m	April 19 1999	April 20 1999
1.4	lowering water level to NAP−2.5 m		April 23 1999
1.5	lowering water level to NAP−3.5 m		April 26 1999
1.6	lowering water level to NAP−4.0 m		April 27 1999
1.7	evaluation of test data	April 28 1999	May 7 1999
1.8	lowering water level to NAP−4.5 m		May 10 1999
1.9	lowering water level to NAP−5.0 m		May 11 1999
Stage 2: sand mound			
2.1	performance of measurements		May 17 1999
2.2	fill with water to NAP−1.5 m		May 18 1999
2.3	construction of sand mound		May 19 1999
2.4	lowering water level to NAP−3.5 m		May 21 1999
2.5	lowering water level to NAP−5.0 m		May 26 1999
Stage 3: long-term field test			
3	monitoring long-term performance	May 11 1999	August 18 1999
Stage 4: additional load increase (1)			
4.1	lowering water level to NAP−5.5 m		August 19 1999
4.2	46 days after *Stage 4.1*		October 5 1999
Stage 5: additional load increase (2)			
5.1	lowering water level to NAP−6.0 m		October 5 1999
5.2	112 days after *Stage 5.1*		January 26 2000
Stage 6: water infiltration			
6.1	water addition behind the AZ13	January 26 2000	January 27 2000
End of test: January 31 2000			

Table 4.4: *Test sequence*

The following six test stages are highlighted:

- Enabling works

- Stage 1: short-term field test

- Stage 2: sand mound

- Stage 3: long-term field test

- Stage 4: additional load increase (1)

- Stage 5: additional load increase (2)

- Stage 6: water addition

The enabling works are presented in Section 4.3.1, the six stages are described hereafter, and a summary of the test procedure including the time schedule is presented in Table 4.4.

Stage 1: Short-term field test

The short-term field test was carried out in 3 main substages:

- After construction of the test setup, a dry excavation was carried out to NAP−4.0 m: both soil and water were removed to this level. The excavator worked from a temporary sand fill of about 2 m, which was constructed behind the east wall. A compact excavator worked on the inside of the excavation

- The water level in the excavation was raised to NAP−1.5 m and the excavation was subsequently deepened to a level of NAP−7.0 m. During the excavation the water level was maintained at NAP−1.5 m

- Next the water level in the excavation was lowered to NAP−5.0 m in 5 steps. The intermediate steps were −2.5, −3.5, −4.0 and NAP−4.5 m. After the third step to NAP−4.0 m a step was introduced to evaluate the measurement results so far and to estimate the present load of the AZ13 wall

Stage 2: Sand mound

During the test, the initial results showed that the load on the active side of the AZ13 wall was insufficient so an embankment of 9×9 m was built immediately behind the wall, see Figure 4.14, to a level of NAP+1 m. The procedure used to construct the sand mound, is outlined in Table 4.4.

Stage 3: Long-term field test

The situation which was obtained after construction of the sand mound, was maintained and monitored for a period of 80 days.

Figure 4.14*: Sand mound behind the AZ13-test wall (May 19 1999)*

Stage 4 and 5: Additional load increase

As the initial test results showed that a plastic hinge could not be generated within the required time limit, two more attempts were made to increase the load on the AZ13 piles.

- **Stage 4:** The water level inside the excavation was lowered to NAP−5.5 m (Aug. 19)

- **Stage 5:** The water level inside the excavation was lowered to NAP−6.0 m (Oct. 5)

These actions resulted in yielding of the outermost fibre and in a slow generation of a fully plastic cross-section.

Stage 6: Water addition

A few days before the end of the test a fully plastic cross-section was almost generated. However, as neither the displacement of the AZ13 wall nor the strain distribution along the pile altered over a 2 week period, it was decided to force the generation of the plastic hinge as described below.

As a result of the continuously increasing wall displacements, two holes had been observed in the greenfield; the sand had evidently flowed into the troughs of the sheet piles. This meant that two perfect sand drains had been generated which were used to increase the water pressure against the back of the sheet pile wall. Water addition took place for 2 days: on the first day, a total of 2 m^3 water was added with an inflow rate of 0.4 m^3/hour and on the second day, a total of 6 m^3 with a rate of 2.2 m^3/hour. This action resulted in a rotation of the plastic hinge and redistribution of the bending moment. Stage 6 concerns the situation of the AZ13 wall before and after the rotation in the plastic hinge.

4.4   Test results

4.4.1   General

In this section an overview of the most important measured results is given. First some remarks are made on the interpretation of measured data, followed by the measured results for the AZ13-wall and the L607K-wall. The measured results for the LX32-walls are not treated in this thesis, but reference is made to Kort [49].

   This section gives a report of the observations and interpretation of the measured results. A more elaborate evaluation of the measured results including back-analyses is given in Chapter 6.

NOTE: *For the measurement results presented in this section, the measured data points, indicated with the $\diamond$ and $\times$-marks, are interconnected by straight lines. These straight lines do not have a physical meaning but serve to improve the visibility of the measured results.*

Appendix H provides an overview of the test results in numerical format. For a complete report including all the measurement results, reference is made to Kort [49].

4.4.2   On the interpretation of measured data

Derivation of the wall displacements from the inclinometer measurements

The lateral and transverse displacement curves of the four test walls were determined from inclinometer measurements. Generally the displacement curve obtained from an inclinometer measurement should be linked to the wall by means of a known reference point. Although sufficient data was available from the geodetic XY-measurements at the top of each casing, the displacement curve has not been linked to this geodetic data. After consideration of the inclinometer measurements from all the piles together with the available geodetic data, it was found that the accuracy of the geodetic data was within ± 10 mm, which is in some cases more than 10% of the maximum displacement. More satisfactory results, especially with respect to the interaction between the AZ13 and L607K-walls, could be obtained assuming that the toe of the piles did not displace. Therefore the displacement curves have been linked to the wall by linear extrapolation of the lowest two measurement points to the undisplaced pile toe. For more detailed information see Kort [49].

Derivation of the bending moment from the measured strains

The bending moment in test piles A4 and H5 were derived with strain gauge readings. Yhe gauges were positioned in 10 measurement planes at 4 positions as shown in Figure 4.15.

   The bending moment in the AZ13 pile is derived from its curvature using the $M - \kappa$ curve in Figure 4.16. This is the $M - \kappa$ curve from the 4-point bending test on test pile A4, see Section 4.2, because both the strain gauges and the inclinometer casing, from which most of the behaviour of the AZ13 test wall is interpreted, were installed on the same pile A4.
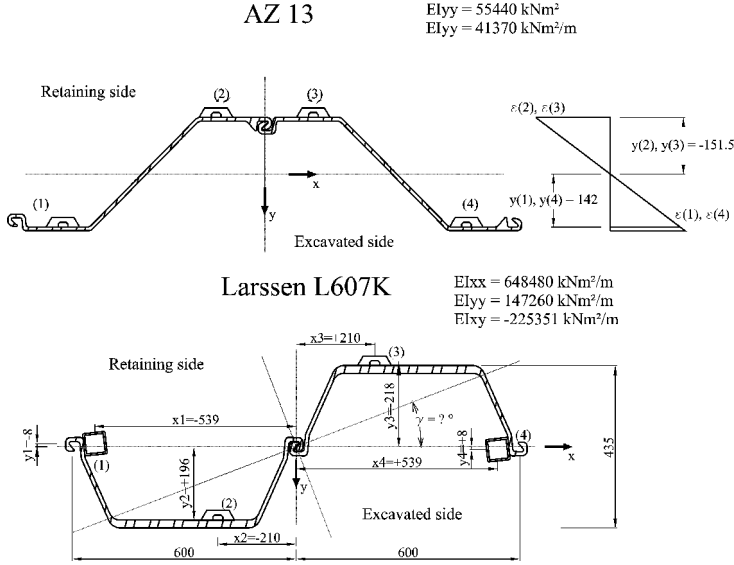
Figure 4.15: *Dimensions of AZ13 and Larssen 607K and position of strain gauges*

The curvature is determined from the four strain gauge measurements according to equation (4.1).

$$\kappa_y = \frac{\varepsilon_1 - \varepsilon_2 - \varepsilon_3 + \varepsilon_4}{y_1 - y_2 - y_3 + y_4} \tag{4.1}$$

The bending moment in the AZ13 pile follows from the $M - \kappa$ curve.

For the double Larssen 607K pile the bending moment is derived according to the theory of elasticity:

$$M_x = EI_{xx}\kappa_x + EI_{xy}\kappa_y \tag{4.2}$$
$$M_y = EI_{xy}\kappa_x + EI_{yy}\kappa_y \tag{4.3}$$

where κ_x and κ_y are derived from

$$\varepsilon_i(x_i, y_i) = \varepsilon + \kappa_x x_i + \kappa_y y_i \tag{4.4}$$

where $\varepsilon_i(x_i, y_i)$ is the strain measured at one of the points 1 to 4, see Figure 4.15. After elaboration, the following relationships for the curvatures κ_x and κ_y are found.

$$\kappa_x = \frac{\varepsilon_1(y_2 - y_3) + (\varepsilon_3(y_1 - y_4) + \varepsilon_4(y_3 - y_2)) - \varepsilon_2(y_1 - y_4)}{x_1(y_2 - y_3) + (x_3(y_1 - y_4) + x_4(y_3 - y_2)) - x_2(y_1 - y_4)} \tag{4.5}$$

$$\kappa_y = -\frac{\varepsilon_1(x_2 - x_3) + (\varepsilon_3(x_1 - x_4) + \varepsilon_4(x_3 - x_2)) - \varepsilon_2(x_1 - x_4)}{x_1(y_2 - y_3) + (x_3(y_1 - y_4) + x_4(y_3 - y_2)) - x_2(y_1 - y_4)} \tag{4.6}$$
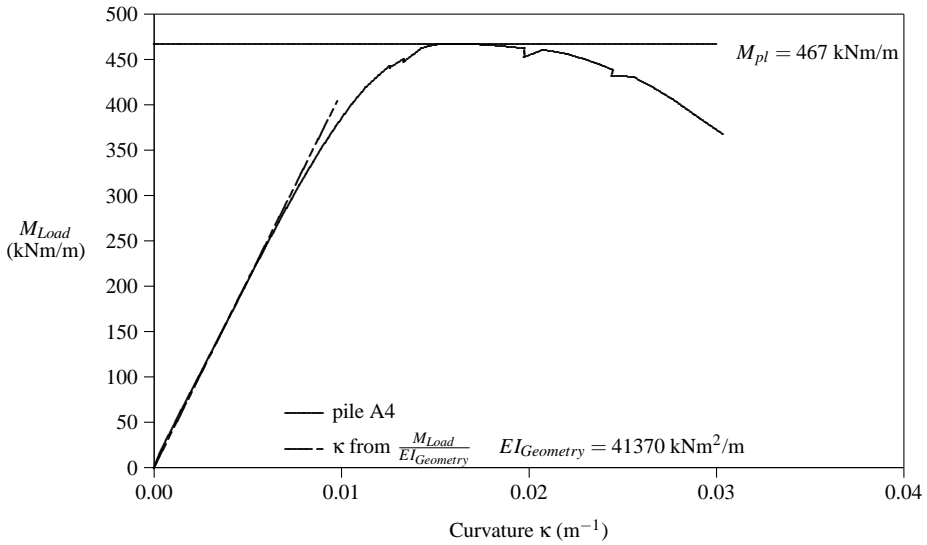
Figure 4.16: *Moment-curvature curve, determined from the bending tests at TNO [12]*

Effective earth pressure

The effective earth pressure (σ') is determined from the difference between the measured earth pressure (σ) and water pressure (u). The piezometer is located 208.8 mm higher than the earth pressure cell, and therefore the measured water pressure is corrected by 2.088 kPa. The effective earth pressure is determined as follows:

$$\sigma' = \sigma - (u + 2.088) \tag{4.7}$$

Evaluation of the measurement results shows the occurrence of *negative earth pressure*. An observed negative earth pressure would mean that the water pressure on the sheet pile is larger than the earth pressure. Both parameters have been measured with different devices which were calibrated in a pressure chamber in advance.

According to Bruzzi et al. [16] an earth pressure cell cannot provide results of the same quality as, for example, a displacement transducer. The contact pressure distribution is not uniform over the diaphragm, as a result of arching effects in the soil around the cell and because the contact between the discrete soil particles and the cell is not continuous. Therefore the scaling factor in water cannot be used to obtain the stress value in soil, without an additional calibration in the soil.

It should therefore be accepted that the interpretation of effective earth pressure is subject to a relatively large error. The measurements of the earth pressure cells can not be interpreted as an absolute behaviour but merely as a relative change of earth pressure. Therefore presentation of negative effective earth pressure indicates probably nothing more but an effective earth pressure of close to zero.

Strut force

The strut and waling forces have not been corrected for temperature variations. The measured average daily variation of the strut force was approximately 2 kN/m, or 10 kN in each strut, and, because the struts were painted white, the average daily temperature variation in the struts was about $\Delta T = 20^o$. Heating of the part of the strut between the stiff HE 600B beams will hardly lead to an increase in the measured strut force, because the accompanying forces are carried by the two side walls. Therefore the influencing length is the overhang of about $\ell = 2.5$ m. A daily temperature variation in the strut of 20° would involve a strain variation of

$$\varepsilon_{\Delta T} = \alpha\,\Delta T = 12 \cdot 10^{-6}\, 20 = 24 \cdot 10^{-5} \tag{4.8}$$

In one strut ($2\times$HE 300A sections, $EA = 4725,000$ kN) with an overhang of $\ell = 2.5$ m, a maximum compressive force $F_{c,\Delta T}$ can occur if the strut is prevented from elongating, of

$$F_{c,\Delta T} = EA\,\varepsilon_{\Delta T} = 1134 \text{ kN} \tag{4.9}$$

or a maximum displacement $u_{\Delta T}$, in the case of a strut that is free to elongate, of

$$u_{\Delta T} = \varepsilon_{\Delta T}\, \ell = 0.6 \text{ mm} \tag{4.10}$$

It may be expected that a maximum elongation of the struts of $\ell = 0.6$ mm can be taken up by the test walls and therefore the measured daily variation of 2 kN/m is probable.

4.4.3 Initial measurements

On April 13 1999 at 7.00 hours, just before the start of the field test, the initial measurements of the earth and water pressures on both the AZ13 and the L607K-walls were taken. The results of these measurements are presented in Figure 4.17.
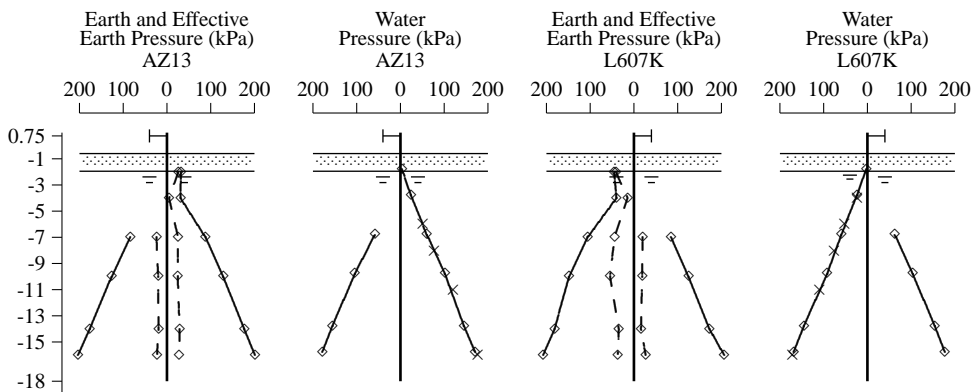
Figure 4.17: *April 13 1999: Inital measurements of the earth, water and effective earth pressure on the AZ13 and the L607K-walls. The* solid lines *indicate the earth pressure and water pressure respectively, and the* dashed lines *the effective earth pressure. The* ×*-marks represent the water pressure 1.5 m behind the test wall.*

4.4.4 Measured results AZ13-wall

In Table 4.5 an overview is given of the measured maximum displacement and the maximum span and fixed moments for the different stages of the test. The measured curves of displacement, bending moment, earth and water pressure for the AZ13-wall are presented in Figures 4.18 to 4.30. In the bending moment diagrams, the measured strut force in kN/m is shown using a convention of positive for compression loading.

			Measured results AZ13-wall			
Date	*Excavation Level* (m NAP)	*Water Level* (m NAP)	*Sand Mound*	w_{max} (mm)	M_s (kNm/m)	M_f (kNm/m)
April 15	-4.0	-4.0	No	33	73	-24
April 22	-7.0	-1.5	No	35	68	-20
May 11	-7.0	-5.0	No	109	206	-30
May 26	-7.0	-5.0	Yes	150	269	-38
June 11	-7.0	-5.0	Yes	-	331	-42
August 11	-7.0	-5.0	Yes	230	355	-40
August 20	-7.0	-5.5	Yes	238	366	-45
October 4	-7.0	-5.5	Yes	282	408	-48
October 13	-7.0	-6.0	Yes	283	397	-39
November 26	-7.0	-6.0	Yes	340	460	-48
December 20	-7.0	-6.0	Yes	385	467	-56
January 2	-7.0	-6.0	Yes	473	-	-67
January 18	-7.0	-6.0	Yes	-	467	-65
January 31	-7.0	-6.0	Yes	1104	-	-270

Table 4.5: *Measured results AZ13*

Figures 4.18 to 4.20 give the results of Stages 1.1, 1.2 and 1.9 of the short-term field test, see Table 4.4 and of Stages I to III to be predicted, see Chapter 5. In Stage III the maximum lateral wall displacement was $w_{max} = 109$ mm and the maximum bending moment was $M_{max} = 206$ kNm/m. This bending moment was far below the expected yield moment of approximately $M_{pl} = 467$ kNm/m. Based on the results measured during the evaluation period (April 28 - May 6) it was anticipated that a plastic hinge could not be generated within the available testing period. To force an increase of the bending moment, it was decided to build a sand mound about 10 metres square and 2 metre high behind the AZ13-wall. Firstly, the state of the construction was monitored, after which the excavation was refilled with water. The sand mound was then built and finally the water level inside the excavation was lowered again, first to NAP−3.5 m and finally to NAP−5.0 m.

The sand mound led to an increase of the wall deflections of the AZ13, see Figures 4.20 and 4.21. On May 26, the maximum lateral wall displacement had increased to $w_{max} = 150$ mm and the maximum bending moment to $M_{max} = 269$ kNm/m. The sand fill led to an increase in strut forces, but as most of the reaction forces could be carried by the east and west walls, the influence of the sand mound on the L607K-wall was limited.

The earth and water pressures did not increase substantially as a result of the sand mound. The extra load caused a pressure increase on the test wall but due to the large deformation capacity of both the soft ground and the wall itself, the extra pressure was immediately transferred into wall displacement (second order effect) and the active earth pressure condition was obtained once again. The direct response of the strut force, bending moment and the tilt sensors (wall displacements) during the construction of the sand mound,
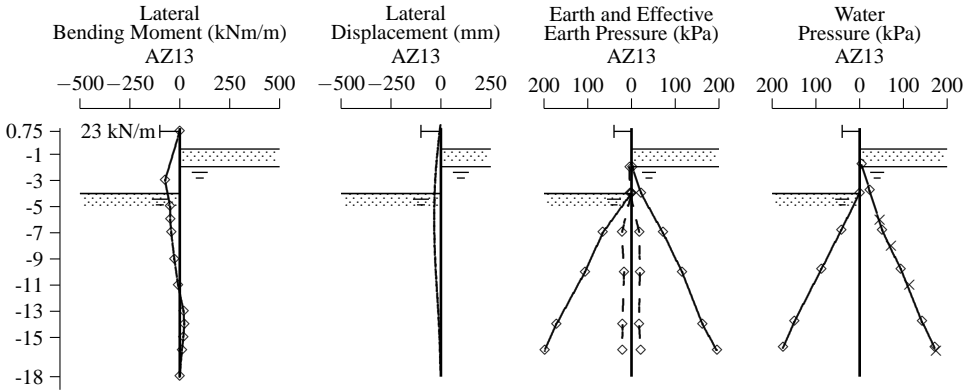
Figure 4.18: *April 15 1999: NAP−4.0 m/NAP−4.0 m and Prediction Stage I*
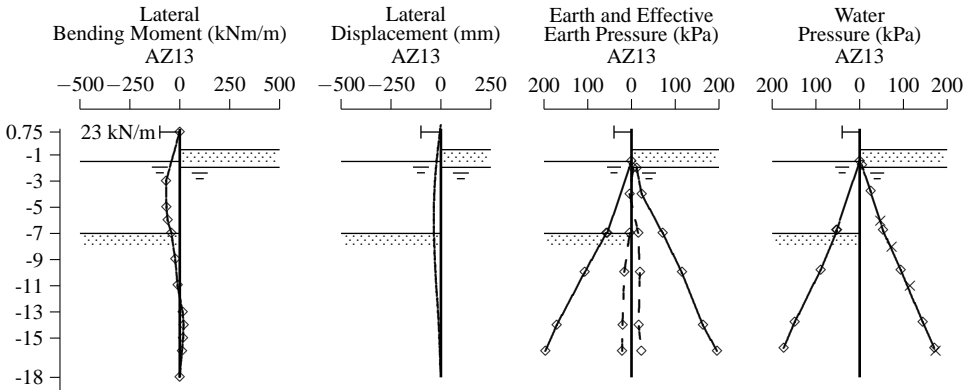
Figure 4.19: *April 22 1999: NAP−7.0 m/NAP−1.5 m and Prediction Stage II*
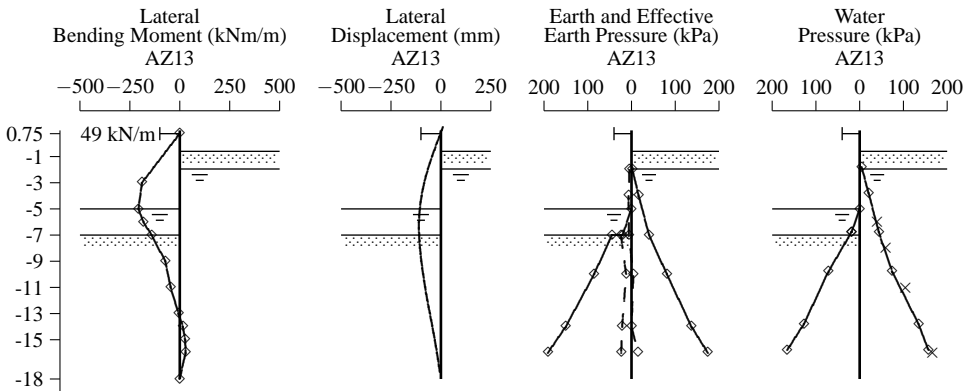
Figure 4.20: *May 11 1999: NAP−7.0 m/NAP−5.0 m and Prediction Stage III*
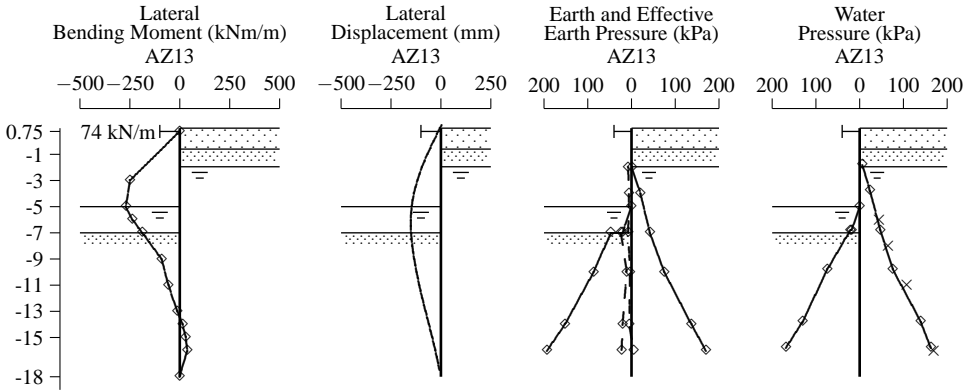
Figure 4.21: *May 26 1999: NAP−7.0 m/NAP−5.0 m with sand mound*
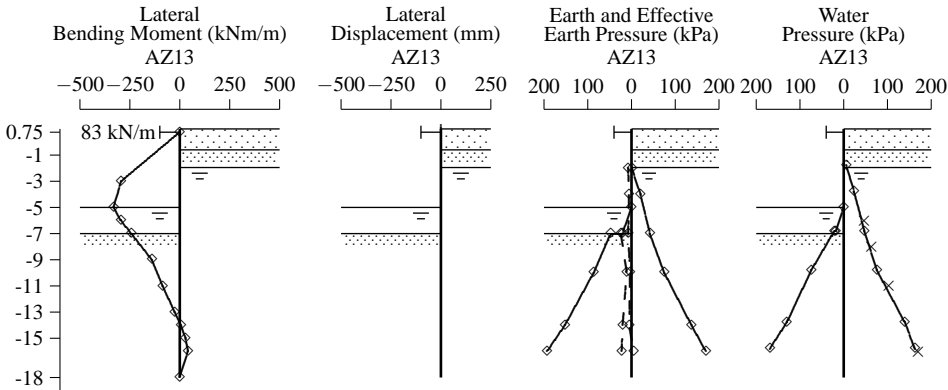
Figure 4.22: *June 11 1999: NAP−7.0 m/NAP−5.0 m with sand mound*
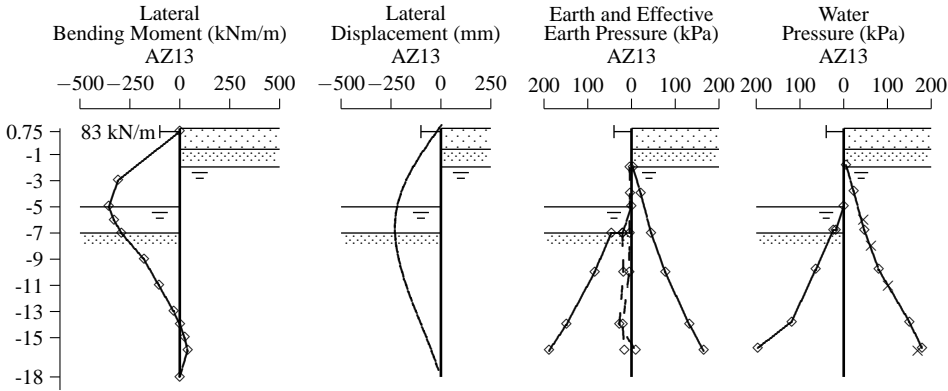
Figure 4.23: *August 11 1999: NAP−7.0 m/NAP−5.0 m with sand mound*
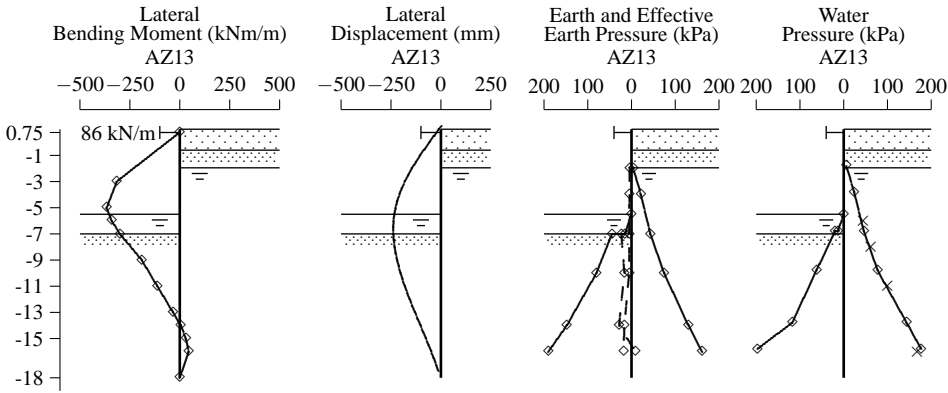
Figure 4.24: *August 20 1999: NAP−7.0 m/NAP−5.5 m with sand mound*
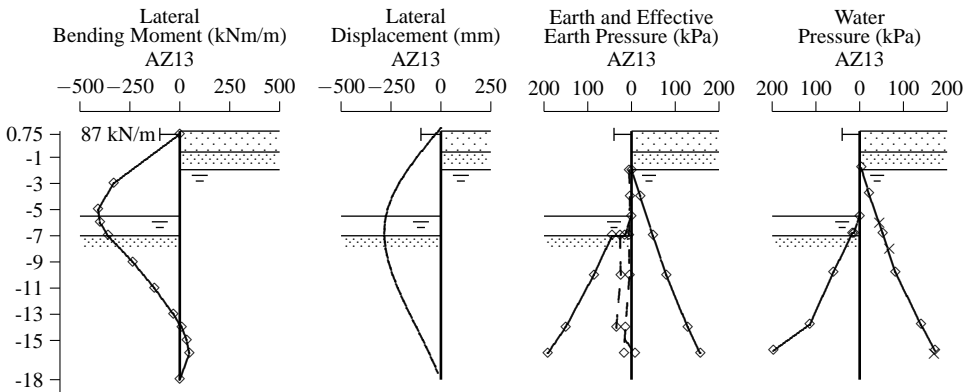
Figure 4.25: *October 4 1999: NAP−7.0 m/NAP−5.5 m with sand mound*
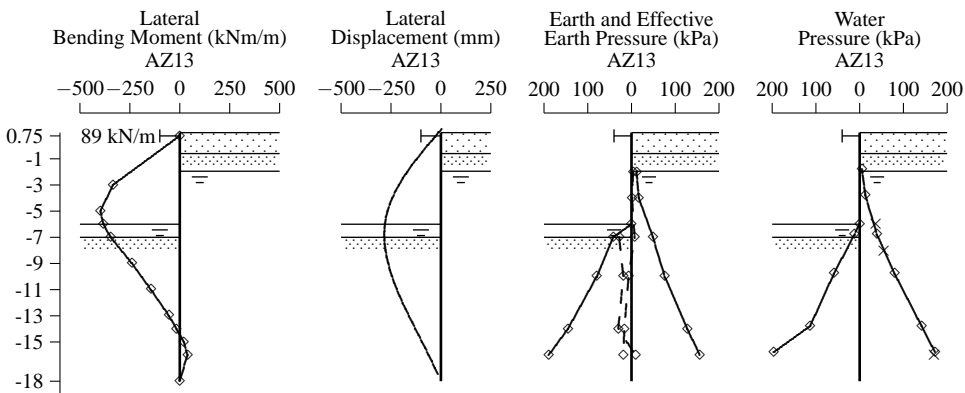
Figure 4.26: *October 13 1999: NAP−7.0 m/NAP−6.0 m with sand mound*
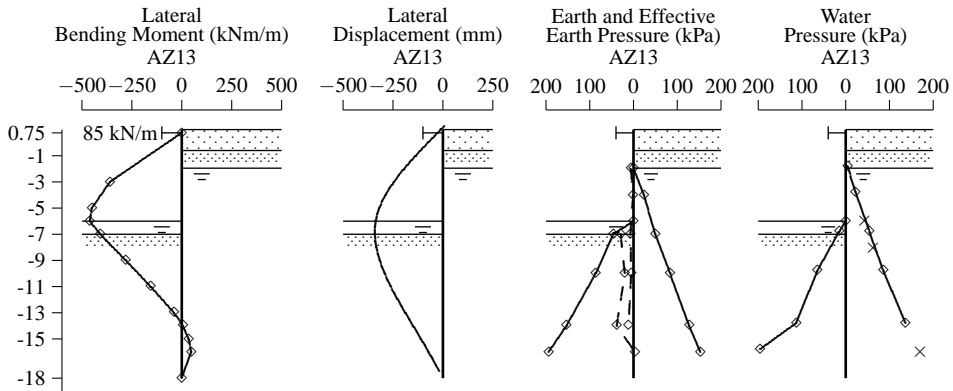
Figure 4.27: *November 26 1999: NAP−7.0 m/NAP−6.0 m with sand mound*
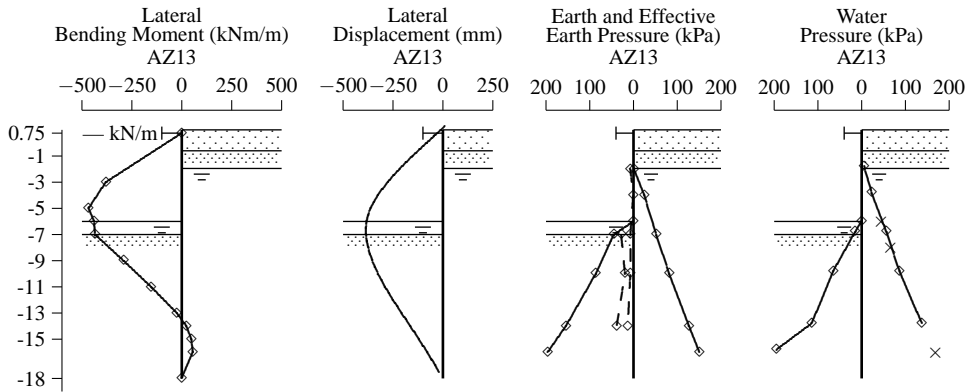
Figure 4.28: *December 20 1999: NAP−7.0 m/NAP−6.0 m with sand mound*
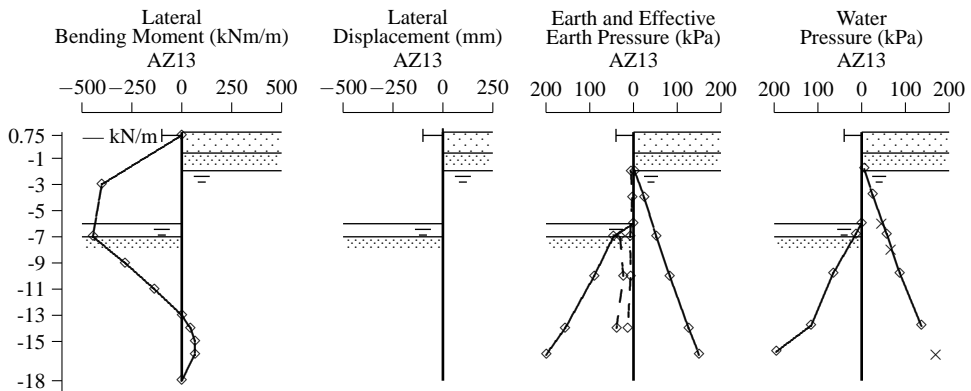
Figure 4.29: *January 2 2000: NAP−7.0 m/NAP−6.0 m with sand mound. The distribution of the bending moment between NAP−3 m and NAP−7 m could not be determined and is therefore, cumbersomely, represented as a straight line*
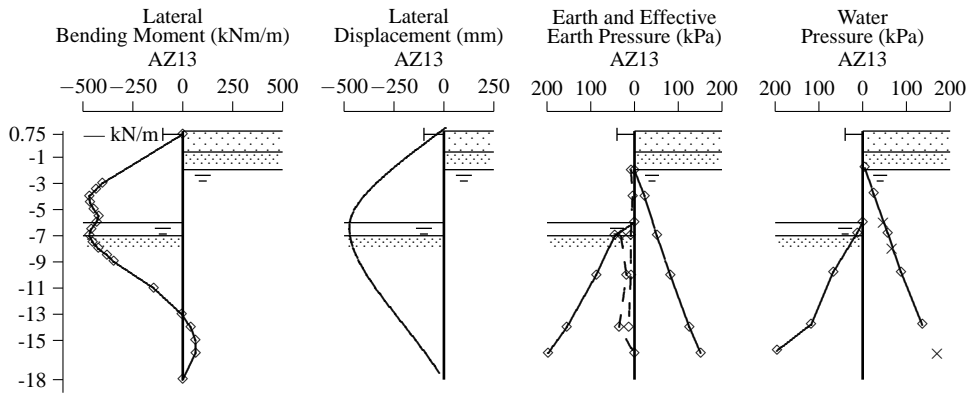
Figure 4.30: *January 18 2000: NAP−7.0 m/NAP−6.0 m with sand mound*
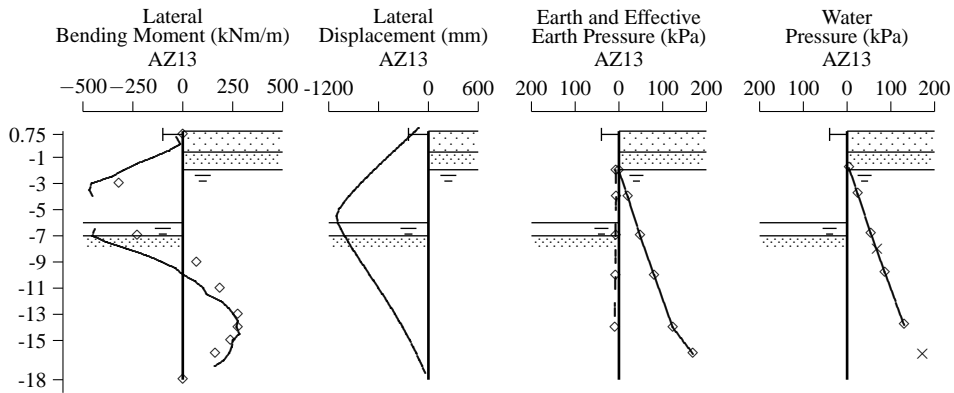
Figure 4.31: *January 28 & 31 2000: NAP−7.0 m/NAP−6.0 m with sand mound*

support this mechanism. However, the effects of 3-dimensional spread of the load from the sand mound certainly cannot be denied.

An other important phenomenon is the direct response of the construction to refilling of the excavation. The displacements and bending moments in the wall gave an immediate and large response as the excavation was refilled, as did the earth pressures at NAP−2.0 m and NAP−4.0 m. This is mainly due to the large deformation capacity of the soft ground together with the undrained soil response.

Figures 4.21 to 4.23 show the results of the long-term field test. These results cannot be compared to the results to be predicted because of the sand mound. On August 11 the maximum displacement had increased to $w_{max} = 230$ mm and the maximum bending moment to $M_{max} = 355$ kNm/m. The bending moment increased at a logarithmic rate with respect to time, and it was expected that it would take more than three years to obtain the yield moment in the AZ13-wall.

Therefore a second attempt was undertaken to increase the load on the AZ13-wall by lowering the water level to NAP−5.5 m. The direct response, see Figures 4.23 and 4.24 showed a minimal response from the wall: $w_{max} = 238$ mm and $M_{max} = 366$ kNm/m. After

more than a month, on October 4, $w_{max} = 282$ mm and $M_{max} = 408$ kNm/m.

According to Kort [49], on October 4 the ultimate fibres started to yield, but not significantly. The maximum elastic bending moment observed in the field test was approximately $M_{el;max} = 408$ kNm/m, see Figure 4.25.

Nevertheless, to generate a plastic hinge within the available time limit, a second additional load increase was required. The water level inside the excavation was lowered to NAP−6.0 m. Figures 4.26 to 4.30 show the measurements which resulted from lowering of the water level to NAP−6.0 m.

It was towards the end of December that the first traces of the plastic hinge became visible. Two holes in the sand about 2 metres depth and with a diameter of 1 metre were generated in two troughs of the sheet pile wall; the sand had evidently flowed into the troughs between the clay and the sheet pile wall.

In Figure 4.30 it is clearly shown that on January 18 the state of the cross-section was beyond the full-plastic state. In this state the moment curve is derived both from the strain measurements and where information was missing, the results from the inclinometer measurements were used. The maximum curvature was $\kappa = 0.026$ m^{-1}. Transformation of the curvature into bending moment according to Figure 4.16 results in a *dent* in the moment curve. However, a clear *kink* in the displacement curve was not observed. Therefore, although the full-plastic cross-section had already be reached, a *plastic hinge* had not been generated.

As the measured strains and slope of the wall at strut level did not alter in the period from January 2 to 18, it was decided to pour water behind the sheet pile wall. In two days about 8000 litres was added via the sand troughs. Finally some active slip planes were generated causing an increase in the earth pressure, and therefore sufficient load to generate the plastic hinge.

The final state of the cross-section is presented in Figure 4.31. This state had been measured for more than one day, as the plastic hinge was developed on January 27 but the inclinometer measurements were carried out on January 31. Between January 27 and 31 the wall moved slightly more but enough for most of the instrumentation to be lost.

The results in Figure 4.30 are compared to those of Figure 4.31:

- On January 18, no rotation of the plastic hinge was observed but on January 31 $\varphi_{pl} = 0.18$ rad

- As a result of rotation in the plastic hinge, the cantilever moment increased from $M = 65$ kNm/m to $M = 284$ kNm/m

- As a result of rotation of the plastic hinge, the cross-sectional resistance decreased to a value which is beyond the range of the bending tests

- Although plastification of the cross-section is distributed over 5 metre, the plastic rotation in the hinge is concentrated over a length of only 1 metre

Figures 4.32 and 4.33 show two photo's of the final state of the field test. The first photo shows the plastic hinge taken from inside the excavation and a large deflection of the wall is clearly visible. In the second photo, a global overview of the test site is shown after the plastic hinge was formed, and an active slip plane in the sand mound is clearly visible. Originally the height of the mound was approximately at strut level but when the plastic hinge was generated, the sand slid into the space behind the deflected wall.

Figure 4.32: *Plastically deformed wall (January 31 2000)*

Figure 4.33: *Final state of the field test (January 31 2000)*

4.4.5   Measured results L607K-wall

In Table 4.6 two tabular overviews are given of the measurement results for the L607K-wall. The first table gives a summary of the measured maximum displacement and the maximum field and cantilever moments for the different stages of the test, all in the lateral direction. The second table gives a summary of the measured transverse displacement in the three test piles and of the measured transverse moment, measured in pile H5. The measured curves for the displacement, bending moment, earth and water pressures on the Larssen 607K-

Measured results Larssen 607K-wall in lateral direction					
Date	*Excavation Level* (m NAP)	*Water Level* (m NAP)	$w_{y,max}$ (mm)	$M_{y,f}$ (kNm/m)	$M_{y,c}$ (kNm/m)
April 15	-4.0	-4.0	27	87	-12
April 22	-7.0	-1.5	29	109	-11
May 11	-7.0	-5.0	85	337	-18
May 26	-7.0	-5.0	96	356	-11
June 11	-7.0	-5.0	-	413	-4
August 11	-7.0	-5.0	131	460	0

Measured results Larssen 607K-wall in transverse direction					
Date	*Excavation Level* (m NAP)	*Water Level* (m NAP)	$w_{x,max,H2}$ (mm)	$w_{x,max,H4}$ (mm)	$w_{x,max,H6}$ (mm)	$M_{x,f}$ (kNm/m)
April 15	-4.0	-4.0	12	9	9	-113
April 22	-7.0	-1.5	15	13	14	-101
May 11	-7.0	-5.0	29	20	11	-264
May 26	-7.0	-5.0	30	23	14	-277
June 11	-7.0	-5.0	-	-	-	-317
August 11	-7.0	-5.0	32	28	14	-380

Table 4.6: *Measured results Larssen 607K in lateral and transverse direction*

wall are presented in Figures 4.34 to 4.39. In the bending moment diagrams, the measured strut force in kN/m is shown using the convention of positive for compression. The lateral displacements are derived from the measurements of pile H4.

Figures 4.34 to 4.36 give the results for Stages 1.1, 1.2 and 1.9 of the short-term field test. On May 11 the maximum lateral wall displacement was $w_{max} = 85$ mm and the maximum bending moment was $M_{max} = 337$ kNm/m. Compared with the AZ13-wall ($w_{max} = 109$ mm and $M_{max} = 206$ kNm/m) the L607K-wall gave a lower maximum displacement and a higher maximum bending moment. These differences can be explained by the bending stiffness of both test walls. The bending stiffness of the L607K-wall ($EI = 0.7$ to 1.0×147063 kNm^2/m) is 2.5 to 3.5 times larger than the bending stiffness of the AZ13-wall ($EI = 41370$ kNm^2/m). It may be expected that the stiffest wall gives the lowest wall displacements and the highest bending moments.

Between May 20 and 26 the sand mound was built behind the AZ13-wall. Therefore the excavation was refilled to NAP-1.5 m and subsequently drained to NAP-5.0 m. As a result of the undrained response of both test walls to this unloading-reloading, the effects of this sudden refill on the L607K-wall were small, and therefore not considered in the evaluation of the long-term test results.

Figures 4.36 to 4.39 show the test results for the long-term field test, the Stages IV to VI of the prediction exercise. In the long-term field test, the wall displacement increased from $w_{max} = 85$ mm to $w_{max} = 131$ mm and the maximum bending moment from $M_{max} = 337$ kNm/m to $M_{max} = 460$ kNm/m after three months.

Figures 4.40 to 4.44 show the bending moment in pile H3 and the displacements of piles H2, H4 and H6 in the transverse direction. The results should be viewed from the excavation towards the test wall. During the test, the top of the L607K-wall moved about 10 to 15 cm towards the West. This movement was caused by the positioning of the excavator, which worked from a 1.5 m high temporary sand mound behind the east wall.

Oblique bending can be recognised from the amount of curvature in the transverse direction. In the dry excavation and after the under water excavation, see Figures 4.40 and 4.41, the amount of oblique bending was small. In Stage 1.9, after lowering the water level to NAP-5.0 m, oblique bending occurred in pile H2 and H4 but not in pile H6. Also during the long-term field test, most oblique bending occurred in pile H2 and H4 and hardly in pile H6.

As the soil in front of and behind the three piles is comparable, the reason for these large differences may be found in variation in the interlock friction. In Section 4.3.1 it was noted that pile S4, the interface pile in the South-West corner (see Figure 4.7), had a very high driving resistance and could only be vibrated to the required depth with a heavier vibrator. Therefore the contact force in the interlocks between pile S4 and H7 may have become very high and, obviously, also the contact forced between pile H7 and H6. These high contact forces prevent the free interlocks from slipping and may explain why oblique bending did not occur in pile H6, and why more oblique bending occurred in pile H2 than pile H4.

For quantitative interpretations and back analyses of various stages of the field test reference is made to Chapter 6.
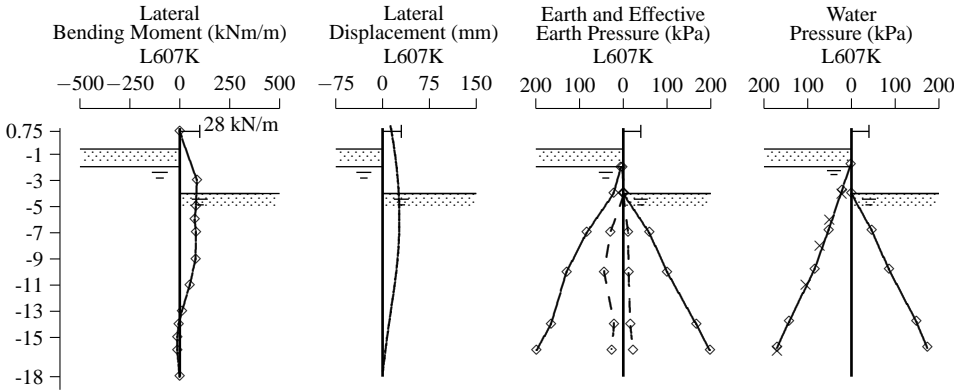
Figure 4.34: *April 15 1999: NAP−4.0 m/NAP−4.0 m and Prediction Stage I*
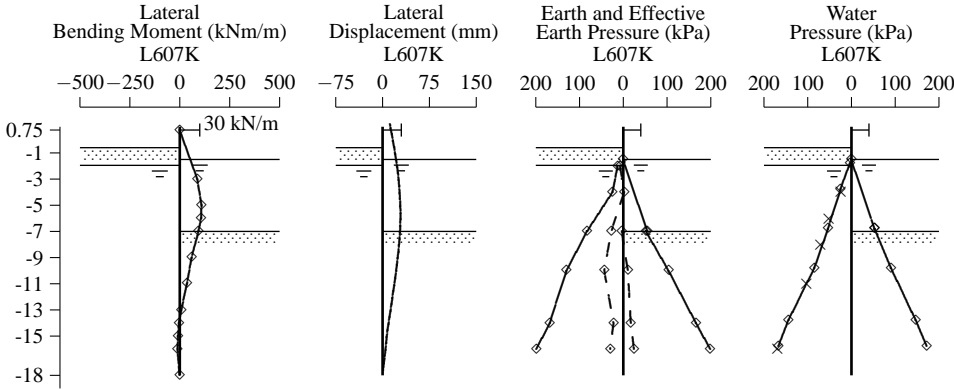
Figure 4.35: *April 22 1999: NAP−7.0 m/NAP−1.5 m and Prediction Stage II*
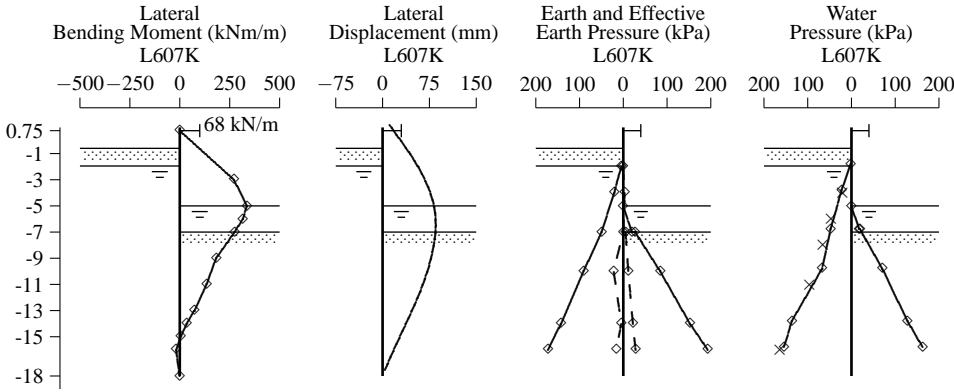
Figure 4.36: *May 11 1999: NAP−7.0 m/NAP−5.0 m and Prediction Stage III*
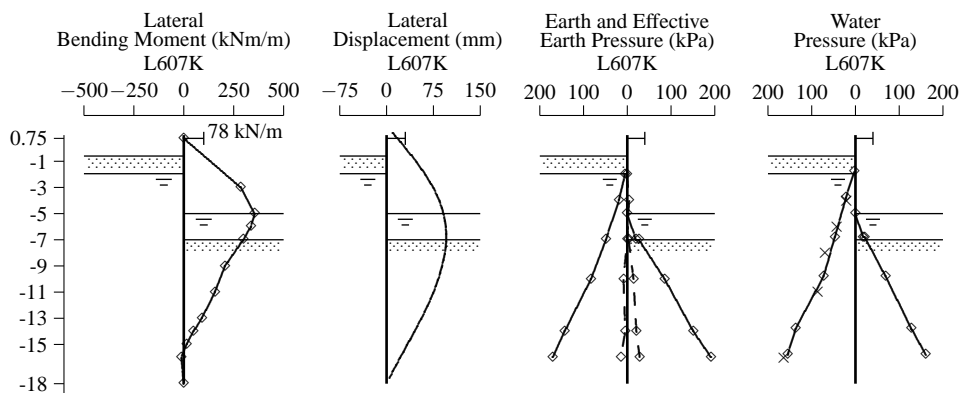
Figure 4.37: *May 26 1999: NAP−7.0 m/NAP−5.0 m with sand mound behind AZ13*
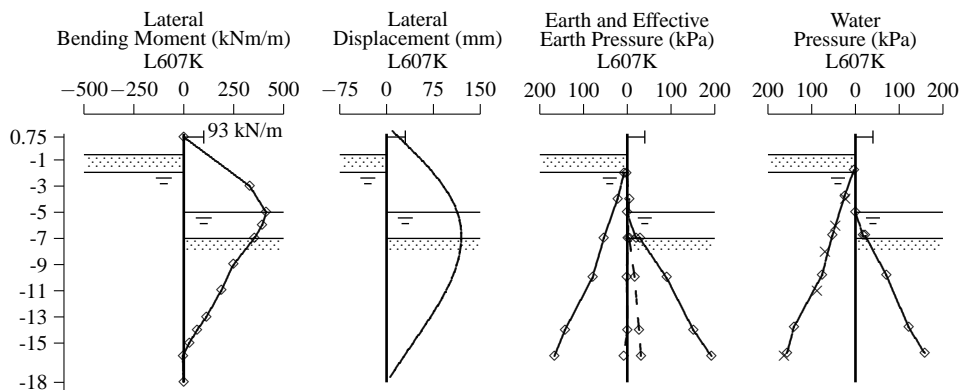
Figure 4.38: *June 11 1999: NAP−7.0 m/NAP−5.0 m and Prediction Stage IV*
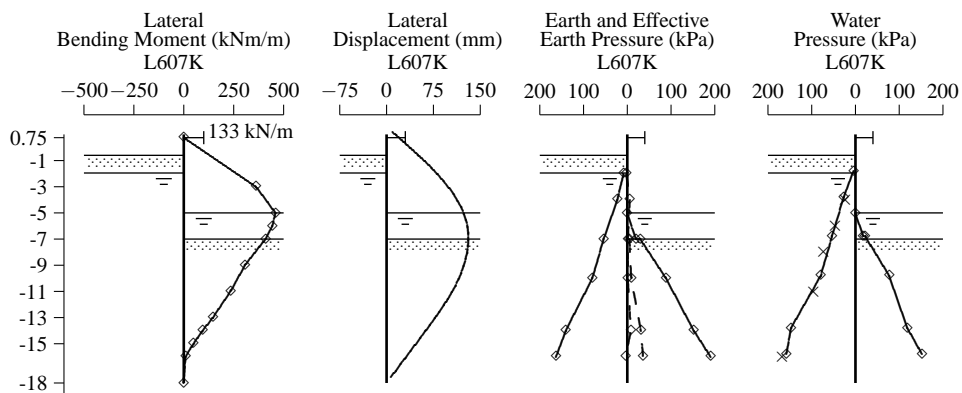
Figure 4.39: *August 11 1999: NAP−7.0 m/NAP−5.0 m and Prediction Stage V*
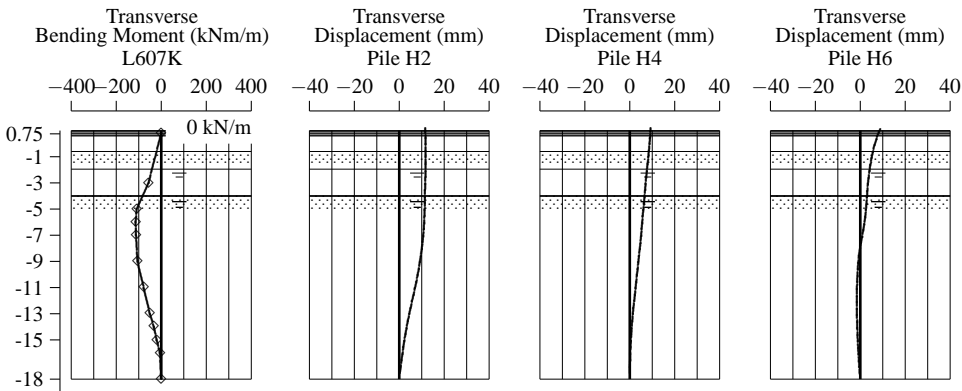
Figure 4.40: *April 15 1999: results in the transverse direction for NAP−4.0 m/NAP−4.0 m, to be viewed from the excavation towards the wall*
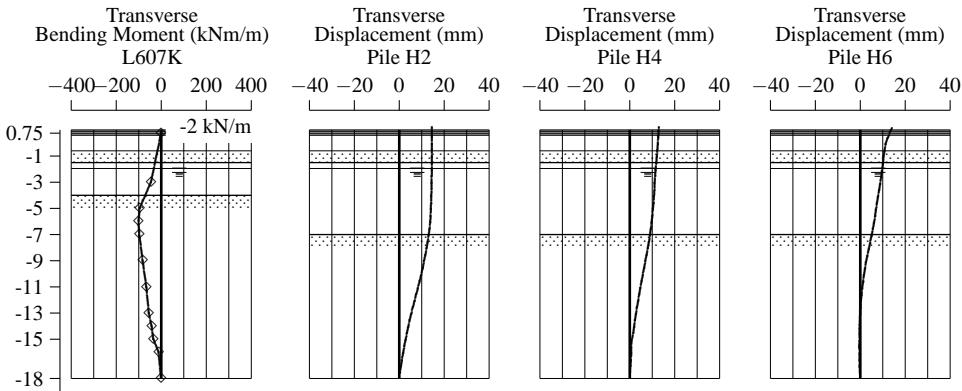
Figure 4.41: *April 22 1999: results in the transverse direction for NAP−7.0 m/NAP−1.5 m*
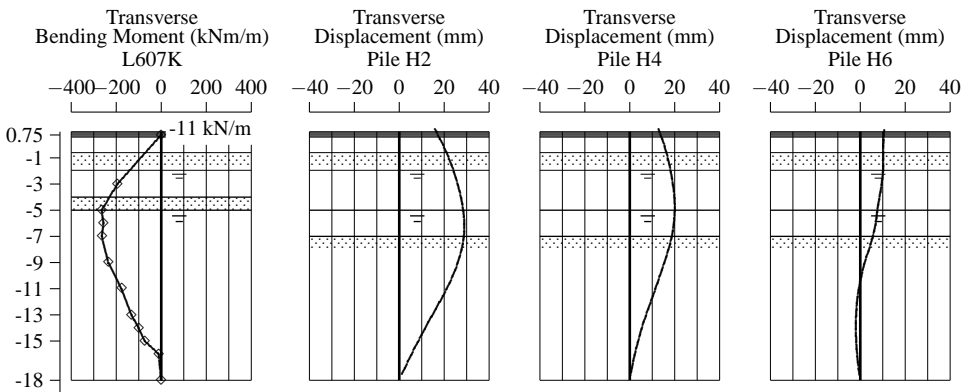
Figure 4.42: *May 11 1999: results in the transverse direction for NAP−7.0 m/NAP−5.0 m*
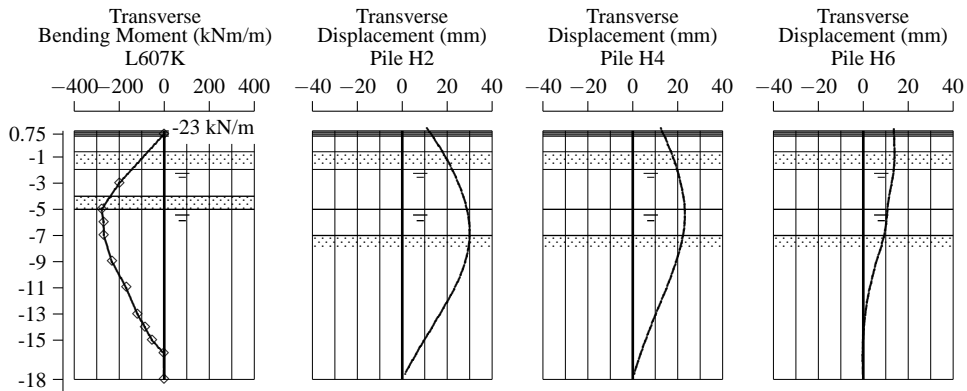
Figure 4.43: *May 26 1999: results in the transverse direction for NAP−7.0 m/NAP−5.0 m, with sand mound behind AZ13*
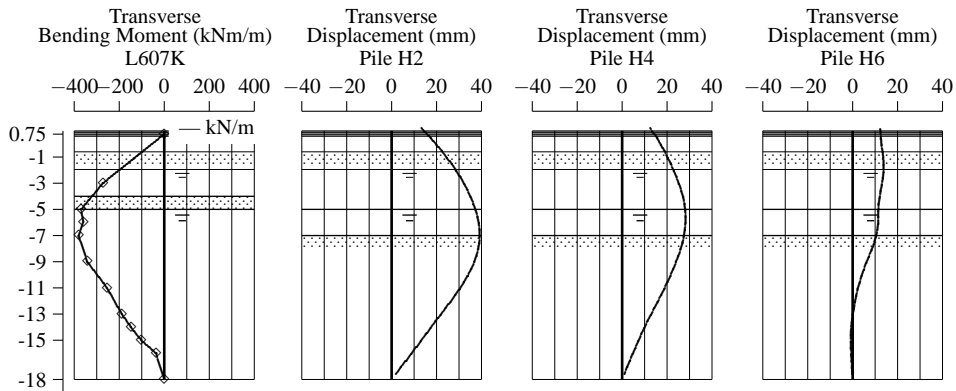
Figure 4.44: *August 11 1999: measurement results in the transverse direction for NAP−7.0 m/NAP−5.0 m, with sand mound behind AZ13*

4.5 Long-term behaviour with respect to $\log t$

In the previous sections it is shown how the actions on the sheet pile walls and the accompanying action effects increase in time. It is interesting to follow some of the action effects against the logarithm of time. In Figure 4.45, the development of the following action effects are plotted against $\log t$:

- inclination of the AZ13-wall at strut level, which is a measure of the wall displacement

- the strut force in both walls

- the bending moment in both walls at NAP−5.0 m depth

The relationship between the tilt (wall displacement) and lateral bending moment on the one hand, and $\log t$ on the other hand, is clearly visible. These measurements, however, are evaluated in Section 6.7.

Finally it is noted that the extraordinary increase in strut force for the L607K is due to the extraordinary increase in the South-West strut force, and is probably not reliable, see Kort [49].
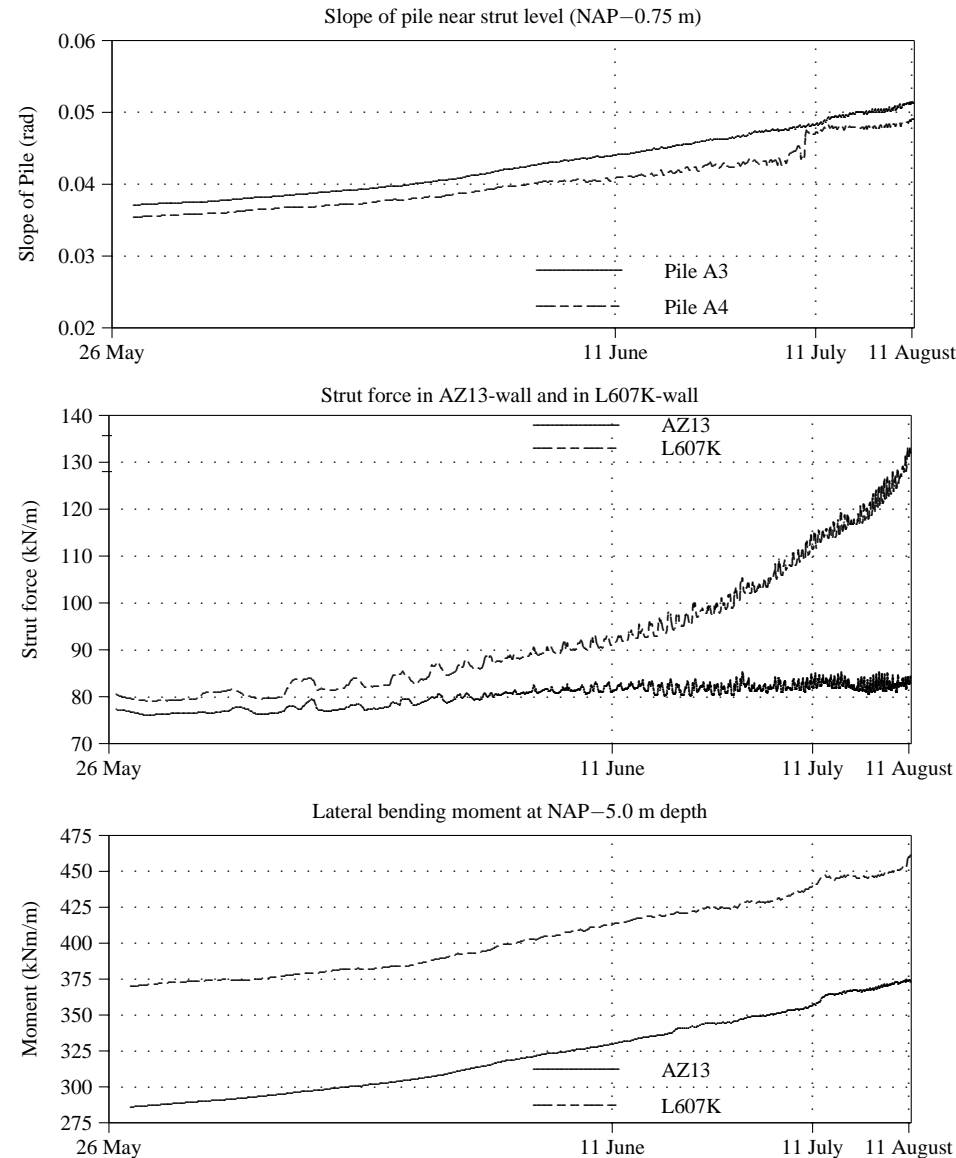
Figure 4.45: *Development of action effects against* log(*time*) *during the long-term field test*

4.6 Consistency check of the measurement results

Before the measured behaviour of the sheet pile walls can be compared to the various calculations, the consistency of the measurement results should be investigated. When the sheet pile wall is in an elastic state, the displacements, measured with an inclinometer, the bending moment, measured with strain gauges, and the earth and water pressure, measured with pressure cells, may be considered as *consistent* if the measurement results are in accordance with equation (4.11).

$$\frac{d^4 w(x)}{dx^4} = \frac{q(x)}{EI} \tag{4.11}$$

In the theoretically perfect case, when measurement errors are absent, the consistency of the measurements would be easy to verify. In practice, however, measurement errors make a consistency check more difficult.

Firstly, a small error in measured displacement generally leads to a large error of the fourth derivative [76] and secondly, DiBiagio [31] and Bruzzi *et al.* [16] demonstrated that earth pressures on sheet piles are extremely difficult to measure accurately.

It is well-known from other large scale field tests [35, 88] that a deviation of about 10% may be expected between the earth pressures determined from the measured deflection and the earth pressures measured with the earth pressure cells on the sheet pile. In literature, various applications of consistency checks for laboratory and field tests are given [34, 46, 58, 88].

The method presented by Boissier *et al.* [9] forms a starting-point for the consistency checks made in this section. Based on the measured displacements, bending moment and earth pressure distributions, a function $g(x) \equiv w(x)$ is determined which satisfies the conditions expressed by equation (4.11), using the least squares method. The actions on the sheet pile walls are described by two high degree polynomials, $e(x)$ on the excavated side and $r(x)$ on the retained side, see Figure 4.46.
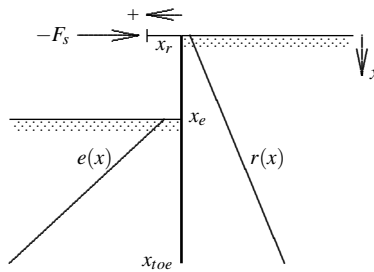
Figure 4.46: *Actions on a sheet pile wall*

Superposition leads to an earth pressure difference $q(x)$.

$$e(x) = \sum_{j=0}^{m-4} \beta'_j (x_e - x)^j \qquad\qquad r(x) = \sum_{j=0}^{n-4} \alpha'_j (x_r - x)^j \tag{4.12}$$

After four successive integrations, a function $g(x)$ can be defined which is equivalent to the wall displacement:

$$w(x) \equiv g(x) = \begin{cases} \sum_{j=0}^{n} \alpha_j (x_r - x)^j & \text{if } x_r \geq x \geq x_e \\ \sum_{j=0}^{n} \alpha_j (x_r - x)^j + \sum_{j=4}^{m} \beta_j (x_e - x)^j & \text{if } x_e \geq x \geq x_{toe} \end{cases} \quad (4.13)$$

Equivalent functions for the bending moment and earth pressure difference follow from the second and fourth derivative of $g(x)$.

The measurements taken in the field are described as follows:

- y_i with $(i = 1, 2, ..., \mathcal{N})$ measured displacement of the wall in x_i

- Δy_i with $(i = 1, 2, ..., \mathcal{N} - 1)$ measured difference of the displacement between x_i' and x_{i+1}' with $x_i' = (x_i + x_{i+1})/2$

- M_i with $(i =, 1, 2, ..., \mathcal{M})$ measured bending moment in x_i

- F_s measured strut force at top of the wall

- q_i with $(i = 1, 2, ..., Q)$ measured earth pressure difference in x_i

The following boundary conditions apply:

- $M(x_r) = 0$ and $M(x_{toe}) = 0$

- $V(x_r) = -F_s$ and $V(x_{toe}) = 0$

The function $g(x)$ can be found by the principle of least squares. The sum of squared errors to be minimised is

$$\Psi = \alpha \sum_{i=1}^{\mathcal{N}} \left(y_i - g(x_i) \right)^2 + \beta \sum_{i=1}^{\mathcal{N}-1} \left(\frac{\Delta y_i}{\Delta x_i'} - \Delta g_i \right)^2 + \gamma \sum_{i=1}^{\mathcal{M}} \left(-\frac{M_i}{EI} - g''(x_i) \right)^2$$

$$+ \delta \left(-\frac{F_s}{EI} - g'''(x_i) \right)^2 + \varepsilon \sum_{i=1}^{Q} \left(\frac{q_i}{EI} - g^{iv}(x_i) \right)^2 \quad (4.14)$$

The coefficients α, β, γ, δ, ε are correction factors which take differences in size and precision of the parameters into account. These factors can be adjusted by engineering judgement but the degree of the polynomials on the retaining and excavated side (n and m) should be estimated with care; too high estimation of n and m will lead to oscillation of the solution.

Minimisation of Ψ leads to α_j ($j \in \{0, .., n\}$) and β_j ($j \in \{4..m\}$) and finally to the earth pressure distribution on the retained side $r(x)$ and on the excavated side $e(x)$.

In Figure 4.47, the consistency check for the AZ13-wall is given for the state of May 11 1999. The bending moment at NAP-0.6 m is derived from a strut force of $F_s = 49$ kN/m. In the displacement curve only 25% of the total available measurement points are presented. The calculation is made using $n = 8$, $m = 10$ and α to $\varepsilon = 1$. The measurements show good consistency between the displacements and bending moments. The moment distribution below NAP-13 m and the resulting earth pressure seem to oscillate but an identical result was obtained for $n = 7$ and $m = 12$.
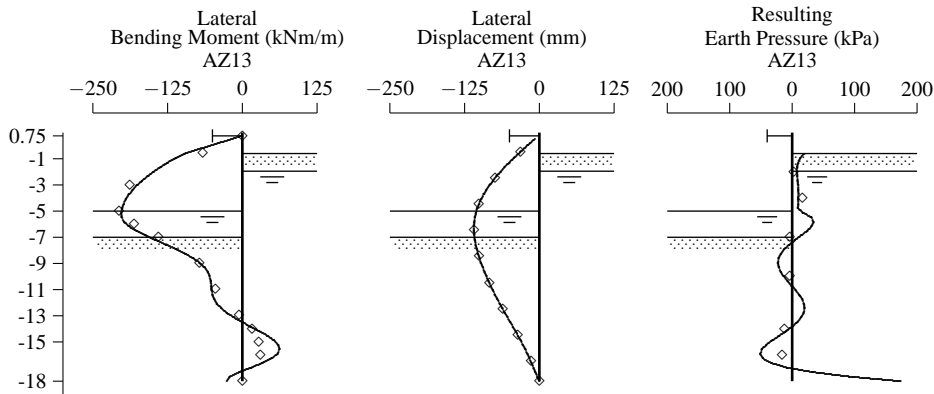
Figure 4.47: *Consistency check for AZ13-wall on May 11 1999: NAP−7.0 m/NAP−5.0 m and Prediction Stage III. The ⋄-marks indicate the measured data points, the polynomial is drawn with the solid line.*

The resulting earth pressure distribution on the AZ13-wall is further analysed in Chapter 6. In this section it is merely concluded that the measured displacements and bending moments for the AZ13-wall are consistent, and that the measured earth pressures can be explained from the displacements and bending moments from the field test.

The consistency check presented in this section is not suitable for verification of the measurements of the L607K-wall, because the method does not account for oblique bending. Figure 4.48 shows the consistency check performed by Kort [49]. This check is based on a best estimate of two 8th degree polynomials of the displacements in the x and y-directions, derived from the inclinometer measurements.
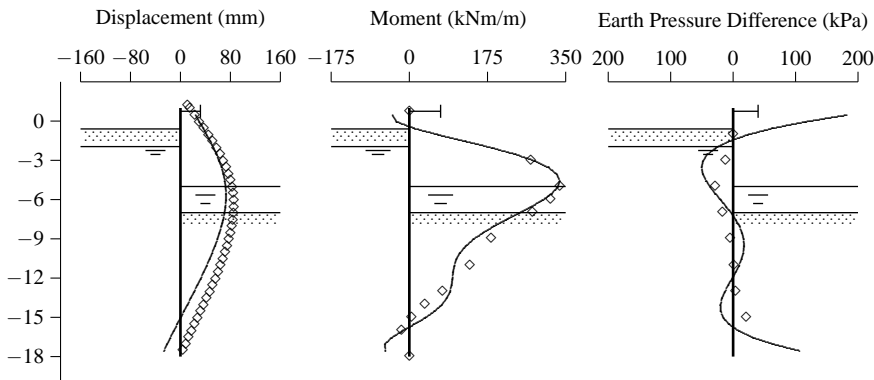
Figure 4.48: *Consistency of the earth pressure measurements on the L607K: May 11. The solid curves indicate the polynomials, the ⋄-marks the measurements. Results are plotted for the y-direction.*

The result of the analysis is given only for the lateral-direction. The result of the earth pressure analysis for the L607K is less robust than for the AZ13, as the inclinometer data in the x-direction has a relatively large measurement error, because of the small deformations.

Nevertheless comparison between the derived earth pressure difference and the measured values does not give any indication for serious concern over the values of the measured earth pressures.

Chapter 5

Predictions for the sheet pile wall field test

5.1 Introduction

For the Rotterdam sheet pile wall field test, specialists in steel sheet piling were invited to predict the behaviour of the sheet pile walls. The aims of the prediction exercise were:

- to validate the state-of-the-art calculation models for steel sheet pile walls in soft soil, including short-term and long-term behaviour

- to introduce the new phenomena of plastic design and oblique bending according to Eurocode 3, part 5 to the practising design engineers

This chapter gives an overview of the prediction exercise and the submitted predictions, and gives an evaluation of the six best predictions.

5.2 Overview and aim of the prediction exercise

The prediction exercise was organised on two levels. Each participant was free to submit one or more predictions for one or both levels. The predictions had to be submitted before the start of the field test, and therefore all predictions can be classified as type A (before the event).

Prediction level 1 was focused on practising design engineers. The aim of this prediction level was to make geotechnical design engineers aware of plastic hinges and oblique bending in steel sheet piling, especially as these phenomena have a large influence on the design and construction of safer and more economic sheet pile walls.

For prediction level 1 a comprehensive set of results of the field and laboratory tests was provided. This parameter set is given in Tables 5.1 and 5.2.

Level (m NAP) from	to	Soil type	γ_{avg} (kN/m³)	Level (m NAP)	Triaxial compression $\varepsilon = 0.01$ c'	φ'	$\varepsilon = 0.02$ c'	φ'	$\varepsilon = 0.03$ c'	φ'	failure c'	φ'	Triax. ext. failure c'	φ'	Field vane test $c_{u,peak}$
-1.50	-5.75	clay, silty slightly sandy	16.0	-2.63	6.9	22.1	7.3	28.3	8.1	29.9	7.7	35.5			123
				-3.02											
			17.6	-3.69	5.2	25.4	6.0	30.2	6.0	33.7	3.9	42.0			27.3
				-4.02											52.6
				-5.02											
			16.7	-5.40	6.2	20.1	5.5	28.7	4.7	34	0	47.2			
-5.75	-9.00	peat	10.0	-6.02									2	44	78.1
				-6.65											
			10.3	-6.82	6.7	14.1	9.1	21.6	10.5	27.2	14.1	51.9			58.6
				-7.02											60.3
				-8.02											
			10.0	-8.83	8.7	8.3	9.7	16.0	10.1	22.4	2.7	61.7			
-9.00	-10.50	peat, very clayey	11.4	-9.02	10.0	12.0	11.8	20.1	12.5	26.5	8.0	73.3			67.3
				-9.97											61.3
				-10.02											
-10.50	-12.50	clay, humous	13.9	-11.25	6.3	14.9	7.1	20.3	7.8	23.6	8.7	37.2			41.1
				-11.45											34.1
				-12.02											
-12.50	-16.10	clay, slightly sandy	16.2	-12.85	7.2	22.9	6.9	28.5	6.8	31.4	6.8	35.7	1	30	34.0
				-13.02											
			16.6	-13.70											
			16.4	-13.88	6.9	20.3	7.9	25.7	8.7	28.7	9.2	36.6			35.8
				-14.02											29.8
				-15.02											
			16.4	-15.63	3.7	24	5.4	29.5	6.3	32.5	5.2	39.6			
				-15.77											
			16.1	-15.93	7.9	19.3	9.4	24.6	10.2	27.5	7.8	37.8			31.7
-16.10	-17.00	clay, highly silty	12.3	-16.52											30.7
-17.00	-17.50	clay, slightly sandy	16.7												
-17.50	-18.50	sand, silty, medium coarse	20.0	-17.85	4.6	34.0	9.8	37.2	11.6	38.0	11.5	38.3			

Table 5.1: *Strength parameters for Prediction level 1*

Level (m NAP) from	to	Soil type	Level test (m NAP)	Menard pressiometer E (MPa)	p'_l (MPa)	Oedometer tests Keverling Buisman (NEN 5118 [62]) $1/C_{p1}$	$1/C_{p2}$	$1/C_{s1}$	$1/C_{s2}$	$e\log p$ $C_C(<p_c)$	$C_C(>p_c)$	C_s
+0.50	-1.50	sand										
-1.50	-5.75	clay, silty	-2.20 -2.30	2.4	0.48	0.0077	0.0017	0.0154	0.0041	0.04	0.16	
		slightly	-3.20 -3.55	1.8	0.34	0.0050	0.0013	0.0088	0.0023	0.02	0.06	0.01
		sandy	-4.20 -5.20 -5.55	1.3 1.8	0.21 0.27	0.0139	0.0028	0.0271	0.0067	0.09	0.30	
-5.75	-9.00	peat	-6.20 -6.75 -7.20 -8.20 -8.75	0.9 0.9 0.9	0.16 0.14 0.14	0.0536	0.0151	0.1286	0.0400	2.64	9.06	1.02
-9.00	-10.50	peat, very clayey	-9.20 -9.85 -10.20	0.8 1.3	0.14 0.14	0.0440	0.0102	0.1017	0.0317	0.94	3.69	0.69
-10.50	-12.50	clay, humous	-11.20 -11.35	0.6	0.10	0.0457	0.0112	0.1094	0.0359	1.21	4.34	
			-12.20 -12.75	0.6	0.10	0.0444	0.0118	0.0775	0.023	0.44	1.30	0.03
-12.50	-16.10	clay, slightly sandy	-13.20 -13.80	0.5	0.08	0.0315	0.0081	0.0484	0.0142	0.20	0.36	
			-14.20	0.6	0.11	0.0365	0.0072	0.0532	0.0113	0.25	0.53	
			-15.20	0.6	0.11	0.0303	0.0069	0.0569	0.0160	0.19	0.44	0.04
			-15.55 -15.80			0.0340	0.0078	0.0659	0.0144	0.22	0.67	
-16.10	-17.00	clay, highly silty	-16.20 -17.00	5.9	0.22	0.0222	0.0056	0.1200	0.0411	0.28	1.85	0.17
-17.00	-17.50	clay, slightly sandy	-17.20	0.4	0.11							
-17.50	-18.50	sand, silty, medium coarse										
-18.50	-22.00	sand, coarse	-20.20	8.3	1.51							

Table 5.2: *Stiffness parameters for Prediction level 1*

Prediction level 1 comprised two parts:

- Prediction of lateral displacements, lateral bending moments, earth and water pressures on both the AZ13 and the L607K test walls for stage I, II, and III of the field test:

    - Stage I: dry excavation to NAP−4.0 m

    - Stage II: wet excavation to NAP−7.0 m, inside water level on NAP−1.5 m

    - Stage III: lowering the internal water level to NAP−5.0 m

    This part can be considered as a real prediction for the field test

- The same questions for two imaginary walls:

    - L607K composed of single piles

    - A Z20-wall (Z-section with $W = 2000 \text{ cm}^3/\text{m}$) that could have been used, if a design with plastic hinges would not be permitted

    This part can be regarded as educational to make geotechnical design engineers aware of plastic hinges and oblique bending in steel sheet piling.

The imaginary walls were introduced to emphasise the phenomena of plastic hinges and oblique bending. The single-L607K can be compared to the double-L607K and the Z20 would have been needed if a plastic hinge would not be permitted.

Prediction level 2 was focused on the scientific aspects of the test and on the short and long-term behaviour of the sheet pile walls. The aim of prediction level 2 was to provide a benchmark to geotechnical engineers who specialise in the design of complex retaining structures using calculation tools with advanced soil models.

The participants were requested to assess the soil parameters using the complete soil investigation report [32]. Three main stages from the short-term field test were considered along with three stages from the long-term field test. The stages to be predicted are denoted as stage I to stage VI as follows:

- Stage I: Dry excavation to NAP−4.0 m

- Stage II: Excavation under water to NAP−7.0 m, water level on NAP−1.5 m

- Stage III: Lowering water level to NAP−5.0 m

- Stage IV: Stage III after 1 month

- Stage V: Stage III after 3 months

- Stage VI: Stage III after 6 months

The wall types which had to be used for prediction level 2, are the same 4 wall types as were asked for prediction level 1: AZ13, L607K-Double, L607K-Single and Z20.

For both levels, the predictors were asked to submit details about the calculation model they used. For prediction level 1, information was requested about the soil model, the wall

friction angle and the eventual reduction of the bending stiffness for the single and double U-piles. Additional questions for prediction level 2 concerned soil parameters and the types of soil tests they had used. The complete documentation of the prediction exercise is reported by CUR [28] and by Kort and Kelleners [50].

Twenty predictors submitted one or two predictions and a total of twenty-three predictions were received. A complete report of the submitted predictions giving details on individual predictions for every type of sheet pile and every prediction stage is provided by Kort and Kelleners [50].

5.3 Evaluation of submitted predictions

5.3.1 General

In this thesis, emphasis is put on Prediction Stage III and on the wall types AZ13 and L607K-double, because the predictions made with these wall types can be compared to the results measured in the test.

A total of twenty-three predictions were submitted: 12 for level 1 and 11 for level 2. Geographically, 19 predictions came from the Netherlands, 2 from Germany, 1 from France and 1 from the UK.

The predictions were submitted anonymously and as the background and professional experience of a predictor is not known, it is not possible to judge whether choices made in a prediction are well-considered or the result of blunders or gross errors.

5.3.2 Subdivision in prediction levels

An overview all the submitted predictions for Stage III, categorised into level 1 and level 2, is presented in Figure 5.1 for the AZ 13-wall and Figure 5.2 for the L607K-wall. A first conclusion that can be drawn from these figures is that in almost every prediction the maximum displacement and bending moment is significantly larger than measured.

In spite of the fact that a parameter set was provided for prediction level 1, it can be concluded that the spread in the submitted predictions is not significantly different for level 1 and level 2 predictions. To study the causes for this general overprediction and to determine lessons that can be drawn from all the entries, a throughout analysis of the predictions for Stage III is necessary.

Table 5.3 gives an overview of the models used for the level 1 predictions. Most of these were carried out with a subgrade reaction model (SRM), but two predictions were made with a finite element model (FEM). In almost every prediction with an SRM use was made of a bi-linear spring characteristic, although most predictors had a multi-linear spring at their disposal. For the determination of earth pressure coefficients, the curved slip plane theory of Kötter was used more frequently than the straight slip plane theory of Müller-Breslau [30] [1]. For the wall friction angle, most predictors used $\delta = 2/3\,\varphi'$ in sand and clay, and $\delta = 0^o$ in peat. In about half of all predictions, a reduction factor was applied to account for loss of stiffness of the double U-pile. According to CUR 166 [27], see Table 3.3, this reduction factor should be $\beta_I = 0.7$.

---

[1]In Prediction 21 earth pressure coefficients from Caquot and Kerisel [18] were applied
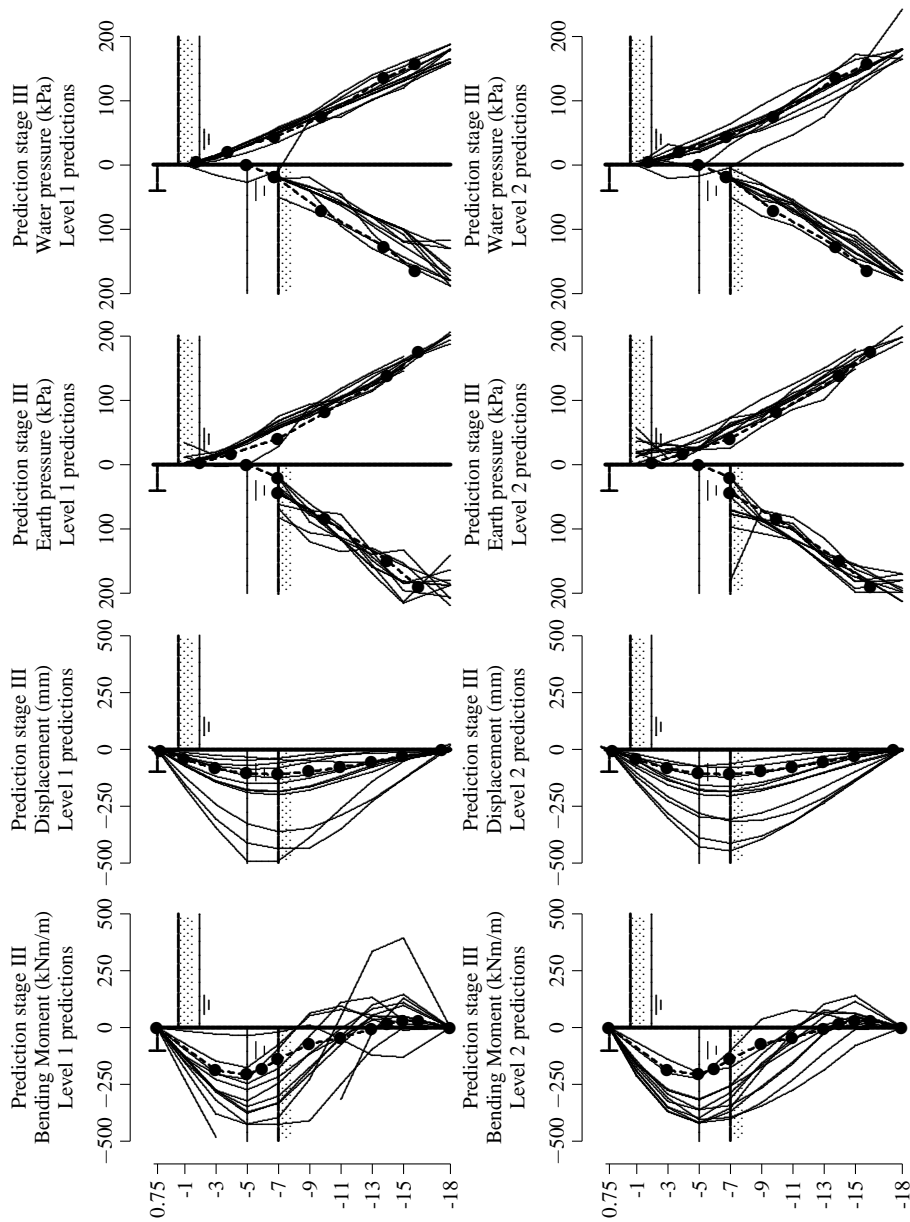
Figure 5.1: *Predictions AZ13 Stage III, subdivision in level 1 and level 2. The •-marks represent the field measurements*
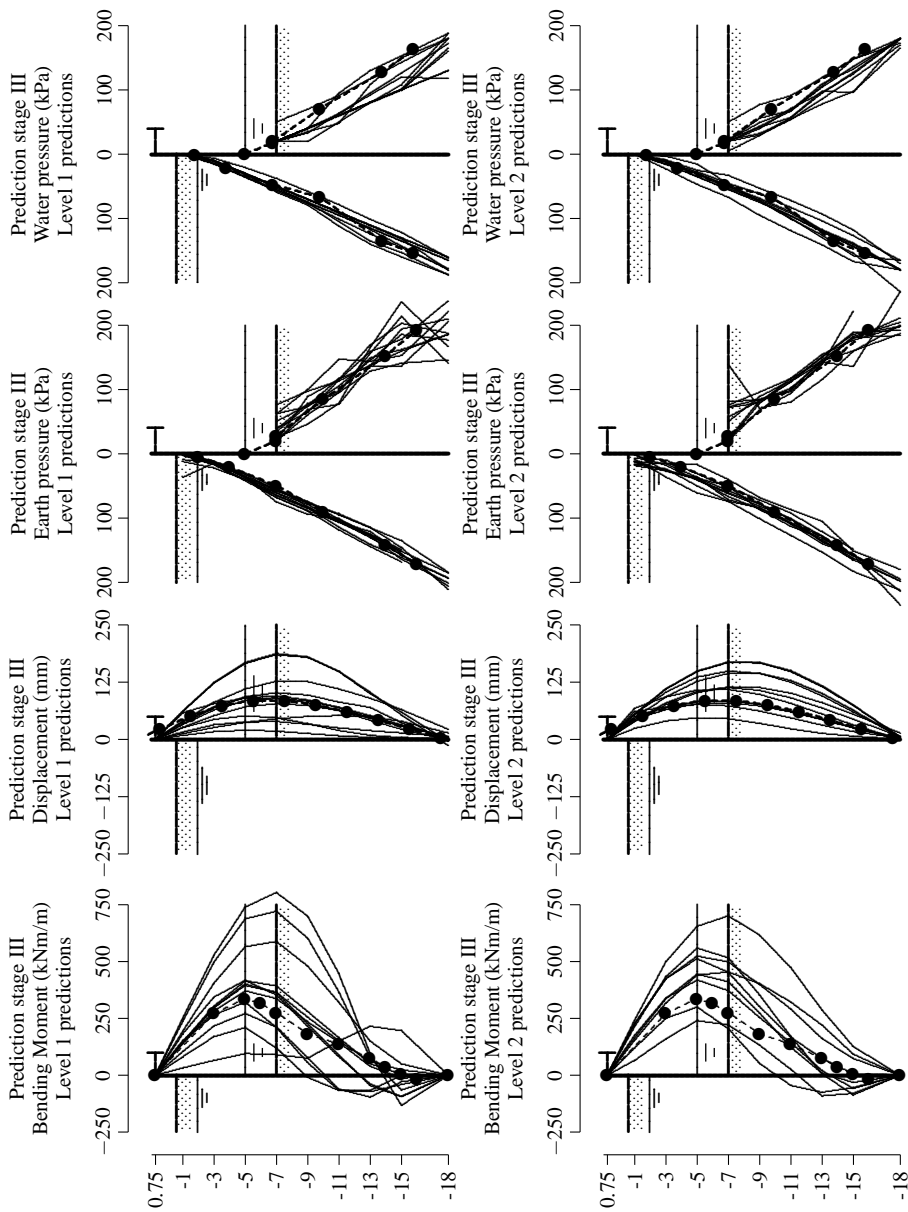
Figure 5.2: *Predictions L607K Stage III, subdivision in level 1 and level 2. The •-marks represent the field measurements*

Predic-tion	Method	Soil model	Slip plane	Wall friction angle				β_I
				sand	clay	peat	other	U-piles
1	SRM	bi-linear	straight	$5/9\varphi'$	$5/12\varphi'$	0	-	calculated
3	SRM	bi-linear	curved	$2/3\varphi'$	$2/3\varphi'$	$2/3\varphi'$	$2/3\varphi'$	-
5	SRM	bi-linear	-	25	10	0	15	-
6	SRM	bi-linear	curved	27.5	17.8	0	-	-
9	FEM	MC dr./HS undr.		-	-	-	-	0.7
10	SRM	bi-linear	straight	$2/3\varphi'$	$2/3\varphi'$	$2/3\varphi'$	$2/3\varphi'$	-
13	FEM	HS/SS		-	-	-	-	0.97
14	SRM	bi-linear	straight	$2/3\varphi'$	$2/3\varphi'$	0	$1/3\varphi'$	1.0
15	Semi-FEM	bi-linear	curved	φ'	φ'	φ'	φ'	1.0
17	SRM	bi-linear	curved	$2/3\varphi'$	$2/3\varphi'$	0	-	0.7
18	SRM	bi-linear	curved	$\varphi'-2.5$	$1/2\varphi'$	0	-	0.7
21	SRM	multi-linear	curved	$2/3\varphi'$	0	0	-	0.8
MC	Mohr-Coulomb Model			SS	Soft Soil Model			
HS	Hardening Soil Model			SSC	Soft Soil Creep Model			

Table 5.3: *Calculation models used for prediction level 1*

Table 5.4 gives an overview of the calculation models used for the level 2 predictions. Predictions 7 and 8, and Predictions 19 and 20 were submitted by one person/team. One level 2 prediction was made with MSHEET [30], the other predictions were all made with PLAXIS version 7. For modelling of the sand layers, most predictors used the Hardening Soil model (HS-model), and the clay and peat layers were modelled both with the HS-model, the Soft Soil model (SS-model) and the Soft Soil Creep model (SSC-model). For a complete description of the various soil models, reference is made to the corresponding PLAXIS manual [80].

Prediction	Method	Soil model			$\tan\delta/\tan\varphi'$			β_I
		sand	clay	peat	sand	clay	peat	U-piles
2	FEM	HS	HS	HS	1	0.5	0.5	0.8
4	SRM				-	-	-	0.8
7	FEM	MC	MC	MC	0.67	0.5	0.5	0.8
8	FEM	HS	SSC	SSC	0.67	0.5	0.5	0.8
11	FEM	HS	HS	SS	0.67	0.5	0.5	1
12	FEM	HS	SS	SS	0.67	0.5	0.5	0.8
16	FEM	HS	SS	SS	-	-	-	-
19	FEM	HS	SSC	SSC	0.7	0.7	0.7	-
20	FEM	HS	HS	HS	0.7	0.7	0.7	-
22	FEM	MC	SSC	SSC	-	-	-	0.8
23	FEM	HS	SS	SS	1	1	1	0.68
MC	Mohr-Coulomb Model			SS	Soft Soil Model			
HS	Hardening Soil Model			SSC	Soft Soil Creep Model			

Table 5.4: *Calculation models used for prediction level 2*

Most predictors chose a wall-friction angle of $\tan\delta = 2/3\tan\varphi'$ in sand and $\tan\delta = 1/2\tan\varphi'$ in clay. In contrast to the level 1 predictions, almost every level 2 predictor reduced the bending stiffness of the L607K-wall to account for oblique bending.

Prediction	c' (kPa)			κ^*			λ^*			AZ13	
	c	p	c	c	p	c	c	p	c	M_f	M_c
2	6.3	9.4	7.5	-	-	-	-	-	-	-361	48
4	4	2	9	-	-	-	-	-	-	-225	76
7	3	3	4	-	-	-	-	-	-	-399	50
8	3	3	4	0.008	0.03	0.034	0.022	0.12	0.073	-419	0
11	6.3	10.3	7.5	-	0.045	-	-	0.19	-	-315	14
12	7	10	7.4	0.0012	0.033	0.047	0.011	0.14	0.072	-421	45
16	6.3	10.3	8	0.003	0.009	0.007	0.017	0.044	0.033	-363	114
19	10	10	10	0.005	0.023	0.016	0.03	0.19	0.098	-420	140
20	10	10	10	-	-	-	-	-	-	-319	65
22	6.3	10.3	8	0.0025	0.033	0.01	0.012	0.13	0.05	-200	76
23	7.8	7.7	7.3	0.0075	0.039	0.011	0.031	0.19	0.081	-406	0
Measured bending moment in AZ13 (kNm/m)										-206	30

Prediction	φ' (^{o})			E_{50} (kPa)			E_{ur} (kPa)			L607K	
	c	p	c	c	p	c	c	p	c	M_f	M_c
2	29.1	19	27.5	-	-	-	18000	2600	4000	701	0
4	35	44	30	-	-	-	-	-	-	300	-75
7	28	37	26	4050	2430	5360	-	-	-	513	0
8	28	37	26	-	-	-	-	-	-	596	0
11	32.5	24.8	30.6	7200	-	2500	35000	-	14000	524	0
12	28	19	27	-	-	-	-	-	-	590	0
16	32.3	24.8	30	-	-	-	-	-	-	419	-58
19	30	30	30	-	-	-	-	-	-	559	-87
20	30	30	30	10970	1350	2860	52660	6490	13740	445	-32
22	32.5	24.8	30	-	-	-	-	-	-	240	-91
23	38.3	57.1	38.8	-	-	-	-	-	-	454	0
Measured bending moment in L607K (kNm/m)										337	-11
c: clay NAP-3.0m		p: peat NAP-7.0m			c: clay NAP-15.0m						

Table 5.5: *Soil parameters used for prediction level 2*

Table 5.5 gives an overview of the most important soil parameters assessed for the level 2 predictions for three important soil layers:

- Clay layer on NAP-3.0 m

- Peat layer on NAP-7.0 m

- Clay layer on NAP-15.0 m

The wide difference between the values selected for the various strength and stiffness parameters, which increase up to a factor of 4, is striking:

- Predictors 4 and 7/8 chose $c' = 2 - 3$ kPa, which corresponds to the value from the triaxial extension test for cohesion in the peat layer. Predictor 23 used $c' = 7.7$ kPa, corresponding to the 1% strain value from the triaxial compression test, Predictor 2 chose $c' = 9.4$ kPa, the 2% strain value, and Predictors 11, 12, 16, 19 and 20 chose $c' = 10$ kPa, the 3% strain value (see also Table 5.1 and Table 5.2)

- Predictor 2 and 12 used $\varphi' = 19^o$ (2% strain value) for the peat layer. Predictors 11, 16 and 22 chose $\varphi' = 24.8^o$ (3% strain value) and Predictors 4, 7/8 and 23 chose $\varphi' > 35^o$, the failure value either for compression or for extension

- The λ^* values from Predictions 12 and 22 are compared to those from Predictions 19 and 23. Predictors 12 and 22 used λ^*-values which can be back-calculated from the $e - \log p$ curves, whereas Predictors 19 and 23 used λ^*-values which can be back calculated from the $z - \log p$ curves

It cannot be concluded that the large differences in parameter choice are due to the fact that the distributed soil parameters have been considered as *model parameters*. Model parameters depend not only on physical soil properties but also on other factors which account for a specific soil model. For example, analysis using a subgrade reaction model with uncoupled springs requires a model parameter to not only cover the physical soil behaviour but also the deficiencies of the SRM, such as modelling of arching.

On the other hand, it can be concluded from the submitted soil parameters, given in Table 5.5, that the current state-of-the-art of parameter assessment for advanced calculations of sheet pile walls is not consistent.

The result of an inconsistent parameter choice is a wide spread of the predicted span and fixed moments. On the basis of Figures 5.1, 5.2, and Table 5.5 some typical observations are given regarding the relationship between parameter choice and predicted result, followed by a qualitative judgement:

- The bending moment in Prediction 4 is very close to the measured bending moment, both for the AZ13 wall and the L607K-wall. On the other hand, Prediction 4 is the only level 2 prediction made with a subgrade reaction model, which is by far the least advanced calculation model

  There may be three important reasons why one of the best predictions has been obtained with an SRM. Firstly, an SRM requires less input parameters than an advanced FE soil model where the outcome is often very sensitive because of the large number of input parameters. Not every parameter has an evident physical quantity that can be measured easily, which makes to very difficult to introduce accurate values. A second reason can be found in the definition of *experience*. For more than 25 years, SRM has been used for design of steel sheet pile walls. This predictor may have gathered wide experience with SRM and measurements in steel sheet piling, so that he is experienced in making predictions with SRM. The third reason may be that the predictor made one or two blunders and accidentally obtained a calculation result close to the measured values. This latter reason may sound weak but can certainly not be ruled out.

- Prediction 22, made with the SSC-model, gave a very good result for the AZ13-wall, see Table 5.4. However, for the L607K-wall the results deviated further from the measured results. The large deviation of the fixed moment is not only the result of an overestimation of the fixed moment capacity. Consider the soil model and soil parameters used in predictions 11, 16 and 22 with respect to the measured bending moment. The strength parameters c' and φ' are exactly the same but the soil models and the stiffness parameters are different. The difference in predicted bending moment for both the AZ13-wall and the L607K-wall, however, is significant

  It appears that a proper choice of the strength parameters only is not sufficient to obtain an accurate prediction. Other variables, such as soil models, stiffness parameters and permeability, are at least of equal importance.

- In Predictions 8 and 12, the bending moments predicted for the L607K-wall are practically the same but both the soil models (SS-model and SSC-model) and the soil

parameters applied are completely different. Nevertheless, the predicted bending moment is not even close to the measured bending moment

It is very possible that the same calculation result can be obtained with different soil models and different soil parameters. This does not mean that every calculation that gives results close to the measured values, is also a good prediction. A prediction is only good when the calculation describes the actual soil behaviour and when the input parameters can be determined from the soil testing in an understandable way.

- The predictions 7/8 and 19/20 were submitted by one person/team who only varied the soil model. Therefore the strength parameters in these predictions are exactly the same and the stiffness parameters are as consistent as possible. Predictions 7 & 8 show that the simple Mohr-Coulomb model gives better results than the more advanced HS and SSC models. Predictions 19 & 20 show that the HS model gives better results than the SSC model

Prediction 7/8 is a typical example of the fact that a more advanced model does not necessarily lead to a better prediction, either because the advanced model is only advanced with respect to a specific soil behaviour (creep) and not so advanced with respect the complicated soil behaviour near sheet piling, e.g., the combination of unloading and shear, and anisotropy, or because this predictor was more experienced in using a simple model than a mode advanced model.

Prediction 19/20 on the other hand can be considered as *equally advanced* but in respect of different characteristics, the SSC-model gives a better description of the creep behaviour of soil and the HS-model gives a better description of the strain-hardening behaviour of soil. Both phenomena are of importance for the real behaviour of the test walls, but it should be realised that none of these two soil models is suitable for anisotropic behaviour of the clay and peat layers. So although the HS-model gives a better result than the SSC-model, this does not mean that the HS-model is the ideal model for this type of soil.

Although on average, the measured values were overpredicted, it may be concluded that a good prediction can be obtained with a subgrade reaction model (Prediction 4) and with a soft soil creep model (Prediction 22), but also with a hardening soil model (level 1 Prediction 13) a good prediction was obtained. This is an important conclusion for design practice, as for normal projects the design engineer does not always have sufficient soil data to use a very advanced model.

Two important lessons can be learned from this prediction competition:

- Parameter assessment should be adapted to the choice of soil model. This means implicitly that the type of soil investigation should be adapted to the choice of soil model, and vice versa

- Using a more advanced model does not automatically guarantee a qualitatively better prediction. Only when a more advanced model is used in combination with well-considered parameter assessment and experience from the design engineer, preferably gained from measurements in a similar project, can a qualitatively better prediction be obtained

5.3.3   Consideration of time-dependent behaviour

For the level 2 predictions, the states 1, 3 and 6 months after Stage III were requested. It is more interesting to compare the predictions for the L607K-wall than for the AZ13-wall, because introduction of the sand mound behind the AZ13-wall means that the long-term predictions and measurements for the AZ13-wall are not comparable anymore.

Table 5.6 gives an overview of the predictions for the long-term behaviour of the L607K-wall. The measurements show that the maximum span moment M_s increased 76 kNm/m (23%) after 1 month and 123 kNm/m (37%) after 3 months. The maximum fixed moment M_f decreased over the long-term period. Few predictors expected an increase of more than 10% after 3 months and only Predictor 22 expected an increase of more than 100 kNm/m after 3 months.

	L607K											
Prediction	2	4	7	8	11	12	16	19	20	22	23	Measured
Maximum span moment M_s (kNm/m)												
Stage III:M_s	701	300	513	596	524	590	419	559	445	240	454	337
Stage IV:M_s	748	-	528	646	543	596	441	632	445	337	-	413
Stage V:M_s	778	-	550	-	546	601	449	-	448	370	-	460
Stage VI:M_s	804	383	573	-	551	606	458	-	450	380	-	-
Increase of maximum span moment M_s (%)												
1 month	7	-	3	8	4	1	5	13	0	40	-	23
3 months	11	-	7	-	4	2	7	-	1	54	-	37
6 months	15	28	12	-	5	3	9	-	1	58	-	-
Maximum fixed moment M_f (kNm/m)												
Stage III:M_f	0	-75	0	0	0	0	-58	-87	-32	-91	0	-18
Stage IV:M_f	0	-	0	0	0	0	-50	-40	-40	-95	-	-4
Stage V:M_f	0	-	0	-	0	0	-51	-	-46	-80	-	0
Stage VI:M_f	0	-95	0	-	0	0	-51	-	-51	-73		-

Table 5.6: *Long-term predictions for the L607K-wall*

A gradual decrease of the maximum fixed moment was only predicted in Prediction 19, made with the SSC model. In Predictions 4 and 20, made with a subgrade reaction model and the HS-model respectively, an increase of the fixed moment was predicted. In Prediction 16 an initial decrease was predicted followed by stabilisation, and in Prediction 22 an initial increase was predicted followed by a decrease of about $\Delta M_c = 20$ kNm/m. The latter two predictions were made with the HS-model. The question of whether the predicted behaviour of the fixed moment is the result of the soil model or of the parameter choice should be answered from back-analyses, see Chapter 6.

In Table 5.7, the permeabilities used by the different predictors are summarised. Prediction 22 (and Prediction 23) were the only ones in which the SS-model was used in combination with a permeability of $k \approx 10^{-7}$ m/s, the other predictors used $k \approx 10^{-9}$ to 10^{-10} m/s which was found from the oedometer tests, generally interpreted with Taylor's method.

The influence of the permeability on the long-term behaviour is investigated in more detail in Section 6.7.
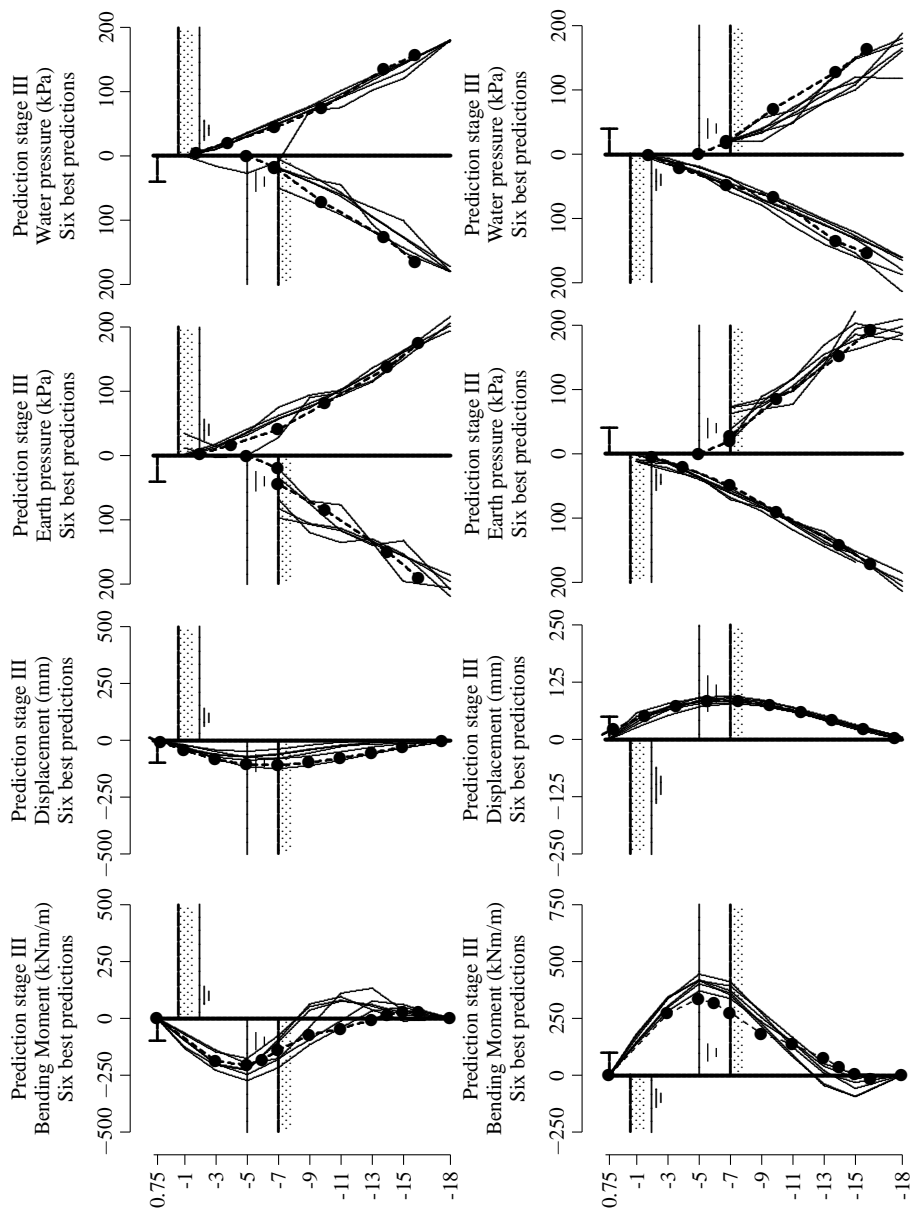
Figure 5.3: *Six best predictions of the AZ13-wall and the L607K-wall, in Stage III. The •-marks represent the field measurements*

Predicted vertical permeability (m/s)				
Prediction	2	7	8	11	12
clay NAP-3m	$5.5\,10^{-9}$	$1\,10^{-9}$	$1\,10^{-9}$	$5.7\,10^{-10}$	$3.7\,10^{-10}$
peat NAP-7m	$7\,10^{-9}$	$1.3\,10^{-9}$	$1.3\,10^{-9}$	$9.3\,10^{-10}$	$9.99\,10^{-10}$
clay NAP-15m	$2\,10^{-9}$	$2.5\,10^{-10}$	$2.5\,10^{-10}$	$2.3\,10^{-10}$	$4.66\,10^{-10}$
Prediction	16	19	20	22	23
clay NAP-3m	$5.8\,10^{-10}$	$6\,10^{-10}$	$6\,10^{-10}$	$6\,10^{-7}$	$9\,10^{-7}$
peat NAP-7m	$8.8\,10^{-10}$	$1\,10^{-9}$	$1\,10^{-9}$	$1\,10^{-7}$	$8\,10^{-7}$
clay NAP-15m	$2.7\,10^{-10}$	$2.2\,10^{-10}$	$2.2\,10^{-10}$	$1\,10^{-7}$	$4.5\,10^{-7}$

Table 5.7: *Predicted vertical permeability for the L607K-wall*

5.3.4   Overview of the six best predictions

In Figure 5.3 and Table 5.8, an overview is presented of the six best predictions for the AZ13-wall and the L607K-wall. The criterion for the best AZ13-predictions is the level of the maximum bending moment, because the implicit aim for the AZ13-wall was to predict whether the maximum elastic moment would be exceeded and a plastic hinge generated. The criterion for the L607K-wall is based both on the accuracy of both the predicted displacements and bending moment.

AZ13 Prediction	level	Calculation model	Soft soil model	M_s (kNm/m)	M_f (kNm/m)	level M_f (m NAP)	w_{max} (mm)
1	1	SRM		-247	133	-13	-89
4	2	SRM		-225	76	-11	-74
13	1	FEM	SS	-274	49	-15	-125
15	1	Semi-FEM	MC	-228	95	-11	-72
18	1	SRM		-176	79	-11	-49
22	2	FEM	SS	-200	76	-13	-81
Measured				-206	30	-16	-109
L607K Prediction	level	Calculation model	Soft soil model	M_s (kNm/m)	M_f (kNm/m)	level M_f (m NAP)	w_{max} (mm)
9	1	FEM	HS	418	-95	-15	95
13	1	FEM	SS	371	-13	-15	91
14	1	SRM		415	0	-18	78
16	2	FEM	SS	419	-58	-15	80
17	1	SRM		402	-94	-15	89
20	2	FEM	HS	445	-32	-15	84
Measured				337	-18	-16	85

Table 5.8: *Overview of the six best predictions*

Four of the six best AZ13 predictions were level 1 and two were level 2. Three predictions were made with a subgrade reaction model, one with the semi-finite element model FREW [7] and two with a finite element model. In both finite element calculations, the soft clay and peat layers were modelled with the PLAXIS SS-model.

Although the six best AZ13 predictions have a maximum span moment close to the measured value, the prediction of the fixed moment is not so promising. In three of the six predictions the fixed moment is generated just below excavation level, see Figure 5.3. This

high fixed moment is caused by a significant overprediction of the effective earth pressures in combination with an underprediction of the water pressure on the excavated side. In Prediction 4 a negative water pressure of -20 kPa just below excavation level was included which accounted for swelling of the peat layer. In Prediction 13 a negative water pressure of about -25 kPa on the retained side was predicted, which suggests undrained response, see Section 6.4. However, Prediction 13 was the only one in which the predicted displacement was larger than 100 mm and the predicted maximum fixed moment was at NAP-15 m.

Furthermore, the prediction of the maximum fixed moment is shown to be the result of underprediction of the displacement and water pressure on the excavated side, and overprediction of the effective earth pressure on both sides of the wall. It can therefore be concluded that none of the six predictions gives an accurate representation of the measured soil behaviour. Nevertheless the predictions show that both the subgrade reaction model and the (semi-)finite element model are suitable tools for the calculation of this sheet pile wall field test.

With regard to the L607K-predictions, four of the six best predictions were also level 1 and two were level 2. Four predictions were made with FEM and two with SRM. Prediction 20 gave the most accurate displacement and Prediction 13 the most accurate bending moment distribution. The spread of the predicted moments and displacements for the L607K-wall was smaller than for the AZ13. As for the AZ13-wall, the L607K predictions all show a slight underprediction of the water pressure on the excavated side in combination with an overprediction of the effective earth pressure. Although the maximum span bending moment is overpredicted in all six predictions, the moment distribution is much better predicted than for the AZ13-wall.

The two main differences between the AZ13 and the L607K-walls are the pile type, Z and double U, but for the predictions, of greater importance is the large difference in bending stiffness, which for the L607K-wall is 3 to 3.5 times larger than for the AZ13-wall. It is striking that the six best L607K entries predicted a maximum bending moment in the range of 325 kNm/m to 375 kNm/m for the AZ13-wall, whereas $M = 206$ kNm/m was measured. This large difference between the predicted and measured bending moment is investigated in Chapter 6.

5.4 Conclusions from the submitted predictions

The two aims of the predictions concerned the state of the art for the calculation models and the introduction of the new plastic design and oblique bending phenomena to design engineers. With regard to the state of the art for the calculation models, the following conclusions can be drawn from the submitted predictions:

- In almost every prediction, the maximum displacement and bending moment is significantly larger than measured, but a few predictions are quite accurate

- Accurate predictions may be obtained from well-considered parameter assessment, but also from errors that cancel each other

- Performing an accurate prediction seems to be possible with both simple and more advanced models. The success of an accurate prediction depends on the *input parameters* applied to the model. An input parameter may be composed of a *physical soil*

property and an *imaginary model factor*. Consequently these input parameters are different for each model

- The imaginary model factor depends both on the geometry and the type of soil, and is therefore more than defined by local experience. From a practical point of view the imaginary model factor should be controlled (simple models and short-term policy), but from a scientific point of view the imaginary model factor should be cancelled (advanced models and long-term policy)

- The design engineer must exercise great skill for a proper assessment of these composed input parameters

The wide spread in parameter choice suggests a general lack of skill in parameter assessment, or an outdated directive. A general trend appears to be the use of advanced soil models but, ironically, to assess the input parameters from triaxial compression tests with 1%, 2% and 3% strain values, whereas in excavations, soil is unloaded and the soil model covers strain hardening.

Summarising it can be concluded that a clear and updated directive for parameter assessment is required which distinguishes between simple, effective calculation models and the advanced state-of-the-art soil models, both in combination with the different stress paths along which the soil is loaded.

Concerning the introduction of the new phenomena of plastic design and oblique bending, it can be concluded that the combination of field test, prediction, and review encourages discussion about plastic design and oblique bending and therefore contributes to a better understanding of these phenomena.

Chapter 6

Evaluation of the sheet pile wall field test

6.1 Introduction

The measurement results of the Rotterdam Sheet Pile Wall Field Test and the results of the 23 type A predictions are presented in Chapter 4 and 5 respectively. This chapter gives a comprehensive evaluation of the observed behaviour of the test walls. Use is made of simple analytical calculations and numerical computations with PLASWALL and PLAXIS.

Initially, the plastic hinge is discussed. A comparison is made between the verification models described in Chapter 2 and the measured plastic rotation. Next, oblique bending of the L607K-wall is evaluated. The reduction factors β_I and β_W are determined for several stages and verified against the theory developed in Chapter 3. In Section 6.4 the measured earth and water pressures are analysed, giving a better insight into the short and long-term behaviour of the test walls.

This chapter concludes with back-analyses; firstly, PLAXIS 3D is used to investigate to what extend 2D calculations are representative of actual 3D behaviour of the excavation. This is followed by back-analyses of the short and long-term test results with PLASWALL and PLAXIS. These back-analyses aim to prove the applicability of the field test to the validation of calculation models for steel sheet pile walls. Therefore the back-analyses focus on explanation of the measured behaviour and validation of the numerical models rather than determination of the proper parameter set for this case.

6.2 Plastic hinge

6.2.1 General

The design rules for plastic design outlined in Chapter 2, are based on thorough laboratory testing and FE analyses of the plastic behaviour of steel sheet piles. During this testing, typical observations were made that form the basis of the design rules, for example the

shape of the plastic hinge and the simplified methods to determine the rotation requirement. In this section these two aspects are evaluated with respect to the field measurements.

6.2.2 Shape of the plastic hinge

The left photo in Figure 6.1 shows the shape of the plastic hinge generated in the field test, and the right photo, a plastically deformed pile after a four-point bending test. Note in the middle of the left photo that the epoxy protection strip for the wiring visibly ripped open.

Figure 6.1: *Shape of plastic hinge observed in field test and in a four-point bending test*

The shape of the plastic hinge is comparable and in agreement with the mechanism described in Section 2.3.2:

- the compression flange buckled and deformed in such a way that the nett height of the cross-section decreased

- the web also deformed out of plane in the opposite direction to the flange deformation

- the plastic kink is rather concentrated but plasticity in the cross-section is over a relatively large portion of the sheet pile, indicated with the two pens in the right photo

6.2.3 Determination of plastic rotation angles in the field test

Figure 6.2 shows the state of the AZ13 piles A2, A4 and A5 when the plastic hinge was fully developed. This state is also referred to as the state on January 31st 2001. The displacements and wall inclinations are compared with the state just before rotation in the plastic hinge occurred. For the accompanying distributions of bending moments and earth pressures reference is made to Figure 4.31.

The plastic hinge was generated in a concentrated zone at approximately NAP−5.5 m. In the displacement curve, the plastic hinge is clearly visible. The amount of plastic rotation in the hinge can be derived from the distribution of the tilt; the straight, almost horizontal, line represents a large change of tilt over a short length of sheet pile. The plastic rotation angle is derived from the start and end points of this line, as indicated in the figure.
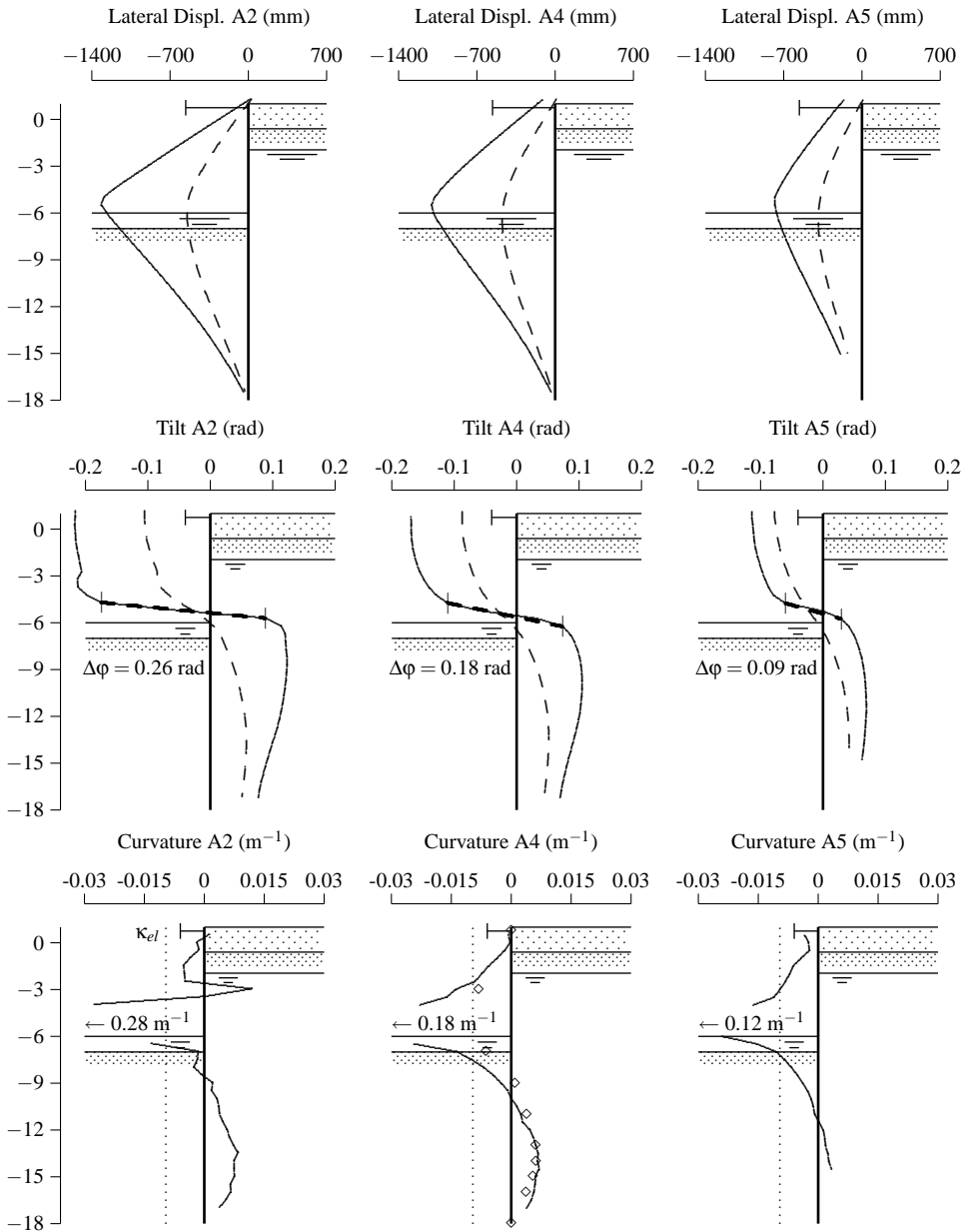
Figure 6.2: *Lateral displacement, wall inclination, and curvature for the AZ13 piles A2, A4 and A5 for the beginning and end of test Part 6, see Table 4.4. The dashed lines indicate the state on January 18 2000 and the solid lines the state on January 31*

The plastic rotation angles in piles A2, A4 and A5 are:

- A2: $\Delta\varphi_{measured} = 0.26$ rad

- A4: $\Delta\varphi_{measured} = 0.18$ rad

- A5: $\Delta\varphi_{measured} = 0.09$ rad

6.2.4 Verification of design methods to the measured plastic angles

In Section 2.4.6, two simplified methods are presented to determine the plastic rotation angle from the displacement curve and the structural properties of the sheet pile wall. Although these methods have been developed as a rotation check in a plastic design, they can be validated against the measured plastic rotation angle $\Delta\varphi_{measured}$. The real structural properties of pile A4, determined just after the field test, are given in Table 6.1.

pile	A cm^2	I cm^4	W cm^3	b mm	b_f mm	t_f mm	f_y N/mm^2	$\frac{b_f}{t_f\varepsilon}$	W_{pl} cm^3	M_{pl} kNm/m	M_u kNm/m
A4	182	25636	1697	1356	387	9.7	315	46.1	1985	467	467

$E = 2.1\,10^8$ kN/m^2

Table 6.1: *Structural properties of pile A4, determined with a four-point bending test*

Method III: simplified assumption based on rotations

In method III the plastic rotation angle $\Delta\varphi_{III}$ is determined according to:

$$\Delta\varphi_{III} = \Phi_R = \varphi_{rot} - \varphi_{pl} \tag{6.1}$$

where φ_{rot} and φ_{pl} are determined in accordance with Figure 6.3.
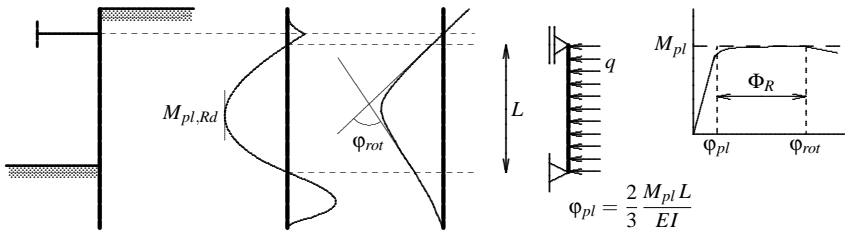
Figure 6.3: *Method III: simplified assumption of Φ_R based on rotations*

The span lengths L were derived from the curvature plots in Figure 6.2:

- A2: $L = 9.25$ m

- A4: $L = 10.50$ m

- A5: $L = 11.75$ m

Using $EI = 39702$ kNm^2/m, $M_{pl} = 467$ kNm/m and the measured data plotted in Figure 6.2, the following plastic rotation angles were found:

- A2: $\Delta\varphi_{III} = 0.27$ rad (measured: 0.26 rad)

- A4: $\Delta\varphi_{III} = 0.19$ rad (measured: 0.18 rad)

- A5: $\Delta\varphi_{III} = 0.09$ rad (measured: 0.09 rad)

Method IV: simplified assumption based on displacements

In method IV the plastic rotation angle $\Delta\varphi_{IV}$ is also determined according to:

$$\Delta\varphi_{IV} = \Phi_R = \varphi_{rot} - \varphi_{pl} \tag{6.2}$$

where φ_{rot} and φ_{pl} are determined in accordance with Figure 6.4.

$$\varphi_{rot} = \frac{w_2 - w_1}{L_1} + \frac{w_2 - w_3}{L_2}$$

$$\varphi_{pl} = \frac{5}{12}\frac{M_{pl}L}{EI}$$
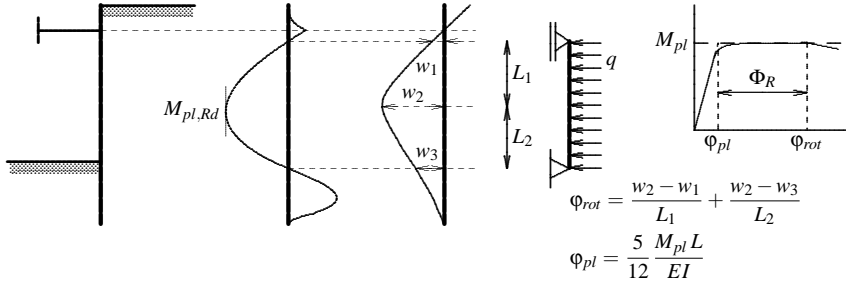
Figure 6.4: *Method IV: simplified assumption of Φ_R based on displacements*

The results are:

- A2: $\Delta\varphi_{IV} = 0.25$ rad (measured: 0.26 rad)

- A4: $\Delta\varphi_{IV} = 0.18$ rad (measured: 0.18 rad)

- A5: $\Delta\varphi_{IV} = 0.09$ rad (measured: 0.09 rad)

The maximum difference in the rotation requirement between the simplified methods III and IV, and the measured values is 0.01 rad, which implies a maximum error of about 5%. Therefore it can be concluded that both Method III and Method IV give good results for plastic rotation in the hinge and are therefore satisfactorily methods to determine the rotation requirement.

6.3 Oblique bending

6.3.1 General

In this section the reduction factors β_I and β_W are determined for various stages of the field test and compared to the design methods presented in Chapter 3.

6.3.2 Method to determine reduction factors

Determination of β_I

In Section 3.4.6 a method is described to determine the reduction factors β_I and β_W from oblique bending calculations with SKEWWALL. This method requires the input of both an oblique bending and a normal bending calculation and was applied to various calculations in order to derive the design rule presented in Section 3.7. However, this method is not applicable to determination of the loss of stiffness and strength that occurred in the field test, because a comparable case with normal bending is missing.

This section starts with the derivation and testing of a second method to determine β_I from a sheet pile wall in oblique bending. The constitutive equations for oblique bending

$$M_x = EI_{xx}\kappa_x + EI_{xy}\kappa_y \tag{6.3}$$
$$M_y = EI_{yx}\kappa_x + EI_{yy}\kappa_y \tag{6.4}$$

are written in the form

$$M_y = \beta_I EI_{yy}\kappa_y \tag{6.5}$$

where

$$\beta_I = \frac{EI_{yx}\kappa_x + EI_{yy}\kappa_y}{EI_{yy}\kappa_y} \tag{6.6}$$

To validate this method, the case presented in Figure 3.10 is considered again. For the calculation results for oblique bending, reference is made to Figure 3.11, Figure 3.12 and Table 3.7.

The left part of Figure 6.5 shows the distribution of β_I with depth determined from equation (6.6). In the same figure, the lateral displacement is plotted. It is shown that the factor β_I does not have a constant value but varies with depth. In this method, the critical value of β_I is assumed at the level of the maximum lateral displacement, indicated by the dotted line; from the figure $\beta_I = 0.62$ is obtained.

In the right part of Figure 6.5, the oblique bending calculation is compared with the normal bending calculation using $\beta_I = 0.62$. This factor is lower than $\beta_I = 0.70$, found with the method described in Section 3.4.6, which also proved to be a useful approximation. However, in Figure 3.14, the displacements were slightly underestimated using $\beta_I = 0.70$, whereas it can be seen in Figure 6.5, that the lateral displacements fit very well for $\beta_I = 0.62$. Therefore it can be concluded that the method presented in this section can be applied to determine β_I from the field measurements.

It is remarked that the method presented in this section and the method in Section 3.4.6 are merely different approaches to determine β_I; it can not be stated that one method is better than the other.
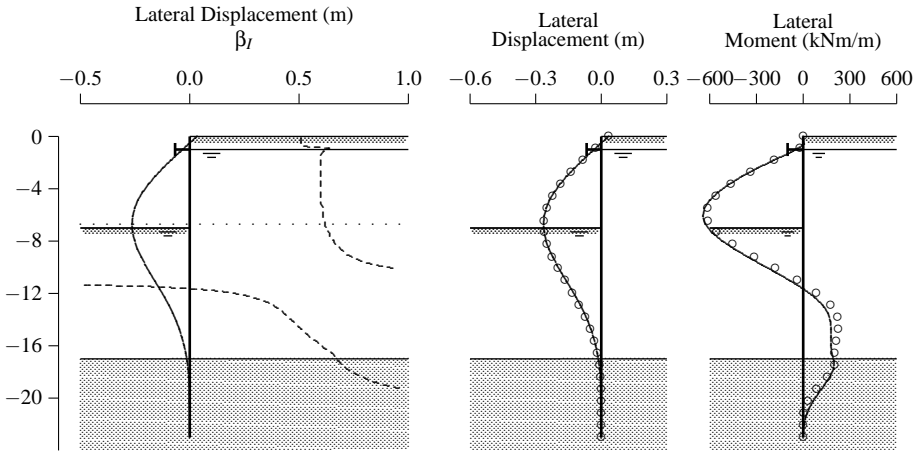
Figure 6.5: *Distribution of* β_I *with depth and oblique bending calculation compared with normal bending using* $\beta_I = 0.62$. *Solid lines represent the oblique bending calculation, the dashed line the distribution of* β_I *with depth, and* ∘*-marks the reduced normal bending calculation*

Determination of β_W

An equivalent section modulus W_{eq} is determined from the maximum bending moment and the strains measured at that level according to

$$W_{eq} = \frac{M_{max}}{\sigma} = \frac{M_{max}}{E\left(\varepsilon + \kappa_x x + \kappa_y y\right)} \tag{6.7}$$

In every test stage, W_{eq} appeared to have a minimum value for $x = +129.6$ mm and $y = -217.5$ mm. The reduction factor follows from

$$\beta_W = \frac{W_{eq}}{W} \tag{6.8}$$

where W is the section modulus for a continuous wall ($W = 3220$ cm^3/m).

6.3.3 Determination of actual reduction factors β_I and β_W in the field test

The reduction factor β_I can be determined from either the displacement measurements (pile H2, H4 and H6) or the strain measurements (pile H5). In practice, measurement errors in field data make the analysis more difficult and therefore it should be realised that the values of β_I determined from the strain measurements in pile H5 may be more accurate than those determined from the inclinometer measurements in piles H2, H4 and H6. However, the reduction factor β_W could only be determined from the strain measurements in pile H5, because it appeared that the influence of ε in equation (6.7) could not be neglected.

Table 6.2 gives an overview of β_I and β_W determined for various test stages. After the dry excavation, the amount of oblique bending was negligible and after the excavation under

Stage	Activity	Date	β_I H2	H4	H5	H6	β_W H5
Stage 1:	short-term field test						
1.1	dry excavation to NAP−4.0 m	Apr. 15 1999	0.60	1.00	0.97	1.00	*0.68*
1.3	excavation under water to NAP−7.0 m	Apr. 22 1999	*0.99*	0.74	0.68	1.00	0.74
1.9	lowering water level to NAP-5.0 m	May 11 1999	0.57	0.68	0.68	0.76	0.73
Stage 3:	long-term field test						
3	end of long-term test	Aug. 11 1999	0.56	0.70	0.69	*0.52*	0.73
Stage 5:	additional load increase: water level on NAP−6.0 m						
5.2	final measurement	Jan. 24 2000	0.58	0.72	0.71	0.80	0.69

Table 6.2: *β_I and β_W determined in various stages of the sheet pile wall field test*

water, β_I and β_W had a constant value during the entire test of $\beta_I = 0.7$ in pile pairs H4 and H5. In pile H2, β_I was generally smaller ($\beta_I = 0.6$) and in pile H6, β_I was generally larger ($\beta_I = 0.8$). During the entire test β_W was about $\beta_W = 0.73$, which should be compared to $\beta_I = 0.68$ in pile H5.
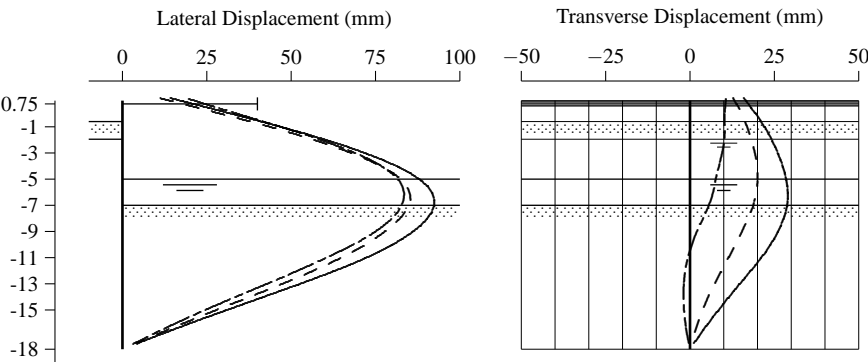
Figure 6.6: *Lateral and transverse displacements in pile H2 (solid line), H4 (dashed line) and H6 (dashed-dotted line) on May 11 1999*

Figure 6.6 shows the lateral and transverse displacements in the three L607K test piles. The lateral displacement and transverse curvature are largest in pile H2 and smallest in pile H6. This is typical for all the test stages and means that a greater loss of stiffness may be expected in pile H2 than in pile H4 and H6. For this reason it can be stated that the value of $\beta_I = 0.99$, measured in pile H2 after the excavation under water and $\beta_I = 0.52$, measured in pile H6 at the end of the long-term field test, are not realistic values but rather the result of measurement inaccuracies. The same applies to $\beta_W = 0.68$ just after the dry excavation.

The different β_I's for the four piles are most probably the result of installation effects. The sheet piles were driven with a rig equipped with a continuously adjustable impact-vibration hammer installed on a leader and therefore precise pile installation was possible. It was observed during installation that the piles near H6 were installed with more effort than the piles near H2. It can therefore be concluded that β_I was not a constant value but varied between $\beta_I = 0.57$ and $\beta_I = 0.78$, depending on the pile installation, with an average of $\beta_I = 0.70$.

15 April 1999
$\gamma = 4.6°$

22 April 1999
$\gamma = 12.2°$

11 May 1999
$\gamma = 13.1°$

11 August 1999
$\gamma = 12.9°$
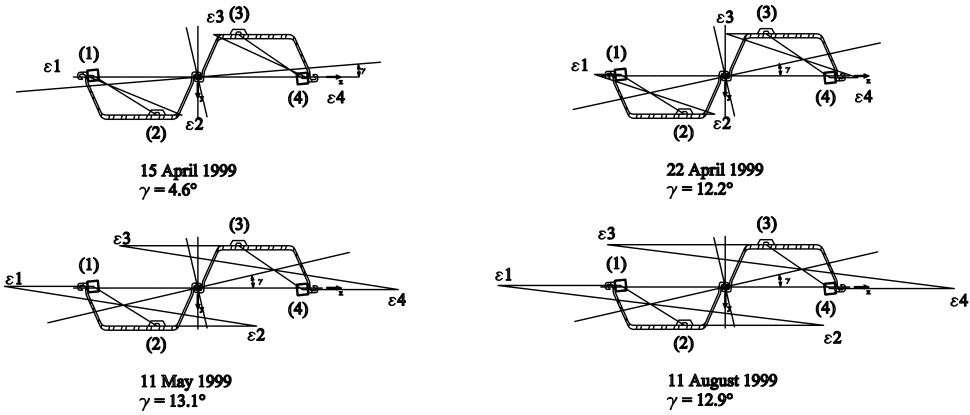
Figure 6.7: *Strain distribution at NAP−5.0 m in pile H5 for various stages of the field test*

Figure 6.7 shows the strain distribution at NAP−5.0 m, in pile H5, for various stages of the field test. NAP−5 m is the level close to the maximum bending moment and is the level where the rotation of the neutral axis is close to the largest value. At this level, rotation of the neutral axis, denoted with γ, may be compared to the rotation of the principle axes of inertia, $\alpha = 20.98^o$: if γ is close to zero, oblique bending is impeded and if γ is close to α, oblique bending occurs.

Rotation of the neutral axes shows that after the dry excavation oblique bending hardly occurred and that during the rest of the field test β_I must have been somewhere halfway between $\beta_{I,0} = 0.47$ and one. The strain distributions confirm the values of β_I's presented in Table 6.2.

6.3.4   General evaluation concerning oblique bending in the field test

Comparing the existing and new design rules presented in Chapter 3, $\beta_I = 0.70$ and $\beta_W = 0.80$ according to CUR 166, and $\beta_I = 0.70$ and $\beta_W = 0.71$ according to the new design rule in Table 3.11. In Table 6.3 the average measured value in the field test of $\beta_I = 0.68$ and $\beta_W = 0.73$ are compared to the design method from CUR 166 and the new method proposed in this thesis.

	CUR 166	new method	measured
β_I	0.70	0.70	0.68
β_W	0.80	0.71	0.73

Table 6.3: *Comparison of β_I and β_W from design methods and the field measurements*

In the new method, $\beta_I = 0.70$ is composed of a theoretical part of $\beta_I = 0.60$ and a practical part of $\beta_I = 0.10$. It is assumed that the theoretical part, where interlock friction is absent, is approximately equal to the measurements in pile H2 ($\beta_I = 0.57$). Both the theoretical part ($\beta_I = 0.60$) and the installation effect ($\beta_{I,6} = 0.10$) seem to be a reasonable estimation. The new design rule also gives a good result for β_W. Therefore the following two general conclusions can be drawn:

- Oblique bending can occur in steel sheet piling

- The loss of stiffness and strength due to oblique bending can be accurately assessed using both the existing CUR rule and the new design rule presented in Chapter 3

6.4   Earth and water pressures

6.4.1   General

The behaviour of a sheet pile wall is governed to a large extent by the behaviour of the soil. The behaviour of the sheet pile wall can therefore be better evaluated when the soil behaviour and the mechanisms in the soil are understood.

In this section the change of earth and water pressures as a function of the wall displacement is investigated. From the rate of change of earth and water pressures it is possible to investigate to what extent the soil behaved as an undrained material during the short-term field test. Furthermore, insight into time-dependent behaviour of the soil can be obtained from the long-term field test.

6.4.2   Measured change in earth and water pressures

The AZ13 test wall was instrumented with two tiltmeters, located just below strut level, so that the inclination of the wall causing a lateral displacement could be measured. This wall inclination is a measure for the wall displacement at a certain depth. The L607K-test wall was not equipped with tiltmeters.

Figure 6.8 shows the change in earth and water pressures on the AZ13 wall against the tilt at strut level. In the bottom graph, the water level in the excavation is coupled to dates on which the various load steps were carried out. An impression of the wall displacements related to the tilt can be derived from Table 6.4, but for a more precise overview of the various activities, see Appendix G.

In Figure 6.9 the change of effective earth pressure is shown. On the retained side, it rapidly decreases to zero at NAP−2 m and NAP−4 m, and slowly decreases at greater depths. On the excavated side, the effective earth pressure remains more or less constant at every depth.

The change in earth and water pressure for the L607K-wall shows a comparable behaviour, and is therefore not treated separately.
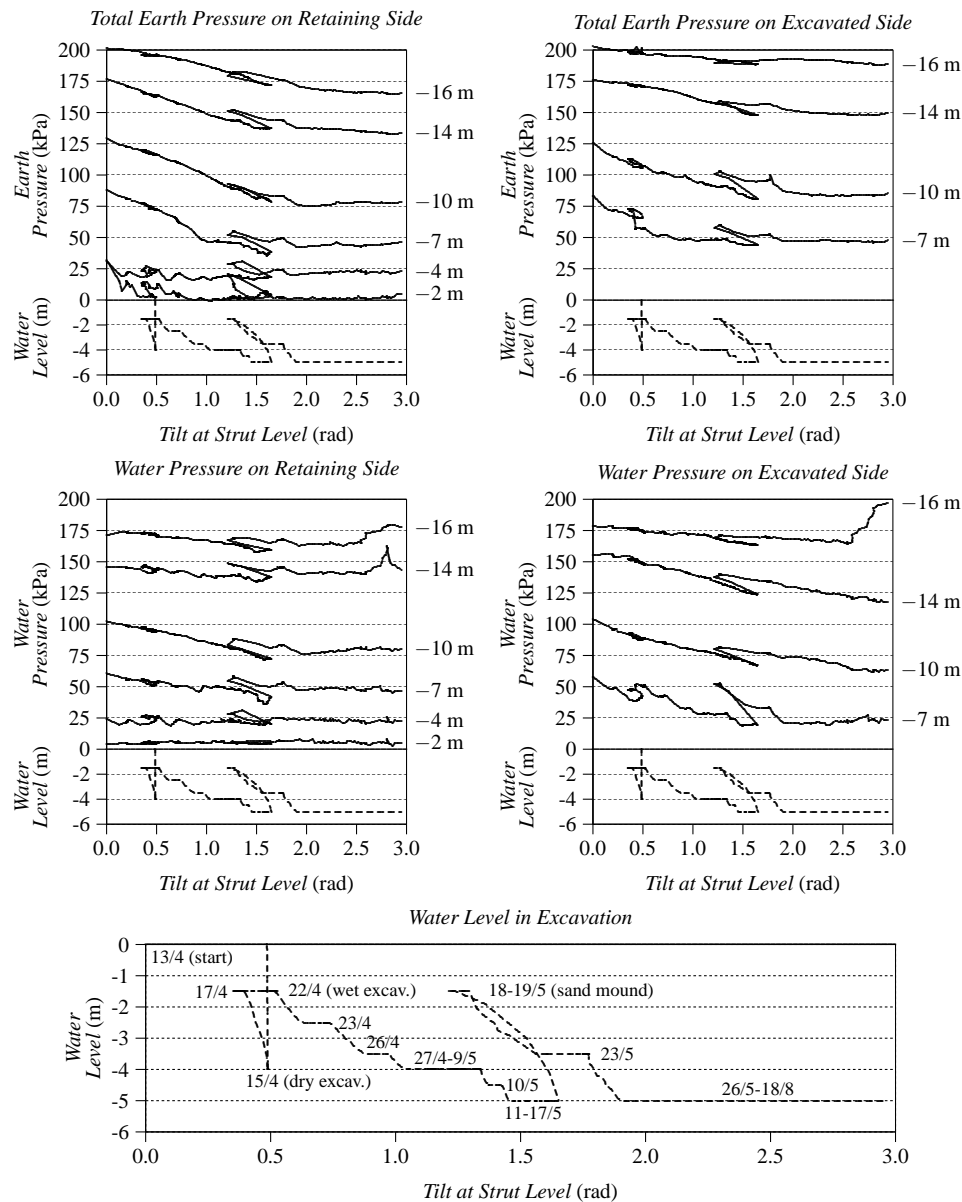
Figure 6.8: *Change of earth and water pressures at different levels NAP, as a function of the tilt at strut level (equivalent to wall displacement). The lower part of the graphs represents the water level inside the excavation. The various test stages are indicated with dates in the bottom graph*

Depth (m NAP)	Lateral Displacement (mm)					
-2	-23	-44	-65	-96	-120	-148
-4	-31	-64	-96	-136	-173	-213
-7	-33	-71	-108	-151	-196	-245
-10	-25	-57	-89	-123	-164	-208
-14	-9	-26	-42	-60	-82	-105
-16	-4	-12	-19	-28	-38	-50
	0.5	1	1.5	2	2.5	3
	Tilt at Strut Level (rad)					

Table 6.4: *Tilt at strut level versus lateral displacement at various depths*
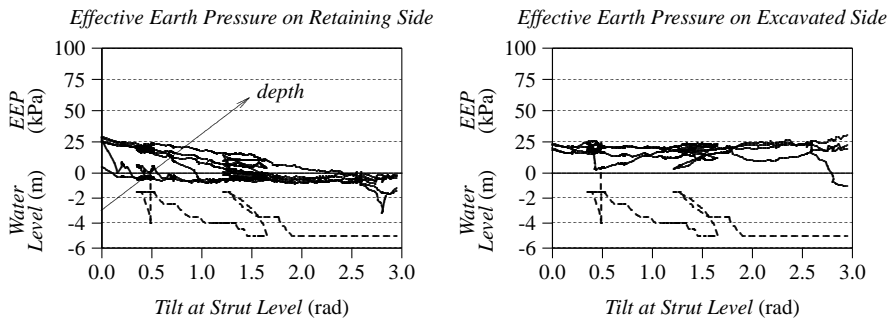
Figure 6.9: *Change of effective earth pressures at different levels NAP, as a function of the tilt at strut level*

6.4.3   Short-term field test

In the short-term field test the tilt around the strut varied between 0 and 1.5 rad. During this period the measured change of water pressure on both sides of the wall was more or less proportional to the change in earth pressure. As a result of the excavation and dewatering, the sheet pile bends and the soil on the retaining side expands. The isotropic soil stress decreases and, if pore water cannot flow in, the water pressure must decrease as well. This behaviour indicates an undrained soil reaction, which is investigated hereafter.

In a porous medium with incompressible grains, where pore water cannot flow in or out (undrained behaviour), the change of pore water pressure Δu is related to the change of isotropic soil stresses $\Delta\sigma$ according to

$$\Delta u = \frac{1}{1 + n\beta K}\left(\Delta p - \frac{K}{D}\Delta q\right) \tag{6.9}$$

where

$$\Delta p = \frac{\Delta\sigma_1 + \Delta\sigma_2 + \Delta\sigma_3}{3} \tag{6.10}$$

$$\Delta q = \sqrt{\frac{1}{2}\left((\Delta\sigma_1 - \Delta\sigma_2)^2 + (\Delta\sigma_2 - \Delta\sigma_3)^2 + (\Delta\sigma_3 - \Delta\sigma_1)^2\right)} \tag{6.11}$$

where n is the porosity, β is the compressibility of the pore water, K is the bulk modulus of the grain skeleton and D is a constant reflecting dilatancy for $D > 0$ and contractancy

when $D < 0$, see Verruijt [86]. When the pore water contains no gas, it may be considered as incompressible ($\beta \approx 0$), but when some gas is present in the pores, the pore water is somewhat compressible and β is of significance. According to Verruijt [81], β may be estimated from

$$\beta = 0.5 \times 10^{-6} + (1 - S)/u \quad (1/\text{kPa}) \tag{6.12}$$

where S is the degree of saturation and u is the pore water pressure.

In spite of its rather theoretical basis, equation (6.9) is used to predict the order of magnitude of the change of pore water pressure related to the change of total earth pressure measured in the field test. Therefore in this simplified approach it is assumed that the total vertical and horizontal stresses in the soil can be represented by principal stresses according to $\sigma_1 = \sigma_v$ and $\sigma_3 = \sigma_h$. Further it is assumed that for this case the soil in shear will not show dilatant or contractant behaviour, i.e., $D = 0$, and that the pore water pressure is not affected by groundwater flow.

Retained side

On the retained side it is assumed that $\Delta\sigma_1$ and $\Delta\varepsilon_2$ do not alter and that the earth pressure reduces by $-\Delta\sigma_3$. This implies that $\Delta\sigma_2 = -\nu\Delta\sigma_3$. Substitution in (6.9) gives

$$\Delta u = -\frac{1}{3(1 + n\beta K)}(1 + \nu)\Delta\sigma_3 \tag{6.13}$$

When the soil is considered as undrained ($\nu = 0.5$) and the pore water is considered as incompressible ($\beta \approx 0$), equation (6.13) reduces to $\Delta u = -\frac{1}{2}\Delta\sigma_3$. However, in the field test it was observed that a significant quantity of gas escaped from the excavation, which indicates that the effect of gas on the compressibility of the pore water cannot be neglected. Reasonable values which can be used for a rough estimation of the compressibility of the pore water are $S = 0.95$ and $u = 50$ kPa. Substitution in (6.12) gives $\beta = 0.001$ m^2/kN and substituting $n = 0.8$ and $K = 625$ kPa in (6.13) finally gives

$$\Delta u = -\frac{1}{3}\Delta\sigma_3 \tag{6.14}$$

It should be realised that the ratio $\frac{1}{3}$ is only a rough estimation and could equally be $\frac{1}{2.5}$ or $\frac{1}{4}$ or so; in the case of drained behaviour, the ratio reduces to zero.

The effective stresses, based on $\Delta\sigma' = \Delta\sigma - \Delta u$, are obtained from

$$\Delta\sigma_1' = \Delta\sigma_2' = +\frac{1}{3}\Delta\sigma_3 \tag{6.15}$$

$$\Delta\sigma_3' = -\frac{2}{3}\Delta\sigma_3 \tag{6.16}$$

Hence, undrained response is obtained if, as a result of a total earth pressure decrease of $-\Delta\sigma_h$:

- the pore water pressure decreases by $\Delta u = -\dfrac{1}{3}\Delta\sigma_h$

- the effective earth pressure decreases by $\Delta\sigma'_h = -\dfrac{2}{3}\Delta\sigma_h$

- the vertical effective stress increases by $\Delta\sigma'_v = +\dfrac{1}{3}\Delta\sigma_h$

Depth (m NAP)	$\Delta\sigma_h$	Δu	$\Delta\sigma'_h$	$\Delta\sigma_h/\Delta u$ (6.14)	$\Delta\sigma_h/\Delta\sigma'_h$ (6.16)
-2	-29.7	0.9	-30.7	-32.0	1.0
-4	-14.5	-3.4	-11.2	4.3	1.3
-7	-47.7	-16.3	-31.5	2.9	1.5
-10	-48.0	-27.8	-20.3	1.7	2.4
-14	-39.5	-10.7	-28.8	3.7	1.4
-16	-26.6	-13.6	-13.0	2.0	2.1
Theoretically				3.0	1.5

Table 6.5: *Measured change of earth and water pressures on the retained side of the AZ13-wall (May 11 1999) compared to the theoretical analysis*

Table 6.5 shows the change in earth and water pressure when the water level inside the excavation was lowered to NAP-5 m (May 11), expressed by the inverse values of the factors in equations (6.14) and (6.16). At NAP-2 m the state of the soil may be considered as fully drained, due to the fact that the groundwater level is approximately at this depth. At the other depths, no clear proof for fully drained behaviour is found, because the change of pore water and effective earth pressures fit quite well with the theoretical values, expected in the case of undrained behaviour.

It is, however, beyond this theoretical consideration to conclude that the pore water contained a significant amount of gas at NAP-4 m, and hardly any gas at NAP-10 m. After all, this analysis implies the assumption that no pore water flow occurred over a period of one month, which is unlikely, and that other effects, such as dilatancy of the soil, were of minor importance, which has not been investigated.

Excavated side

On the excavated side it is assumed that the total vertical stress decreases by $-\Delta\sigma_1$, and the total horizontal stress by $-\Delta\sigma_3$. Again, $\Delta\varepsilon_2 = 0$ and therefore $\Delta\sigma_2 = -\nu\Delta\sigma_1 - \nu\Delta\sigma_3$. Substitution in (6.9) leads to

$$\Delta u = -\frac{1}{3(1+n\beta K)}\left((1+\nu)\Delta\sigma_1 + (1+\nu)\Delta\sigma_3\right) \qquad (6.17)$$

When the soil is considered as undrained ($\nu = 0.5$) and the pore water is considered as incompressible ($\beta \approx 0$), equation (6.17) is reduced to $\Delta u = -\frac{1}{2}\Delta\sigma_1 - \frac{1}{2}\Delta\sigma_3$. As the amount of gas that escaped from the excavation was significant, its effect on the compressibility of

the pore water is not neglected. As for the retained side, substitution of $\beta = 0.001$ m^2/kN, $n = 0.8$ and $K = 625$ kPa in (6.17) gives

$$\Delta u = -\frac{1}{3}\Delta\sigma_1 - \frac{1}{3}\Delta\sigma_3 \tag{6.18}$$

Again it should be realised that the ratio's $\frac{1}{3}$ are rough values and could equally be $\frac{1}{2.5}$ or $\frac{1}{4}$ or so. In the case of drained behaviour, the ratio's reduce to zero and effective stresses based on $\Delta\sigma' = \Delta\sigma - \Delta u$ are obtained:

$$\Delta\sigma'_1 = -\frac{2}{3}\Delta\sigma_1 + \frac{1}{3}\Delta\sigma_3 \tag{6.19}$$

$$\Delta\sigma'_2 = +\frac{1}{3}\Delta\sigma_1 + \frac{1}{3}\Delta\sigma_3 \tag{6.20}$$

$$\Delta\sigma'_3 = +\frac{1}{3}\Delta\sigma_1 - \frac{2}{3}\Delta\sigma_3 \tag{6.21}$$

Hence, undrained response is obtained if, as a result of a total earth pressure decrease of $-\Delta\sigma_h$:

- the pore water pressure decreases by $\Delta u = -\dfrac{1}{3}\Delta\sigma_v - \dfrac{1}{3}\Delta\sigma_h$

- the effective earth pressure decreases by $\Delta\sigma'_h = +\dfrac{1}{3}\Delta\sigma_v - \dfrac{2}{3}\Delta\sigma_h$

- the vertical effective stress decreases by $\Delta\sigma'_v = -\dfrac{2}{3}\Delta\sigma_v + \dfrac{1}{3}\Delta\sigma_h$

As a result of the excavation to NAP-7 m and dewatering to NAP-5 m, the total vertical stress decreased by $\Delta\sigma_v = -80$ kPa.

Depth (m NAP)	Measured Values				Theory	
	$\Delta\sigma_h$	Δu	$\Delta\sigma'_h$	$(\Delta\sigma_v + \Delta\sigma_h)/\Delta u$ (6.18)	$\Delta\sigma'_h$	$\Delta\sigma'_v$
-7	-39.11	-39.41	0.30	3.0	0.59	-40.3
-10	-40.96	-33.06	-7.90	3.7	-0.64	-39.7
-14	-26.28	-28.47	2.19	3.7	9.15	-44.6
-16	-12.28	-13.03	0.75	7.1	18.48	-49.2
Theoretically				3.0		

Table 6.6: *Measured change of earth and water pressures on the excavated side of the AZ13-wall (May 11 1999) compared to the theoretical analysis*

Table 6.6 shows the change of earth and water pressures measured on May 11. The change of earth pressure $\Delta\sigma_h$ is of the same order of magnitude as the change of water pressure Δu, and therefore the change of effective earth pressure $\Delta\sigma'_h \approx 0$. The last two columns in Table 6.6 give the change of effective horizontal and vertical soil stress, calculated using $\Delta\sigma_v = -80$ kPa and the measured value of $\Delta\sigma_h$.

Conclusions concerning undrained behaviour of the soil cannot be drawn. On the other hand, the measurements do not indicate fully drained behaviour of the soil.

Evaluation of measured pore water pressures

Evaluation of the measured pore water pressures is based on the assumption that the soil behaved in an undrained manner and that a significant amount of gas was present in the pore water. In Figure 6.10 the dashed lines show the water pressures calculated from the measured earth pressures according to:

$$\Delta u = \frac{1}{3}\Delta\sigma_h \qquad\qquad\qquad \text{(retained side)} \qquad\qquad (6.22)$$

$$\Delta u = \frac{1}{3}\Delta\sigma_v + \frac{1}{3}\Delta\sigma_h \qquad\qquad \text{(excavated side)} \qquad\qquad (6.23)$$
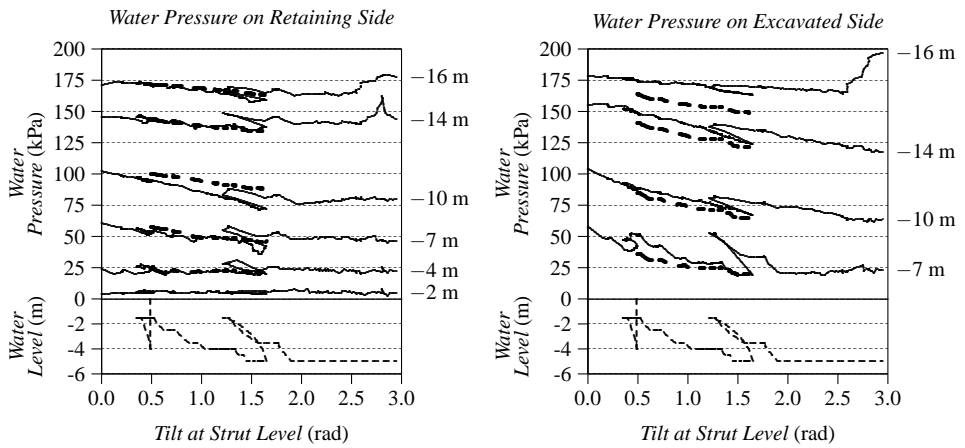
Figure 6.10: *Change of water pressures at different levels NAP, as a function of the* tilt at strut level *(equivalent to wall displacement). The solid lines represent the measured values and the dashed lines were calculated with equations* (6.22) *and* (6.23)

On the retained side the calculated water pressures correspond quite well to the measured values, indicating that the soil reaction on the retained side may not be considered as drained but rather as undrained.

On the excavated side, the measured water pressure difference is significantly smaller than the calculated values. This might indicate that the soil reaction on the excavated side was not fully undrained but was subjected to time dependent behaviour, to a greater extent than the retained side.

6.4.4   Long-term field test

Figure 6.11 shows the displacement, bending moment, and earth and water pressures measured on May 26 and August 11. In this period, the water level inside the excavation was maintained at a constant level, meaning that the changes in bending moment and wall displacement are the result of time-dependent effects in the soil i.e., consolidation and creep. The maximum bending moment increased with $\Delta M = 105$ kNm/m and the maximum wall displacement with $\Delta w = 80$ mm.
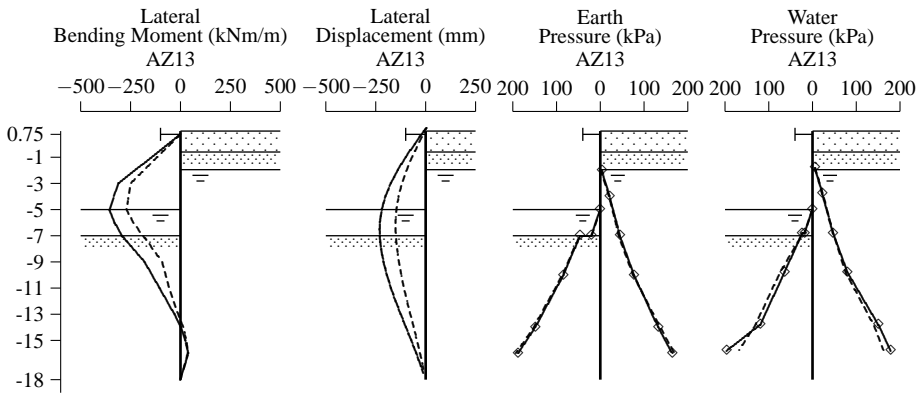
Figure 6.11: *Increase of action effects on the AZ13-wall from May 26 (dashed lines) to August 11 1999 (solid lines)*

The distribution of earth and water pressures was determined at eight measurement points on the retained side and four on the excavated side, and do not show any significant changes. Nevertheless according to engineering beam theory, the differential equations

$$\frac{d^2w}{dx^2} = -\frac{M}{EI} \tag{6.24}$$

$$\frac{d^2M}{dx^2} = -q + kw \tag{6.25}$$

indicate that an increase of displacement and bending moment must be the result of either a change of the resulting earth pressure distribution on the wall (q) or a change of stiffness of the soil (k). In soil, the displacement and bending moment are dependent on both q and k. For example, a decrease of k due to time-dependent effects will lead to an increase of w and consequently to a change of q.

To obtain more insight into the question of where the most significant changes in soil behaviour occurred, the increase of the action effects in the period from May 26 to August 11 is analysed using the consistency check technique described in Section 4.6. This calculation technique was developed for a single layer system, and therefore the calculation results give an indicative view of the change of earth pressure distribution rather than an exact result. The calculation was made with $n = 8$, $m = 7$, α, β, δ, $\varepsilon = 1$ and $\gamma = 1.52$. In the displacement curve only 25% of the total available measurement points are presented, and the results are plotted in Figure 6.12.

The calculated wall displacements fit very well with the measured data points, whereas the calculated bending moment exceeds the measured values above the level of the maximum bending moment. Obviously some accuracy has been lost in the determination of either the displacement increase or the moment increase at that level. Therefore the polynomial gives a slight overestimation of the earth pressure change above NAP-5 m.

The consistency check technique confirms that the increase of lateral displacement and bending moment in the long-term is caused by a relatively small change of earth pressures. It is therefore understandable that this change was hardly detected by the instrumentation.
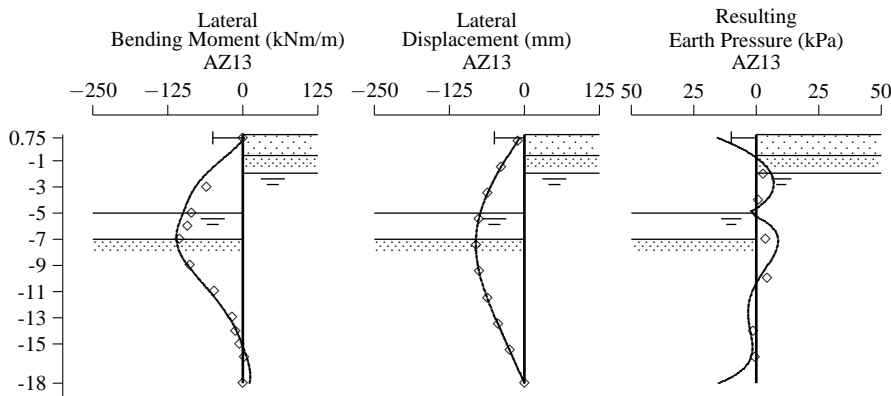
Figure 6.12: *Consistency check for AZ13-wall for the difference in action effects between May 26 and August 11 1999. The ⋄-marks indicate the measured data points, the polynomial is drawn with the solid line.*

	Retaining Side			Excavated Side			Resulting Pressures		
Depth (m NAP)	$\Delta\sigma_h$	Δu	$\Delta\sigma'_h$	$\Delta\sigma_h$	Δu	$\Delta\sigma'_h$	$\Delta\sigma_h$	Δu	$\Delta\sigma'_h$
-2	2.80	-0.70	3.50				2.80	-0.70	3.50
-4	0.77	-1.21	1.98				0.77	-1.21	1.98
-7	2.80	-0.30	3.10	-0.93	2.59	-3.52	3.73	-2.89	6.62
-10	2.02	4.04	-2.01	-2.28	-10.00	7.72	4.30	14.03	-9.73
-14	-4.65			-3.43	-10.87	7.44	-1.22		
-16	-5.15			-4.60			-0.55		

Pressures in (kPa)

NOTE: *The change of water pressures on the retained side at NAP−14 m and NAP−16 m and on the excavated side at NAP−16 m may be disturbed, see also Figure 6.8*

Table 6.7: *Measured changes of earth, water and effective earth pressures during the long-term field test*

In Table 6.7, an overview of the measured changes in earth, water and effective earth pressures is presented. Considering this table together with Figure 6.12 it follows that the increase in displacement and bending moment is mainly generated by the earth pressure change between NAP−7 m and NAP−10 m. At these levels the total earth pressure increased on the retained side and decreased on the excavated side. At a lower level the total earth pressure on both sides decreased. The decrease on the retained side is caused by the wall deflection and on the excavated side by consolidation towards a hydrostatic pore water pressure, see also Figure 6.8. The pressure increase between NAP−7 m and NAP−10 m is partly carried by the strutting and partly by the Pleistocene sand layer.

In Figure 6.8 it is shown that the tilt at the strut level increased from 2 to 3 rad during the long-term field test. The pore water pressure on the retained side hardly altered during this period. One might have expected an increase of water pressure against the sheet pile wall as a result of pore water inflow in the soil behind the sheet pile wall. However, instead of this increase being recorded by the piezometers, the sheet pile wall continued to deflect until the excavated side could carry the additional load. As a result of increasing deflection, the

soil behind the sheet pile wall expanded, which involved a decrease of pore water pressure. The two effects of increasing pore water pressures due to groundwater flow and decreasing pore water pressures due to wall deflection obviously cancelled each other out. On the excavated side, the pore water pressure decreased towards a hydrostatic condition. This decrease indicated that the time-dependent soil behaviour on the excavated side was of significance.

The long-term behaviour can be summarised as follows: as a result of consolidation and creep, the earth pressure on the excavated side redistributed, resulting in greater deflection of the sheet pile wall. The soil on the retained side followed this deflection.

6.5   3D behaviour

PLASWALL and PLAXIS are plane strain models which can be used to simulate infinitely long sheet pile walls rather than cofferdams of limited sizes. To use these models for back-analyses, the 3D behaviour of the test setup must be understood. Recently (April 2001) a pilot version of PLAXIS 3D TUNNEL became available. This version contained a limited number of options, which is the main reason for the simplifications made in these calculations.
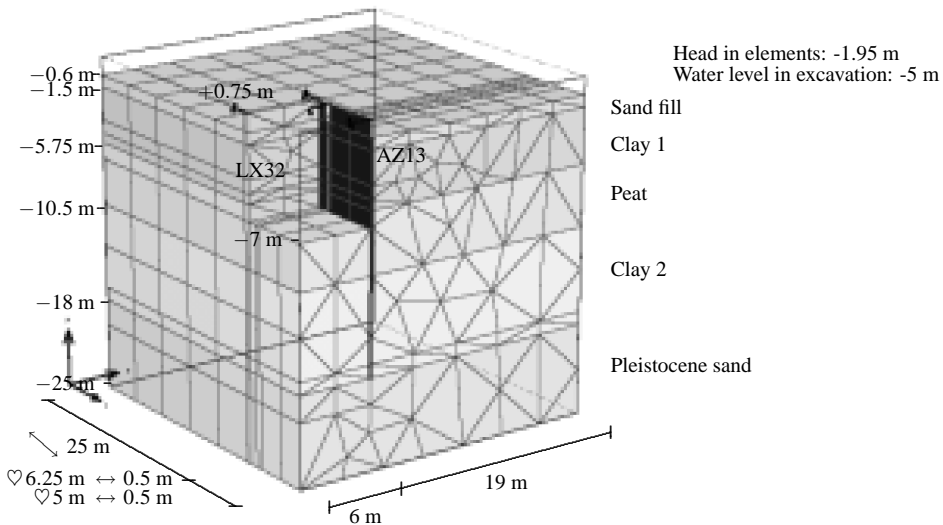
Figure 6.13: *Reference case to investigate the 3D effects in the field test*

Figure 6.13 shows the 3D mesh of a quarter of the excavation. The properties of the clay and peat layers were derived from Prediction 20. To model the initial water pressure distribution and the higher head in the Pleistocene sand layer, a unit weight of the water was applied of $\gamma_{wat} = 11$ kN/m^3. The calculations were carried out 'undrained' without consolidation steps. Relevant dimensions are given in the figure, and the soil and sheet pile properties in Table 6.8.

Soil type	Model	Top layer (m)	$\gamma_{dry/sat}$ (kN/m^3)	G (kPa)	v' (-)	c' (kPa)	φ' (^{o})	E'_{50} (kPa)	n (-)	E'_{ur} (kPa)
Sand fill	MC	-0.6	17/19	8000	0.3	2	35			
Clay 1	HS	-1.5	17		0.2	10	30	10970	0.5	52660
Peat	HS	-5.75	10.5		0.2	10	30	1350	0.7	6490
Clay 2	HS	-10.5	16		0.2	10	30	3860	0.7	13740
Pleistocene	MC	-18	20	40,000	0.2	2	37			
Slurry	MC		17	168	0.49	7	0			
AZ13-wall	$EI = 41370$ kNm^2/m									
LX32-wall	$EI = 75600$ kNm^2/m ($\beta_I = 0.5$)									

Table 6.8: *Soil parameters for comparison between 3D and 2D*

The following calculations were carried out:

0: Reference calculation of a 2D slice (front two element rows)

1: Calculation of the construction without measures for 2D behaviour

2: Calculation with a special interface pile

3: Calculation with a special interface pile and a slurry wall [1]

4: Calculation with a special interface pile and a very smooth slurry wall ($E = 1$ kPa)
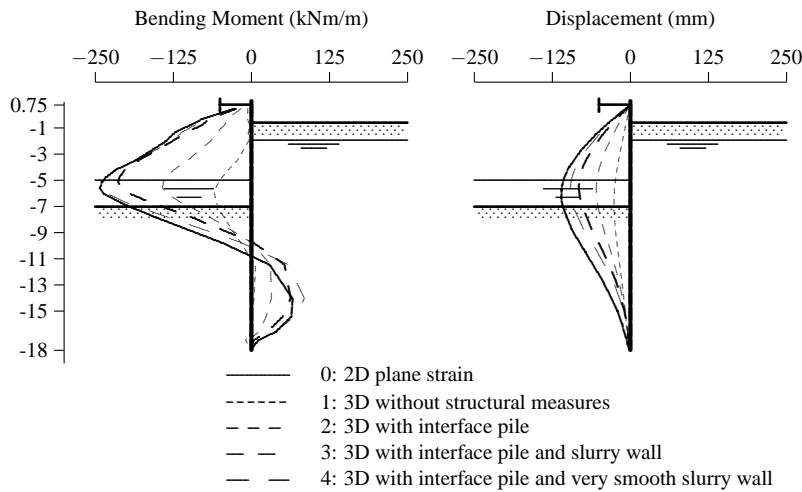
Figure 6.14: *Bending moments and displacements for the five 3D calculations*

Figure 6.14 shows the displacement and moment curves of the 5 calculations. The calculated results show that both the special interface piles and the slurry screen were necessary

---

[1]The properties of the slurry wall were estimated from various triaxial UU tests on samples taken from the slurry wall after the test.

to obtain a model as close to a plane strain situation as possible. It is assumed that calculations 3 may be considered as *equivalent to the measured behaviour*. Comparison between calculation 3 and 0 shows that the 2D model gives an overprediction of about 28 mm (34%) for the maximum displacement and 29 kNm/m (14%) for the maximum bending moment with respect to the *measured behaviour*.

Calculation 3 gives a shorter span length between the points of zero moment than calculation 0, which indicates that the peat layer has extra resistance due to the 3D effects. As a result of the shorter span length, the maximum wall displacement is smaller in calculation 3 than in calculation 0.

When the slurry wall is modelled as *very smooth* (calculation 4), more load is generated on the AZ13-wall, causing larger bending moments and displacements, but the very smooth slurry wall is not sufficient to fully explain the difference between the 3D and the 2D calculation. Explanations for the other differences may be found in 3D effects on the excavated side. Additional calculations, however, proved that the stiffness of the LX32 side walls was of negligible influence.

The 3D calculations indicate that the measured behaviour of the test walls is sensitive to the behaviour of the slurry walls and other 3D effects on the excavated side. For the evaluation of the field test, the use of 2D models for comparison means that somewhat larger displacements and bending moments may be calculated as a result of the missing 3D effects. However, the second point of zero moment cannot be higher than the measured level.

6.6 Back-analysis with the subgrade reaction method

6.6.1 General

The subgrade reaction method is an empirical method for which a lot of experience has been gained in the Dutch engineering practice [27]. The power of this method is its simplicity and reduced calculation time and therefore this method is very practical for relatively simple problems. Since the soil behaviour is simplified by uncoupled elasto-plastic springs, the scientific value of this method is poor. As a result, these back-analyses are made 'through the eyes of the design engineer'.

In Section 6.4 it has been stated that the soil behaviour during the short-term field test was more or less undrained and that during the long-term field test the sheet pile walls kept on deforming to an end-state. Hence, it is decided to make the back-analyses of the short-term field test with undrained soil parameters and of the long-term field test with drained parameters.

In these back-analyses the aim is to estimate the subgrade reaction moduli that can be applied to this field test. The other parameters which are used, are derived from the CPT's and the triaxial tests, as in most practical cases, these are the only tests from which the data are available to the 'design engineer'. Nevertheless, it may be expected that the results from these back-analyses will be close to the results from more advanced back-analyses.

The following back-analyses were carried out with PLASWALL:

- Short-term field test

    - based on undrained parameters
    - based on effective parameters
    - based on both undrained and effective parameters

- Long-term field test

- Limit state

6.6.2   Drained and undrained calculations

The back-analyses are based on both drained and undrained soil parameters. In this section the modelling aspects of drained and undrained soil behaviour are presented.

In a *drained* calculation with the subgrade reaction model, the general input parameters are the soil profile (stratification, volume weights and heads) and the spring characteristic σ'_a, σ'_n, σ'_p, k and Δw, see also Figure 2.23. Consequently the spring represents an effective stiffness parameter which behaves according to

$$\sigma'_h = \sigma_h - u = k(w - \Delta w) \tag{6.26}$$

where u is the measured water pressure.

In an *undrained* calculation, however, an undrained spring characteristic is used which is defined by σ_a, σ_n, σ_p, k_u and Δw. The spring becomes therefore an undrained stiffness parameter which behaves according to

$$\sigma'_h + u = \sigma_h = k_u(w - \Delta w) \tag{6.27}$$

The plastic branches of the springs are described by the following equations:

$$\sigma_a = \sigma_v - 2c_u \not< 0 \tag{6.28}$$
$$\sigma_p = \sigma_v + 2c_u \tag{6.29}$$

where (for a single layer)

$$\sigma_v = \gamma_{sat} z \tag{6.30}$$

The neutral earth pressure σ_n is derived from the initial field measurements, hence the initial stresses are generated with a undrained neutral earth pressure coefficient, K_0^u, such that $K_0^u = \sigma_n / \sigma_v$.

The term $\pm 2c_u$ in equations (6.28) and (6.29) implies a perfectly smooth wall in the case of undrained behaviour. This assumption is often made for undrained calculations e.g., by the German EAU [25] and Kerisel and Absi [47]. In reality wall friction can be of importance and according to Craig [26] and CUR 166 [27] this term may be about $\pm 2.4c_u$. The consequence of the smooth wall assumption on the retained side is negligible because generally $2c_u > \sigma_v$. On the excavated side this assumption is only of influence when the plastic branch of the spring is reached i.e., when the calculated result is not sensitive to the subgrade reaction modulus.

6.6.3 Short-term field test with undrained parameters

The first back-analysis of the short-term field test is based on undrained soil parameters and the following construction stages are considered:

1. Dry excavation to NAP-4.0 m

2. Excavation under water to NAP-7.0 m, water level in the excavation at NAP-1.5 m

3. Lowering of the water level to NAP-5.0 m

Soil type	Top layer (m)	γ (kN/m³)	c_u (kPa)	c' (kPa)	φ' (°)	$k_{u,1}$ (kN/m³)	$k_{u,2}$ (kN/m³)	$k_{u,3}$ (kN/m³)
Sand Fill	-0.6	17		2	35	900	900	250
Silty Clay	-1.6	16.8	34.3			900	600	250
Peat	-5.75	10.1	39.7			800	800	500
Clayey Peat	-9.0	10.1	44.2			1100	750	400
Humous Clay	-10.5	13.9	29.9			1200	850	450
Sandy Clay	-12.5	16.3	50.7			3200	2600	1000
Silty Clay	-16.1	14.5	50.7			12000	12000	5000
Pleistocene Sand	-17	20		2	37	30000	30000	30000

Table 6.9: *Input parameters for back-analysis of the short-term field test with* PLASWALL *based on undrained parameters*

The input parameters are presented in Table 6.9. The spring constants used in the different construction stages are denoted by $k_{u,1}$, $k_{u,2}$ and $k_{u,3}$. The input parameters are based on the following assumptions:

- The calculations are based on undrained soil parameters

- The soil is treated as a *single source*: for each layer, the same soil parameters are chosen for the retained and excavated sides

    This assumption is reasonable for the undrained shear strength but not obvious for the undrained soil stiffness k_u, which is not necessarily equal on both sides of the wall. Nevertheless, in Dutch engineering practice, the spring stiffness is often chosen as equal for both sides of the wall and the Dutch CUR 166 regulation does not give directives for correction of k-values due to excavation.

- The undrained shear strength c_u is derived from triaxial tests with cell pressures approximately equal to the original stress level in the field

    Generally for the design of simple retaining structures, a limited amount of soil investigation is available. In a lot of cases, the available soil investigation comprises only CPT's and triaxial tests. Furthermore, in Dutch engineering practice, the level of the plastic branches is linked to physical soil properties, whenever possible.

- The subgrade reaction modulus is treated as a so-called *model factor* and is not directly related to, for example, a Young's modulus measured in a triaxial test. Furthermore, the subgrade reaction modulus may decrease for increasing wall displacements

The 'real' soil behaviour, which is typically observed in the field test, is taken into account by a correction of the spring stiffness in every construction stage, see Figure 6.15.
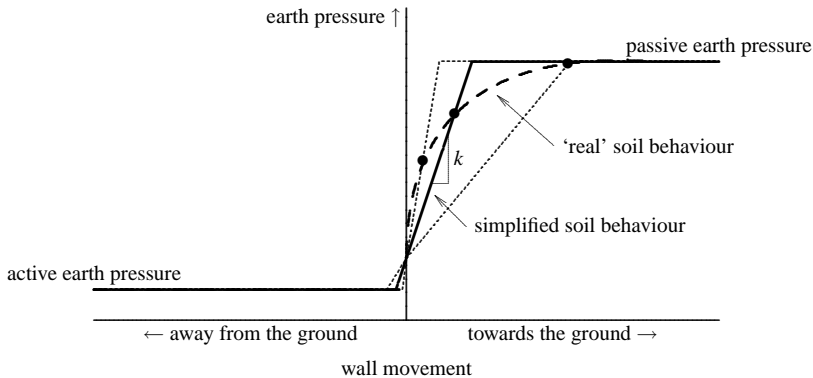
Figure 6.15: *'Real' soil behaviour modelled with springs with varying stiffness*

Respecting these assumptions, only the subgrade reaction modulus k_u is unknown, which has been fitted to the measurements by trial-and-error.

The calculation results for stage 3 are presented in Figure 6.16. It is shown that not only the calculated displacements and bending moments are close to the measured results, but the calculated earth pressures on both sides of the wall are also close to the measured earth pressures at every depth. This result confirms that the combinations of k_u and c_u applied in the different soil layers are reasonable, although both the bending moments and wall deflections were very sensitive for the values of the subgrade reaction moduli.

From the back-analysis of the short-term field test with undrained parameters in PLAS-WALL, the following conclusions can be drawn:

- The assumption that during the short-term field test the soil behaved as an undrained material, is reasonable, but probably not completely correct

- The assumption that the undrained shear strength may be derived from the triaxial tests, is reasonable

- The assumption that the soil parameters may be treated as a 'single source' gives reliable calculation results

- Reasonable values for k_{undr} vary between 250 and 900 kN/m^3 for the upper clay layer, between 400 and 1100 kN/m^3 for the peat layer, and between 1000 and 3200 kN/m^3 for the lower clay layer

Results AZ13
Stage 3: Water level at NAP−5.0 m (May 11 1999)

Figure 6.16: *Back-analysis of the short-term field test with* PLASWALL *based on undrained parameters. The solid lines represent the calculation results and the ◇-marks the field measurements*

6.6.4   Short-term field test with effective parameters

The second back-analysis of the short-term field test is based on effective soil parameters and measured water pressures. This back-analysis of the short-term field test is required to analyse the time-dependent effects of the long-term field test. In this back-analysis the following construction stages are considered:

1. Dry excavation to NAP−4.0 m

2. Excavation under water to NAP−7.0 m, water level in the excavation at NAP−1.5 m

3. Lowering of the water level to NAP−5.0 m

Soil type	Top layer (m)	γ (kN/m^3)	c' (kPa)	φ' (^{o})	k_3 (kN/m^3)	K_a	K_p	h_{ret} (m)	h_{exc} (m)
Sand Fill	-0.6	17	2	35	700	0.27	3.39	-1.95	
Silty Clay	-1.6	16.8	6.3	29.1	700	0.31	4.06	-1.51	-5
Peat	-5.75	10.1	9.4	18.8	700	0.51	1.95	-2.36	-4.94
Clayey Peat	-9.0	11.4	11.8	20.1	400	0.49	2.05	-2.34	-2.68
Humous Clay	-10.5	13.9	7.1	20.3	500	0.44	2.52	-1.32	-1.90
Sandy Clay	-12.5	16.3	7.4	27.1	1400	0.33	3.62	-0.31	-1.11
Silty Clay	-16.1	14.5	9.8	37.2	5000	0.22	6.83	-0.04	0.75
Pleistocene Sand	-17	20	2	37	30000	0.25	4.02	-0.04	0.75
$\delta = 0.5\varphi'$ in clay and $\delta = 0$ in peat									
K_n follows from $K_n = 1 - \sin\varphi'$									

Table 6.10: *Input parameters for back-analysis of the short-term field test with* PLASWALL *based on effective parameters*

Table 6.10 shows the input parameters for this back-analysis. The assumptions made are similar to those for the previous back-analysis:

- The calculations are based on effective soil parameters

    During the long-term field test the sheet pile walls continued to deform to an end-state. This continuing deformation is the result of the time-dependent behaviour of the soil due to consolidation and creep. In Dutch design practice with subgrade reaction models, this end-state is generally assessed using effective strength and stiffness parameters of the soil.

- The soil is treated as a *single source*: for each layer equal soil parameters are chosen on the retained and excavated side

- The effective strength parameters c' and φ' are derived from triaxial tests for axial strains of 2%

    For verification of the serviceability limit state CUR 166 [27] recommends use of c' and φ' from a triaxial test for 2% axial strain, especially as extensive experience exists with these values in combination with subgrade reaction models. For verification of the ultimate limit state, c' and φ' should be determined from the top of the $\sigma - \varepsilon$ curve, or otherwise for 5% axial strain.

- The earth pressure coefficients are assessed with Kötter's curved slip plane theory

    It has been shown in Section 2.6.4 that the outcome of a calculation with a subgrade reaction model depends heavily on the chosen earth pressure theory. In this back-analysis, the intention is to follow existing experience as much as possible. In Dutch design practice, the earth pressure coefficients are often assessed from c', φ' and δ with Kötter's curved slip plane theory, see Appendix D.

- The subgrade reaction modulus is treated as a so-called *model factor* and is not directly related to, for example, a Young's modulus measured in a triaxial test. Furthermore, the subgrade reaction modulus may decrease for increasing wall displacements, see also Figure 6.15

- The water pressure distribution on both sides of the wall is based on measured water pressures in each construction stage

    In the field test, the water pressure distribution was measured at 8 points on the retained side and 4 points on the excavated side. As a result of this limited amount of data, the water pressure distribution is not exactly known. In PLASWALL, input of the water pressure distribution is by the head in a soil layer. From the combination of these two restrictions, a certain error in the contribution of the water pressure to the calculated distribution of bending moment and wall displacements may be expected, which may be of significance. This error is implicitly corrected by the choice of the (empirically determined) subgrade reaction modulus.

Respecting these assumptions, only the subgrade reaction modulus k is unknown, which has been fitted to the measurements by trial-and-error.

The method involving adoption of 2% axial strain values of c' and φ' for both sides of the wall in combination with Kötter's earth pressure theory did not appear to be satisfactory.

Figure 6.17 shows the result of the back-calculation using this approach compared with the field measurements.

Results AZ13
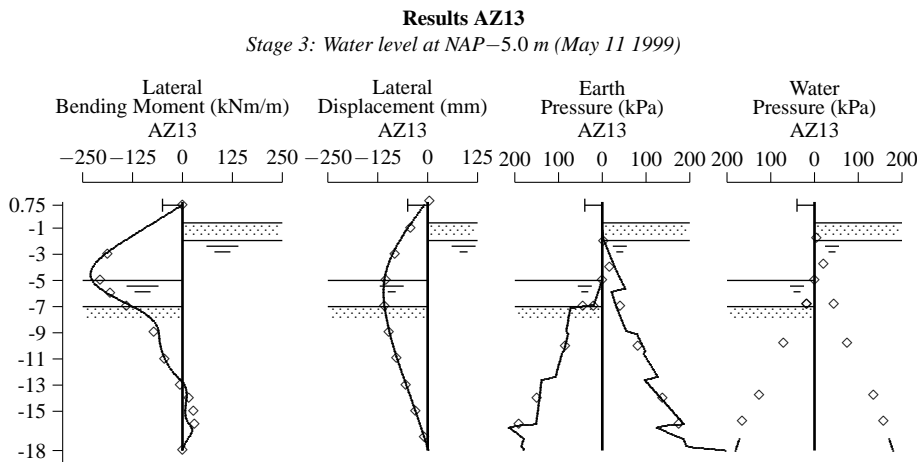*Stage 3: Water level at NAP−5.0 m (May 11 1999)*

Figure 6.17: *Drained back-analysis of the short-term field test with* PLASWALL *based on effective parameters. The solid lines represent the calculation results and the ◇-marks the field measurements*

It is shown that the maximum bending moment is considerably overestimated, $\Delta M = 230$ kNm/m. The choice of the k-values had minor effect on the calculation results, which indicates that most springs are in a plastic state. Typical strength parameters of the peat of $c' = 10$ kPa and $\varphi' = 20^o$ result in an active earth pressure coefficient of approximately $K_a = 0.5$. This gives an active effective earth pressure of

$$\sigma'_a = K_a \left(\sigma_v - u \right) - 2c' \sqrt{K_a} \tag{6.31}$$

In the weightless peat layer, on a level of -7 m, for example, it follows from Table 6.10 that $\sigma_v = 99$ kPa and $u = 46$ kPa, hence $\sigma'_a = 12.3$ kPa. In the field test, however, a typical observation was that the effective earth pressure was approximately zero. The effects of an overestimation of the effective earth pressure on the bending moment are investigated hereafter.

From Figure 6.17, the part of the sheet pile between the points where $M = 0$ is considered as a simply supported beam loaded by a distributed load. The distributed load represents the calculated effective earth pressure, which was not present in the field test. This load is estimated as $q = 10$ kPa. For the span, $L = 14$ m is taken. Overestimation of the maximum bending moment is

$$\Delta M = \frac{1}{8} qL^2 = 245 \text{ kNm/m} \quad \text{(calculated: 230 kNm/m)} \tag{6.32}$$

This simple calculation illustrates that a significant part of the overestimated bending moments and displacements is caused by the effective earth pressure, which is taken into account in the calculation by using effective strength parameters but was not observed in the field test.

6.6.5 Short-term field test with undrained and effective parameters

The back-analysis of the short-term field test was successful with undrained parameters but not with effective parameters, because the active earth pressure was overestimated. However, the back-analysis with undrained parameters can not be used to analyse the long-term field test, because the geometrical boundary conditions do not alter during the test. In order to be able to make a back-analysis for the long-term field test, it is proposed to take undrained parameters on the retained side and effective parameters on the excavated side; the reasons are outlined below.

It has been suggested in Section 6.4.4 that the increase in displacements and moments is generated from the excavated side and that the soil on the retained side more or less followed the deflected wall. As neither the total earth pressure nor the water pressure on the retained side underwent a significant change during the short-term field test, see Figure 6.8, no proof of drained soil behaviour was found. On the other hand, on the excavated side some significant prove for time-dependent effects was found.

In this back-analysis, the following construction stages are considered:

1. Dry excavation to NAP-4.0 m

2. Excavation under water to NAP-7.0 m, water level in the excavation at NAP-1.5 m

3. Lowering of the water level to NAP-5.0 m (May 11)

Depth (m)	γ (kN/m^3)	c' (kPa)	φ' (^{o})	c_u (kPa)	Stage 1 k_1 (kN/m^3)	Stage 2 k_2 (kN/m^3)	Stage 3 k_3 (kN/m^3)	Stage 4 k_4 (kN/m^3)	Stage 5 k_5 (kN/m^3)
+0.35	17	2	35		900	700	300	300	200
-1.6	16.8	6.3	29.1	34.3	900	700	300	300	200
-5.75	10.1	9.4	18.8	39.7	700	700	550	550	300
-9	10.1	11.8	20.1	44.2	700	600	300	300	200
-10.5	13.9	7.1	20.3	29.9	600	500	300	300	200
-12.5	16.3	7.4	27.1	50.7	1800	1800	800	800	600
-16.1	14.5	9.8	37.2	50.7	6000	6000	2000	2000	2000
-17	20	2	37		30000	30000	30000	30000	30000

Table 6.11: *Input parameters for the short-term and long-term field tests in* PLASWALL *based on both undrained and effective parameters*

The input parameters are presented in Table 6.11. Stages 4 and 5 refer to the back-analysis of the long-term field test presented in Section 6.6.6 and are of no importance in this back-analysis. The following assumptions are added to the list in Section 6.6.4:

- The soil on the retained side is assigned undrained parameters

- The soil on the excavated side is assigned effective parameters

- For each soil layer, one subgrade reaction modulus is applied to both sides of the retaining wall

Results AZ13

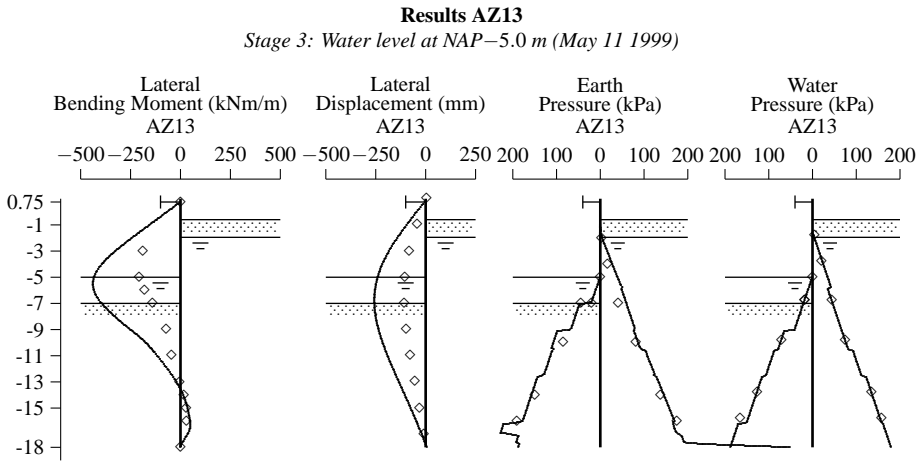*Stage 3: Water level at NAP−5.0 m (May 11 1999)*
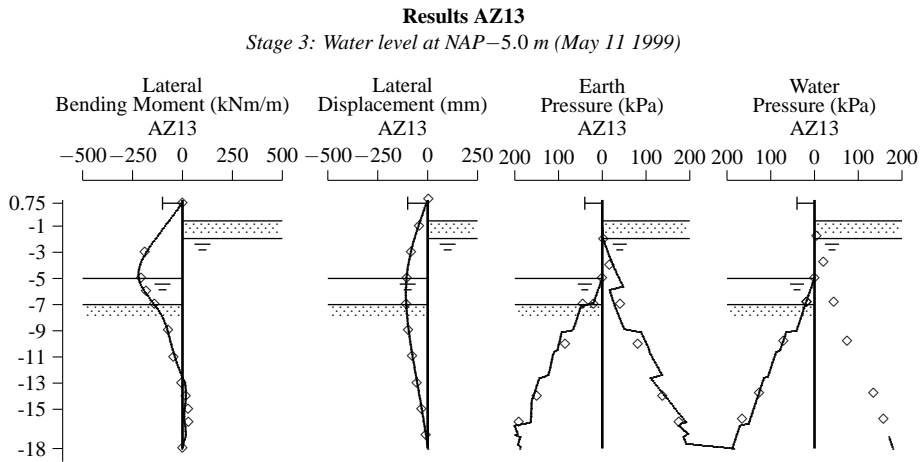
Figure 6.18: *Back-analysis of the short-term field test with* PLASWALL *using both un-drained and effective parameters. The solid lines represent the calculation results and the ⋄-marks the field measurements*

The calculation results of Stage 3 are presented in Figure 6.18. The calculated displacements and bending moment distribution are in agreement with the measurements, although both the bending moments and wall deflections were sensitive for the values of the subgrade reaction moduli. The subgrade reaction moduli used in this back-analysis, see Table 6.11, were of the same order as the moduli used in the undrained analysis presented in Table 6.9. On the basis of the calculated result, it can be concluded that the assumption of undrained parameters on the retained side gives a reliable back-analysis.

6.6.6 Long-term field test

The back-analysis with both the undrained and effective parameters presented in the previous section can be used for back-analysis of the long-term field test. Although the retained side is modelled with undrained parameters, it follows from the measurements in Figures 6.8 and 6.9 that, during the long-term field test (*tilt* from 2 to 3 rad), the earth, water and effective earth pressures hardly altered; an analysis with undrained parameters on the retained side therefore seems to be justified. The back-analysis of the long-term field test is carried out for the following stages:

1. Dry excavation to NAP−4.0 m

2. Excavation under water to NAP−7.0 m, water level in the excavation at NAP−1.5 m

3. Lowering of the water level to NAP−5.0 m (May 11)

4. Positioning of the sand mound with the water level at NAP−5.0 m (May 26)

5. End of the long-term field test (August 11)

For the long-term field test, the sand mound has to be modelled in Stage 4, bit as it had limited dimensions, geometrical effects should taken into account. Therefore the mound is modelled by an increase of the ground surface level but only to NAP+0.35 m, which is 70% of the total increase to NAP+1.0 m. The choice of 70% is supported by the theory of elasticity. In Figure 6.19, the case of a uniform load q distributed over a circular area with radius a on an elastic half plane is considered. The solutions for the vertical and radial stress increase under the centre point of the load are given by Timoshenko and Goodier [72].

$\sigma_{zz}, \sigma_{rr}, u$ (kPa)

$q = 27.2$ kPa, $a = 10$ m

$$\sigma_{zz} = q\left(1 - \frac{z^3}{(a^2 + z^2)^{\frac{3}{2}}}\right)$$

$$\sigma_{rr} = \sigma_{\theta\theta} = \frac{q}{2}\left((1+2\nu) - \frac{2(1+\nu)z}{\sqrt{(a^2+z^2)}} + \left(\frac{z}{\sqrt{(a^2+z^2)}}\right)^3\right)$$

$\nu = 0.5$

$$u = \frac{1}{3}(\sigma_{rr} + \sigma_{\theta\theta} + \sigma_{zz})$$
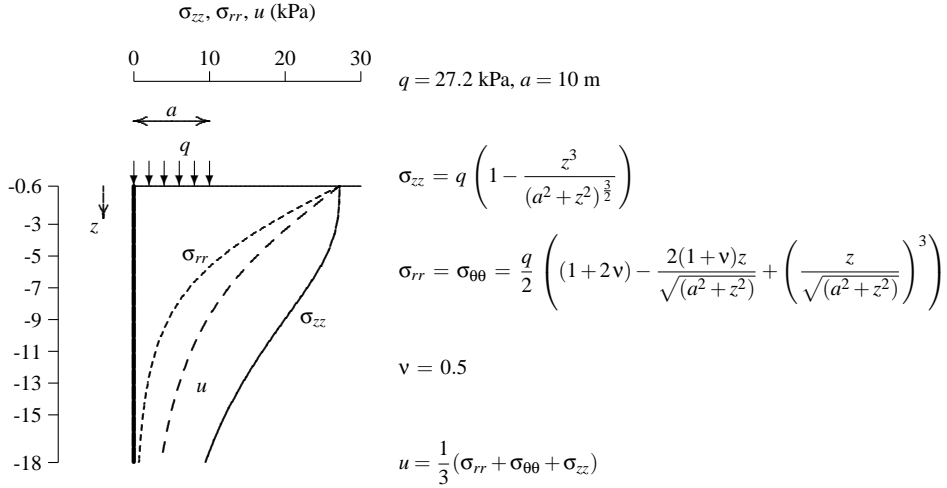
Figure 6.19: *Increase of vertical and radial stresses and pore water pressures produced by a uniform load distributed over a circular area*

The sand mound is considered as a circular distributed load with radius $a = 10$ m. The height of the sand mound is 1.6 m with an average volume weight of $\gamma = 17$ kN/m^3, so the load increase is $q = 27.2$ kPa. The vertical stress increase σ_{zz} is plotted in Figure 6.19 and the average increase over the height is $\sigma_{zz,average} = 19$ kPa, which is 70% of load q. This result means that when the sand mound is modelled by means of an increase of the ground level, only 70% of this increase should be taken into account.

In Figure 6.19 the development of the radial stress increase and the pore water pressure are also plotted. In the back-analysis, however, undrained soil behaviour is assumed on the retained side, so the pore water pressure increase is not taken into account.

The input parameters for the long-term field test are given in Table 6.11 and the calculation results for Stage 5 are presented in Figure 6.20. Similar to those for the short-term field test, it should be noted that not only are the calculated displacements and bending moments close to the measured results, but the calculated earth pressures on both sides of the wall are also quite close to the measured earth pressures at every depth. This result again confirms that the combinations of k on the one hand and c_u, c' and φ' on the other hand, applied in the different soil layers are reasonable. The water pressures on the excavated side are input parameters chosen on the basis of the measured water pressures.

Results AZ13

Stage 5: Water level at NAP−5.0 m with sand mound (August 11 1999)
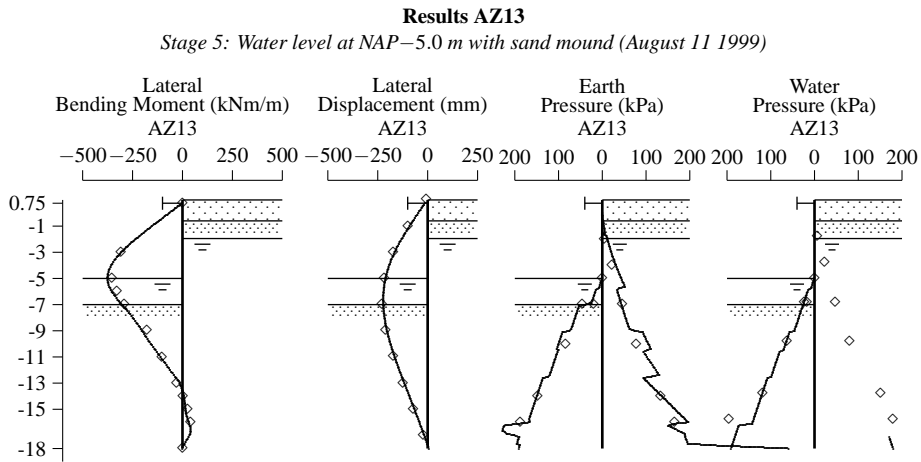
Figure 6.20: *Back-analysis of the long-term field test with* PLASWALL. *The solid lines represent the calculation results and the ⋄-marks the field measurements*

From the back-analysis of the long-term field test with PLASWALL the following conclusions can be drawn:

- Back-analysis based on drained parameters on both sides of the sheet pile wall in combination with Kötter's earth pressure theory is not possible

- The assumption that the retained side can be modelled with undrained shear strength parameters together with the assumption that the excavated side can be modelled with effective strength parameters in combination with the measured water pressure distribution, gives reasonable results

- The assumption that equal k-values can be applied to both sides of the sheet pile wall gives reasonable results

- Reasonable values for k vary between 200 and 900 kN/m^3 for the upper clay layer, between 200 and 700 kN/m^3 for the peat layer, and between 200 and 1800 kN/m^3 for the lower clay layer

6.6.7 Comparison of subgrade reaction moduli with engineering practice

In the three back-analyses already presented, subgrade reaction moduli have been determined. In Table 6.12, these moduli are compared with the moduli presented by CUR 166 [27] and by Van Tol and Brassinga [73], who proposed their moduli on the basis of a back-analysis for the Willemspoortunnel in Rotterdam. Both the values from CUR 166 and from Van Tol and Brassinga are frequently used in Dutch engineering practice.

It is shown that the subgrade reaction moduli determined in the back-analyses are significantly smaller than those generally used in the Dutch engineering practice bbut a clear

Subgrade Reaction Moduli (kN/m³)			
	Clay	Peat	Clay
Depth (m NAP)	-1.6 to -5.75	-5.75 to -10.5	-10.5 to -16.1
c_u (kPa)	35	40	40
Short-term, undrained	250 - 900	400 - 1100	1000 - 3200
Short-term, undrained and effective	300 - 900	300 - 700	300 - 1800
Long-term	200 - 900	200 - 700	200 - 1800
CUR 166	1000 - 4500	1000 - 4000	1100 - 5200
Van Tol and Brassinga	2200 - 4400	2250 - 4500	2300 - 4600

Table 6.12: *Comparison of subgrade reaction moduli with engineering practice*

explanation for this large difference has not been investigated. However, it is known that higher subgrade reaction moduli result in a smaller wall deflection and in a smaller maximum bending moment. Therefore it is suspected that the higher subgrade reaction moduli account for the overestimation of the wall displacements by the earth pressure theories from Müller-Breslau and Kötter.

6.6.8   Limit state

The final state of the test in which the plastic hinge was generated, was close to an ultimate limit state and is therefore the perfect case for back-analysis with a limit state model, but it can also be analysed with a subgrade reaction model. The back-analyses were carried out with the classical model SPOOKS [37] and the subgrade reaction model PLASWALL.

In the ultimate limit state, the water level inside the excavation was at NAP$-$6 m. In this stage, vertical equilibrium is not satisfied, unless wall friction between the soil and the sheet pile is taken into account. SPOOKS does not accept an input that does not satisfy vertical equilibrium of the excavation. In order to generate suitable input parameters for SPOOKS,

$W + T = U$

$A \sum_{i=1}^{n} \gamma_i d_i + T = A u$ (in which A: area of pit and d: thickness of layer)

$146.8 + T/A = 170$ kPa

Hence vertical equilibrium is not satisfied!

Correction of volumetric weights to account for wall friction:

$W + T = U \rightarrow W^* = U$

Solve: $\sum_{i=1}^{n} (\gamma_i + \Delta\gamma_i) d_i = U$

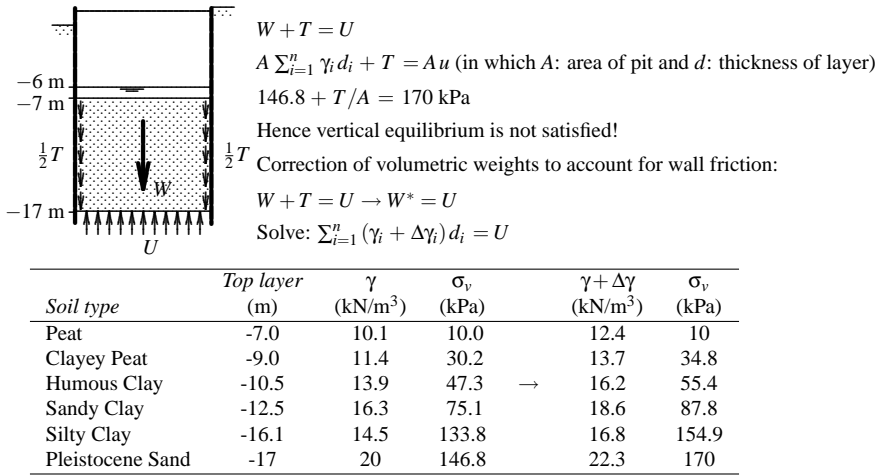| Soil type	Top layer (m)	γ (kN/m³)	σ_v (kPa)		$\gamma + \Delta\gamma$ (kN/m³)	σ_v (kPa)
Peat	-7.0	10.1	10.0		12.4	10
Clayey Peat	-9.0	11.4	30.2		13.7	34.8
Humous Clay	-10.5	13.9	47.3	$\rightarrow$	16.2	55.4
Sandy Clay	-12.5	16.3	75.1		18.6	87.8
Silty Clay	-16.1	14.5	133.8		16.8	154.9
Pleistocene Sand	-17	20	146.8		22.3	170

Figure 6.21: *Correction of vertical weight to account for wall friction*

a correction is applied to the volume weight of the soil layers on the excavated side that account for the contribution of the wall friction to vertical equilibrium. This correction method is explained in Figure 6.21.

The sand mound is modelled by raising the ground surface level on the retained side to NAP+0.35 m, as explained for the back-analysis of the long-term field test, see Section 6.6.6. Furthermore, it is also important to note that in the period November 1999 to January 2000, the groundwater level on the retained side gradually rose from NAP−1.95 m to NAP−1.26 m.

SPOOKS

The input parameters c' and φ' are derived from the peak-value of the $\sigma - \varepsilon$ diagram from triaxial tests. The water pressure distribution is corrected by a hydraulic gradient i, from which the effective volume weight of the pore water follows: $\gamma_w = (1 - i)\,10 \text{ kN/m}^3$. The input parameters are given in Table 6.13. In addition, the level of Pleistocene Sand layer was raised slightly to -16.9 m to obtain a numerical stable result.

Soil type	Top layer (m)	γ_{ret} (kN/m³)	γ_{exc} (kN/m³)	c' (kPa)	φ' (°)
Sand Fill	+0.35	17		2	35
Silty Clay	-1.6	16.8		15.3	19.2
Peat	-5.75	10.1	12.4	13.2	19.7
Clayey Peat	-9.0	11.4	13.7	21.8	15.7
Humous Clay	-10.5	13.9	16.2	8.7	16.7
Sandy Clay	-12.5	16.3	18.6	15	16.8
Silty Clay	-16.1	14.5	16.8	14.5	15
Pleistocene Sand	-16.9	20	22.3	2	37

retained side: $\tan\delta = 0$, $h = -1.26$ m and $i = -0.06$
Excavated side: $\tan\delta = 0.4\tan\varphi'$, $h = -6$ m and $i = -0.5$

Table 6.13: *Input parameters for the back-analysis of the limit state with* SPOOKS

Figure 6.22 shows the calculation results. The calculated minimum wall length of 20 m is 2 m longer than the real length. The calculated plastic moment is $M_{pl} = 466.04$ kNm/m and the fixed end moment is $M = 265.64$ kNm/m.

From the back-analysis of the limit state with SPOOKS the following conclusions can be drawn:

• Back-analysis based on drained parameters on both sides of the sheet pile wall in combination Brinch Hansen's earth pressure theory is possible

• The input parameters c' and φ' derived from the peak-value of the $\sigma - \varepsilon$ diagram from triaxial tests, give a satisfactory result

• The corrections of the ground level on the retained side and of the volume weights on the excavated side were effective
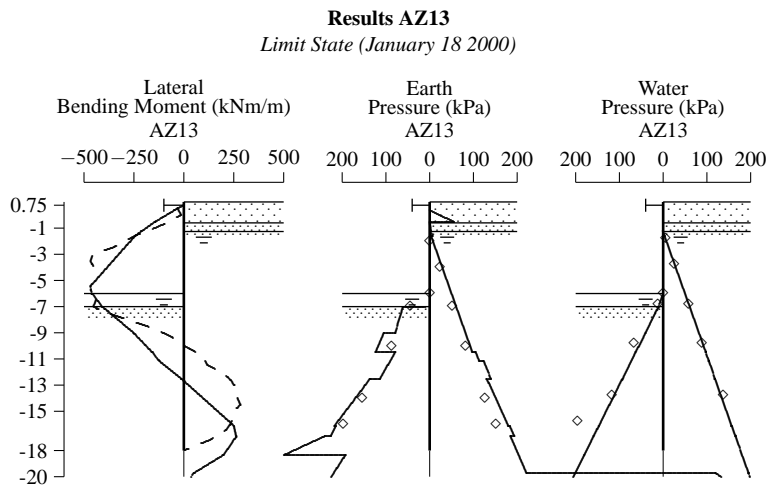
Figure 6.22: *Back-analysis of the limit state with* SPOOKS. *The solid lines represent the calculation results and the dashed lines and ◇-marks the field measurements*

PLASWALL

This back-analysis with PLASWALL is an ulimate limit state calculation and does therefore not account for construction stages. The input parameters of this back-analysis are presented in Table 6.14. The active and passive earth pressure coefficients were chosen such that they are as compatible as possible with Brinch-Hansen's earth pressure theory.

Soil type	Top layer (m)	γ (kN/m^3)	c' (kPa)	φ' (^{o})	k (kN/m^3)	K_a	K_p	h_{ret} (m)	h_{exc} (m)
Sand Fill	-0.6	17	2	35	100	0.18	4.35	-1.26	
Silty Clay	-1.6	16.8	15.3	19.2	100	0.20	2.00	-1.25	
Peat	-5.75	10.1	13.2	19.7	200	0.20	2.85	-1.03	-5.57
Clayey Peat	-9.0	11.4	21.8	15.7	100	0.20	1.12	-0.99	-3.09
Humous Clay	-10.5	13.9	8.7	16.7	100	0.32	2.35	-0.55	-2.56
	-11.18	13.9	8.7	16.7	100	0.56	2.35	-0.55	-2.56
Sandy Clay	-12.5	16.3	15	16.8	500	0.56	2.47	-0.12	-2.03
Silty Clay	-16.1	14.5	14.5	15	2000	0.59	2.56	1.47	1.05
Pleistocene Sand	-17	20	2	37	30000	0.25	7.13	1.47	1.05

$M_{pl} = 467$ kNm/m
K_n follows from $K_n = 1 - \sin\varphi'$
Volume weight on the excavated side follows from Figure 6.21

Table 6.14: *Input parameters for the back-analysis of the limit state with* PLASWALL

    The calculation results are presented in Figure 6.23 and are compared to the state of the excavation on January 18 2000, just before the large rotation in the plastic hinge occurred. The calculated plastic rotation of the hinge amounts to $\Delta\varphi = 0.043$ rad. In the comparable stage of the field test, no clear plastic rotation was measured. This means that this back-analysis gives a slight overestimation compared to the measured behaviour.
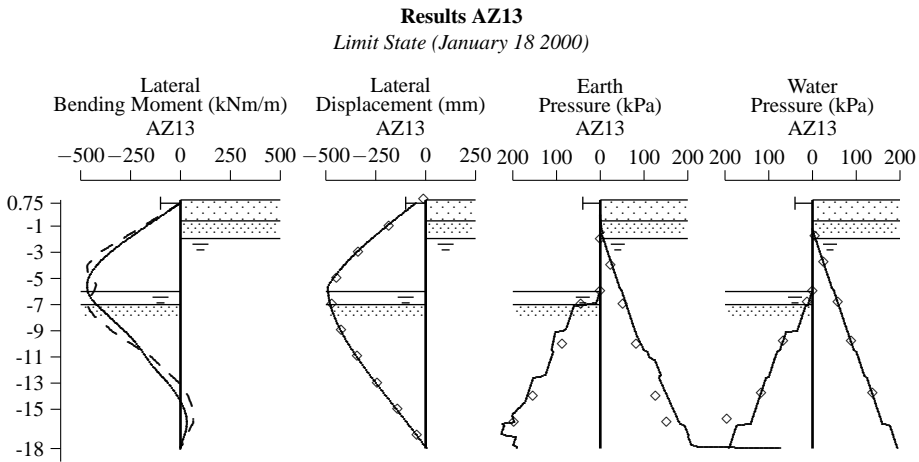
Figure 6.23: *Back-analysis of the long-term field test with* PLASWALL. *The solid lines represent the calculation results, the dashed lines and ⋄-marks the field measurements*

From the back-analysis of the limit state with PLASWALL the following conclusions can be drawn:

- Back-analysis based on drained parameters on both sides of the sheet pile wall in combination with Brinch Hansen's earth pressure theory is possible

- The input parameters c' and φ' derived from the peak-value of the $\sigma - \varepsilon$ diagram from triaxial tests, give a satisfactory result

- The corrections of the ground level on the retained side and of the volume weights on the excavated side were effective

6.7 Back-analysis with the finite element method

6.7.1 General

The finite element method can be considered as a tool of the highest order for a back-analysis. Combined with an appropriate soil model, the real soil behaviour can be modelled quite accurately. Soil is a complex material that is highly stress-dependent and therefore its behaviour is closely linked to the stress path along which the soil is loaded. In deep excavation problems, different soil areas are loaded by different stress paths. On the retained side, the soil is unloaded mainly in the horizontal direction but on the excavated side it is unloaded in both the vertical direction and to a lesser extent in horizontal direction.

The back-analyses made in this section focus on the application of different material models, each with its specific characteristics, such as shear hardening or creep. By back-analyses with several material models, insight is obtained into the effects of these characteristics on the behaviour of the sheet pile walls and a better explanation of the measured behaviour of the sheet pile walls can be given.

6.7.2 Choice of soil model

The back-analyses described in this section are made with PLAXIS 7.2 [80] which has various advanced soil models available that are able to describe stress-dependent soil behaviour, such as the Soft-Soil Model (SS-model), the Hardening-Soil model (HS-model) and the Soft-Soil-Creep model (SSC-model).

The SS-model is a modification of the Cam-Clay model and is especially suitable for problems where compression of soil is dominant rather than shear. In this respect the SSC-model is an extension of the SS-model that accounts for creep in the soil. A limitation of the SSC-model, however, is that, particularly for unloading problems, the range of elastic soil behaviour tends to be overpredicted [80].

The HS-model includes a hyperbolic stress-strain relationship and strain hardening of soil loaded in shear. As in the SSC-model, a cap yield surface has been implemented in the HS-model to account for plastic soil behaviour in compression. All these features combine to give a rather realistic description of the real soil behaviour. An important limitation of the HS-model is that it does not account for other complex soil behaviour, such as softening in the case of large deformations, creep and anisotropy.

Regarding the choice of soil model, the PLAXIS manual recommends for this case to use the HS-model. Recent studies by Freiseder and Schweiger [33] and Callisto *et al.*, [17] support the applicability of the PLAXIS HS-model for excavation problems in soft soil. Furthermore, Predictions 19 and 20, reported in Chapter 5, were made with the SSC-model and with the HS-model respectively, using comparable soil parameters. Better results were obtained with the HS-model than with the SSC-model. Because of these considerations the HS-model is used for the short-term field test and both the HS-model and the SSC-model for the long-term field test. The SSC-model was only applied to the soft clay and peat layers.

6.7.3 Determination of soil parameters

The soil parameters used in the back-analyses are presented in Table 6.15. The soil parameters were obtained mainly from the CU triaxial tests. The strength parameters c' and φ' have

Soil type	Top layer (m)	γ (kN/m^3)	c' (kPa)	φ' (^{o})	E_{50}^{ref} (kPa)	E_{oed}^{ref} (kPa)	m	k (m/day)
Sand Mound	+0.75	11.9	2	35	45000	45000	0.5	1
Sand Fill	-0.6	17	2	35	45000	45000	0.5	1
Silty Clay	-1.6	16.8	15.3	19.2	11245	5623	0.9	$5.07\,10^{-5}$
Peat	-5.75	11.0	13.2	19.7	2210	1070	0.65	$9.60\,10^{-5}$
Clayey Peat	-9.0	11.9	21.8	15.7	2833	5574	1	$7.88\,10^{-5}$
Humous Clay	-10.5	13.9	8.7	16.7	4829	8930	1	$2.28\,10^{-5}$
Sandy Clay	-12.5	16.3	15	16.8	6924	3204	0.9	$1.96\,10^{-5}$
Silty Clay	-16.1	14.5	14.5	15	8850	18180	1	$2.97\,10^{-5}$
Pleistocene Sand	-17	20	2	37	45000	45000	0.5	1

$E_{ur}^{ref} = 5 E_{50}^{ref}$
Peat: $k_h = 8.64\,10^{-5}$ m/day; Sandy Clay: $k_h = 2.86\,10^{-5}$ m/day
Larssen 607K: $\beta_l = 0.7$
$\psi' = \varphi' - 30^o \not< 0$

Table 6.15: *Input parameters for the back-analysis with* PLAXIS

been redetermined from the peak-value of the $\sigma - \varepsilon$ diagram and the reference stiffness E_{50}^{ref} is determined using

$$E_{50} = E_{50}^{ref} \left(\frac{c' \cot \varphi' + \sigma_3'}{c' \cot \varphi' + p^{ref}} \right)^m \tag{6.33}$$

where E_{50} is the stiffness measured in the triaxial test for confining pressure σ_3' and $p^{ref} = 100$ kPa as a reference pressure. The power m was derived from a best estimate of the three stages in one triaxial test. For the oedometric stiffness the minimum value recommended by the program was used, as the values found in the oedometer tests were too low to be accepted by PLAXIS.

The stiffness of the upper silty clay layer was not trusted and was therefore determined from the oedometer tests using the following relations:

$$\lambda^* = \frac{C_c}{2.3 \, (1+e)} \tag{6.34}$$

$$E_{oed}^{ref} = \frac{p^{ref}}{\lambda^*} \tag{6.35}$$

$$E_{50}^{ref} = 2 \, E_{oed}^{ref} \tag{6.36}$$

From the soil investigation it appears that a reasonable choice of the unloading stiffness is $E_{ur}^{ref} = 5 \times E_{50}^{ref}$, which is taken for all soil layers.

Parameters for the SSC-model were derived from Table 6.15 in accordance with the PLAXIS manual [80]:

$$\lambda^* = \frac{p^{ref}}{E_{oed}^{ref}} \tag{6.37}$$

$$\kappa^* = \frac{3 p^{ref} \, (1 - 2 \nu_{ur})}{E_{ur}^{ref}} \tag{6.38}$$

$$\mu^* = \frac{1}{25} \lambda^* \tag{6.39}$$

where $\nu_{ur} = 0.2$ The permeabilities of the soft clay and peat layers were derived from the oedometer tests using the Taylor interpretation; this parameter is referred to as k_{oed}. The low volume weight of the sand mound accounts for its geometrical effects.

6.7.4 Calculation model

Figure 6.24 shows a typical FE mesh; 15-noded triangular soil elements and 5-noded beam elements were applied. Interface elements were used to model slip between the soil and sheet pile. The interface strength parameter was set at $R = 1$, which represents a rough interface.
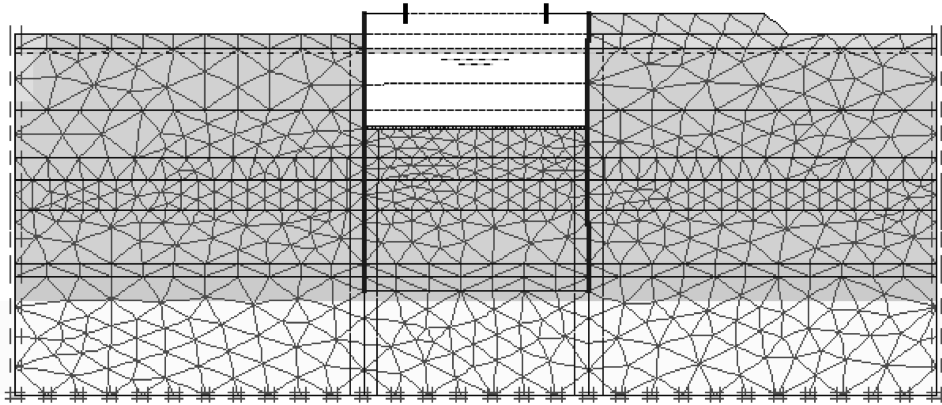
Figure 6.24: *Finite element mesh used for the back analysis*

Other assumptions on which the calculation was based are as follows:

- The calculations are based on undrained soil behaviour

- The initial groundwater pressure is modelled as follows: the head in the layers above -9 m is set to $h = -1.6$ m, the head below -17 m is set to $h = 0$ m and the heads in the intermediate layers are derived from linear interpolation

- The sand fill is included in the initial stress determination, which implies that the consolidation effects of the sand fill are negligible at the start of the test

- Excavation is taken into account by removal of soil elements

- Change of water level inside the excavation is modelled by giving the empty blocks in the excavation a head of water. The heads in the soil elements were not modified

- Excavation under water to NAP-7 m and lowering of the water level to NAP-5 m is modelled in one calculation stage. Similar calculations in which intermediate construction stages were taken into account, gave negligibly different results

- To obtain numerically stable results, the *tension cut-off* parameter in the peat layer was set to 1 kPa

- The switch to the SSC-model was made with a plastic 0-step

The calculated stages are given in Table 6.16.

6.7.5   Calculation results

Table 6.17 shows an overview of the various calculations and the results. Four calculations for the long-term field test were carried out. The calculation with $20 \times k_{oed}$ is based on the observation of Leroueil *et al.* [56]. They found that an evaluation of the coefficient

Stage	Description
1	Installation of sheet pile walls
2	Excavation to NAP−7 m and water level at NAP−5 m (short-term field test)
3	Construction of the sand mound
HS-model	
4	80 Days consolidation (long-term field test)
SSC-model	
4	Switch to SSC-model
5	80 Days consolidation (long-term field test)

Table 6.16: *Time scedule for the* PLAXIS *calculation*

of consolidation using the methods of Taylor and Casagrande can lead to underestimation of the permeability and determined consolidation coefficients using measurements from settlements of embankments, which are 3 to 200 times larger, with an average of factor 20.

The calculations with the HS-model don't account for creep, and in the calculation with the SSC-model and $\lambda^*/\mu^* = 400$ the creep effect is negligibly small. Only the calculation with $\lambda^*/\mu^* = 25$ takes creep into account, but without shear hardening.

	AZ13		Larssen 607K	
Stage	w_{max} (mm)	M_{max} (kNm/m)	w_{max} (mm)	M_{max} (kNm/m)
3: Short-term field test	117 (109)	245 (206)	78 (85)	345 (356)
Hardening soil model				
5: Long-term field test with $k = k_{oed}$	233 (230)	435 (355)	86 (131)	362 (460)
5: Long-term field test with $k = 20 \times k_{oed}$	303 (230)	504 (355)	116 (131)	434 (460)
Soft soil creep model				
5: Long-term field test with $\lambda^*/\mu^* = 400$	215 (230)	414 (355)	87 (131)	368 (460)
5: Long-term field test with $\lambda^*/\mu^* = 25$	343 (230)	545 (355)	139 (131)	505 (460)

Table 6.17: *Calculation results of the back-analysis with* PLAXIS *compared to field measurements. Measured results between brackets*

The results in Table 6.17 show that the short-term calculation gives reasonable values for both the AZ13-wall and the L607K-wall, although for the AZ13-side, the displacements and moments were somewhat overpredicted. For the long-term field test it can be stated that the better the prediction for the L607K-wall, it was the worse for the AZ13-wall. The best long-term prediction for the L607K-wall was obtained with the SSC-model and $\lambda^*/\mu^* = 25$.

The explanation for the poor prediction of the AZ13-wall might be the sand mound and 3D behaviour. The sensitivity of the slurry walls to the behaviour of the test wall is shown in Figure 6.14. Significant overpredictions of displacements and moments can be found with an improperly functioning slurry wall. A logical explanation for the overpredictions might therefore be that the slurry wall was pushed-in by the sand mound in such a way that the active earth pressure wedge could not move freely against the surrounding soil. However, this mechanism can not be proven from the field measurements.

For this reason the back-analysis of the long-term field test is focused on the L607K-wall. Figure 6.25 shows the increase of wall displacement at NAP−2 m measured in the period between May 26 and August 11, compared to five calculations of the long-term field test. Figure 6.26 shows the same plot on a $\log t$ scale. The bottom two lines in Figure 6.25

show some difference between the predictions with the HS-model with k_{oed}, and the SSC-model with $\lambda^*/\mu^* = 400$, both of which only take consolidation into account. These differences are negligible compared to the measured behaviour and therefore in this case, the influence of creep may be assessed with the SSC-model.
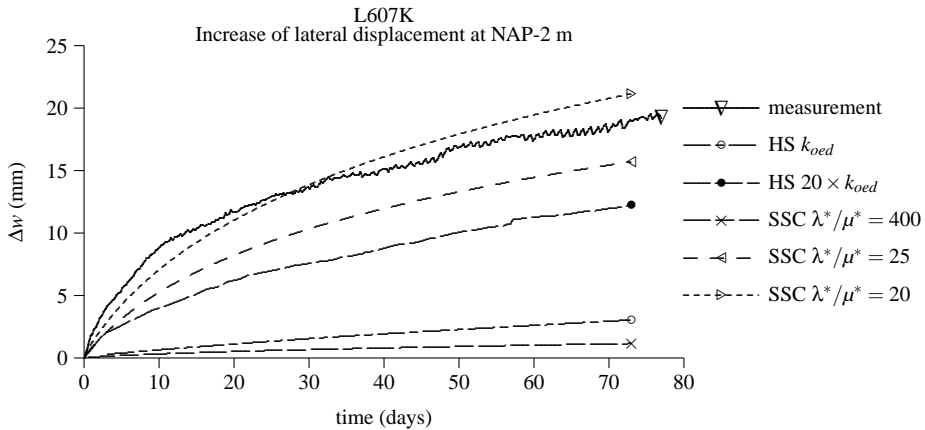

Figure 6.25: *Increase in lateral displacement at NAP−2 m against time after installation of the sand mound*
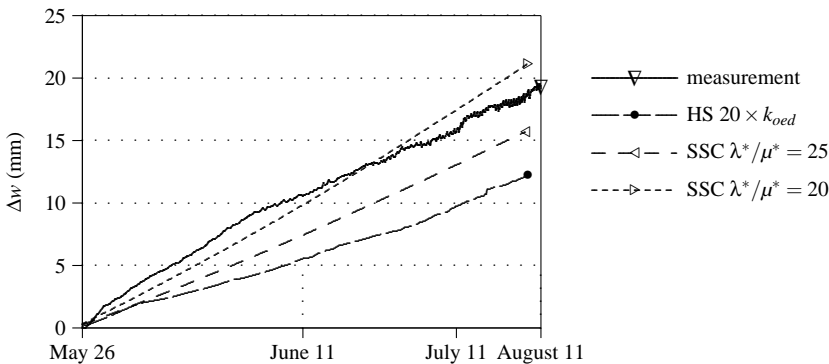

Figure 6.26: *Increase of lateral displacement at NAP−2 m against* $\log t$ *after installation of the sand mound*

In Section 4.5, typical field measurements of the long-term field test are presented with respect to $\log t$. Figure 6.26 shows the increase in wall displacement at NAP−2 m on a $\log t$ scale compared to the better long-term calculations. Perfect single logarithmic relations are found with the SSC-model and not with the HS-model. However, the HS-calculation shows an almost linear increase with $\log t$. The long-term behaviour of the field test can be explained both by consolidation and creep. A clear distinction between these phenomena can not be made from the measurements.

The Figures 6.25 and 6.26 show that the behaviour during the long-term field test can be better explained on the basis of creep with $\lambda^*/\mu^* = 20$ to 25, than from underestimation of the permeability by a factor 20. Therefore, it can be concluded that creep might have had a significant influence on the long-term behaviour of the field test.

6.7.6 Evaluation of calculated results

Figure 6.27 shows the results of the back-analysis of the short and long-term field tests, where the long-term field test was predicted with the SSC-model and $\lambda^*/\mu^* = 25$. Although the calculated results are close to the measured values, it should be realised that this back-analysis is rather simple.
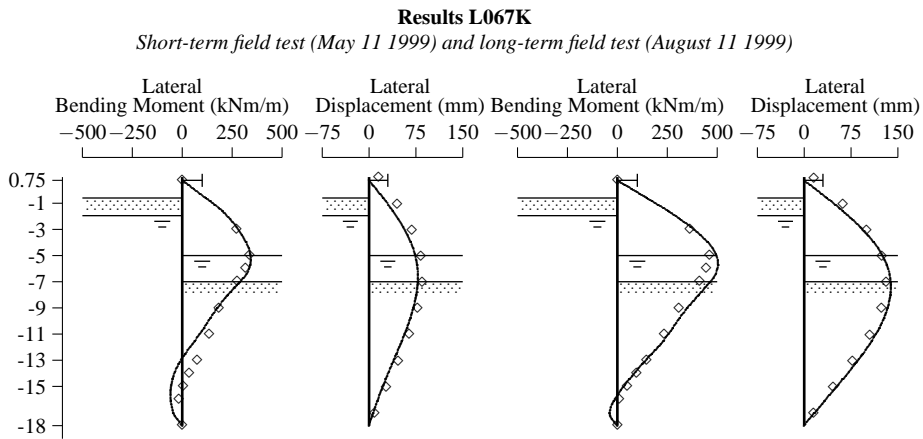
Results L067K

Short-term field test (May 11 1999) and long-term field test (August 11 1999)

Figure 6.27: *Back-analysis with* PLAXIS. *Left, the short-term field test and right, the long-term field test with the SSC-model and* $\lambda^*/\mu^* = 25$

Some important shortcomings of this back-analysis are:

- the stiffness parameters of all but the top silty clay layer were determined from triaxial tests

- the calculation was carried out with different material models to model the same layer

- groundwater is assumed to be incompressible, which could not be concluded from the field measurements

- the time-dependent effects between the different construction stages were not taken into account in the calculations

- the additional soil investigation, such as the oedometer tests, the vane tests and the cone pressiometer tests have been given little or no consideration

In spite of the shortcomings of this back-analysis with PLAXIS, the following conclusions can be drawn regarding the short and long-term field tests:

- back-analysis of the short-term field test gives results that are in reasonable agreement with the measurements

- all back-analyses of the long-term field test overestimate the maximum bending moment in the AZ13-wall. Possibly the bentonite screens have not functioned properly during the long-term field test

- the back-analyses of the long-term field test that do not account for increased permeability or for creep, underestimate the bending moment in the L607K-wall

- the bending moment in the L607K-wall is better assessed by the back-analyses of the long-term field test that account for increased permeability or for creep

- the behaviour of the long-term field test can be explained both by consolidation and creep

- creep might have had a significant influence on the long-term behaviour of the field test

Chapter 7

Discussion of results and conclusions

7.1 Introduction

The global objective of this study was to contribute to the process of filling-in gaps in our knowledge which became apparent when Eurocode 3, part 5 was drafted with particular reference to the topics of plastic design and oblique bending. The investigation of plastic design was of interest because an important material saving may be expected when plastic design is applied, and the intention behind the investigation of oblique bending of double U-piles was to obtain insight into the safety level of this type of sheet piling with regard to the structural stiffness and strength.

The development of the Structural Eurocodes and their anticipated role in the design of steel sheet piling, together with the knowledge of plastic design and oblique bending developed earlier in the ECSC research project [39], inspired the Geotechnical Laboratory of Delft University and the CUR to carry out the full-scale steel sheet pile wall field test near Rotterdam.

Within the framework of this field test, a prediction exercise was organised to validate the state-of-the-art calculation models for steel sheet pile walls in soft soil and to introduce the new phenomena of plastic design and oblique bending according to Eurocode 3, part 5 to the practising design engineers.

The research presented in this thesis focused on the following research topics involving interaction between soft soil and steel sheet piling:

- The structural and geotechnical aspects of plastic hinges

- The phenomenon of *oblique bending* and design rules that take it into account

- The effects of short and long-term behaviour of soft soil on the performance of steel sheet pile walls

For the investigation of these three topics, use was made of different research techniques, varying from analytical and numerical calculations to full-scale laboratory and field testing.

These techniques proved to be useful for the investigation of plastic design and oblique bending. The effects of short and long-term behaviour of soft soil on the performance of steel sheet pile walls was investigated by means of the full-scale field test and various numerical simulations of this test.

7.2 Plastic design

Investigation of the structural and geotechnical aspects of plastic design has lead to a wider insight into steel sheet pile wall design with plastic hinges. Investigation of the structural aspects had already shown [38] that the rotation capacity of a steel sheet pile is determined by the slenderness of the compression flange and the steel grade, expressed by the $\frac{b_f}{t_f \varepsilon}$ ratio. Dependent upon the cross-sectional geometry, many steel sheet piles have a limited rotation capacity or no rotation capacity at all. Consequently not every sheet pile profile can be used in plastic design.

With regard to the geotechnical aspects of plastic design, the rotation in the plastic hinge resulting from the geotechnical calculations, which is defined as the rotation requirement, depends upon the geometry of the entire sheet pile wall. Typical design cases, for which it can be proven that the rotation requirement will never exceed the rotation capacity of the sheet pile, could not be defined. Therefore in cases where rotation in the plastic hinge is accepted, a rotation check should always be part of the verification of the sheet piling. Simple suitable methods for such a rotation check are presented in Section 2.4.6.

In addition to these simplified methods, the subgrade reaction model PLASWALL was developed that accounts for moment redistribution and a plastic hinge when a certain maximum moment is reached. The calculation results obtained with PLASWALL are highly dependent upon the earth pressure model applied. From a study with four different earth pressure models compared to a finite element calculation, it could be concluded that a close result could only be obtained when Brinch Hansen's earth pressure model was applied; the strength of Brinch Hansen's earth pressure theory is that the earth pressure distribution is related to the deformation of the retaining wall. A significant overestimation of the design bending moment was found with the other three earth pressure models. This result may prove the practicality of applying Brinch Hansen's earth pressure theory to the limit earth pressure distribution in a subgrade reaction model.

The practical applicability of plastic design in comparison to the 'conventional' elastic design method was demonstrated with the design examples in Section 2.7. The example in Section 2.7.3 showed a possible material saving of 26%, which is typical for plastic design. This might have increased had the wall length been optimised as well.

In the first test wall of the sheet pile wall field test a plastic hinge was generated in the sheet pile wall with a plastic rotation of about $\Delta \varphi = 0.2$ rad. The structure with the plastic hinge proved to be a stable earth and water retaining structure with a very large wall deflection and a clear increase in the fixed moment, to carry the redistributed moment. A stable wall with rotation in the plastic hinge could be obtained, because the available embedment length was sufficient.

The generation of the plastic hinge was as expected on the basis of observations of many four-point bending tests. Therefore the application of the structural design rules for plastic design given in ENV 1993-5, which are based on the theory derived from a large number of

bending tests [38, 39], to this sheet pile wall field test proved to be successful.

The following point regarding plastic design must not be overlooked. The combination of 'possible material saving' together with the safety requirement of 'sufficient wall length' could lead to designs of longer and lighter sheet piling in future. If this is the case, the drivability of the sheet piling may more often become the critical factor in a design. It is, however, not obvious that the sheet piling will become longer compared to elastic design. The possible failure modes in the ground associated with plastic design, listed in Figures 2.6 and 2.15, indicate that plastic design should not necessarily lead to an increase in embedment length, because the fixed moment should not always be fully developed. Clever positioning of struts can be of more importance than the embedment length. Plastic design gives the design engineer a lot of freedom to choose clever and innovative solutions.

7.3   Oblique bending

Investigation of the oblique bending phenomenon has resulted in the statement that oblique bending can occur in steel sheet piling. In this thesis, a design rule is proposed to take oblique bending into account.

To develop this design rule, the subgrade reaction model SKEWWALL was built. The applicability of SKEWWALL to the investigation of oblique bending was verified with an experimental four point bending test on two double U-piles and to 3D numerical simulations with DIANA. The success of this verification meant that SKEWWALL could be used to develop the new design rule to account for oblique bending.

In the development of the new design rule the approach presented in ENV 1993-5 [24] was closely followed. Six major effects that influence oblique bending, were distinguished and by means of a thorough study with SKEWWALL, most of these influences could be quantified. This design rule is presented in Section 3.7 and its workability was illustrated with two design examples.

Oblique bending was investigated in the second test wall of the sheet pile wall field test. The measurements, presented in Figures 6.6 and 6.7, showed that oblique bending can occur in steel sheet piling and that loss of strength and stiffness should be taken into account in the design. The amount of loss of structural resistance varied from pile to pile and in this field test, average values of $\beta_I = 0.68$ and $\beta_W = 0.73$ were found. These values could be determined with reasonable accuracy from the design rule proposed in this thesis.

The following critical comment is made regarding oblique bending. A design that accounts for oblique bending results in a better prediction of the wall displacement and in a more considered choice of the required section. These are both safety aspects and should not be regarded as giving a less economic structure. Nevertheless, it is tempting for the design engineer to avoid the complex design rule for U-piles and to choose Z-piles instead. In this way the Z-pile will be designated as a 'designer's pile'. This negative development should be avoided, for example, by taking into account the drivability and the reusability of the sheet piling in the design. When this occurs, the designer can make a properly considered choice of the profile.

7.4   Full-scale field test

Apart from the investigation of plastic design and oblique bending, the Rotterdam sheet pile wall field test revealed many other new results that are of interest for steel sheet pile wall design in soft soil.

The behaviour of the short-term field test could be explained by undrained behaviour of the soil in combination with some significant compressibility of the pore water. The long-term behaviour seemed to be dominated by the time-dependent soil behaviour on the excavated side.

The measured results from the short-term field test could be reproduced by a back-analyses with PLASWALL based on *undrained* soil parameters from the triaxial tests. The back-analysis with *effective* soil parameters in combination with Kötter's earth pressure theory led to a significant overestimation of the wall deflection and bending moment. This overestimation is ascribed to the active earth pressure coefficient determined with Kötter's earth pressure theory, which was too high for this case. A more practical approximation was obtained when undrained soil parameters were applied to the retained side and effective parameters on the excavated side.

The subgrade reaction moduli determined with these back-analyses were significantly lower than the values that are generally used in Dutch design practice. A clear explanation for this large difference was not investigated but it was suspected that the higher subgrade reaction moduli account for overestimation of the wall displacements when used in combination with the earth pressure theories of Müller-Breslau and Kötter.

During the long-term field test, displacements of and bending moment in the test walls increased in proportional to $\log t$. This increase was ascribed to the consolidation and creep effects of the soft soil layers. A first back-analysis with PLAXIS indicated that for the short-term field test a more accurate prediction was obtained with the soil model that accounted for shear hardening, and that for the long-term behaviour in this test, creep was probably of more importance than consolidation. Therefore interesting results are expected when a back-analysis is made with a soil model that includes both shear hardening and creep.

The full-scale field test can also serve as a *benchmark* against which numerical or centrifuge models can be validated. For example, in the back-analysis with PLAXIS, the need for a soil model which accounts for both shear hardening and creep, became evident. When inverse analysis techniques are used to determine parameters, as was carried out, for example, by Bakker [3] for the Karlsruhe field test, the 3D effects should be appreciated.

7.5   Design of steel sheet piling

The topics of plastic design and oblique bending focus on a more economical use of steel sheet piles. More economical use, however, is only acceptable when the predicted load on the sheet pile wall is reliable, i.e., when the concept of limit state design is sufficiently mastered. The prediction can be made with either simple tools or with more advanced calculation models, provided that the soil behaviour is modelled correctly and that the soil parameters are determined properly.

For the prediction exercise, where 20 engineers were provided with the same soil investigation data, 23 predictions were submitted. The scatter of the predicted wall displacements

and bending moments, presented in the Figures 5.1 and 5.2, was large, which suggests that the reliability of predicted wall performance is quite inaccurate. Similar results have been obtained previously in geotechnical engineering, for example, at the sheet pile wall field test in Karlsruhe [88].

The parameters used in the predictions proved that a unique set of soil data does not automatically guarantee a unique set of model parameters. The most important factor in the choice of calculation model and parameter determination in steel sheet piling is the skill and experience of the design engineer.

This wide scatter of results indicates that, on average, the prediction of displacement and bending moment in steel sheet piling is insufficiently mastered. However, as prediction of displacement and bending moment forms the basis of limit state design, the wide scatter also indicates that, on average, limit state design of steel sheet piling is insufficiently mastered.

Summarising, it can be concluded from this research that it is worthwhile taking plastic hinges into account, provided that the design engineer is able to make an accurate prediction of the intermediate construction stages, and necessary to take oblique bending into account.

7.6 Recommendations and outlook

The theory behind plastic design and oblique bending presented in Chapters 2 and 3 respectively, has become available to improve the draft of Eurocode 3, part 5. It is expected that this Eurocode will be used as a basis for design of steel sheet piling.

With regard to application of plastic design, it is noted that the sections which are available today, are optimised for *elastic design*, i.e., structural failure is defined by yielding of the outermost fibre, and therefore most sections have a small rotation capacity or no rotation capacity at all. However, when sections will become available that are optimised for *plastic design*, i.e., sections with an equal full-plastic moment resistance but with more rotation capacity, the amount of material saving might increase.

As in most countries, plastic design and oblique bending have been seldom applied, and are therefore rather unknown, experience with these phenomena must be gained. Valuable experience from field studies of steel sheet piling in general, and in particular from cases involving double U-piles, may be obtained, relatively simply, by monitoring with an inclinometer in combination with strain gauges and a permanent tilt sensor; for cases involving single U-piles, strain gauges are indispensable. The experience gained from field studies can also be used to improve the design rules for U-piles.

The full-scale field test can be used as a benchmark for the verification of advanced material models in finite element programs, developed recently or to be developed in the future. The extensive amount of soil data [32] might be a good starting point for thorough back-analyses.

Bibliography

[1] NEN 6740. Geotechniek TGB 1990 Basiseisen en belastingen, 1991.

[2] E.J. Aukema and A.G. Joling. A 3D numerical simulation of oblique bending in a steel sheet pile wall: A quantification of soil influence. Master's thesis, Delft University of Technology, Geotechnical Laboratory, January 1997. Report number 416.

[3] K.J. Bakker. *Soil retaining structures Development of models for structural analysis*. PhD thesis, Delft University of Technology, 2000.

[4] J. Balay. Recommandations pour le choix des paramètres de calcul des écrans de soutènement par la méthode aux modules de réaction. Technical report, Ministère de l'Urbanisme, du Logement et des Transports & Laboratoire Central des Ponts et Chaussées, 1984.

[5] J. Balay, R. Frank, and L. Harfouche. Programme DENEBOLA pour le calcul des soutènements par la méthode des modules de réaction. *Bulletin Liaison Laboratoire des Ponts et Chaussées*, 120:3–12, 1982.

[6] M. Bats and D.R. Smit. Metingen van de vervormingen van damwanden in de bouwsleuf voor de aanleg van de metrotunnel in de SCHIEDAMSEWEG over de periode van mei t/m september 1984. Technical report, Gemeentewerken Rotterdam. Ingenieursbureau Waterbouw, juni 1985.

[7] G. Bell. FREW *17 GEO Suite for Windows*. Oasys GEO, London, 1999.

[8] H. Blum. *Einspannungsverhältnisse bei Bohlwerken und deren vereinfachte Berechnung mit Hilfe von "ideeller" und "stellvertretender" Belastung*. PhD thesis, Technische Hochschule Carolo Wilhelmina zu Braunschweig, 1931.

[9] D. Boissier, J. Gielly, R. Kastner, and J.C. Mangin. Détermination des moments et des pressions exercées sur un écran à partir des mesures inclinométriques. *Canadian Geotechnical Journal*, 15:522–536, 1978.

[10] M.D. Bolton and R.W. Whittle. A non-linear elastic/perfectly plastic analysis for plane strain undrained expansion tests. *Géotechnique*, 49(1):133–141, 1999.

[11] J.E. Bowles. *Foundation Analysis and Design*. Mc.Graw-Hill, 1988.

[12] E.L.M.G. van den Brande and A.W. Tomà. Bending test on steel piles. Technical Report 006/01469.01.01, TNO Building and Construction Research, June 2000.

[13] J. Brinch Hansen. *Earth Pressure Calculation*. PhD thesis, University of Copenhagen, 1953.

[14] J. Brinch Hansen. The internal forces in a circle of rupture. The Danish Geotechnical Institute, 1957. Bulletin No.2.

[15] J. Brinch Hansen and H. Lundgren. *Hauptprobleme der Bodenmechanik*. Springer-Verlag, 1960.

[16] D. Bruzzi, A. Zattoni, and G. Pezzetti. Pressure cells: How to obtain better results. In C.F. Leung, S.A. Tan, and K.K. Phoon, editors, *Field Measurements in Geomechanics*, pages 61–65. A.A. Balkema, Rotterdam, 1999. FMGM99: Singapore, 1-3 December 1999.

[17] L. Callisto, Amorosi A, and S. Rampello. The influence of pre-failure soil modelling on the behaviour of open excavations. In F.B.J. Barends, J. Lindenberg, H.J. Luger, L. de Quelerij, and A. Verruijt, editors, *Geotechnical Engineering for Transportation Infrastructure*, volume 1, pages 89–96. A.A. Balkema. Rotterdam, 1999. Proceedings XII ECSMGE.

[18] A. Caquot and J. Kerisel. *Tables de butée, de poussée et de force portante des fondations*. Paris: Gauthiers-Villars, 1948.

[19] CEN European Committee for Standardization. *Metallic materials - Tensile testing - Part 1: Methods of test (at ambient temperature)*, March 1990.

[20] CEN European Committee for Standardization. *Eurocode 3: Design of Steel Structures, Part 1.1: General Rules and Rules for Buildings*, 1992. ENV 1993-1-1.

[21] CEN European Committee for Standardization. *Eurocode 1: Basis of Design and Actions on Structures, Part 1: Basis of Design*, 1994. ENV 1991-1.

[22] CEN European Committee for Standardization. *Eurocode 7: Geotechnical Design, Part 1: General Rules*, 1994. ENV 1997-1.

[23] CEN European Committee for Standardization. *Hot rolled sheet piling of non alloy steels - Part 1: Technical delivery conditions*, April 1994.

[24] CEN European Committee for Standardization. *Eurocode 3: Design of Steel Structures Part 5: Piling*, 1997. ENV 1993-5.

[25] Committee for Waterfront Structures of the Society for Harbour Engineering and the German Society for Soil Mechanics and Foundation Engineering. *Recommendations of the Committee for Waterfront Structures, Harbours and Waterways EAU 1990*, sixth english edition, 1992.

[26] R.E. Craig. *Soil Mechanics*. E & F.N. Spon, 6th edition, 1997.

[27] CUR Civieltechnisch Centrum Uitvoering Research en Regelgeving. *Damwandconstructies*, 1994. Publicatie 166.

[28] CUR committee C119. Sheet pile wall field test Rotterdam: prediction document, 1999.

[29] Commissie Damwanden. *Scheve Buiging*. KIvI, afdeling Tunneltechniek en Ondergrondse Werken & Geotechniek, Den Haag, januari 1987.

[30] Delft Geotechnics. MSHEET, 1995.

[31] E. DiBiagio. Field instrumentation - a geotechnical tool. *Norwegian geotechnical institute publication*, 115:29–40, 1977.

[32] CUR Centre for Civil Engineering Research and Codes. Sheet Pile Wall Field Test at Rotterdam-Pernis: Site Investigation and Laboratory Testing. Technical Report R035498_1, MOS Grondmechanica B.V., October 1998.

[33] M.G. Freiseder and H.F. Schweiger. Performance of the 'hardening soil model' for a deep excavation problem. In R.B.J. Brinkgreve, editor, *Beyond 2000 in Computational Geotechnics Ten Years of* PLAXIS *International*, pages 263–270. A.A. Balkema. Rotterdam, 1999.

[34] J. Gattermann. *Interpretation von geotechnischen Messungen an Kaimauern in einem Tidehafen*. PhD thesis, Technische Universität Carolo Wilhelmina zu Braunschweig, 1998.

[35] J.P. Gigan. Expérimentation d'un rideau de palplanches ancré par tirants actifs. *Bulletin Liaison Laboratoire des Ponts et Chaussées*, 129:5–20, 1984.

[36] A.E. Groen. *Three-Dimensional Elasto-Plastic Analysis of Soils*. PhD thesis, Delft University of Technology, 1997.

[37] F. Haahr and N. Mortensen. *Spooks/W User's Manual*. Danish Geotechnical Institute, November 1996.

[38] R. Hartmann-Linden. *Tragfähigkeit von Stahlspundwänden*. PhD thesis, RWTH Aachen, Lehrstuhl für Stahlbau, 1997.

[39] R. Hartmann-Linden, A. Kort, M. Meyrer, A. Schmitt, G. Sedlacek, and F. van Tol. Development of Unified Design Rules for Steel Sheet Piles and Introduction in Eurocode 3, Part 5. CEC Agreement 7210-SA 127/523/840, ECSC, April 1997. Draft Final Report.

[40] P. Hebert, R. Quedinel, and P.Y. Reynauld. Report on an experiment conducted during the construction of a sheet-piling wharf at the port of Le Havre (roll on/roll off pier no.3). In 7de *Internationale Havenkongres. Antwerpen*, pages 1.12/1–1.12/8. KVIV, mei 1978.

[41] M. Hetényi. *Beams on Elastic Foundation*. The University of Michigan Press, 1946.

[42] J.A.W. Hockx. Methods to Reduce Oblique Bending in a Steel Sheet Pile Wall: A 3D Numerical Simulation. Master's thesis, Delft University of Technology, Geotechnical Laboratory, April 1998. Report number 440.

[43] G.T. Houlsby and N.J. Withers. Analysis of the cone pressuremeter test in clay. *Géotechnique*, 38(4):575–587, December 1988.

[44] HSP HOESCH SPUNDWAND UND PROFIL. Spundwandhandbuch Profiltafeln, April 1998.

[45] E. Juaristi. Influence of interlock friction on the flexural stiffness of a double U steel sheet pile wall. Technical Report LTI-MOD-96AE-ISPC, Centre de recherche public Henri Tudor, 1998.

[46] R.. Kastner, F. Masrouri, J. Monnet, and R. Fages. Soutènements flexibles, essais sur modèle, calculs. In *Proceedings XI ICSMFE San Francisco*, pages 2103–2106, 1985.

[47] J. Kerisel and E. Absi. *Active and Passive Earth Pressure Tables*. Balkema, Rotterdam, 3rd edition, 1990.

[48] D.A. Kort. Transfer matrix method for design of sheet pile walls. In *International Conference on Geotechnical and Geological Engineering*, page 621, 2000. GeoEng 2000, Melbourne.

[49] D.A. Kort. Test results of the Rotterdam sheet pile wall field test. Technical Report 483, Delft University of Technology, Geotechnical Laboratory, September 2001.

[50] D.A. Kort and N.A.P.M. Kelleners. Sheet pile wall field test Rotterdam: Prediction results. Technical Report 477, Delft University of Technology, Geotechnical Laboratory, May 2000.

[51] D.A. Kort and A.F. van Tol. Analytical and 2-D numerical considerations on large scale oblique bending tests. Technical Report 409, Delft University of Technology, Geotechnical Laboratory, September 1996.

[52] D.A. Kort and A.F. van Tol. Rotation requirement in a steel sheet pile wall. Technical Report 413, Delft University of Technology, Geotechnical Laboratory, March 1997.

[53] D.A. Kort, A.F. van Tol, and A. Jonker. Predictions for the Rotterdam sheet pile wall field test. In *Proceedings of the fifteenth international conference on soil mechanics and geotechnical engineering. Istanbul*, pages 1289–1293. A.A. Balkema, 2001.

[54] D.A. Kort, A.F. van Tol, and A. Jonker. The Rotterdam sheet pile wall field test: Test setup. In *Proceedings of the International Symposium on Geotechnical Aspects of Underground Construction in Soft Ground*, pages 537–542, 2000. IS-Tokyo'99.

[55] T.W. Lambe and R.V. Whitman. *Soil Mechanics*. John Wiley & Sons, 1969.

[56] S. Leroueil, J.-P. Magnan, and F. Tavenas. *Embankments on Soft Clays*. Chichester, England: Ellis Horwood, 1990. Translated by D. Muir Wood.

[57] PROFILARBED Luxembourg. Steel sheet piling & steel sheet piles, 1995.

[58] R. Marte and S. Semprich. Back analysis of internal forces and earth pressure acting on horizontally loaded piles and walls using deformation measurements. In C.F. Leung, S.A. Tan, and K.K. Phoon, editors, *Field Measurements in Geomechanics*, pages 217–222. A.A. Balkema, Rotterdam, 1999. FMGM99: Singapore, 1-3 December 1999.

[59] H. Müller-Breslau. *Erddruck auf Stützmauern*. Alfred Kröner Verlag, 1906.

[60] B.G. Neal. *The Plastic Methods of Structural Analysis*. Science paperbacks, 3rd edition, 1985.

[61] NEN Nederlands Normalisatie Instituut. *Bepaling van ongedraineerde schuifsterkte;Terrein-vinproef*, 1997. NEN 5106.

[62] NEN Nederlands Normalistatie Instituut. *Bepaling van de een-dimensionale samendrukkingseigenschappen van de grond*, 1997. NEN 5118.

[63] E.C. Pestel and F.A. Leckie. *Matrix Methods in Elastomechanics*. Mc Graw-Hill Book Compagny, inc., New York, 1963.

[64] A.J.M. Peters. Damwandveldproef: data-acquisitiesysteem en metingen. Technical Report CO-383560-51, GeoDelft, april 1999.

[65] W.D. Pilkey and W. Wunderlich. *Mechanics of Structures, Variational and Computational Methods*. CRC Press, Boca Raton, 1994.

[66] P.W. Rowe. Anchored sheet-pile walls. *Proceedings of the Institution of Civil Engineers*, 1:27–70, 1952.

[67] R. Schillings and P. Boeraeve. Oblique bending tests: Serie A. Technical report, CRIF Department of Steel Construction. Liège, September 1996. ECSC-Project 7210-SA 127/523/840.

[68] G. Sedlacek, M. Feldmann, R. Hartmann, W. Dahl, and B. Kalinowski. Determination of b/t-ratios in order to classify Steel Sheet Pile Wall Sections for plastic design. Technical report, RWTH Aachen, Institute for Steel Construction, September 1994.

[69] J.S. Steenfelt. Theoretical aspects of basement excavation support. basement excavations, theory, design and litigation. *Workshop notes, University of Queensland*, 1:1–60, 1988.

[70] J.S. Steenfelt and F. Haahr. Impact of safety factors in design of retaining structures. In *Proceedings International Symposium on Limit State Design*, volume 1, pages 295–304, 1993. ISLSD 93 Copenhagen.

[71] S. Timoshenko and D.H. Young. *Elements of Strength of Materials*. Van Nostrand, London, 5th edition, 1968.

[72] S.P. Timoshenko and J.N. Goodier. *Theory of Elasticity*. McGraw-Hill, 3rd edition, 1970.

[73] A.F. van Tol and H.E. Brassinga. Evaluatie gedrag grondkeringen bouwput Binnenrotte. *Civiele Techniek*, 1:24–28, 1993.

[74] A.F. Van Tol and D.A. Kort. Limit state design for steel sheet pile walls. In *Proceedings of the Fourteenth International Conference on Soil Mechanics and Foundation Engineering*, volume 2, pages 1351–1354, 1997. XIV ICSMFE Hamburg.

[75] A.F. van Tol and D.A. Kort. Stalen damwand voorbij de uiterste vezel. *Geotechniek*, pages 5–8, Oktober 1998.

[76] J. van Kan. *Numerieke wiskunde voor technici*. Delftse Uitgevers Maatschappij, 1988.

[77] J.-F. vanden Berghe, A. Holeyman, E. Juaristi, and A. Schmitt. Interlock friction in a sheet pile wall: laboratory tests. In *Proceedings of the fifteenth international conference on soil mechanics and geotechnical engineering. Istanbul*, pages 1273–1276. A.A. Balkema, 2001.

[78] J.-F. vanden Berghe, A. Holeyman, and B. Sine. Détermination de la loi de comportement de l'interface entre palplanches. Technical Report 263/3-97, Université Catholique de Louvain, Laboratoire de Génie Civil, September 1998.

[79] P.A. Vermeer and R.B.J. Brinkgreve. PLAXIS *Finite Element Code for Soil and Rock Analyses*. Plaxis B.V., 6th edition, 1995.

[80] P.A. Vermeer and R.B.J. Brinkgreve. PLAXIS *Finite Element Code for Soil and Rock Analyses*. Plaxis B.V., 7th edition, 1998.

[81] A. Verruijt. *Theory of Groundwater Flow*. Macmillan, 1970.

[82] A. Verruijt. Numerieke berekening van verend ondersteunde liggers. *Cement*, 35:659–662, 1983.

[83] A. Verruijt. *Toegepaste Mechanica II*. Delftse Uitgeverers Maatschappij, 1983.

[84] A. Verruijt. *Grondmechanica*. Delftse Uitgevers Maatschappij, 1987.

[85] A. Verruijt. *Computational Geomechanics*. Kluwer Academic Publishers, Dordrecht, 1995.

[86] A. Verruijt. *Grondmechanica*. Delftse Uitgevers Maatschappij, 1999.

[87] A. Verruijt. SPW99, 1999. Delft University of Technology.

[88] P.A. von Wolffersdorff. Vervormungsprognosen für Stützkonstruktionen. Technical Report Heft 141, Veröffentlichungen des Institutes für Bodenmechanik und Felsmechanik der Universität Fridericiana in Karlsruhe, 1997.

[89] A. Weißenbach. Berechnung von mehrfach gestützten Baugrubenspundwänden und Trägerbohlwänden nach dem Traglastverfahren. *Strasse Brücke Tunnel*, pages 17–23, 38–42, 67–74, 130–136, 1969.

[90] A. Weißenbach. *Baugruben, Teil II: Berechnungsgrundlagen*. Verlag von Wilhelm Ernst & Sohn, 1975.

[91] A. Weißenbach. *Baugruben, Teil III: Berechnungsverfahren*. Verlag von Wilhelm Ernst & Sohn, 1977.

[92] R. Windels. Berechnung von Bohlwerken nach dem Traglastverfahren. *Die Bautechnik*, pages 212–220, Juni 1959.

[93] R. Windels. Berechnung von Bohlwerken mit geradlinig begrenzten Erddruckflächen nach dem Traglastverfahren. *Die Bautechnik*, 10:339–345, 1963.

[94] R. Windels. Bohlwände und Traglastverfahren. *Die Bautechnik*, 9:300–305, 1970.

[95] R. Windels. Traglasten von Balkenquerschnitten bei Angriff von Biegemomenten, Längs- und Querkraft. *Der Stahlbau*, 1:10–16, 1970.

[96] F.C. de Witte et al. DIANA *User's Manual*. TNO Building and Construction Research, 7th edition, 2000.

Appendix A

Sign conventions for bending

A.1 Definitions for engineering beam theory

Stress

$$\sigma_{zz} = -E\left(x\frac{d^2 w_x}{dz^2} + y\frac{d^2 w_y}{dz^2}\right) \tag{A.1}$$

Bending moment

$$M_x = \int_A \sigma_{zz}\, x\, dA \qquad M_y = \int_A \sigma_{zz}\, y\, dA \tag{A.2}$$

Moment of inertia

$$I_{xx} = \int_A x^2\, dA \qquad I_{xy} = \int_A xy\, dA \tag{A.3}$$

$$I_{yx} = \int_A yx\, dA \qquad I_{yy} = \int_A y^2\, dA \tag{A.4}$$

Kinematical equations

$$\frac{dw_x(z)}{dz} = -\varphi_x(z) \qquad\qquad \frac{dw_y(z)}{dz} = -\varphi_y(z) \tag{A.5}$$

$$\frac{d\varphi_x(z)}{dz} = \kappa_x(z) \qquad\qquad \frac{d\varphi_y(z)}{dz} = \kappa_y(z) \tag{A.6}$$

Constitutive equations

$$M_x = -EI_{xx}\frac{d^2 w_x}{dz^2} - EI_{xy}\frac{d^2 w_y}{dz^2} \tag{A.7}$$

$$M_y = -EI_{yx}\frac{d^2 w_x}{dz^2} - EI_{yy}\frac{d^2 w_y}{dz^2} \tag{A.8}$$

Equilibrium equations

$$\frac{dM_x(z)}{dz} = V_x(z) \qquad \frac{dM_y(z)}{dz} = V_y(z) \tag{A.9}$$

$$\frac{dV_x(z)}{dz} = -q_x(z) \qquad \frac{dV_y(z)}{dz} = -q_y(z) \tag{A.10}$$
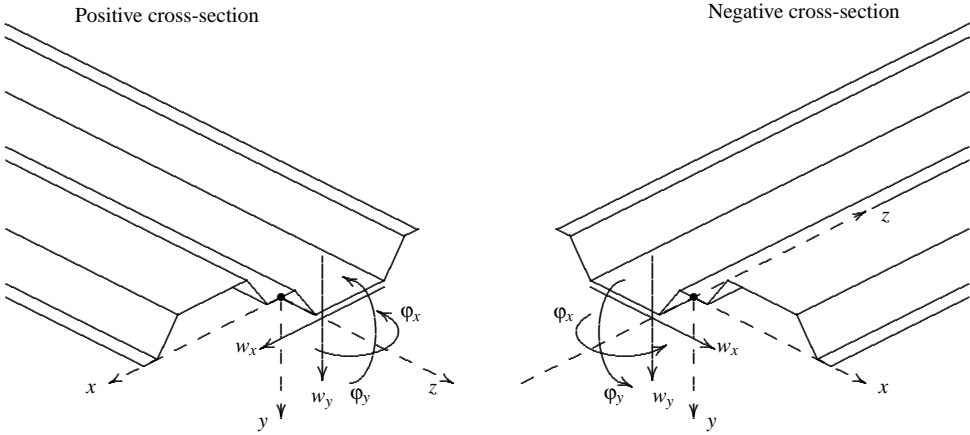
A.2   Local sign convention

Figure A.1: *Sign convention for a positive and a negative cross-section. Positive displacements and slopes are shown. Note the contradiction between the positive direction defined for φ_x and orthogonality*
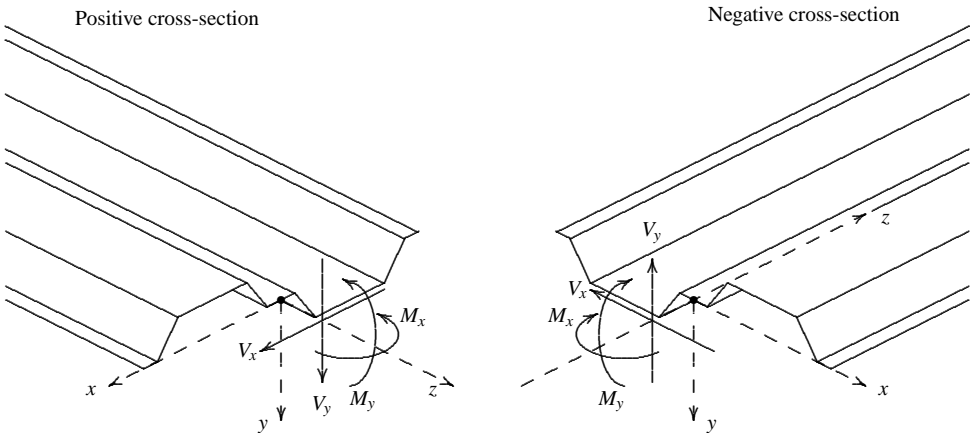

Figure A.2: *Sign convention for a positive and a negative cross-section. Positive forces and moments are shown*

A.3   Global sign convention
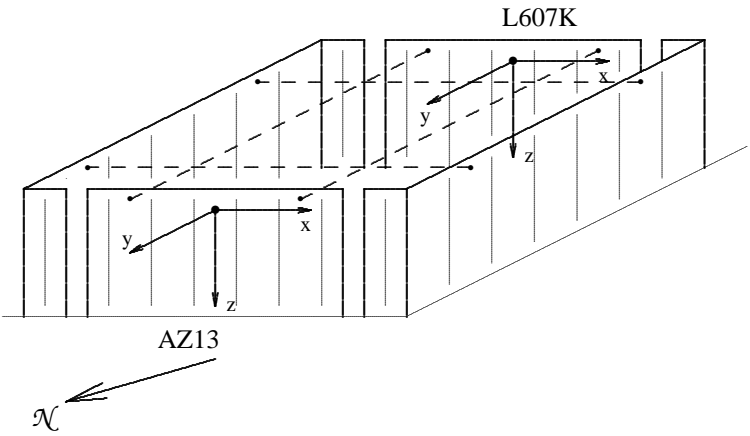
Figure A.3: *Sign convention of the local beams in the global construction*

Appendix B

The transfer matrix method

B.1 Basic equations

The behaviour of a beam loaded with a distributed load and subjected to bending can be described with the kinematic, constitutive and equilibrium equations for bending, see Figure B.1. The sign convention is presented in Appendix A.

Figure B.1: *Beam loaded with a distributed load*

The kinematic equations are

$$\frac{dw(x)}{dx} = -\varphi(x) \tag{B.1}$$

$$\frac{d\varphi(x)}{dx} = \kappa(x) \tag{B.2}$$

The constitutive equation is

$$\kappa(x) = \frac{M(x)}{EI} \tag{B.3}$$

The equilibrium equations are

$$\frac{dM(x)}{dx} = V(x) \tag{B.4}$$

$$\frac{dV(x)}{dx} = -q(x) \tag{B.5}$$

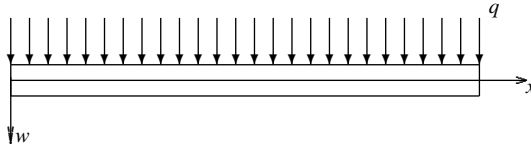The general differential equation for beams subjected to bending are derived from these three sets of equations

$$\frac{d^4 w(x)}{dx^4} = \frac{q(x)}{EI} \tag{B.6}$$

A basic solution for the displacement for a linear distributed load from q_L to q_R over an element of length ℓ is

$$w(x) = w_0 - \varphi_0 x - \frac{M_0 x^2}{2EI} - \frac{V_0 x^3}{6EI} + \frac{q_L x^4}{24EI} + \frac{(q_R - q_L)x^5}{120EI\ell} \tag{B.7}$$

in which w_0, φ_0, M_0, V_0 are the displacement, rotation, moment and shear force for $x = 0$. The basic solution for the rotation, bending moment and shear force are

$$\varphi(x) = \varphi_0 + \frac{M_0 x}{EI} + \frac{V_0 x^2}{2EI} - \frac{q_L x^3}{6EI} - \frac{(q_R - q_L)x^4}{24EI\ell} \tag{B.8}$$

$$M(x) = M_0 + V_0 x - \frac{1}{2} q_L x^2 - \frac{1}{6} \frac{(q_R - q_L)}{\ell} x^3 \tag{B.9}$$

$$V(x) = V_0 - q_L x - \frac{1}{2} \frac{(q_R - q_L)}{\ell} x^2 \tag{B.10}$$

B.2   State vectors and transfer matrices

Consider an element of length ℓ loaded with a linear distributed load, see Figure B.2. Denote the displacement, rotation, bending moment and shear force for $x = \ell$ by w_1, φ_1, M_1 and V_1 and the linear distributed load at both ends of the elements as $q_0 = q_L$ and $q_1 = q_R$ [63, 65]. It follows that

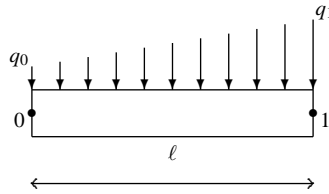**Figure B.2**: *An element of length ℓ*

$$w_1 = w_0 - \varphi_0 \ell - \frac{M_0 \ell^2}{2EI} - \frac{V_0 \ell^3}{6EI} + \frac{(4q_0 + q_1)\ell^4}{120EI} \tag{B.11}$$

$$\varphi_1 = \varphi_0 + \frac{M_0 \ell}{EI} + \frac{V_0 \ell^2}{2EI} - \frac{(3q_0 + q_1)\ell^3}{24EI} \tag{B.12}$$

$$M_1 = M_0 + V_0 \ell - \frac{1}{6}(2q_0 + q_1)\ell^2 \tag{B.13}$$

$$V_1 = V_0 - \frac{1}{2}(q_0 + q_1)\ell \tag{B.14}$$

This is written in matrix form as

$$
\begin{bmatrix} w_1 \\ \varphi_1 \\ M_1 \\ V_1 \\ 1 \end{bmatrix} = \begin{bmatrix} 1 & -\ell & -\dfrac{\ell^2}{2EI} & -\dfrac{\ell^3}{6EI} & \dfrac{(4q_0+q_1)\ell^4}{120EI} \\[2mm] 0 & 1 & \dfrac{\ell}{EI} & \dfrac{\ell^2}{2EI} & -\dfrac{(3q_0+q_1)\ell^3}{24EI} \\[2mm] 0 & 0 & 1 & \ell & -\dfrac{(2q_0+q_1)\ell^2}{6} \\[2mm] 0 & 0 & 0 & 1 & -(q_0+q_1)\dfrac{\ell}{2} \\[2mm] 0 & 0 & 0 & 0 & 1 \end{bmatrix} \begin{bmatrix} w_0 \\ \varphi_0 \\ M_0 \\ V_0 \\ 1 \end{bmatrix} \qquad (B.15)
$$

or, more generally, as

$$ \mathbf{z_1} = \mathbf{F^1 z_0} \qquad (B.16) $$

The vectors $\mathbf{z_0}$ and $\mathbf{z_1}$ are called *state vectors*, because they describe the state of node 0 and 1 and matrix $\mathbf{F^1}$ is referred to as the *transfer field matrix*, since it *transfers* the state vector from 0 to 1. The state vectors $\mathbf{z_0}$ and $\mathbf{z_1}$ represent the *exact* solution at points 0 and 1.

B.3   Solving the transfer equations

The system drawn in Figure B.3 is a typical system to describe with state vectors and transfer matrices. It follows that [63, 65]
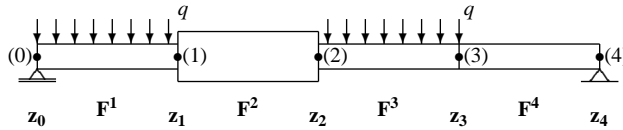
Figure B.3: *A typical system which can be described with the transfer matrix method*

$$ \mathbf{z_1} = \mathbf{F^1 z_0} \qquad (B.17) $$
$$ \mathbf{z_2} = \mathbf{F^2 z_1} \qquad (B.18) $$
$$ \mathbf{z_3} = \mathbf{F^3 z_2} \qquad (B.19) $$
$$ \mathbf{z_4} = \mathbf{F^4 z_3} \qquad (B.20) $$

Hence

$$ \mathbf{z_4} = \mathbf{F^4 F^3 F^2 F^1 z_0} \qquad (B.21) $$

or, more generally,

$$ \mathbf{z_n} = \mathbf{F^n F^{n-1}} \quad \ldots \quad \mathbf{F^2 F^1 z_0} \qquad (B.22) $$

Four boundary conditions are required to solve this system of equations: two on the left hand side and two on the right. For example, in the case of Figure B.3 the boundary conditions are $w_0 = M_0 = 0$ and $w_4 = M_4 = 0$.

The beam response problem is a boundary value problem, since the only unknown parameter is the initial state vector $\mathbf{z_0}$. In general the four state variables w_0, φ_0, M_0 and V_0 of $\mathbf{z_0}$ are determined from the two boundary conditions that occur at each end of the beam. This requires two *sweeps* along the beam for a complete transfer matrix solution. First, the global transfer matrix $\mathbf{T} = \mathbf{F^n F^{n-1}} \dots \mathbf{F^2 F^1}$ is constructed. The four boundary conditions are applied and the four state variables w_0, φ_0, M_0 and V_0 of $\mathbf{z_0}$ are solved outlined below.

When, after the first sweep the system of equations, $\mathbf{z_n} = \mathbf{T z_0}$ is obtained, both $\mathbf{z_n}$ and $\mathbf{z_0}$ have two known and two unknown state variables. We denote the known state variables $\mathbf{z^*_{n;1}}$ and $\mathbf{z^*_{0;1}}$ and the unknown state variables $\mathbf{z_{n;2}}$ and $\mathbf{z_{0;2}}$. The system of equations can be written as

$$\mathbf{z^*_{n;1}} = \mathbf{T_{11} z^*_{0;1}} + \mathbf{T_{12} z_{0;2}} \tag{B.23}$$

$$\mathbf{z_{n;2}} = \mathbf{T_{21} z^*_{0;1}} + \mathbf{T_{22} z_{0;2}} \tag{B.24}$$

Now we can derive the unknown part of the initial state vector $\mathbf{z_{0;2}}$ from (B.23).

When the entire initial state vector $\mathbf{z_0}$ is known, a second sweep along the member can be made to compute the state variables w, φ, M and V at every node of the beam.

B.4   Point occurrences

The transfer matrix can also be used to describe local occurrences, such as concentrated forces or nodal springs, see Figure B.4.
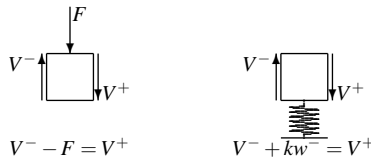
Figure B.4: *Point occurrences*

Examples of transfer matrices for an infinite short element loaded by a concentrated force F and supported by a spring with stiffness k are respectively

$$
\begin{bmatrix} w^+ \\ \varphi^+ \\ M^+ \\ V^+ \\ 1 \end{bmatrix} =
\begin{bmatrix}
1 & 0 & 0 & 0 & 0 \\
0 & 1 & 0 & 0 & 0 \\
0 & 0 & 1 & 0 & 0 \\
0 & 0 & 0 & 1 & -F \\
0 & 0 & 0 & 0 & 1
\end{bmatrix}
\begin{bmatrix} w^- \\ \varphi^- \\ M^- \\ V^- \\ 1 \end{bmatrix}
\tag{B.25}
$$

$$
\begin{bmatrix} w^+ \\ \varphi^+ \\ M^+ \\ V^+ \\ 1 \end{bmatrix} = \begin{bmatrix} 1 & 0 & 0 & 0 & 0 \\ 0 & 1 & 0 & 0 & 0 \\ 0 & 0 & 1 & 0 & 0 \\ k & 0 & 0 & 1 & 0 \\ 0 & 0 & 0 & 0 & 1 \end{bmatrix} \begin{bmatrix} w^- \\ \varphi^- \\ M^- \\ V^- \\ 1 \end{bmatrix}
\tag{B.26}
$$

These transfer matrices describe the change of the state vector at a point and are therefore referred to as the *transfer point matrix* $\mathbf{P}$.

As an example, the transfer matrix for a beam of length ℓ with a stiffness EI and with a concentrated load F at midspan is, see Figure B.5
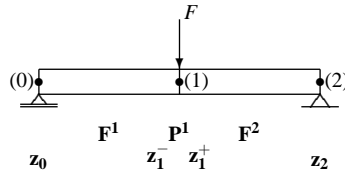
Figure B.5: *Beam loaded with a concentrated load*

$$
\mathbf{z}_1^- = \mathbf{F}^1 \mathbf{z}_0
\tag{B.27}
$$

$$
\mathbf{z}_1^+ = \mathbf{P}^1 \mathbf{z}_1^-
\tag{B.28}
$$

$$
\mathbf{z}_2 = \mathbf{F}^2 \mathbf{z}_1^+
\tag{B.29}
$$

or, more generally,

$$
\mathbf{z}_n = \mathbf{F}^n \mathbf{P}^{n-1} \mathbf{F}^{n-1} \quad \dots \quad \mathbf{F}^2 \mathbf{P}^1 \mathbf{F}^1 \mathbf{z}_0
\tag{B.30}
$$

which can be solved in the manner described in Section B.3.

B.5   Intermediate boundary conditions

Intermediate supports or moment releasing hinges bring on boundary conditions which occur at positions other than at one of the ends of the construction, see Figure B.6.

Figure B.6: *A statically indeterminate system suitable for the transfer matrix method*

The transfer matrix equation $\mathbf{z}_n = \mathbf{T}\mathbf{z}_0$ cannot be solved with the method described previously, since the effects of the intermediate boundary conditions are unknown and therefore the transfer matrix $\mathbf{T}$ is also unknown.

The state vector of an intermediate condition has one fixed state variable and one discontinuous state variable, as illustrated in Figure B.7 for the intermediate support and for the intermediate moment release. The system in Figure B.6 can be simplified by replacing an intermediate fixed state variable by the accompanying action effect: the intermediate supports are replaced by the unknown reaction forces R_1 and R_3 and the moment release by the unknown reaction *kink* $\Delta\varphi_4$.

fixed conditions $\qquad w = 0 \qquad\qquad M = 0$

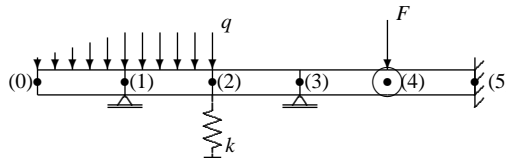intermediate conditions $\qquad V^- - R = V^+ \qquad \varphi^- + \Delta\varphi = \varphi^+$

R
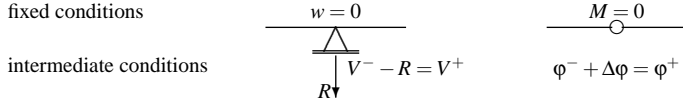
Figure B.7: *Fixed and discontinuous state variables*

The basic idea for the solution of this system is to *append* the known intermediate boundary condition to $\mathbf{z_n}$ and the accompagnying unknown discontinuous state variable to $\mathbf{z_0}$ [63]. The number of degrees of freedom of the transfer matrix equation $\mathbf{z_n} = \mathbf{T}\,\mathbf{z_0}$ is extended with the number of intermediate boundary conditions and can be solved in the same manner as described in Section B.3. The procedure is illustrated with a simplified but typical example [48].

Example

As a typical example for explaining how the plastic hinge is taken into account, consider the beam in Figure B.8.

q

(0) (1) (2) (3) (4)

2ℓ
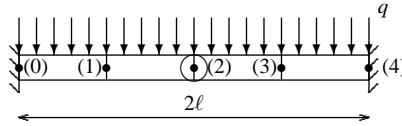
Figure B.8: *A typical system to describe with the transfer matrix method*

To describe the system properly, the boundary conditions at the left and right hand side and at midspan are required. At the hinge the moment is $M_2 = 0$ and a reaction kink $\Delta\varphi_2$ applies, which is unknown. The boundary conditions are

- left hand side: $w_0 = 0$ and $\varphi_0 = 0$
- midspan: $M_2 = 0$ and $\varphi_2^+ = \varphi_2^- + \Delta\varphi_2$
- right hand side: $w_4 = 0$ and $\varphi_4 = 0$

The additional unknown $\Delta\varphi_2$ from the intermediate hinge is introduced and appended to the transfer matrix. The state vector becomes

$$\mathbf{z_i} = \begin{pmatrix} w_i & \varphi_i & M_i & V_i & 1 & \Delta\varphi_2 \end{pmatrix}^T \qquad (B.31)$$

The transfer field matrix for the four elements and the transfer point matrix for node 2 are

$$\mathbf{F^1} = \mathbf{F^2} = \mathbf{F^3} = \mathbf{F^4} = \begin{bmatrix} 1 & -\dfrac{\ell}{2} & -\dfrac{\ell^2}{8EI} & -\dfrac{\ell^3}{48EI} & \dfrac{q\ell^4}{384EI} & 0 \\[2ex] 0 & 1 & \dfrac{\ell}{2EI} & \dfrac{\ell^2}{8EI} & -\dfrac{q\ell^3}{48EI} & 0 \\[2ex] 0 & 0 & 1 & \dfrac{\ell}{2} & -\dfrac{q\ell^2}{8} & 0 \\[2ex] 0 & 0 & 0 & 1 & -\dfrac{q\ell}{2} & 0 \\[2ex] 0 & 0 & 0 & 0 & 1 & 0 \\[2ex] 0 & 0 & 0 & 0 & 0 & 1 \end{bmatrix} \quad \text{(B.32)}$$

$$\mathbf{P^2} = \begin{bmatrix} 1 & 0 & 0 & 0 & 0 & 0 \\ 0 & 1 & 0 & 0 & 0 & 1 \\ 0 & 0 & 1 & 0 & 0 & 0 \\ 0 & 0 & 0 & 1 & 0 & 0 \\ 0 & 0 & 0 & 0 & 1 & 0 \\ 0 & 0 & 0 & 0 & 0 & 1 \end{bmatrix} \quad \text{(B.33)}$$

It follows that

$$\mathbf{z_2^+} = \mathbf{P^2 F^2 F^1 z_0} \quad \text{(B.34)}$$
$$\mathbf{z_4} = \mathbf{F^4 F^3 P^2 F^2 F^1 z_0} \quad \text{(B.35)}$$

Substituting transfer matrices (B.32) and (B.33) and the given boundary conditions into (B.34) and (B.35) we obtain the following equations, after elaboration.

$$\begin{bmatrix} M_2 \\ w_4 \\ \varphi_4 \\ 1 \end{bmatrix} = \begin{bmatrix} 1 & \ell & -\dfrac{q\ell}{2} & 0 \\[2ex] -\dfrac{2\ell^2}{EI} & -\dfrac{4}{3}\dfrac{\ell^3}{EI} & \dfrac{2}{3}\dfrac{q\ell^4}{EI} & -\ell \\[2ex] \dfrac{2\ell}{EI} & \dfrac{2\ell^2}{EI} & -\dfrac{4}{3}\dfrac{\ell^3}{EI} & 1 \\[2ex] 0 & 0 & 0 & 1 \end{bmatrix} \begin{bmatrix} M_0 \\ V_0 \\ 1 \\ \Delta\varphi_2 \end{bmatrix} + \begin{bmatrix} 0 & 0 \\ 1 & -2\ell \\ 0 & 1 \\ 0 & 0 \end{bmatrix} \begin{bmatrix} w_0 \\ \varphi_0 \end{bmatrix}$$

(B.36)

with $\begin{bmatrix} M_2 & w_4 & \varphi_4 & 1 \end{bmatrix}^T = \begin{bmatrix} 0 & 0 & 0 & 1 \end{bmatrix}^T$
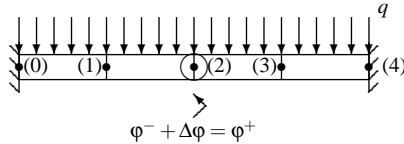
Figure B.9: *The system has been prepared for the second sweep. The intermediate hinge is taken into account by the* kink $\Delta\varphi_2$.

The solution of the initial state vector is

$$\mathbf{z_0} = \begin{bmatrix} 0 & 0 & -\dfrac{q\ell^2}{2} & q\ell & 1 \end{bmatrix}^T \quad \text{(B.37)}$$

and the kink at the hinge has an angle of $\Delta\varphi_2 = \dfrac{q\ell^3}{3EI}$. Now all the boundary conditions are known and the second sweep can be carried out in accordance with (B.30). The state vector at every node can now be calculated, see Figure B.9.

B.6 Oblique bending and interlock friction

B.6.1 Oblique bending

The behaviour of a beam with an asymmetric cross-section, loaded with a distributed load, which is subjected to bending in two directions can be described with the kinematic, constitutive and equilibrium equations for oblique bending, see Figure B.10. The sign convention is presented in Appendix A.
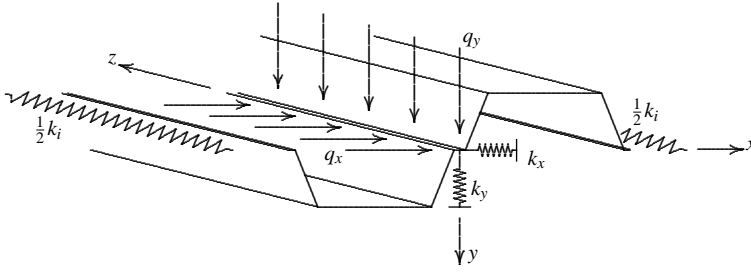
Figure B.10*: Beam with an asymmetrical cross-section restrained by shear springs*

The kinematic equations are

$$\frac{dw_x(z)}{dz} = -\varphi_x(z) \qquad\qquad \frac{dw_y(z)}{dz} = -\varphi_y(z) \qquad\qquad \text{(B.38)}$$

$$\frac{d\varphi_x(z)}{dz} = \kappa_x(z) \qquad\qquad \frac{d\varphi_y(z)}{dz} = \kappa_y(z) \qquad\qquad \text{(B.39)}$$

The constitutive equations are [83]

$$\begin{bmatrix} \kappa_x(z) \\ \kappa_y(z) \end{bmatrix} = \frac{1}{det} \begin{bmatrix} EI_{yy} & -EI_{xy} \\ -EI_{yx} & EI_{xx} \end{bmatrix} \begin{bmatrix} M_x(z) \\ M_y(z) \end{bmatrix} \qquad\qquad \text{(B.40)}$$

in which

$$det = EI_{xx}EI_{yy} - EI_{xy}EI_{yx} \qquad\qquad \text{(B.41)}$$

The equilibrium equations are

$$\frac{dM_x(z)}{dz} = V_x(z) \qquad\qquad \frac{dM_y(z)}{dz} = V_y(z) \qquad\qquad \text{(B.42)}$$

$$\frac{dV_x(z)}{dz} = -q_x(z) \qquad\qquad \frac{dV_y(z)}{dz} = -q_y(z) \qquad\qquad \text{(B.43)}$$

On the basis of these equations, the following general displacement functions for $w_x(z)$ and $w_y(z)$ can be found.

$$w_x(z) = w_{x0} - \varphi_{x0}z - \frac{EI_{yy}}{det}\frac{M_{x0}z^2}{2} - \frac{EI_{yy}}{det}\frac{V_{x0}z^3}{6} + \frac{EI_{yy}}{det}\frac{q_{x0}z^4}{24} + \frac{EI_{yy}}{det}\frac{q_{x1}z^5}{120\ell}$$
$$+ \frac{EI_{xy}}{det}\frac{M_{y0}z^2}{2} + \frac{EI_{xy}}{det}\frac{V_{y0}z^3}{6} - \frac{EI_{xy}}{det}\frac{q_{y0}z^4}{24} - \frac{EI_{xy}}{det}\frac{q_{y1}z^5}{120\ell} \quad \text{(B.44)}$$

and

$$w_y(z) = \frac{EI_{xy}}{det}\frac{M_{x0}z^2}{2} + \frac{EI_{xy}}{det}\frac{V_{x0}z^3}{6} - \frac{EI_{xy}}{det}\frac{q_{x0}z^4}{24} - \frac{EI_{xy}}{det}\frac{q_{x1}z^5}{120\ell}$$
$$+ w_{y0} - \varphi_{y0}z - \frac{EI_{xx}}{det}\frac{M_{y0}z^2}{2} - \frac{EI_{xx}}{det}\frac{V_{y0}z^3}{6} + \frac{EI_{xx}}{det}\frac{q_{y0}z^4}{24} + \frac{EI_{xx}}{det}\frac{q_{y1}z^5}{120\ell}$$

$$\text{(B.45)}$$

A beam with an asymmetric cross-section, loaded with a linear distributed load, can be described with the basic equation of the transfer matrix method as follows.

$$\mathbf{z_1} = \mathbf{F^1 z_0} \quad \text{(B.16)}$$

In (B.16) the state vectors are described by

$$\mathbf{z_0} = [w_{x0}\ \varphi_{x0}\ M_{x0}\ V_{x0}\ 1\ w_{y0}\ \varphi_{y0}\ M_{y0}\ V_{y0}\ 1]^T \quad \text{(B.46)}$$
$$\mathbf{z_1} = [w_{x1}\ \varphi_{x1}\ M_{x1}\ V_{x1}\ 1\ w_{y1}\ \varphi_{y1}\ M_{y1}\ V_{y1}\ 1]^T \quad \text{(B.47)}$$

and the transfer matrix for oblique bending by (B.49). The stress distribution in the cross-section can be described by

$$\sigma(x,y) = E\varepsilon(x,y) = E(\varepsilon_{xx} + \kappa_y y + \kappa_z z) \quad \text{(B.48)}$$

$$
\mathbf{F^1} =
\begin{bmatrix}
1 & -\ell & -\dfrac{EI_{yy}}{det}\dfrac{\ell^2}{2} & -\dfrac{EI_{yy}}{det}\dfrac{\ell^3}{6} & \dfrac{EI_{yy}}{det}\dfrac{(4q_{x0}+q_{x1})\ell^4}{120} & 0 & 0 & \dfrac{EI_{xy}}{det}\dfrac{\ell^2}{2} & \dfrac{EI_{xy}}{det}\dfrac{\ell^3}{6} & \dfrac{EI_{xy}}{det}\dfrac{(4q_{y0}+q_{y1})\ell^4}{120} \\[2ex]
0 & 1 & \dfrac{EI_{yy}}{det}\ell & \dfrac{EI_{yy}}{det}\dfrac{\ell^2}{2} & \dfrac{EI_{yy}}{det}\dfrac{(3q_{x0}+q_{x1})\ell^3}{24} & 0 & 0 & -\dfrac{EI_{xy}}{det}\ell & -\dfrac{EI_{xy}}{det}\dfrac{\ell^2}{2} & \dfrac{EI_{xy}}{det}\dfrac{(3q_{y0}+q_{y1})\ell^3}{24} \\[2ex]
0 & 0 & 1 & \ell & -\dfrac{(2q_{x0}+q_{x1})\ell^2}{6} & 0 & 0 & 0 & 0 & 0 \\[2ex]
0 & 0 & 0 & 1 & -\dfrac{(q_{x0}+q_{x1})\ell}{2} & 0 & 0 & 0 & 0 & 0 \\[1ex]
0 & 0 & 0 & 0 & 1 & 0 & 0 & 0 & 0 & 0 \\[1ex]
0 & 0 & \dfrac{EI_{xy}}{det}\dfrac{\ell^2}{2} & \dfrac{EI_{xy}}{det}\dfrac{\ell^3}{6} & \dfrac{EI_{xy}}{det}\dfrac{(4q_{x0}+q_{x1})\ell^4}{120} & 1 & -\ell & -\dfrac{EI_{xx}}{det}\dfrac{\ell^2}{2} & \dfrac{EI_{xx}}{det}\dfrac{\ell^3}{6} & \dfrac{EI_{xx}}{det}\dfrac{(4q_{y0}+q_{y1})\ell^4}{120} \\[2ex]
0 & 0 & -\dfrac{EI_{xy}}{det}\ell & -\dfrac{EI_{xy}}{det}\dfrac{\ell^2}{2} & \dfrac{EI_{xy}}{det}\dfrac{(3q_{x0}+q_{x1})\ell^3}{24} & 0 & 1 & \dfrac{EI_{xx}}{det}\ell & -\dfrac{EI_{xx}}{det}\dfrac{\ell^2}{2} & \dfrac{EI_{xx}}{det}\dfrac{(3q_{y0}+q_{y1})\ell^3}{24} \\[2ex]
0 & 0 & 0 & 0 & 0 & 0 & 0 & 1 & \ell & -\dfrac{(2q_{y0}+q_{y1})\ell^2}{6} \\[2ex]
0 & 0 & 0 & 0 & 0 & 0 & 0 & 0 & 1 & -\dfrac{(q_{y0}+q_{y1})\ell}{2} \\[1ex]
0 & 0 & 0 & 0 & 0 & 0 & 0 & 0 & 0 & 1
\end{bmatrix}
$$

(B.49)

B.6.2 Interlock friction

Interlock friction can be taken into account with the shear springs in Figure B.10. The transfer point matrix of the nodal shear spring is derived as shown in Figure B.11.

$$T = \tfrac{1}{2}k_i\Delta x\tfrac{1}{2}b\varphi_x$$

$$M_x^- + \tfrac{1}{4}k_i\Delta x b^2\varphi_x = M_x^+$$
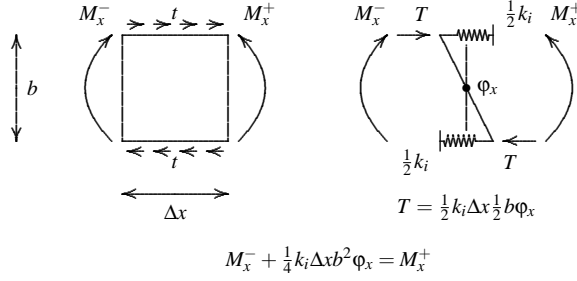
Figure B.11: *Nodal interlock spring model (top view)*

With $\Delta x = \tfrac{1}{2}\ell_i + \tfrac{1}{2}\ell_{i+1}$, the transfer point matrix for interlock friction is

$$\mathbf{P} = \begin{bmatrix} 1 & 0 & 0 & 0 & 0 & 0 & 0 & 0 & 0 & 0 \\ 0 & 1 & 0 & 0 & 0 & 0 & 0 & 0 & 0 & 0 \\ 0 & \tfrac{1}{8}k_i b^2(\ell_i+\ell_{i+1}) & 1 & 0 & 0 & 0 & 0 & 0 & 0 & 0 \\ 0 & 0 & 0 & 1 & 0 & 0 & 0 & 0 & 0 & 0 \\ 0 & 0 & 0 & 0 & 1 & 0 & 0 & 0 & 0 & 0 \\ 0 & 0 & 0 & 0 & 0 & 1 & 0 & 0 & 0 & 0 \\ 0 & 0 & 0 & 0 & 0 & 0 & 1 & 0 & 0 & 0 \\ 0 & 0 & 0 & 0 & 0 & 0 & 0 & 1 & 0 & 0 \\ 0 & 0 & 0 & 0 & 0 & 0 & 0 & 0 & 1 & 0 \\ 0 & 0 & 0 & 0 & 0 & 0 & 0 & 0 & 0 & 1 \end{bmatrix} \tag{B.50}$$

The spring characteristics for interlock friction can be extended with plastic branches in the same manner as for the soil springs.

Appendix C

Elasto-plastic beam on an elastic foundation

In this appendix an elasto-plastic beam with infinite length supported by an elastic foundation and loaded by a steadily increasing concentrated load $2F$ is considered, see Figure C.1. After formation of a plastic hinge in the beam, the load is further increased until a second and third plastic hinge are about to be formed. At that moment the uncoupled beam is about to permit a kinematic mechanism motion. Subsequently the beam is unloaded to 50% of its original load.
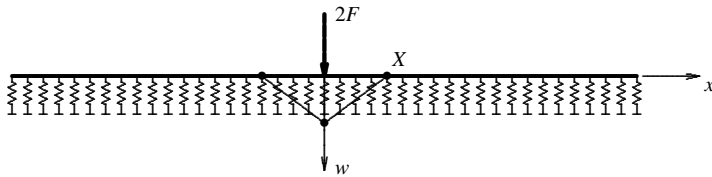
Figure C.1: *Elasto-plastic beam on an elastic foundation*

The distribution of displacement and bending moment is determined. Winkler's assumption of subgrade reaction with uncoupled springs allows for the following reduced differential equation:

$$EI\frac{d^4w(x)}{dx^4} + kw(x) = 0 \tag{C.1}$$

Solutions of this differential equation for different boundary conditions are extensively described by Hetényi [41]. For the problem of the elasto-plastic beam on an elastic foundation, two different systems are identified, see Figure C.2.

When load $2F$ is steadily increased, the maximum bending moment directly under the load increases until the plastic moment capacity of the beam is reached: one plastic hinge is formed. For this situation the displacement and bending moment distribution of the right
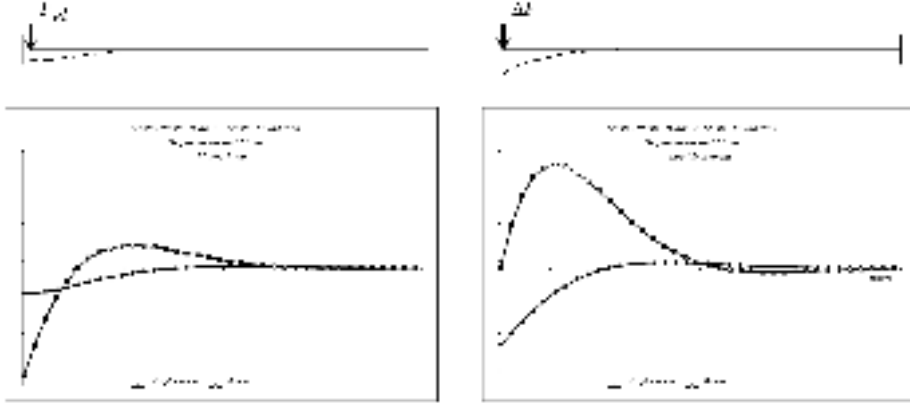
Figure C.2: *Two different systems to consider for the elasto-plastic beam*

half of the beam are shown in Figure C.2, *left*. The equations in (C.2) describe the displacement, rotation, bending moment and shear force in the elastic stage:

$$\begin{cases} w_{el}(x) = -\dfrac{F_{el}\lambda\sqrt{2}}{k} e^{-\lambda x} \sin\left(\lambda x + \dfrac{\pi}{4}\right) \\[2mm] \varphi_{el}(x) = \dfrac{2F_{el}\lambda^2}{k} e^{-\lambda x} \sin(\lambda x) \\[2mm] M_{el}(x) = -\dfrac{F_{el}}{\lambda\sqrt{2}} e^{-\lambda x} \sin\left(\lambda x - \dfrac{\pi}{4}\right) \\[2mm] V_{el}(x) = F_{el} e^{-\lambda x} \sin\left(\lambda x - \dfrac{\pi}{2}\right) \end{cases} \tag{C.2}$$

where

$$\lambda = \sqrt[4]{\dfrac{k}{4EI}} \tag{C.3}$$

Next the load is increased by $2\Delta F$. As a result of the plastic hinge generated directly under the load, the boundary conditions change. The following equations describe the displacement, rotation, bending moment and shear force of the right part of the beam due to the load increase $2\Delta F$ and Figure C.2, *right* shows the displacement and bending moment distribution:

$$\begin{cases} \Delta w(x) = -\dfrac{2\Delta F\lambda}{k} e^{-\lambda x} \sin\left(\lambda x + \dfrac{\pi}{2}\right) \\[2mm] \Delta\varphi(x) = \dfrac{2\Delta F\lambda^2\sqrt{2}}{k} e^{-\lambda x} \sin\left(\lambda x + \dfrac{\pi}{4}\right) \\[2mm] \Delta M(x) = -\dfrac{\Delta F}{\lambda} e^{-\lambda x} \sin(\lambda x) \\[2mm] \Delta V(x) = \Delta F\sqrt{2} e^{-\lambda x} \sin\left(\lambda x - \dfrac{\pi}{4}\right) \end{cases} \tag{C.4}$$

The behaviour of the beam with three plastic hinges is described by the sum of the elastic

contribution and the incremental contribution, according to:

$$f_{pl}(x) = f_{el}(x) + \Delta f(x) \tag{C.5}$$

where for $f_{el}(x)$ is substituted $w_{el}(x)$, $\varphi_{el}(x)$, $M_{el}(x)$, etc. Three plastic hinges are obtained when a total load of $2F + 2\Delta F$ acts on the beam. The choice of ΔF is governed by the negative bending moment in the field that may not exceed the maximum positive bending moment directly under the load; the load increase ΔF must be so chosen that a negative moment equal to the plastic moment under the load can be formed, but for the determination of the load increase ΔF, the position of the second plastic hinge X must also be known, see Figure C.1.

The unknowns ΔF and X can be described with the following implicit equations:

$$e^{-\lambda X} + (\cos \lambda X - \sin \lambda X) = 0 \tag{C.6}$$

$$\Delta F = \frac{F_{el}}{\tan \lambda X} - F_{el} \tag{C.7}$$

The solution for the maximum negative bending moment is:

$$\Delta F = 1.434 \, F_{el} \tag{C.8}$$

$$\lambda X = 1.038 \tag{C.9}$$

Hence the full-plastic load is

$$F_{pl} = F_{el} + \Delta F = 2.434 F_{el} \tag{C.10}$$

Subsequently the beam is unloaded to 50% of the maximum load. Unloading is taken into account by substituting a negative load F_{unl} in the elastic solution (C.2) of:

$$F_{unl} = -\frac{1}{2}(F_{el} + \Delta F) = -1.217 F_{el} \tag{C.11}$$

A summary of the case of the infinitely long elasto-plastic beam on an elastic foundation loaded with a concentrated load $2F_{el} + 2\Delta F$ and subsequently unloaded to $F_{el} + \Delta F$, is given by the following equations and figures:

- Generation of the first plastic hinge

$$
\begin{cases}
w_{el}(x) = -\dfrac{F_{el}\lambda\sqrt{2}}{k} e^{-\lambda x} \sin\left(\lambda x + \dfrac{\pi}{4}\right) \\[2mm]
\varphi_{el}(x) = \dfrac{2F_{el}\lambda^2}{k} e^{-\lambda x} \sin(\lambda x) \\[2mm]
M_{el}(x) = -\dfrac{F_{el}}{\lambda\sqrt{2}} e^{-\lambda x} \sin\left(\lambda x - \dfrac{\pi}{4}\right) \\[2mm]
V_{el}(x) = F_{el}\, e^{-\lambda x} \sin\left(\lambda x - \dfrac{\pi}{2}\right)
\end{cases} \tag{C.12}
$$

Figure C.3: *Elastic vertical displacement and bending moment distribution. The solid line is calculated with* PLASWALL, *the ×-marks indicate the analytical solution*

- Just before generation of the second and third plastic hinge

$$\begin{cases} w_{pl}(x) = -\dfrac{F_{el}\lambda\sqrt{2}}{k} e^{-\lambda x} \sin\left(\lambda x + \dfrac{\pi}{4}\right) - \dfrac{2\Delta F\lambda}{k} e^{-\lambda x} \sin\left(\lambda x + \dfrac{\pi}{2}\right) \\[2mm] \varphi_{pl}(x) = \dfrac{2F_{el}\lambda^2}{k} e^{-\lambda x} \sin\left(\lambda x\right) + \dfrac{2\Delta F\lambda^2\sqrt{2}}{k} e^{-\lambda x} \sin\left(\lambda x + \dfrac{\pi}{4}\right) \\[2mm] M_{pl}(x) = -\dfrac{F_{el}}{\lambda\sqrt{2}} e^{-\lambda x} \sin\left(\lambda x - \dfrac{\pi}{4}\right) - \dfrac{\Delta F}{\lambda} e^{-\lambda x} \sin\left(\lambda x\right) \\[2mm] V_{pl}(x) = F_{el} e^{-\lambda x} \sin\left(\lambda x - \dfrac{\pi}{2}\right) + \Delta F\sqrt{2} e^{-\lambda x} \sin\left(\lambda x - \dfrac{\pi}{4}\right) \end{cases} \quad \text{(C.13)}$$
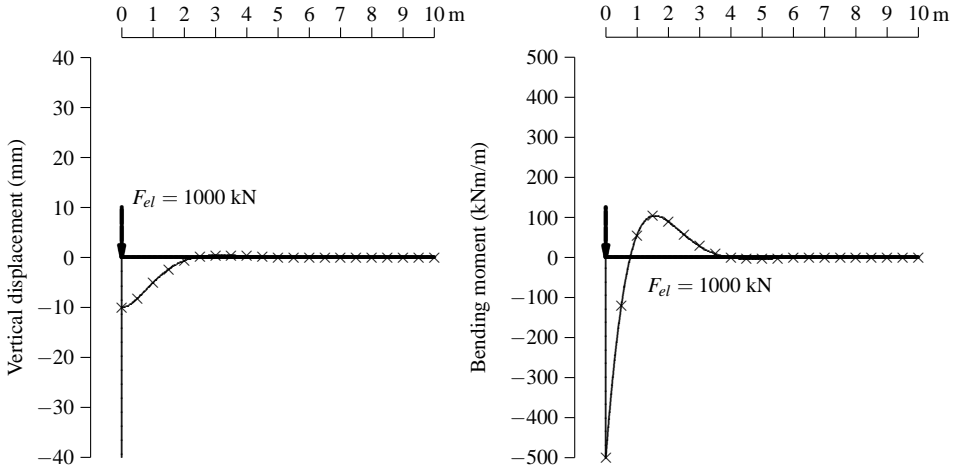
where

$$\Delta F = 1.434 F_{el} \quad\quad\quad\quad \text{(C.14)}$$

Figure C.4: *Vertical displacement and bending moment distribution just before generation of the second and third plastic hinge.*

- Subsequently 50% unloading

$$
\begin{cases}
w_{unl}(x) = -\dfrac{(1-1.217)F_{el}\lambda\sqrt{2}}{k}\,e^{-\lambda x}\sin\left(\lambda x+\dfrac{\pi}{4}\right) - \dfrac{2\Delta F\lambda}{k}\,e^{-\lambda x}\sin\left(\lambda x+\dfrac{\pi}{2}\right) \\[2ex]
\varphi_{el}(x) = \dfrac{2(1-1.217)F_{el}\lambda^2}{k}\,e^{-\lambda x}\sin\left(\lambda x\right) + \dfrac{2\Delta F\lambda^2\sqrt{2}}{k}\,e^{-\lambda x}\sin\left(\lambda x+\dfrac{\pi}{4}\right) \\[2ex]
M_{unl}(x) = -\dfrac{(1-1.217)F_{el}}{\lambda\sqrt{2}}\,e^{-\lambda x}\sin\left(\lambda x-\dfrac{\pi}{4}\right) - \dfrac{\Delta F}{\lambda}\,e^{-\lambda x}\sin\left(\lambda x\right) \\[2ex]
V_{unl}(x) = (1-1.217)F_{el}\,e^{-\lambda x}\sin\left(\lambda x-\dfrac{\pi}{2}\right) + \Delta F\sqrt{2}\,e^{-\lambda x}\sin\left(\lambda x-\dfrac{\pi}{4}\right)
\end{cases}
$$

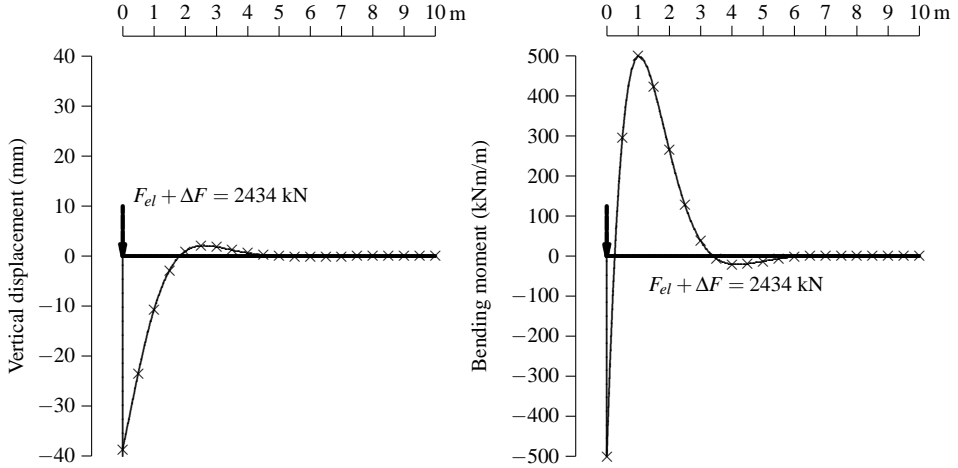$$\text{(C.15)}$$

where

$$\Delta F = 1.434 F_{el} \tag{C.16}$$
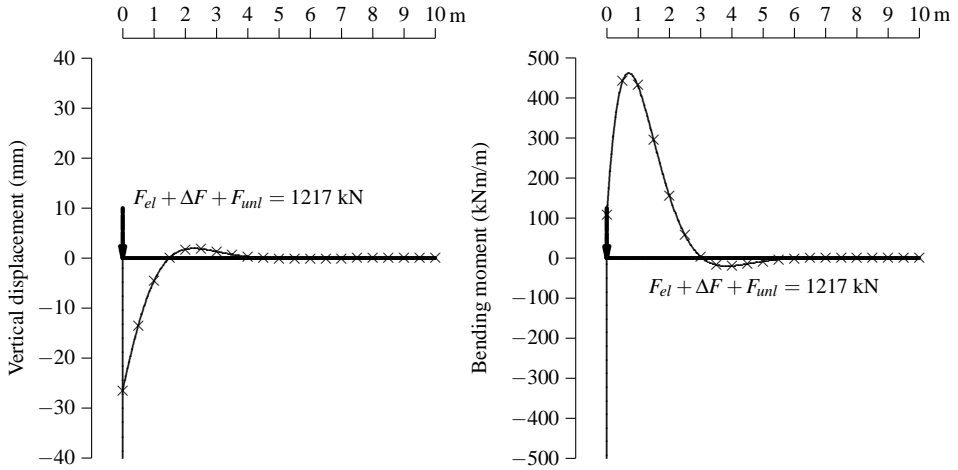
Figure C.5: *Vertical displacement and bending moment distribution after 50% unloading.*

Appendix D

Earth pressure theories

For practical applications of the subgrade reaction method it is desirable to describe the spring characteristic with the earth pressure coefficients K_a, K_n and K_p and to derive these coefficients from physical soil parameters, such as c', φ' and δ. Examples of earth pressure theories where K_a and K_p are calculated from physical soil parameters are those of Müller-Breslau, Kötter, Brinch Hansen, and Kerisel and Absi.

Müller-Breslau

Müller-Breslau [59] provided a general solution for the active and passive earth pressure coefficients of a cohesionless soil wedge failing along a straight slip plane. In the Dutch code NEN 6740 [1] this theory is extended for cohesive soil. The levels of the active and passive spring branches for a vertical wall and horizontal ground levels, without surcharge, are determined by

$$\sigma'_a = K_{ca}c' + K_{\varphi a}\sigma'_v \tag{D.1}$$
$$\sigma'_n = K_n\sigma'_v \tag{D.2}$$
$$\sigma'_p = K_{cp}c' + K_{\varphi p}\sigma'_v \tag{D.3}$$

where

$$K_{ca} = -\frac{2\cos\varphi'\cos\delta}{1+\sin(\varphi'+\delta)} \quad \text{and} \quad K_{\varphi a} = \frac{\cos^2\varphi'}{\left(\sqrt{\dfrac{\sin\varphi'\sin(\varphi'+\delta)}{\cos\delta}}+1\right)^2} \tag{D.4}$$

$$K_n = 1 - \sin\varphi' \tag{D.5}$$

$$K_{cp} = \frac{2\cos\varphi'\cos\delta}{1-\sin(\varphi'-\delta)} \quad \text{and} \quad K_{\varphi p} = \frac{\cos^2\varphi'}{\left(\sqrt{\dfrac{\sin\varphi'\sin(\varphi'-\delta)}{\cos\delta}}-1\right)^2} \tag{D.6}$$

Kötter

The earth pressure theory of the curved slip plane is generally ascribed to Kötter. In this theory the levels of the active and passive spring branches for a vertical wall and horizontal ground levels, without surcharge, are determined by [30]

$$\sigma_a' = K_a \sigma_v' - 2c' \sqrt{K_a} \tag{D.7}$$
$$\sigma_n' = K_n \sigma_v' \tag{D.8}$$
$$\sigma_p' = K_p \sigma_v' + 2c' \sqrt{K_p} \tag{D.9}$$
$$\tag{D.10}$$

where in case of weightless and cohesionless soil

$$K_a = \frac{1 - \sin\varphi' \, \sin(2\alpha + \varphi')}{1 + \sin\varphi'} \, e^{(-\frac{\pi}{2} + \varphi' + 2\alpha)\tan\varphi'} \tag{D.11}$$

$$\text{with } \alpha: \ \cos(2\alpha + \varphi' - \delta) = \frac{\sin\delta}{\sin\varphi'} \tag{D.12}$$

$$K_n = 1 - \sin\varphi' \tag{D.13}$$

$$K_p = \frac{1 + \sin\varphi' \, \sin(2\alpha - \varphi')}{1 - \sin\varphi'} \, e^{(+\frac{\pi}{2} + \varphi' - 2\alpha)\tan\varphi'} \tag{D.14}$$

$$\text{with } \alpha: \ \cos(2\alpha - \varphi' + \delta) = \frac{\sin\delta}{\sin\varphi'} \tag{D.15}$$

Brinch Hansen

In the theories of Müller-Breslau and Kötter the earth pressure coefficients depend on the assumption of soil failure according to a straight or curved slip plane. In Brinch-Hansen's earth pressure theory, however, the failure mechanism in the soil depends on the shape of the deformed retaining wall [13]. This means that for the same problem other earth pressure coefficients are found when the passive earth wedge fails than in the case of e.g., anchor failure. Consequently, arching in the soil is implicitly taken into account. Brinch Hansen's earth pressure theory was developed for rigid walls with a frictionless hinge, and is still used for plastic design.

As the Brinch Hansen earth pressure coefficients cannot be determined by a straight-forward formula, the computer program SPOOKS [37] is used to determine the appropriate earth pressure coefficients.

Kerisel and Absi

Kerisel and Absi [47] provide tabulated active and passive earth coefficients for weightless cohesionless soil without surcharge. These coefficients are determined from c', φ', and δ, and applied to the equations (D.7) and (D.9).

Appendix E

Technical drawings

The following technical drawings were made for the Rotterdam Sheet Pile Wall Field Test.

1. Location of test site

2. Soil investigation

3. Cofferdam details

4. Steel framing

5. Interface pile

6. Instrumentation AZ13 pile A3

7. Instrumentation AZ13 pile A4

8. Instrumentation L607K pile H3

9. Instrumentation L607K pile H5

10. Measurement tubes

Drawing no. 1: Location of test site
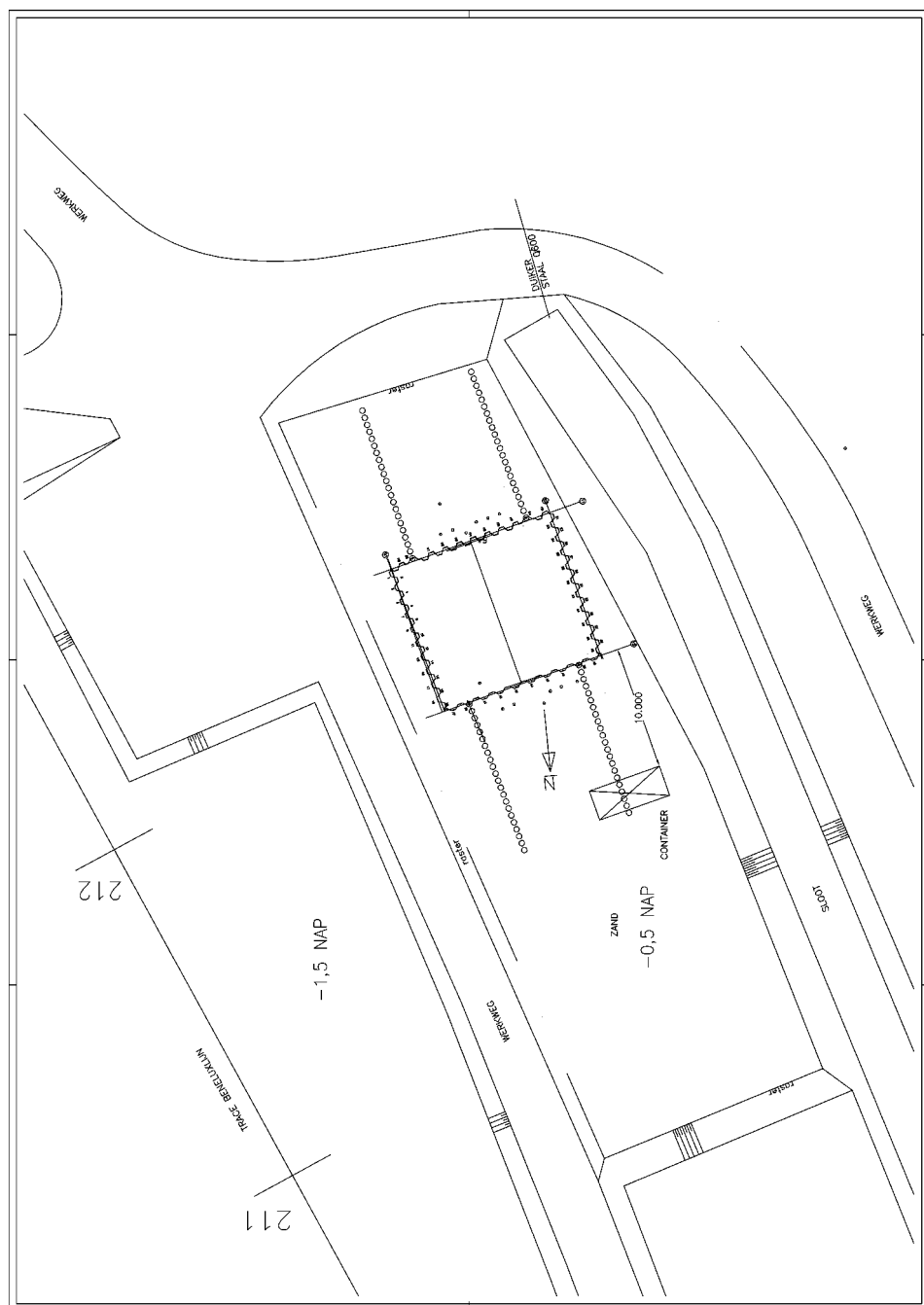
Drawing no. 2: Soil investigation

TEST LOCATION

Drawing no. 3: Cofferdam details
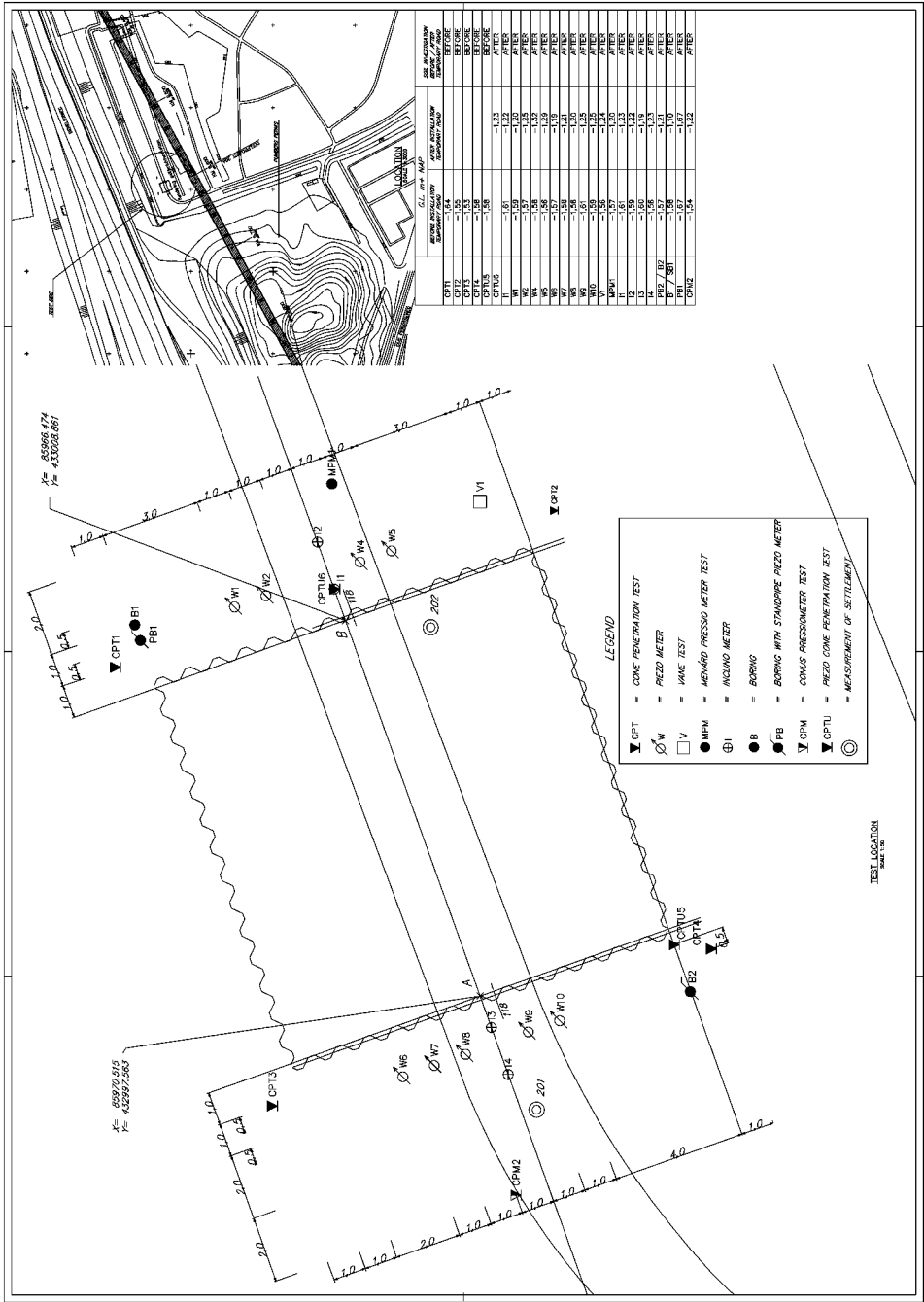
Drawing no. 4: Steel framing
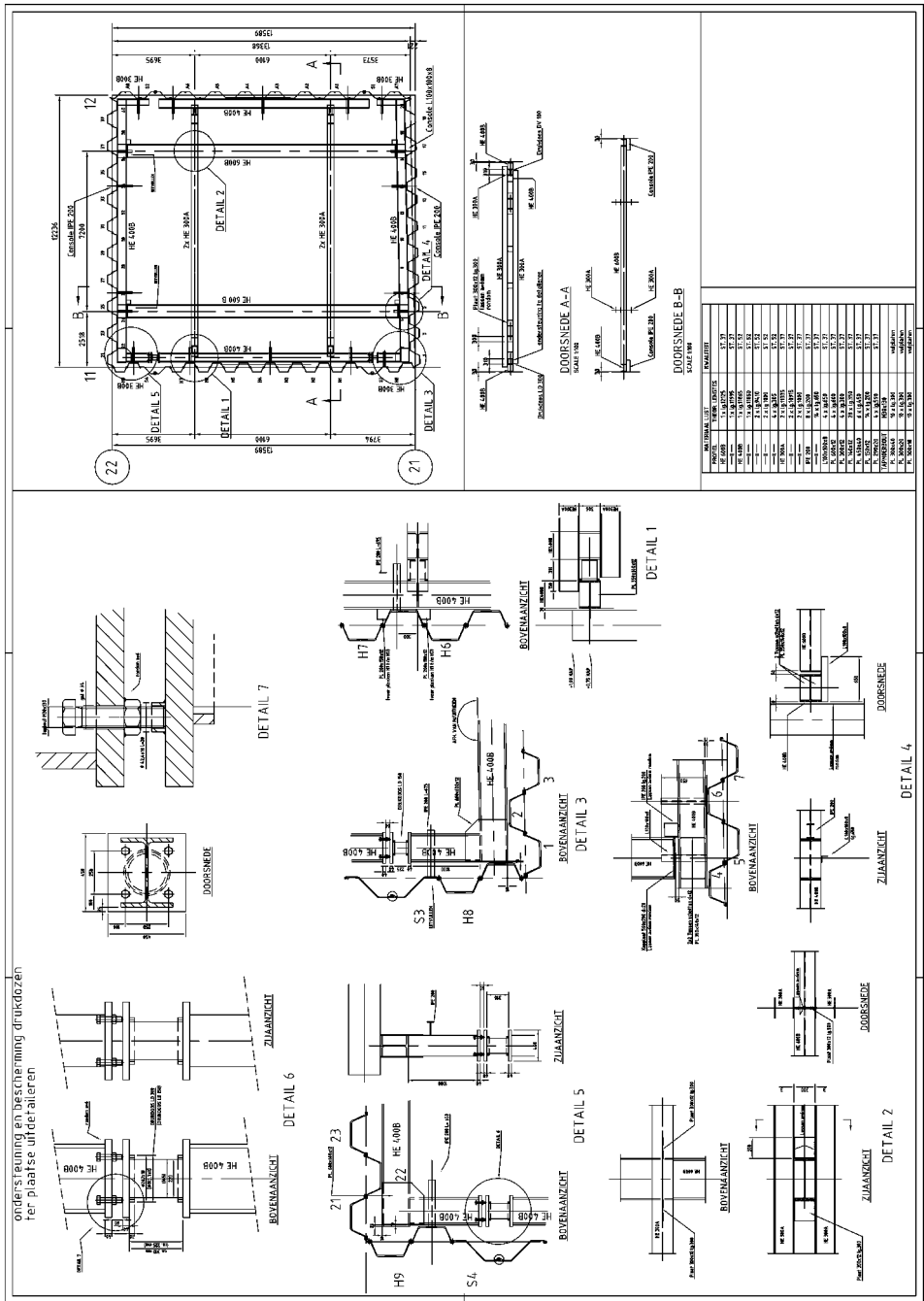
Drawing no. 5: Interface pile

Special Interface Pile

top

19000

1000

2000

500
250
250

200
100

Gap ⊿ 16000 × 100mm

X — X

Section X-X

114
200
72

M10 ⟨68×⟩
Ø16

100

Bulb steel 100 × 8

VLDPE-foil 2mm

Gap ⊿ 16000 × 100 mm
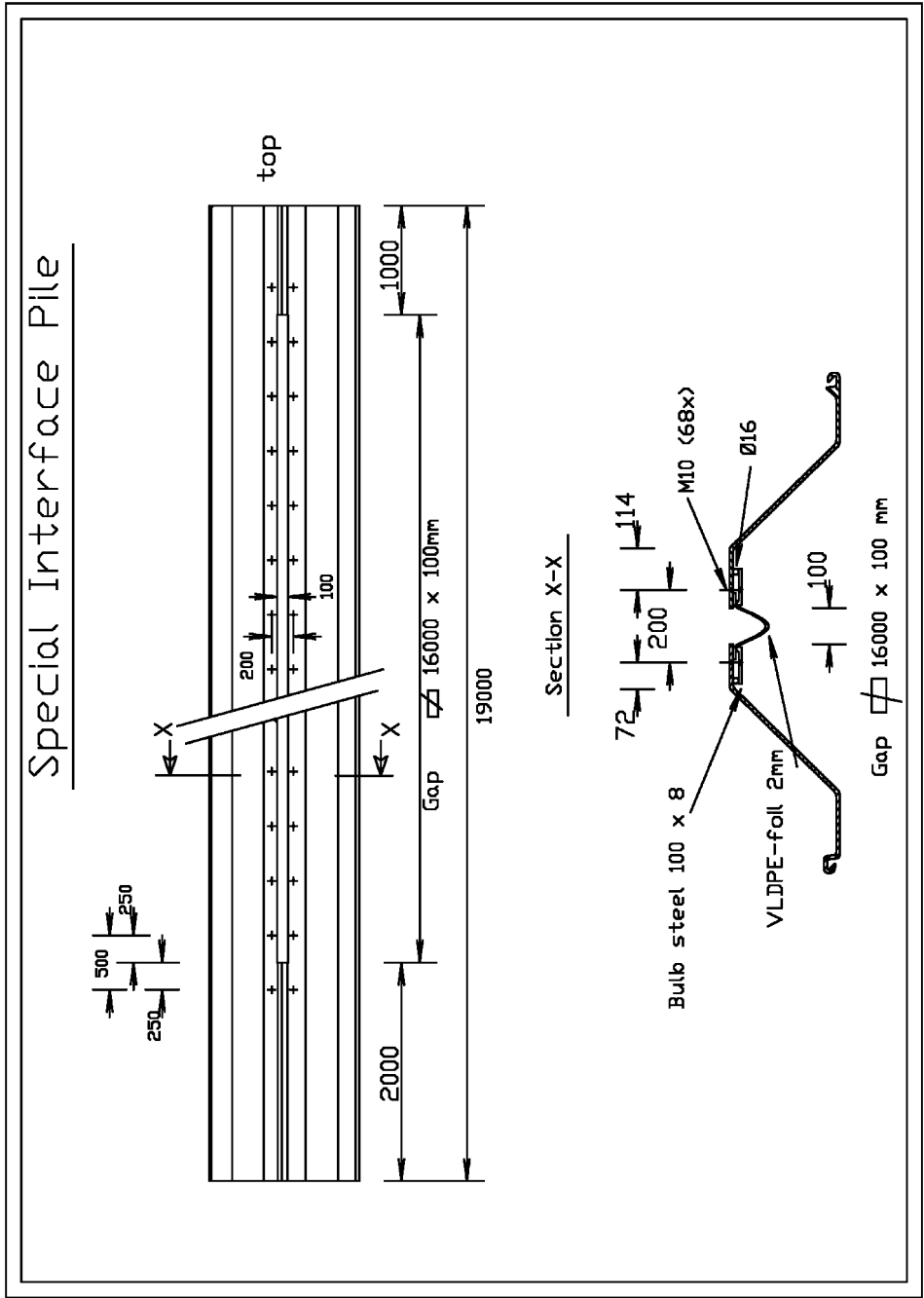
Drawing no. 6: Instrumentation AZ13 pile A3
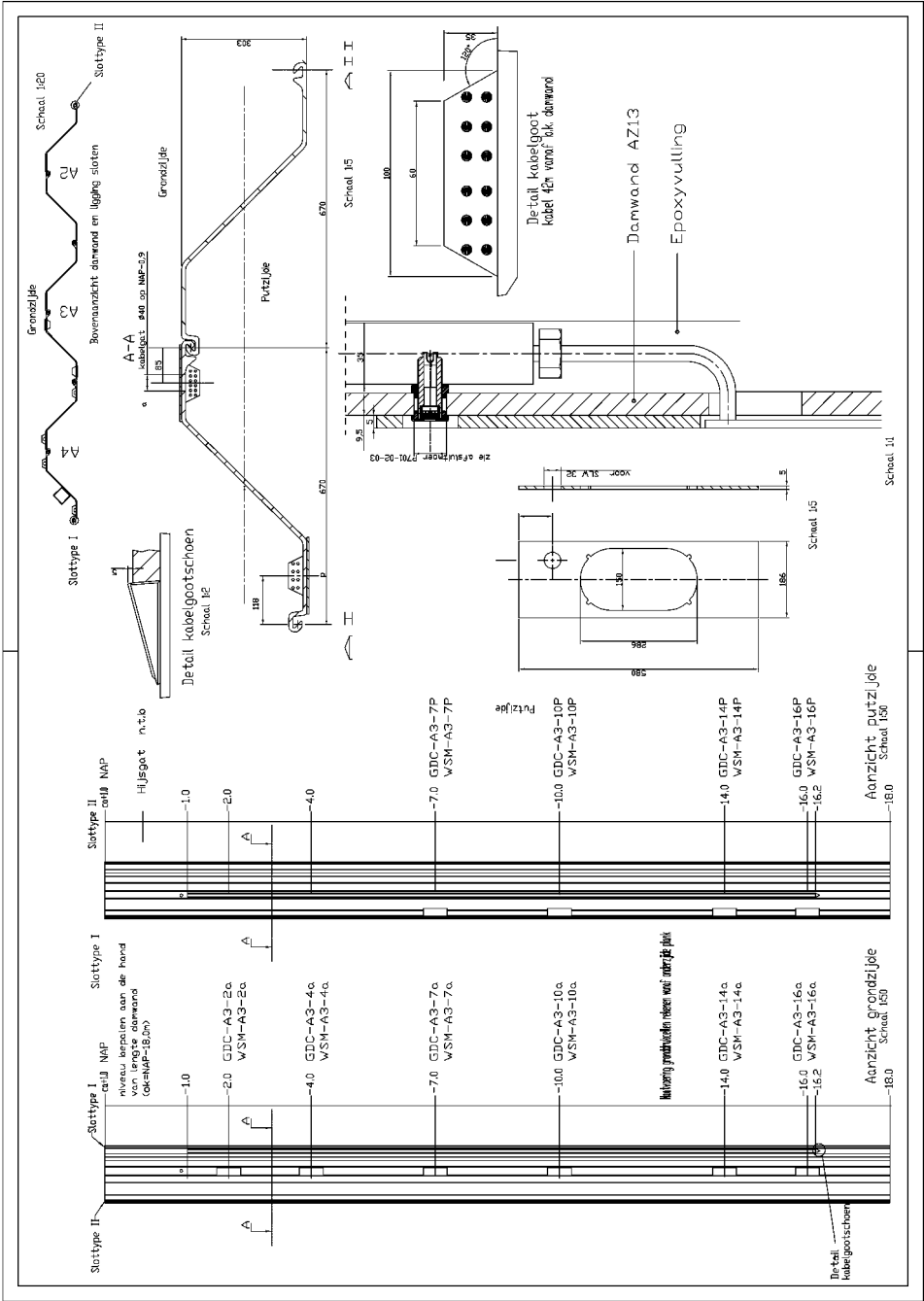
Drawing no. 7: Instrumentation AZ13 pile A4
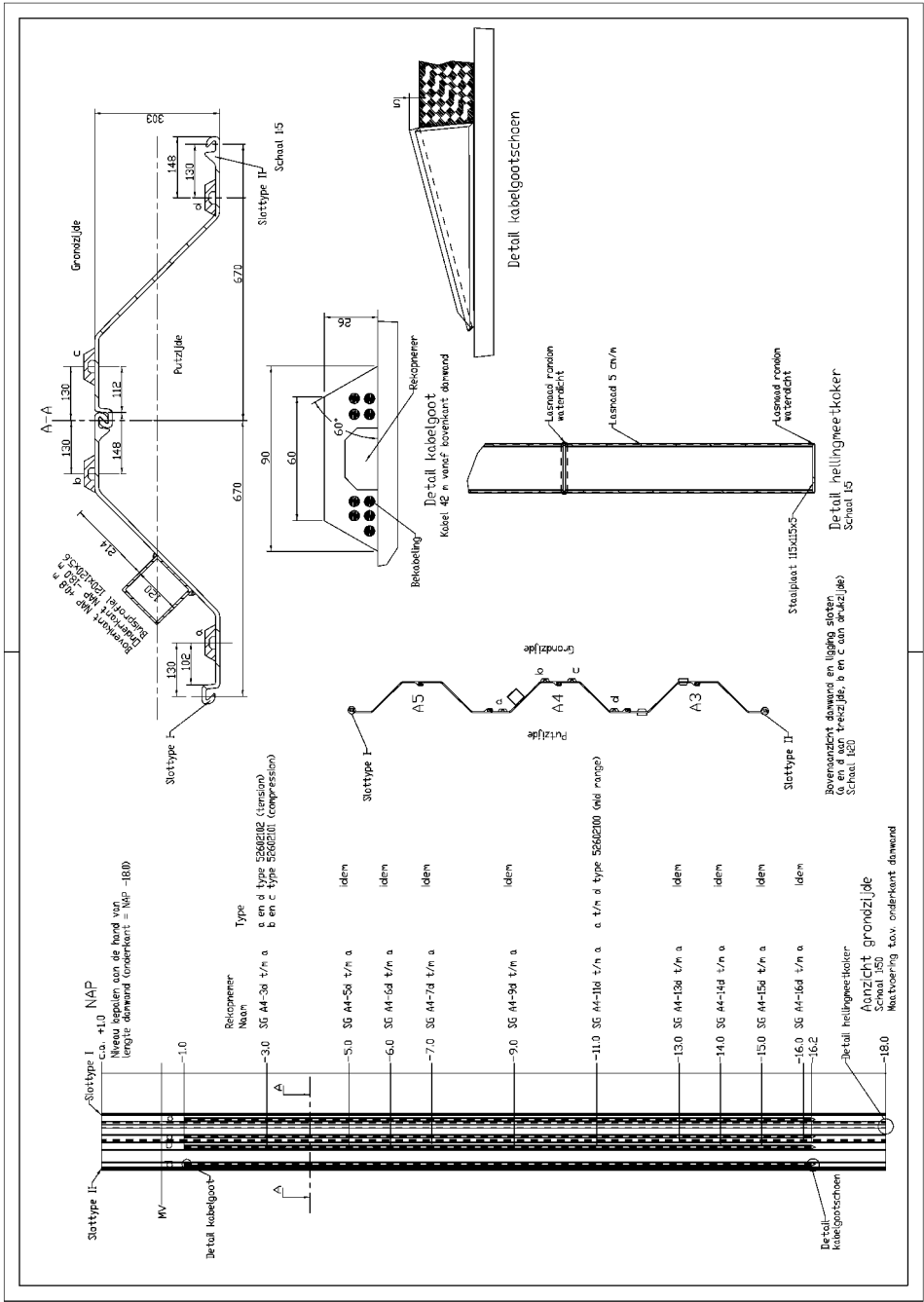
Drawing no. 8: Instrumentation L607K pile H3

Drawing no. 9: Instrumentation L607K pile H5
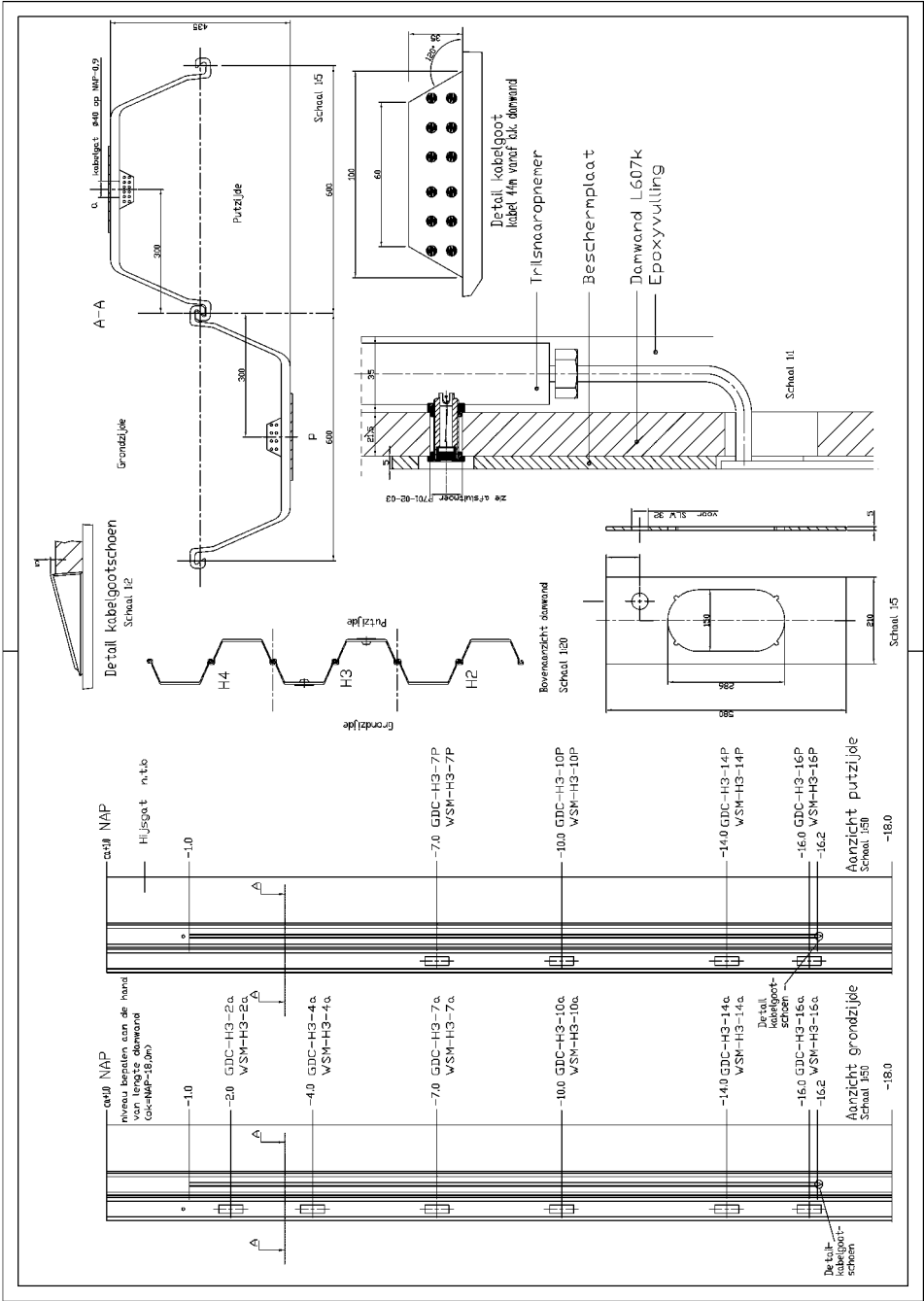
Drawing no. 10: Measurement tubes
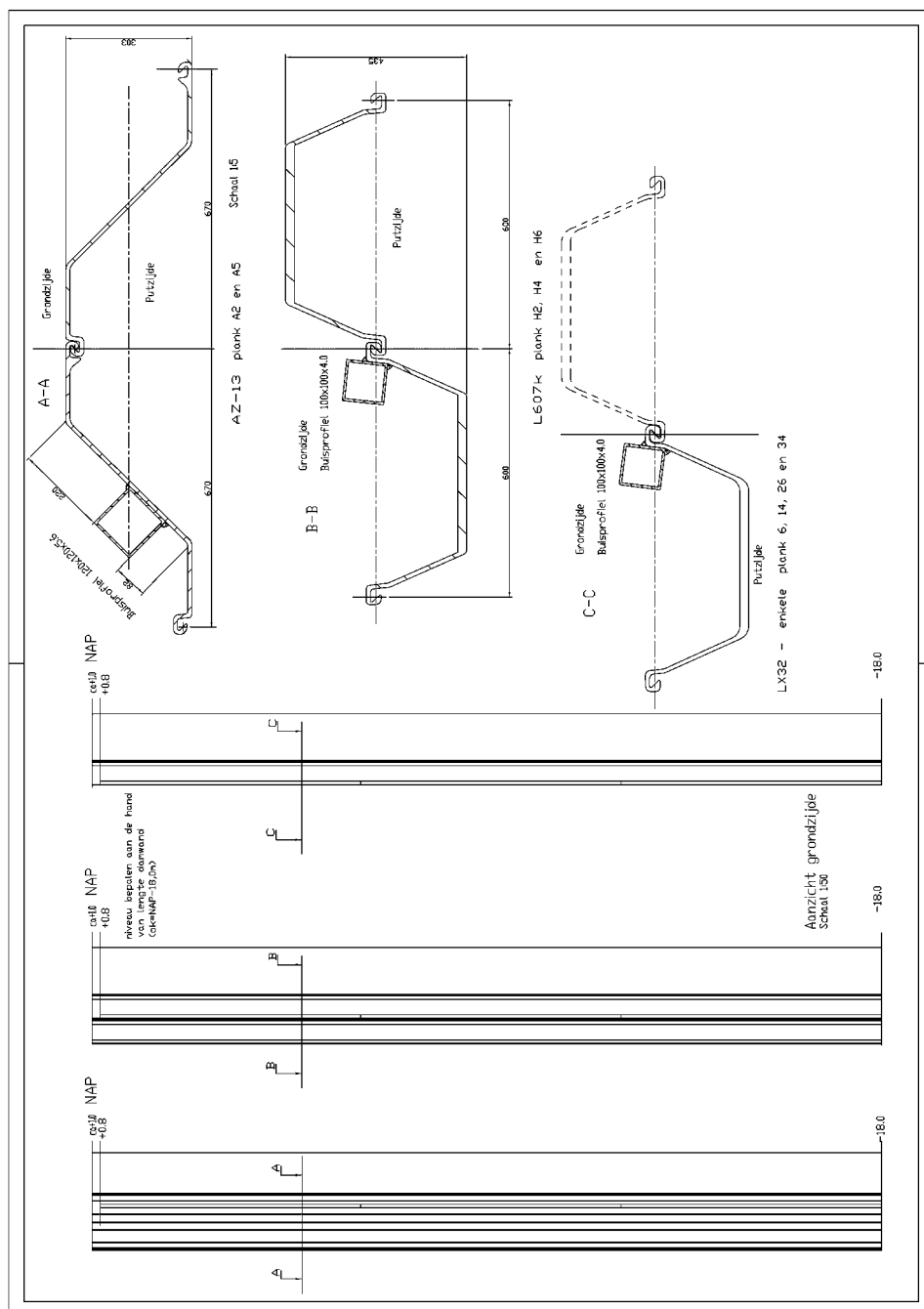
Appendix F

Site investigation and laboratory testing

This appendix contains the results of the following site investigations and laboratory tests:

- Borings
- Cone penetration tests
- In-situ vane tests
- Triaxial tests
- Oedometer tests
- Volume weights
- Cone pressiometer tests
- Water content
- Ménard pressiometer tests
- Atterberg values

These results give a comprehensive summary of the soil investigation carried out for the Rotterdam sheet pile wall field test. For the complete report of the soil investigation, see reference [32].

Boring B2
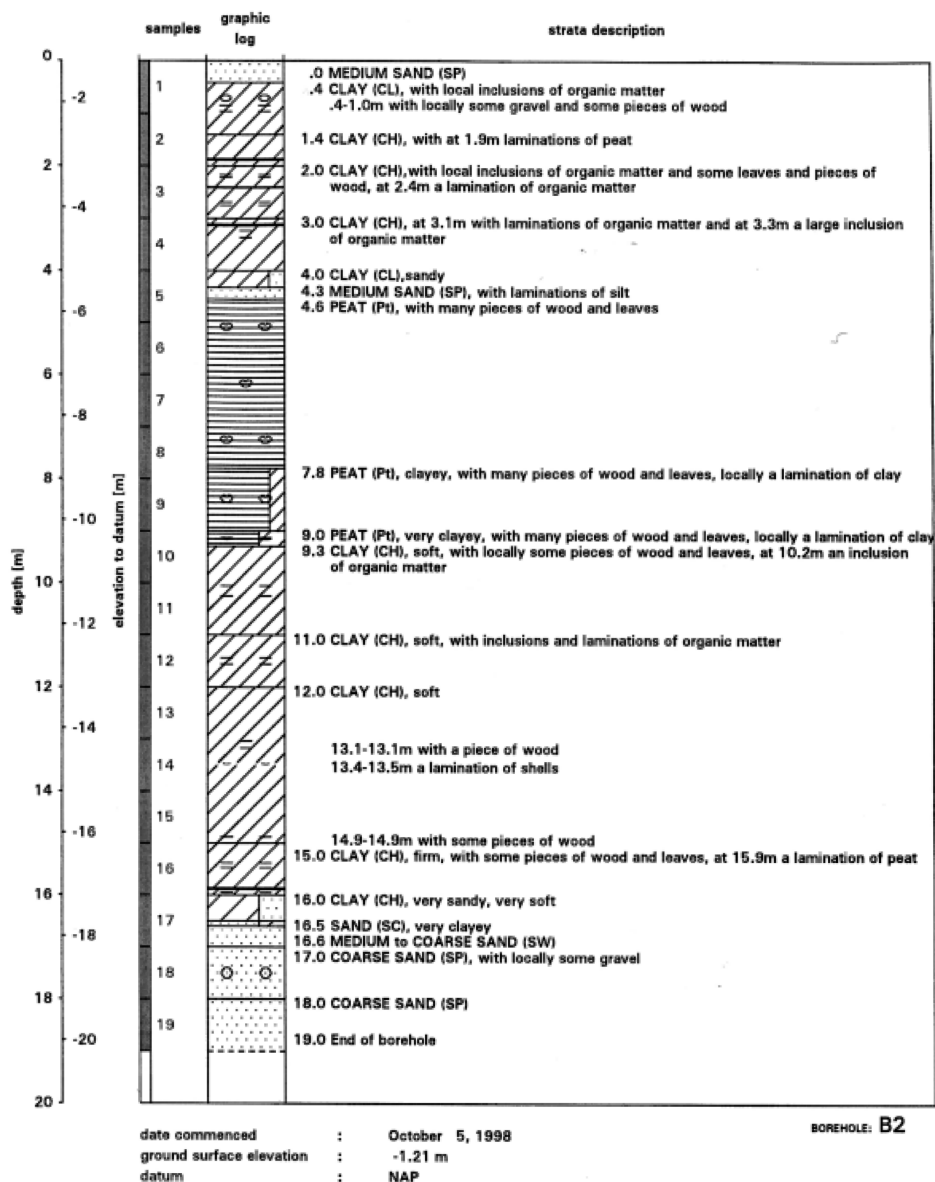
Figure F.1: *Log of boring B2*
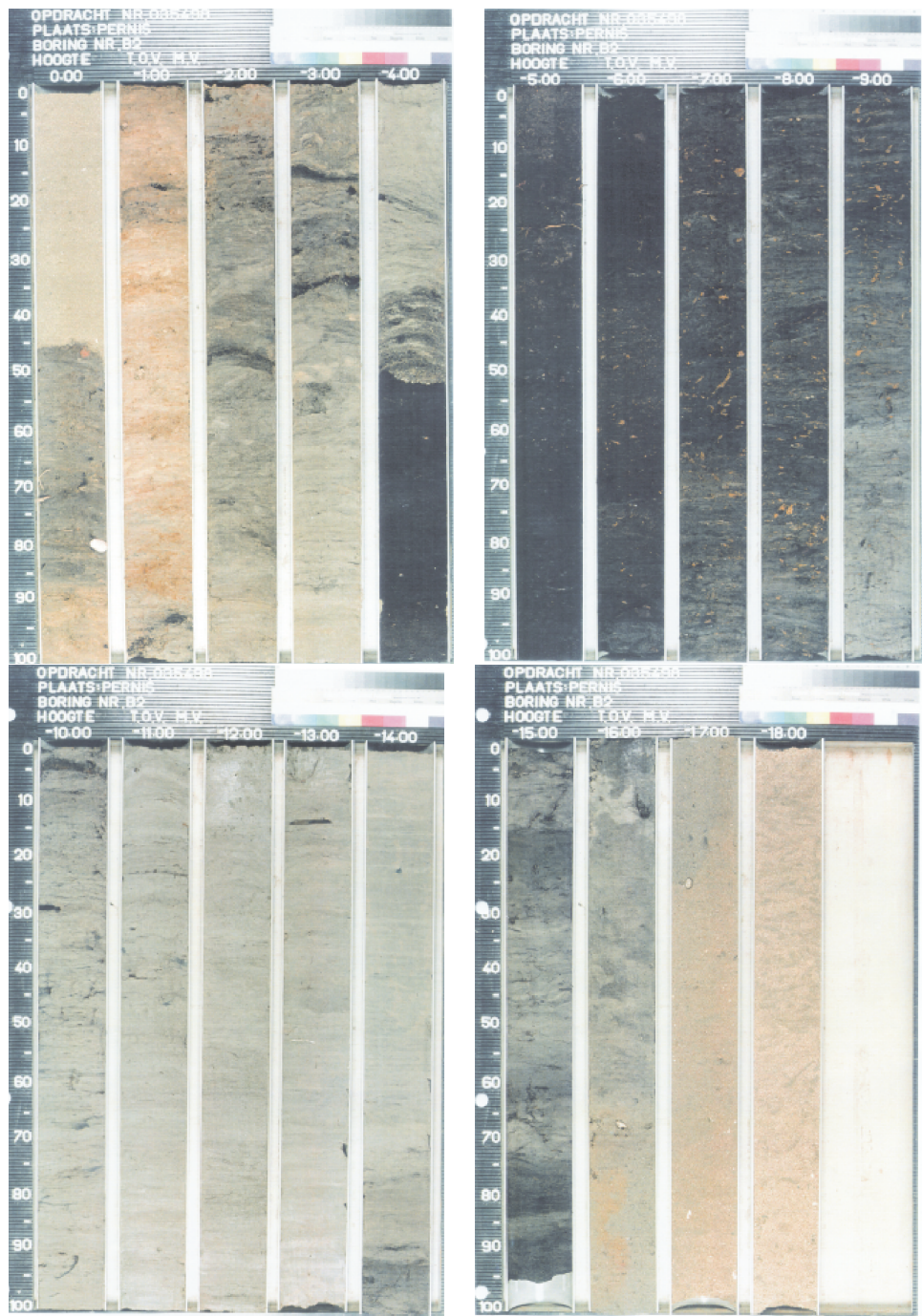
Figure F.2: *Photograph of boring B2. Depth with respect to ground level (NAP-1.21 m)*

Cone penetration tests
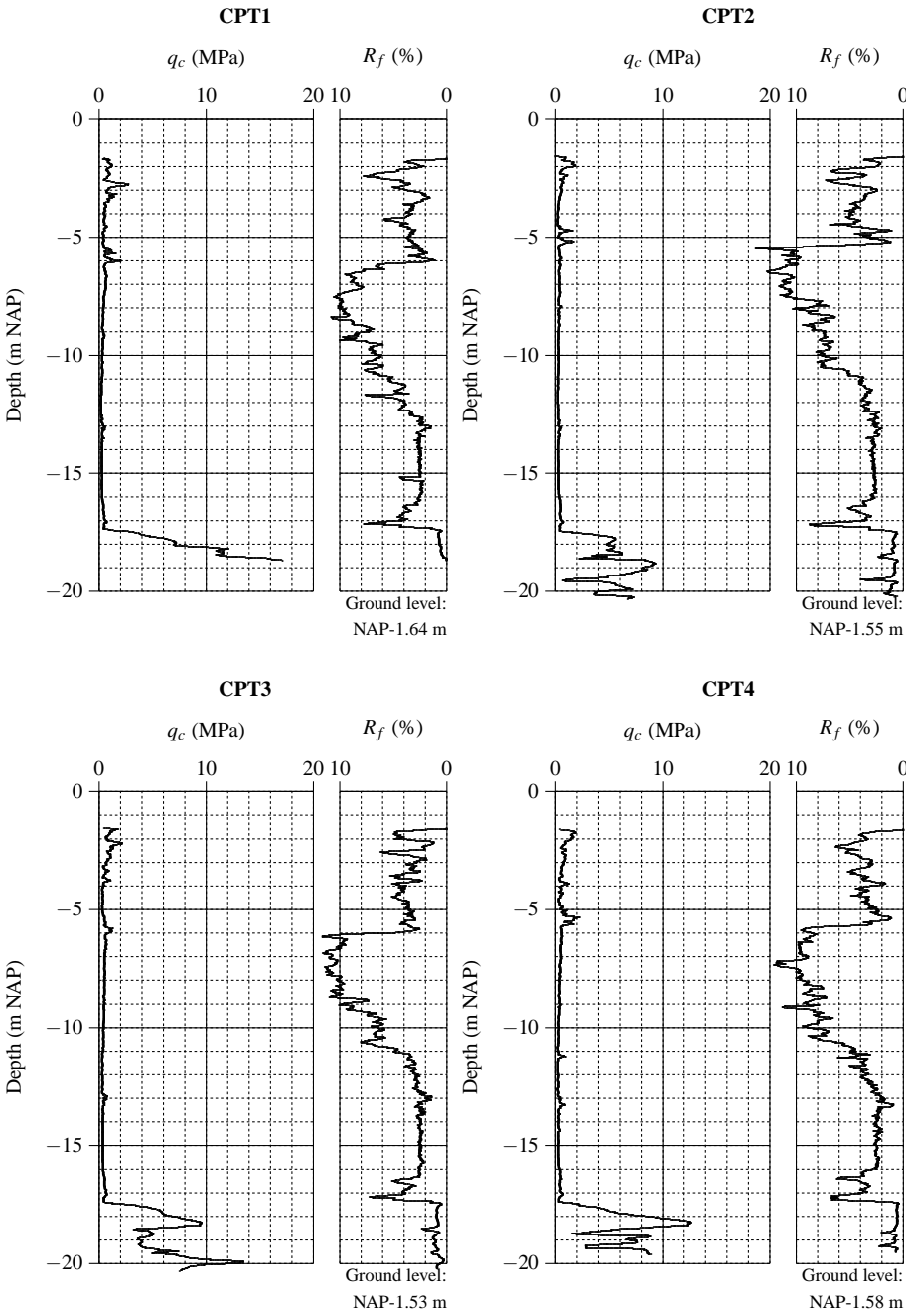
Figure F.3: *CPT1 to CPT4*
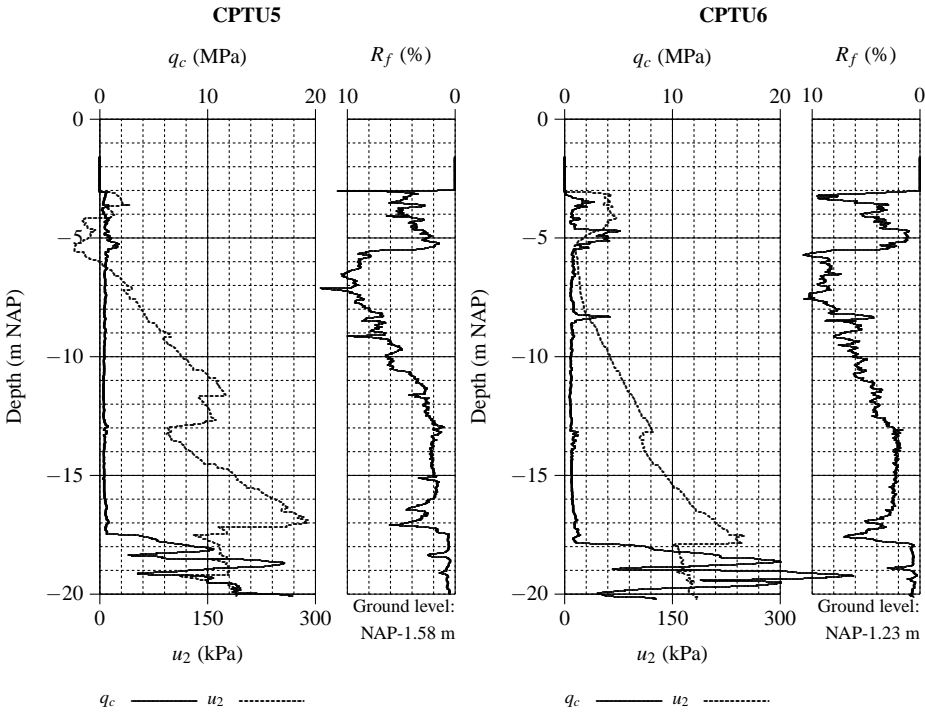
Figure F.4: *CPTU5 & CPTU6*
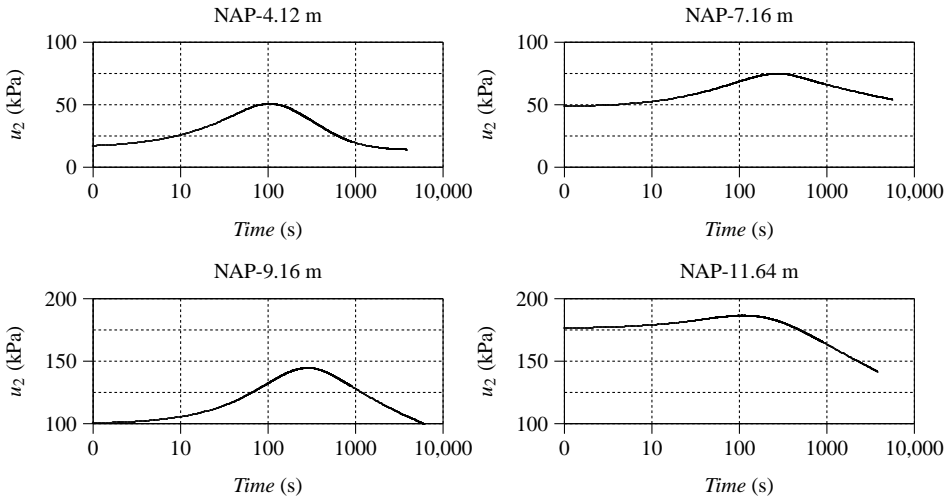
Figure F.5: *Piezo cone dissipation tests 1-4*
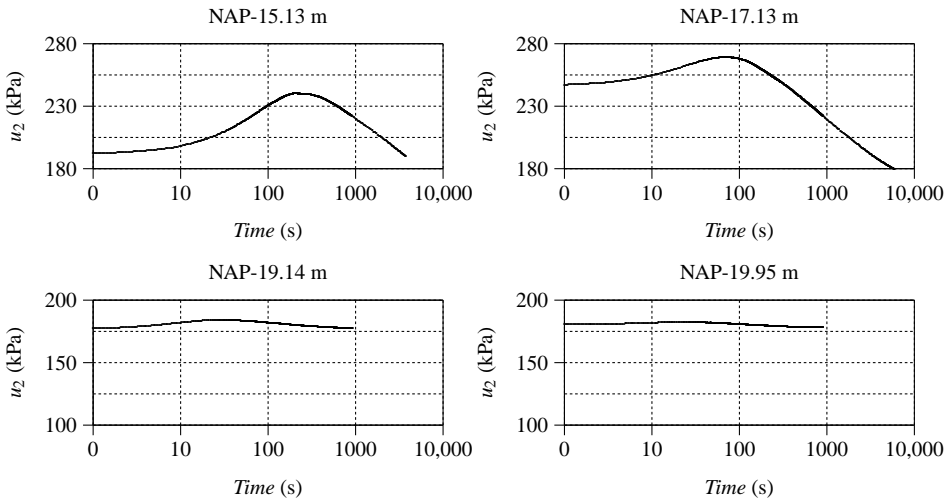
Figure F.6: *Piezo cone dissipation tests 5-8*

In-situ vane V1

The in-situ vane tests were executed according to the Dutch standard NEN 5106 [61], with the following simplification: The residual shear strength $f_{u,rest}$ was not measured in order to reduce the total time of the test and so to limit costs. The specifications of the equipment are given in Table F.1.

Geonor H-10 SGI vane borer			
height of blade:	110 mm	diameter of blade:	55 mm
diameter of rod:	16 mm	diameter of protective shoe:	65 mm
rate of vane rotation:	0.1 ^{o}/sec	accuracy of measurement:	$\pm$0.5 kPa

Table F.1: *Specifications of equipment for the in-situ vane tests*
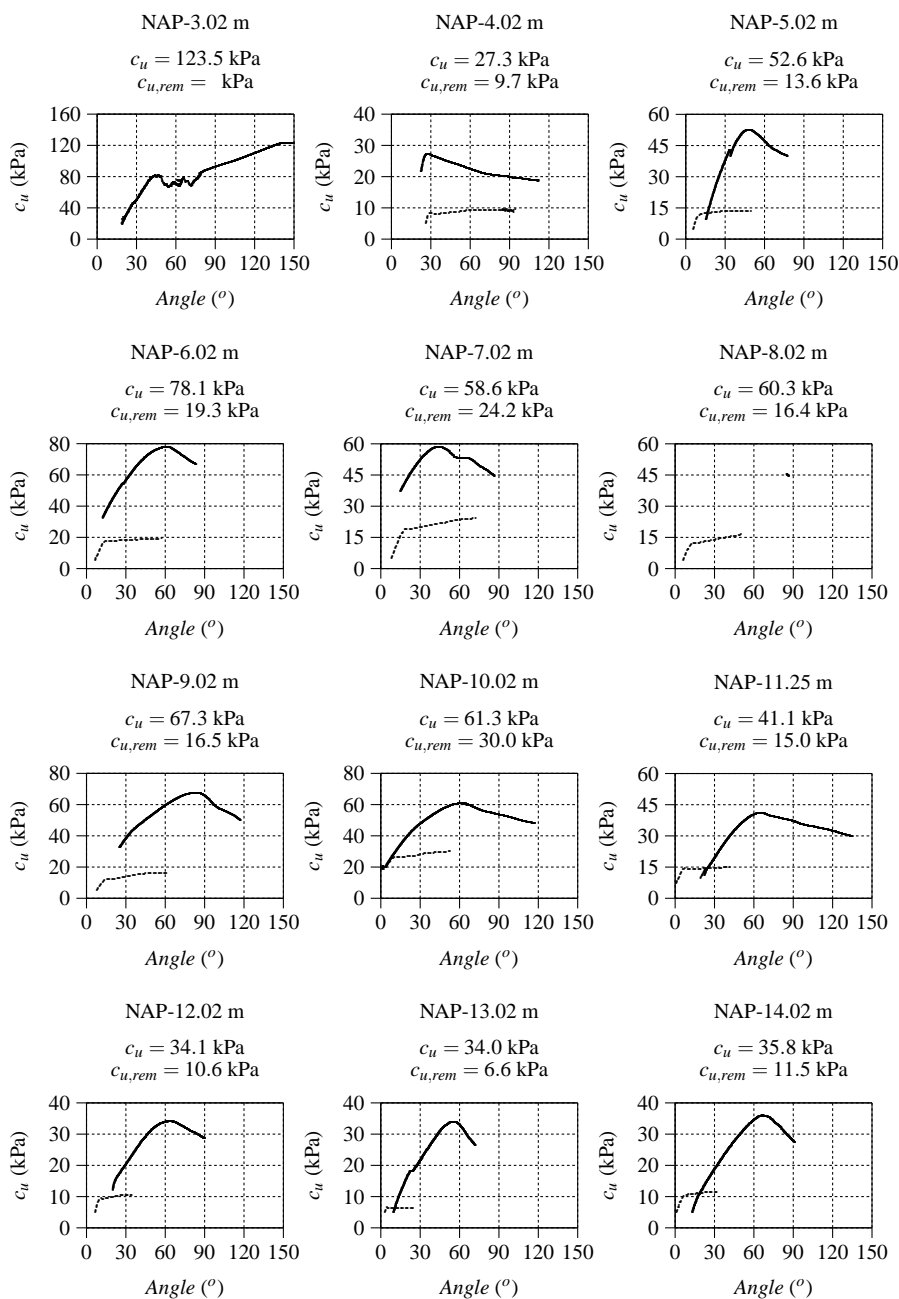
Figure F.7: *In-situ vane test 1-12*

NAP-15.02 m

$c_u = 29.8$ kPa
$c_{u,rem} = 7.3$ kPa

NAP-15.77 m

$c_u = 31.7$ kPa
$c_{u,rem} = 8.3$ kPa

NAP-16.52 m

$c_u = 30.7$ kPa
$c_{u,rem} = 6.4$ kPa
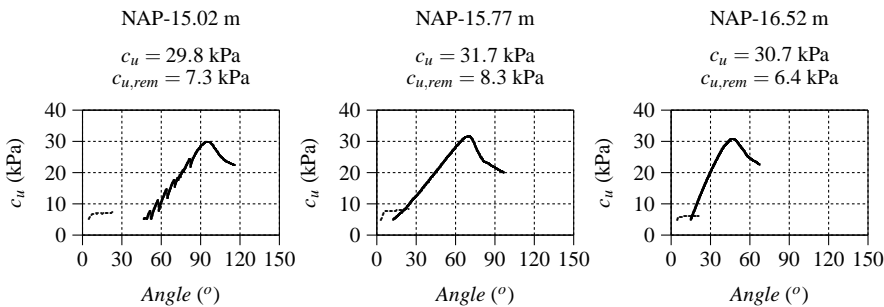
Figure F.8: *In-situ vane tests 13-15*

Triaxial tests

				Triaxial compression							
Level	E_u^{50} (MPa)			σ_3' (kPa)			c_u (kPa)			Peak Values*	
(m NAP)	Stage 1	Stage 2	Stage 3	St.1	St.2	St.3	St.1	St.2	St.3	c' (kPa)	φ'
-2.63	3.1	3.2	4.1	10	17	24	21.1	27.4	29.6	11.5	21.3
-3.69	1.9	3.3	3.1	14	24	34	29.2	36.4	40	16.1	20.3
-5.4	1.6	4.1	4.3	22	38	54	31.6	39.1	43.8	18.3	16.0
-6.82	2.1	2.2	2.4	22	38	54	33	41.3	53.1	12.1	22.7
-8.83	1.8	3.1	2.7	24	44	66	26.7	38.1	43.9	14.3	16.7
-9.97	2.1	3.2	3.8	22	45	66	38.7	44.2	55	21.8	15.7
-11.45	2.7	5.2	5.7	24	49	74	24.6	29.9	45.8	8.7	16.7
-12.96	3.7	3.7	6.8	32	64	96	42.3	58	78.7	15.5	21.0
-13.89	4.1	8.6	14.1	36	72	109	35.3	47	59.6	17.9	14.3
-15.63	5.6	10.2	20.3	41	81	119	33.1	49.1	64.5	12.3	17.0
-15.93	7.4	10.4	20.3	42	84	126	33.6	48.8	63.4	14.5	15.0
-17.875	17.9	40.2	55.5	50	100	150					
				Triaxial extension							
-6.65	2.6	2.5	11.3	25	50	75	22	38	50	13	34.5
-13.7	15.3	22.6	33.5	40	80	120	23	33	45	9.9	27

*Peak values determined by the Author

Table F.2: *Triaxial tests*

Oedometer tests

Level (m NAP)	p_c (kPa)	$C_C(< p_c)$	$C_C(> p_c)$	C_s	Taylor c_v 90% (m^2/s)	m_v (1/MPa)	E_{oed} (MPa)	k (m/s)
-2.3	17	0.04	0.16		$3.80\,10^{-7}$	0.18	5.6	$6.30\,10^{-10}$
-3.55	21	0.02	0.06	0.01	$8.50\,10^{-7}$	0.069	14.5	$6.14\,10^{-10}$
-5.5	35	0.09	0.3		$1.50\,10^{-7}$	0.37	2.7	$5.18\,10^{-10}$
-6.75	34	2.64	9.06	1.02	$9.30\,10^{-8}$	0.84	1.2	$7.81\,10^{-10}$
-8.75	41	0.94	3.69		$1.10\,10^{-7}$	1.2	0.8	$1.44\,10^{-9}$
-9.85	41	1.21	4.34	0.69	$1.20\,10^{-7}$	0.76	1.3	$9.12\,10^{-10}$
-11.35	48	0.44	1.3		$3.20\,10^{-8}$	0.85	1.2	$2.64\,10^{-10}$
-12.75	43	0.2	0.36	0.03	$3.00\,10^{-8}$	0.58	1.7	$1.74\,10^{-10}$
-13.8	56	0.25	0.53		$5.40\,10^{-8}$	0.51	2.0	$2.86\,10^{-10}$
-15.55	59	0.19	0.44	0.04	$6.00\,10^{-8}$	0.39	2.6	$2.46\,10^{-10}$
-15.8	70	0.22	0.67		$4.70\,10^{-8}$	0.44	2.3	$2.02\,10^{-10}$
-17	71	0.28	1.85	0.17	$5.40\,10^{-8}$	0.66	1.5	$3.43\,10^{-10}$
Horizontal tests								
-6.75	20	0.7	3.62	0.6	$2.50\,10^{-7}$	0.26	3.8	$7.02\,10^{-10}$
-13.8	24	0.14	0.32	0.03	$6.20\,10^{-8}$	0.64	1.6	$4.16\,10^{-10}$

Table F.3: *Oedometer tests*

Volume weights
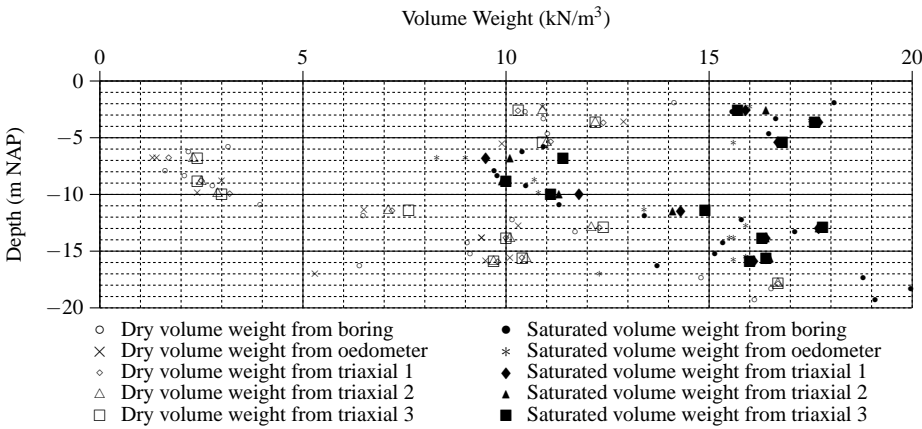
Figure F.9: *Volume weights*

Cone pressiometer tests

Depth	linear					non-linear					
	P_0	C_u	I_r	P_l	G_{min}	P_0	G_{min}	I_r	G_{r-1}	α	β
m-NAP	(kPa)	(kPa)		(kPa)	(MPa)	(kPa)	(MPa)	(MPa)	(MPa)	(kPa)	
-2.22	51	36	379	300	14	77	4.6	128	6.21	268	0.735
-4.22	62	20	172	183	3.4	64	2.0	101	2.09	594	0.724
-5.22	67	23	251	218	5.8	68	3.4	149	3.2	584	0.673
-6.72	110	32	33	254	1.1	94	1.2	38	1.6	478	0.742
-8.22	117	30	40	257	1.2	99	1.4	47	1.5	409	0.681
-10.22	155	18	53	246	1	148	1.0	55	1	356	0.724
-11.72	161	11	190	228	2.1	163	0.9	84	0.9	163	0.617
-13.22	126	19	425	262	8.2	140	2.5	130	1.8	358	0.659
-15.22	206	12	123	278	1.5	205	0.9	76	0.9	129	0.561
-16.22	183	10	69	237	0.7	181	0.5	45	0.7	107	0.613
-19.22	640	404	200	3188	81	767	53	130	53.9	3137	0.894

Depth	Depth of the middle of the inflatable part of the probe
P_0	Horizontal total stress at rest
C_u	Shear strength according to Houlsby and Withers [43]
I_r	Rigidity Index: ratio between G_{min} and C_u
P_l	Pressure at failure
G_{min}	Shear modulus at failure
G_{r-1}	Shear modulus at unload/reload cycles (1st unloading-reloading loop)
α	Stiffness constant according to Bolton and Whittle [10] (1st unloading-reloading loop)
β	Exponent of elasticity according to Bolton and Whittle [10] (1st unloading-reloading loop)

Table F.4: *Cone pressiometer test CPM1*

Water content
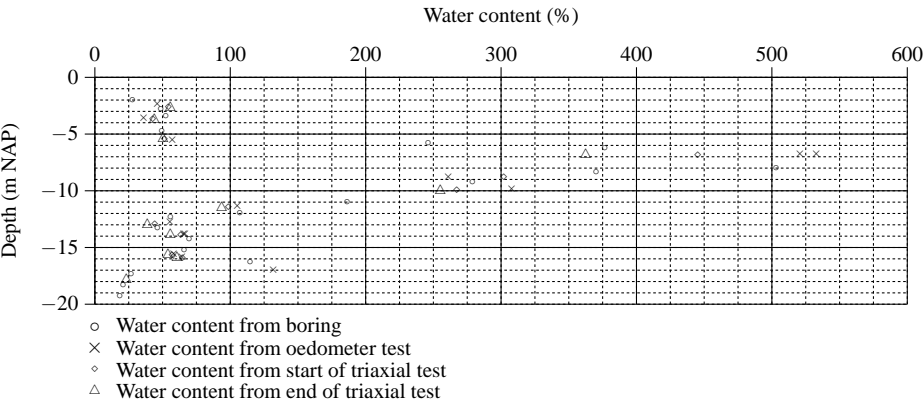
Figure F.10: *Water content*

Ménard pressiometer tests MPM1

Depth	M 1		Average per layer		Soil type
m-NAP	P'_l (MPa)	E (MPa)	$P'_{l,avg}$ (MPa)	E_{avg} (MPa)	
-2.30	0.48	2.4	0.4	2.1	Sand
-3.30	0.34	1.8			Silt
-4.30	0.21	1.3	0.24	1.5	Peat
-5.30	0.27	1.8			-
-6.30	0.16	0.9	0.14	0.9	Organic silt
-7.30	0.14	0.9			-
-8.30	0.14	0.9			-
-9.30	0.14	0.8			-
-10.30	0.14	1.3			-
-11.30	0.10	0.6	0.10	0.6	Clayey silt or silty clay
-12.30	0.10	0.6			-
-13.30	0.08	0.5			-
-14.30	0.11	0.6			-
-15.30	0.11	0.6			-
-16.30	0.22	5.9			Clay?
-17.30	0.11	0.4			Suspected test or soft layer
-18.30	0.86	7.1	0.71	4.4	Silty sand
-19.30	0.59	3.2			-
-20.30	1.51	8.3	1.45	8.6	Sand
-21.00	1.39	8.9			-
P'_l	Effective horizontal stress at failure				
E	Pressuremeter modulus over the central pseudo-elastic part of the test				

Table F.5: *Cone pressiometer tests and Ménard pressiometer tests*
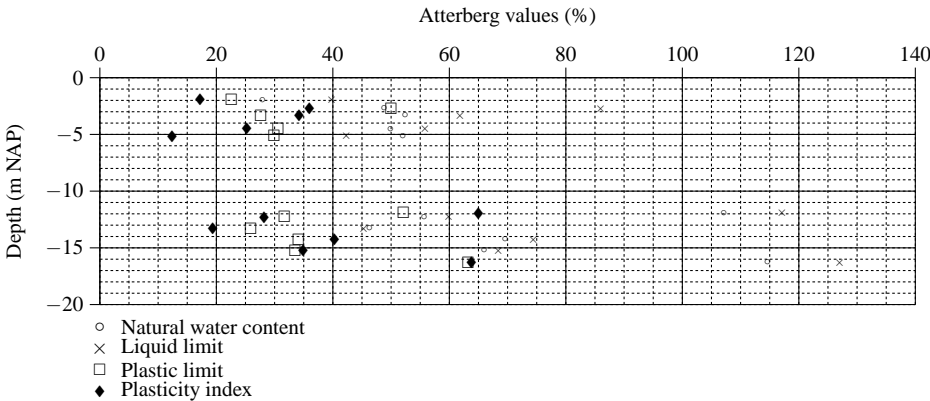
Atterberg values

Figure F.11: *Atterberg values*

Appendix G

Test procedure

Stage 1.1

13 April 1999 7:00 hours

Beginning of the dry excavation to NAP−4.0 m

Beginning of the on-line measurements

15 April 1999 17:00 hours

Measurement of the inclinometer, geodetical measurements and levelling of the settlement pawns

To be predicted Stage I
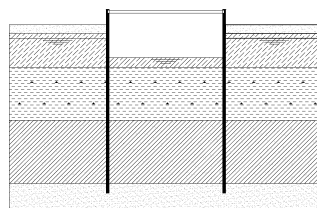
soil NAP−4.0 m
water NAP−4.0 m

Stage 1.2

16 April 1999 7:00 hours

Beginning of refill with water to NAP−1.5 m

17 April 1999 17:00 hours

On-line measurement for Stage 1.2
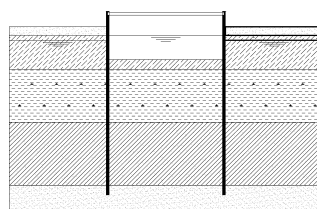
soil NAP−4.0 m
water NAP−1.5 m

Stage 1.3

19 April 1999 7:00 hours

Beginning of the wet excavation to NAP−7.0 m

22 April 1999 17:00 hours

Measurement of the inclinometer, geodetical measurements and levelling of the settlement pawns

To be predicted Stage II
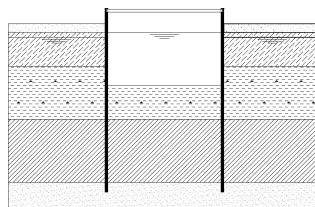
soil NAP−7.0 m
water NAP−1.5 m

Stage 1.4
23 April 1999 7:00 hours
Lowering of the water level to NAP−2.5 m
23 April 1999 17:00 hours
Measurement of the inclinometer, geodetical measurements and levelling of the settlement pawns
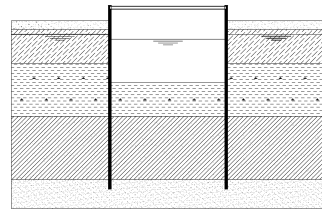
soil NAP−7.0 m
water NAP−2.5 m

Stage 1.5
26 April 1999 7:00 hours
Lowering of the water level to NAP−3.5 m
26 April 1999 17:00 hours
Measurement of the inclinometer, geodetical measurements and levelling of the settlement pawns
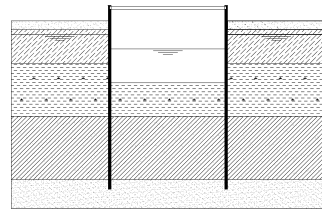
soil NAP−7.0 m
water NAP−3.5 m

Stage 1.6
27 April 1999 7:00 hours
Lowering of the water level to NAP−4.0 m
27 April 1999 17:00 hours
Measurement of the inclinometer, geodetical measurements and levelling of the settlement pawns
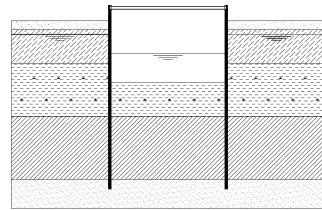
soil NAP−7.0 m
water NAP−4.0 m

Stage 1.7
6 May 1999 17:00 hours
Evaluation of the test data
Measurement of the inclinometer, geodetical measurements and levelling of the settlement pawns
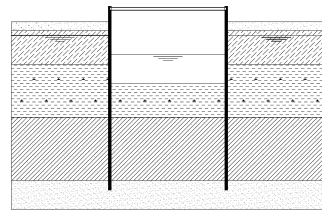
soil NAP−7.0 m
water NAP−4.0 m

Stage 1.8
10 May 1999 7:00 hours
Lowering of the water level to NAP−4.5 m
10 May 1999 17:00 hours
Measurement of the inclinometer, geodetical measurements and levelling of the settlement pawns
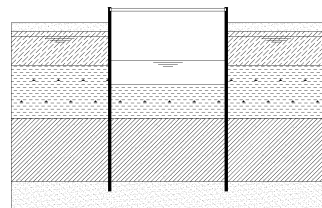
soil NAP−7.0 m
water NAP−4.5 m

Stage 1.9
11 May 1999 7:00 hours
Lowering of the water level to NAP−5.0 m
11 May 1999 17:00 hours
Measurement of the inclinometer, geodetical measurements and levelling of the settlement pawns

To be predicted Stage III

soil NAP−7.0 m
water NAP−5.0 m

Stage 2
Construction of sand fill behind AZ13-wall
17 May 1999 17:00 hours
Measurement of the inclinometer, geodetical measurements and levelling of the settlement pawns
18 May 1999 7:00 hours
Beginning of refill with water to NAP−1.5 m
18 May 1999 17:00 hours
End of refill.

19 May 1999 7:00 hours
Construction of sand fill
20 May 1999 17:00 hours
Measurement of the inclinometer, geodetical measurements and levelling of the settlement pawns

soil NAP−7.0 m
water NAP−1.5 m

soil NAP−7.0 m
water NAP−1.5 m

21 May 1999 7:00 hours
Lowering of the water level to NAP−3.5 m
21 May 1999 17:00 hours
Measurement of the inclinometer

soil NAP−7.0 m
water NAP−3.5 m

26 May 1999 7:00 hours
Lowering of the water level to NAP−5.0 m
26 May 1999 17:00 hours
Measurement of the inclinometer and geodetical measurements
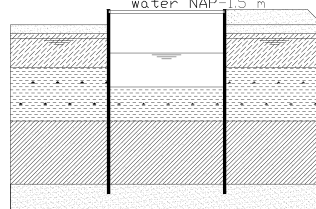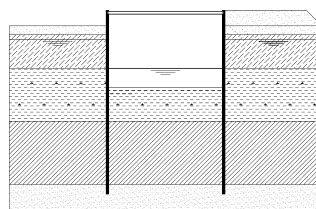
soil NAP−7.0 m
water NAP−5.0 m

Stage 3

26 May 1999 17:00 hours
Measurement of the inclinometer and geodetical measurements
11 June 17:00 hours
After 1 month of the long-term field test
11 & 12 August 1999
Measurement of the inclinometer, geodetical measurements and levelling of the settlement pawns
11 August 1999 17:00 hours
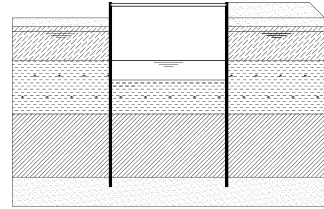

```
soil  NAP−7.0 m
water NAP−5.0 m
```

To be predicted Stage V for L607K double U

Stage 4

19 August 1999 7:00 hours
Lowering of the water level to NAP−5.5 m
20 August 1999 17:00 hours
Measurement of the inclinometer casings A2, A4, A5
4 October 1999 17:00 hours
Measurement of the inclinometer
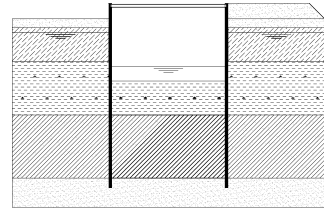

```
soil  NAP−7.0 m
water NAP−5.5 m
```

Stage 5

5 October 1999 7:00 hours
Lowering of the water level to NAP−6.0 m
13 October 1999 17:00 hours
Measurement of the inclinometer casings A2, A4, A5, H4
24 November 1999 17:00 hours
Levelling of the settlement pawns
26 November 1999 17:00 hours
Measurement of the inclinometer
20 December 1999 17:00 hours
Measurement of the inclinometer casings A2, A4, A5 and levelling of the settlement pawns
19 January 2000 17:00 hours
Levelling of the settlement pawns
24 January 2000 17:00 hours
Measurement of the inclinometer
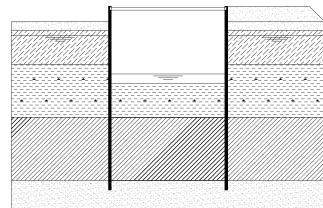

```
soil  NAP−7.0 m
water NAP−6.0 m
```

Stage 6

26 January and 27 January 2000
Water infiltration behind the AZ13 wall
31 January 2000 17:00 hours
Measurement of the inclinometer casings A2, A4, A5
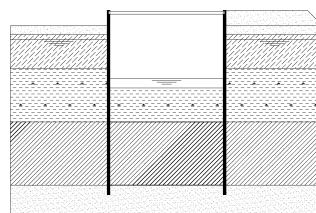
soil NAP−7.0 m
water NAP−6.0 m

Appendix H

Measured results

13-Apr Initial measurement

15-Apr Stage 1.1: dry excavation to NAP−4.0 m
   Prediction Stage I

22-Apr Stage 1.3: excavation under water to NAP−7.0 m
   Prediction Stage II

11-May Stage 1.9: lowering water level to NAP−5.0 m
   Prediction Stage III

26-May Stage 2.5: sand fill & lowering water level to NAP−5.0 m

11-Jun Stage 3: 1 month after 11 May
   Prediction Stage IV

11-Aug Stage 3: 3 months after 11 May
   Prediction Stage V

20-Aug Stage 4: water level on NAP−5.5 m

4-Oct Stage 4: water level on NAP−5.5 m

13-Oct Stage 5: water level on NAP−6.0 m
   start of yielding in the outermost fibre

26-Nov Stage 5: water level on NAP−6.0 m

20-Dec Stage 5: water level on NAP−6.0 m

2-Jan Stage 5: water level on NAP−6.0 m
   observation of holes *behind the sheet pile wall*

18-Jan Stage 5: water level on NAP−6.0 m

28/31-Jan Stage 6: water level on NAP−6.0 m
   plastic hinge

AZ13 test wall

Lateral Displacement, Strut Force and Tilt at Strut Level, part 1-3

	13-Apr	15-Apr	22-Apr	11-May	26-May	11-Jun	11-Aug
Depth (m NAP)				Lateral displacement (mm)			
1.015	-	-3.34	-1.99	4.85	-3.55	-	-7.57
0.515	-	-6.96	-5.78	-7.42	-19.58	-	-30.72
0.015	-	-10.52	-9.69	-19.62	-35.78	-	-53.85
-0.485	-	-14.05	-13.61	-31.71	-51.65	-	-76.71
-0.985	-	-17.40	-17.34	-43.38	-66.83	-	-98.72
-1.485	-	-20.48	-20.79	-54.41	-81.09	-	-119.59
-1.985	-	-23.20	-23.86	-64.64	-94.26	-	-139.05
-2.485	-	-25.59	-26.53	-74.01	-106.27	-	-156.97
-2.985	-	-27.61	-28.87	-82.44	-117.03	-	-173.26
-3.485	-	-29.22	-30.79	-89.79	-126.35	-	-187.62
-3.985	-	-30.46	-32.31	-96.03	-134.28	-	-199.99
-4.485	-	-31.32	-33.48	-101.05	-140.54	-	-210.23
-4.985	-	-31.96	-34.35	-104.83	-145.29	-	-218.32
-5.485	-	-32.42	-34.88	-107.47	-148.41	-	-224.22
-5.985	-	-32.54	-35.02	-108.91	-150.01	-	-227.97
-6.485	-	-32.50	-34.71	-109.17	-150.05	-	-229.51
-6.985	-	-32.08	-34.06	-108.33	-148.68	-	-228.96
-7.485	-	-31.40	-33.12	-106.49	-146.09	-	-226.56
-7.985	-	-30.47	-32.03	-103.87	-142.47	-	-222.54
-8.485	-	-29.33	-30.83	-100.69	-138.06	-	-217.12
-8.985	-	-28.00	-29.54	-97.05	-132.98	-	-210.43
-9.485	-	-26.43	-28.01	-92.95	-127.35	-	-202.49
-9.985	-	-24.72	-26.38	-88.45	-121.28	-	-193.63
-10.485	-	-22.86	-24.59	-83.60	-114.78	-	-183.91
-10.985	-	-20.88	-22.64	-78.43	-107.87	-	-173.38
-11.485	-	-18.81	-20.46	-72.86	-100.53	-	-162.09
-11.985	-	-16.67	-17.83	-66.98	-92.68	-	-150.10
-12.485	-	-14.60	-15.69	-60.86	-84.58	-	-137.54
-12.985	-	-12.59	-13.63	-54.57	-76.18	-	-124.57
-13.485	-	-10.77	-11.71	-48.29	-67.72	-	-111.42
-13.985	-	-9.13	-9.97	-42.08	-59.27	-	-98.19
-14.485	-	-7.68	-8.43	-36.05	-50.99	-	-85.01
-14.985	-	-6.32	-7.00	-30.16	-42.86	-	-71.94
-15.485	-	-5.11	-5.61	-24.47	-34.92	-	-58.98
-15.985	-	-3.96	-4.34	-19.03	-27.27	-	-46.36
-16.485	-	-2.87	-3.16	-13.91	-20.00	-	-34.17
-16.985	-	-1.86	-2.06	-9.10	-13.08	-	-22.50
-17.485	-	-0.94	-1.05	-4.62	-6.64	-	-11.42
Depth (m NAP)				Strut force (kN/m)			
+0.75	0	-22.94	-23.06	-49.38	-74.45	-82.70	-84.32
Depth (m NAP)				Inclination (rad)			
± +0.75	0	0.487	0.519	1.499	1.974	2.432	2.874

Table H.1: *Measurement results of the displacements and strut force for the AZ13 test wall, part 1-3*

AZ13 test wall

Lateral Displacement, Strut Force and Tilt at Strut Level, part 4-6

	20-Aug	4-Oct	13-Oct	26-Nov	20-Dec	2-Jan	18-Jan	28/31-Jan
Depth (m NAP)	Lateral displacement (mm)							
1.015	-8.65	-11.75	-10.41	-8.75	-8.36	-11.67	-	-153.13
0.515	-32.50	-39.04	-38.11	-40.77	-44.28	-55.14	-	-237.60
0.015	-56.31	-66.16	-65.67	-72.70	-80.18	-98.57	-	-321.90
-0.485	-79.78	-92.96	-92.86	-104.37	-115.85	-141.75	-	-406.14
-0.985	-102.43	-118.87	-119.13	-135.23	-150.75	-184.10	-	-490.00
-1.485	-123.88	-143.54	-144.03	-164.84	-184.43	-225.15	-	-572.98
-1.985	-143.91	-166.78	-167.42	-192.96	-216.54	-264.54	-	-654.56
-2.485	-162.40	-188.43	-189.12	-219.42	-246.91	-302.14	-	-734.31
-2.985	-179.23	-208.41	-208.99	-244.04	-275.32	-337.65	-	-811.79
-3.485	-194.09	-226.28	-226.74	-266.40	-301.33	-370.46	-	-885.83
-3.985	-206.97	-241.99	-242.34	-286.36	-324.72	-400.24	-	-955.84
-4.485	-217.64	-255.25	-255.46	-303.55	-344.85	-426.01	-	-1020.15
-4.985	-226.10	-265.97	-266.07	-317.70	-361.32	-447.01	-	-1075.20
-5.485	-232.33	-274.10	-274.06	-328.52	-373.57	-462.11	-	-1104.39
-5.985	-236.32	-279.48	-279.44	-335.83	-381.34	-470.61	-	-1087.89
-6.485	-238.03	-282.22	-282.29	-339.63	-384.85	-472.75	-	-1050.94
-6.985	-237.58	-282.35	-282.59	-340.12	-384.38	-469.81	-	-1007.91
-7.485	-235.21	-280.15	-280.65	-337.67	-380.57	-462.85	-	-961.48
-7.985	-231.12	-275.74	-276.67	-332.63	-373.82	-452.50	-	-912.56
-8.485	-225.54	-269.44	-270.85	-325.26	-364.54	-439.29	-	-861.92
-8.985	-218.61	-261.33	-263.32	-315.73	-353.01	-423.63	-	-810.16
-9.485	-210.39	-251.60	-254.27	-304.21	-339.37	-405.78	-	-757.77
-9.985	-201.22	-240.62	-243.90	-291.14	-324.06	-386.14	-	-705.19
-10.485	-191.13	-228.49	-232.38	-276.61	-307.25	-365.01	-	-652.62
-10.985	-180.17	-215.33	-219.76	-260.80	-289.15	-342.50	-	-600.41
-11.485	-168.40	-201.17	-206.11	-243.81	-269.83	-318.80	-	-548.80
-11.985	-155.89	-186.19	-191.48	-225.81	-249.52	-294.11	-	-497.92
-12.485	-142.76	-170.61	-176.09	-207.08	-228.50	-268.78	-	-448.20
-12.985	-129.26	-154.59	-160.09	-187.87	-206.97	-243.05	-	-399.87
-13.485	-115.56	-138.32	-143.74	-168.39	-185.24	-217.22	-	-353.09
-13.985	-101.79	-121.97	-127.14	-148.75	-163.45	-191.48	-	-308.01
-14.485	-88.10	-105.69	-110.48	-129.15	-141.74	-165.92	-	-264.58
-14.985	-74.51	-89.52	-93.83	-109.66	-120.26	-140.67	-	-222.91
-15.485	-61.07	-73.54	-77.26	-90.31	-99.08	-115.83	-	-182.78
-15.985	-47.98	-57.94	-60.96	-71.35	-78.29	-91.53	-	-144.15
-16.485	-35.38	-42.80	-45.12	-52.90	-58.09	-67.95	-	-106.94
-16.985	-23.29	-28.27	-29.83	-35.07	-38.50	-45.06	-	-71.00
-17.485	-11.82	-14.34	-15.14	-17.79	-19.53	-22.86	-	-36.02
Depth (m NAP)	Strut force (kN/m)							
+0.75	-85.70	-86.69	-88.85	-84.67	-	-	-	-
Depth (m NAP)	Inclination (rad)							
± +0.75	2.897	3.487	3.544	4.204	4.808	5.580	5.844	10.886

Table H.2: *Measurement results of the displacements and strut force for the AZ13 test wall, part 4-6*

AZ13 test wall

Bending Moment, Earth Pressure and Water pressure, part 1-3

	13-Apr	15-Apr	22-Apr	11-May	26-May	11-Jun	11-Aug
Depth (m NAP)	Lateral bending moment (kNm/m)						
-3	-	-72.58	-67.89	-188.22	-248.93	-293.04	-309.44
-5	-	-47.84	-66.03	-206.24	-269.20	-331.12	-354.63
-6	-	-46.85	-59.81	-181.14	-236.38	-294.32	-328.79
-7	-	-41.75	-41.04	-140.29	-186.63	-242.51	-292.01
-9	-	-26.58	-21.82	-71.89	-90.54	-138.88	-178.82
-11	-	-7.52	-10.04	-44.84	-56.16	-85.18	-104.07
-13	-	19.86	15.10	-5.61	-11.83	-25.16	-29.49
-14	-	23.72	19.79	16.19	14.48	6.05	2.24
-15	-	18.75	17.24	27.68	30.83	29.06	25.26
-16	-	11.48	11.88	30.08	37.90	42.12	39.89
Depth (m NAP)	Earth pressure on retaining side (kN/m^2)						
-2	32.19	2.38	11.95	2.46	1.11	1.20	3.91
-4	31.30	22.26	23.79	16.78	20.80	22.64	21.57
-7	88.37	72.20	71.87	40.62	42.41	43.93	45.21
-10	129.30	115.92	115.80	81.25	75.31	77.55	77.33
-14	176.88	162.54	163.43	137.42	137.32	136.10	132.67
-16	201.32	195.51	195.74	174.76	170.27	166.25	165.12
Depth (m NAP)	Earth pressure on excavated side (kN/m^2)						
-7	83.52	65.46	57.34	44.41	46.92	47.34	45.99
-10	126.00	105.89	107.09	85.04	86.15	83.72	83.87
-14	176.21	171.39	170.37	149.93	151.84	149.02	148.41
-16	202.95	197.84	196.61	190.67	192.71	191.24	188.11
Depth (m NAP)	Water pressure on retaining side (kN/m^2)						
-2	5.91	6.61	7.44	6.84	8.45	8.36	7.75
-4	26.25	25.39	27.67	22.89	26.03	25.17	24.82
-7	62.66	53.71	56.05	46.37	49.64	51.45	49.34
-10	104.38	96.44	96.38	76.63	78.15	81.35	82.18
-14	147.59	144.97	146.62	136.90	142.05	143.87	152.54
-16	173.20	173.89	172.99	159.60	165.24	166.25	181.15
Depth (m NAP)	Water pressure on excavated side (kN/m^2)						
-7	59.98	43.75	53.66	20.58	22.89	24.53	25.49
-10	106.24	89.33	90.95	73.18	75.65	69.83	65.65
-14	157.39	151.03	150.15	128.92	131.95	126.55	121.08
-16	180.55	177.20	175.51	167.52	170.51	169.03	198.22
Depth (m NAP)	Water pressure 1.5 m behind retaining wall (kN/m^2)						
-6	51.27	46.26	47.80	39.51	44.10	46.40	45.29
-8	76.67	71.82	73.60	59.59	65.27	63.70	62.73
-11	120.39	114.03	114.90	104.46	107.92	102.95	101.14
-16	176.38	174.76	173.95	166.38	169.00	170.02	169.03

Table H.3: *Measurement results of the bending moments, earth pressure and water pressure for the AZ13 test wall, part 1-3*

AZ13 test wall

Bending Moment, Earth Pressure and Water pressure, part 4-6

	20-Aug	4-Oct	13-Oct	26-Nov	20-Dec	2-Jan	18-Jan	28/31-Jan
Depth (m NAP)	Lateral bending moment (kNm/m)							
-3	-315.26	-330.00	-333.81	-358.86	-379.60	-399.85	-401.71	-455.41
-5	-365.61	-408.45	-396.63	-449.52	-466.75	-	-445.03	-
-6	-339.94	-398.59	-381.56	-459.75	-438.82	-	-431.61	-
-7	-299.43	-359.08	-345.34	-407.43	-433.73	-444.51	-466.56	-450.06
-9	-189.46	-235.01	-238.65	-279.69	-291.06	-283.10	-344.17	-102.87
-11	-111.50	-126.80	-143.71	-155.09	-152.88	-136.78	-145.39	103.10
-13	-33.04	-31.11	-53.56	-38.08	-24.25	1.65	-5.39	253.94
-14	5.48	10.17	-15.84	6.66	23.55	44.22	39.96	269.85
-15	31.65	35.48	20.79	35.44	48.71	66.71	63.80	250.76
-16	45.35	48.01	39.49	47.81	55.79	66.69	64.96	232.46
Depth (m NAP)	Earth pressure on retaining side (kN/m^2)							
-2	4.54	0.90	11.82	0.98	1.29	2.72	-0.16	-0.56
-4	21.84	20.54	17.08	24.14	24.84	25.10	23.47	20.58
-7	43.45	49.44	49.33	50.04	52.30	52.65	51.60	48.79
-10	74.84	79.84	76.11	83.96	81.97	83.24	82.12	80.66
-14	130.43	128.89	128.09	127.73	127.21	126.27	125.76	123.04
-16	161.69	157.81	156.27	153.20	150.75	150.09	151.51	169.22
Depth (m NAP)	Earth pressure on excavated side (kN/m^2)							
-7	44.30	44.16	41.46	45.72	44.36	45.47	44.83	-
-10	79.80	85.74	79.08	86.13	85.90	89.56	87.16	-
-14	147.49	150.26	144.97	152.99	154.24	155.99	154.45	-
-16	189.67	191.20	188.89	193.77	196.09	199.08	197.46	-
Depth (m NAP)	Water pressure on retaining side (kN/m^2)							
-2	8.47	5.99	7.66	6.65	8.11	8.13	7.36	6.57
-4	26.18	23.53	15.46	24.70	25.20	27.57	27.51	26.65
-7	48.44	54.99	41.88	56.63	59.02	59.75	59.67	56.30
-10	79.77	83.95	82.34	88.66	88.75	89.49	90.13	88.25
-14	146.37	142.39	144.07	138.89	139.95	139.03	138.84	132.78
-16	179.33	174.79	174.73	-	-	-	-	-
Depth (m NAP)	Water pressure on excavated side (kN/m^2)							
-7	21.54	18.40	13.72	16.63	16.62	15.06	14.27	-
-10	63.93	61.59	60.73	66.63	66.70	66.66	69.07	-
-14	119.44	115.85	114.99	115.01	115.95	117.48	119.70	-
-16	198.88	199.41	198.49	197.74	196.48	197.20	197.73	-
Depth (m NAP)	Water pressure 1.5 m behind retaining wall (kN/m^2)							
-6	44.25	45.19	37.04	42.43	44.06	45.36	46.38	-
-8	61.87	68.19	54.95	62.55	65.36	66.54	66.42	68.54
-11	99.99	-	-	-	-	-	-	-
-16	168.02	169.82	169.94	170.28	168.29	169.17	170.23	172.25

Table H.4: *Measurement results of the bending moments, earth pressure and water pressure for the AZ13 test wall, part 4-6*

L607K test wall
Lateral Displacement and Strut Force

	13-Apr	15-Apr	22-Apr	11-May	26-May	11-Jun	11-Aug
Depth (m NAP)	Lateral displacement (mm)						
0.94	-	-13.83	-12.90	-15.14	-14.29	-	-15.54
0.44	-	-15.63	-14.93	-22.83	-23.14	-	-27.38
-0.06	-	-17.30	-16.82	-30.15	-31.48	-	-38.88
-0.56	-	-18.88	-18.69	-37.60	-39.99	-	-50.38
-1.06	-	-20.36	-20.48	-44.72	-48.22	-	-61.64
-1.56	-	-21.72	-22.07	-51.45	-55.79	-	-72.28
-2.06	-	-22.90	-23.51	-57.64	-62.79	-	-82.03
-2.56	-	-23.94	-24.93	-63.35	-69.35	-	-91.39
-3.06	-	-24.87	-26.03	-68.56	-75.44	-	-99.84
-3.56	-	-25.60	-26.76	-73.18	-80.61	-	-107.39
-4.06	-	-26.19	-27.58	-77.16	-85.06	-	-113.99
-4.56	-	-26.62	-28.20	-80.38	-88.77	-	-119.53
-5.06	-	-26.91	-28.64	-82.85	-91.63	-	-124.04
-5.56	-	-27.03	-28.88	-84.45	-93.76	-	-127.49
-6.06	-	-27.07	-28.84	-85.26	-95.22	-	-129.94
-6.56	-	-27.01	-28.59	-85.41	-95.91	-	-131.07
-7.06	-	-26.77	-28.12	-84.88	-95.79	-	-131.24
-7.56	-	-26.40	-27.43	-83.70	-94.97	-	-130.55
-8.06	-	-25.89	-26.59	-82.04	-93.49	-	-129.16
-8.56	-	-25.03	-25.57	-79.98	-91.26	-	-126.67
-9.06	-	-24.14	-24.35	-77.51	-88.76	-	-123.60
-9.56	-	-23.16	-23.12	-74.67	-85.91	-	-119.94
-10.06	-	-21.99	-21.89	-71.57	-82.66	-	-115.66
-10.56	-	-20.70	-20.47	-68.12	-79.02	-	-110.53
-11.06	-	-19.38	-19.01	-64.37	-74.99	-	-104.87
-11.56	-	-17.90	-17.51	-60.35	-70.59	-	-98.58
-12.06	-	-16.38	-15.94	-56.02	-65.83	-	-91.82
-12.56	-	-14.77	-14.38	-51.46	-60.80	-	-84.69
-13.06	-	-13.31	-12.81	-46.80	-55.51	-	-77.41
-13.56	-	-11.75	-11.18	-41.96	-49.97	-	-69.82
-14.06	-	-10.26	-9.63	-37.08	-44.38	-	-62.18
-14.56	-	-8.80	-8.08	-32.15	-38.67	-	-54.20
-15.06	-	-7.34	-6.86	-27.24	-32.90	-	-46.32
-15.56	-	-5.99	-5.82	-22.43	-27.19	-	-38.48
-16.06	-	-4.70	-4.90	-17.62	-21.54	-	-30.61
-16.56	-	-3.39	-3.64	-12.97	-15.88	-	-22.73
-17.06	-	-2.00	-2.38	-8.45	-10.33	-	-14.96
-17.56	-	-0.94	-1.11	-3.96	-4.84	-	-7.00
Depth (m NAP)	Strut force (kN/m)						
+0.75	-	-27.61	-29.55	-67.77	-78.20	-92.97	-133.28

Table H.5: *Measurement results of the displacements and strut force for the L607K test wall*

L607K test wall

Bending Moment, Earth Pressure and Water pressure

	13-Apr	15-Apr	22-Apr	11-May	26-May	11-Jun	11-Aug
Depth (m NAP)	Lateral bending moment (kNm/m)						
-3	-	86.52	88.58	271.89	285.59	330.93	362.24
-5	-	81.82	109.41	336.88	355.85	413.22	460.47
-6	-	75.58	107.57	316.05	337.20	393.23	443.98
-7	-	81.61	94.15	275.47	299.20	353.34	410.45
-9	-	80.01	59.83	183.12	207.19	249.58	307.51
-11	-	50.95	36.57	135.53	156.82	188.18	234.70
-13	-	11.16	8.45	74.17	91.24	113.90	146.45
-14	-	-4.96	-3.20	34.82	49.30	67.58	95.03
-15	-	-11.51	-8.04	5.04	15.55	28.32	49.19
-16	-	-11.95	-10.90	-17.69	-10.72	-3.81	9.52
Depth (m NAP)	Earth pressure on retaining side (kN/m^2)						
-2	44.91	5.46	12.49	4.37	4.94	6.85	8.04
-4	39.58	21.60	24.39	20.47	18.84	21.99	22.52
-7	105.48	83.40	82.67	49.32	48.56	53.39	53.63
-10	148.05	129.43	129.75	90.31	82.61	79.12	79.55
-14	181.07	164.96	167.75	141.95	142.79	141.98	140.36
-16	207.18	198.30	198.42	171.85	170.61	166.17	162.77
Depth (m NAP)	Earth pressure on excavated side (kN/m^2)						
-7	85.01	59.77	52.15	27.45	26.80	29.24	29.91
-10	125.30	100.42	103.69	84.63	85.69	89.99	88.80
-14	172.93	167.13	166.64	152.68	151.32	151.30	152.29
-16	206.60	198.48	198.86	193.30	192.00	192.68	190.78
Depth (m NAP)	Water pressure on retaining side (kN/m^2)						
-2	4.37	3.51	5.17	3.69	4.48	5.30	6.21
-4	25.45	23.72	27.01	24.11	23.27	26.60	28.52
-7	61.52	54.06	55.47	49.51	48.80	54.92	55.25
-10	93.95	86.00	86.66	68.72	74.37	78.03	80.91
-14	146.86	144.28	145.82	137.78	138.44	142.55	148.88
-16	170.47	171.93	168.82	155.91	156.51	158.18	159.68
Depth (m NAP)	Water pressure on excavated side (kN/m^2)						
-7	64.83	48.47	55.39	21.98	23.55	24.41	24.56
-10	106.09	87.86	92.76	72.87	71.15	72.88	79.52
-14	156.40	150.88	149.22	130.32	130.19	124.09	120.93
-16	179.35	175.92	174.16	165.02	163.22	160.90	154.32
Depth (m NAP)	Water pressure 1.5 m behind retaining wall (kN/m^2)						
-4	23.97	22.25	24.13	20.98	21.00	23.03	23.33
-6	52.75	50.55	51.79	46.68	42.75	46.06	46.54
-8	76.43	72.10	71.14	65.78	69.34	69.36	72.86
-11	109.70	104.70	103.20	96.03	86.30	87.93	96.45
-16	171.26	169.71	169.43	163.70	163.83	163.24	168.02

Table H.6: *Measurement results of the bending moments, earth pressure and water pressure for the L607K test wall*

Surface settlements behind both test walls

AZ13 test wall
Settlements of ground surface, part 1-3

Distance (m)	13-Apr	15-Apr	22-Apr	11-May	26-May	11-Jun	11-Aug
				Settlement (mm)			
1	-	-4.2	-6.75	-37.2	-	-	-314.2
2.5	-	-5.6	-7.9	-39.9	-	-	-304.7
4.5	-	-4.55	-6.25	-34.95	-	-	-273.2
7	-	-3.15	-4	-26.9	-	-	-205.1
10	-	-1.25	-1.4	-13.75	-	-	-

Table H.7: *Measurement results of the ground surface settlements behind the AZ13 test wall, part 1-3*

AZ13 test wall
Settlements of ground surface, part 4-6

Distance (m)	20-Aug	4-Oct	13-Oct	26-Nov	20-Dec	2-Jan	18-Jan	28/31-Jan
				Settlement (mm)				
1	-	-	-	-478	-572.4	-	-753.4	-
2.5	-	-	-	-440.6	-484.5	-	-543	-
4.5	-	-	-	-383	-410.6	-	-443.9	-
7	-	-	-	-290.3	-307.6	-	-323.5	-
10	-	-	-	-	-	-	-	-

Table H.8: *Measurement results of the ground surface settlements behind the AZ13 test wall, part 4-6*

L607K test wall
Settlements of ground surface

Distance (m)	13-Apr	15-Apr	22-Apr	11-May	26-May	11-Jun	11-Aug
				Settlement (mm)			
1	-	-6.3	-12.95	-34.65	-	-	-61.1
2.5	-	-5.7	-10.55	-32.1	-	-	-55.4
4.5	-	-4.3	-7.2	-24.8	-	-	-44.45
7	-	-2.95	-5.25	-18.95	-	-	-35
10	-	-1.65	-4.1	-14.35	-	-	-26.7

Table H.9: *Measurement results of the ground surface settlements behind the L607K test wall*

Samenvatting

Stalen damwanden in slappe grond

Het onderzoek dat is beschreven in dit proefschrift, richt zich op een tweetal recente ontwikkelingen op het gebied van stalen damwandconstructies: *Ontwerpen met Plastische Scharnieren* en *Scheve Buiging*. In het eerste deel van dit proefschrift wordt de theoretische achtergrond van deze twee onderwerpen behandeld. In het tweede deel van dit proefschrift wordt het ontwerpen met plastische scharnieren en scheve buiging onderzocht in een damwandveldproef die in 1999 is uitgevoerd in Pernis.

In 1953 ontwikkelde Brinch Hansen een ontwerpmethode waarbij één of meerdere plastische scharnieren in de damwand konden ontstaan. Sinds die tijd wordt deze methode met name in Denemarken veelvuldig toegepast bij het ontwerpen van damwandconstructies. Het ontwerpen met plastische scharnieren kan leiden tot een materiaalbesparing van maximaal 35%, verdeeld in 15% tot 20% wanneer in plaats van vloei in de uiterste vezel het volplastisch moment in rekening wordt gebracht en in ongeveer 20% wanneer rotatie in het plastisch scharnier wordt toegelaten.

Drie klassieke ontwerpmethoden met plastische scharnieren worden gepresenteerd: de methoden van Brinch Hansen, Windels en Weißenbach. Deze drie methoden zijn gericht op de geotechnische kant van het ontwerp en gaan uit van een oneindige rotatiecapaciteit van de damwand. In werkelijkheid is de rotatiecapaciteit van de damwand echter beperkt vanwege de dunwandige vorm van de plank.

In het kader van dit promotieonderzoek zijn een groot aantal geotechnische berekeningen uitgevoerd waarbij is onderzocht hoe de beperkte rotatiecapaciteit van de damwand in rekening kan worden gebracht. Hiertoe is het verenmodel PLASWALL ontwikkeld waarin een plastisch scharnier kan worden gegenereerd en de benodigde rotatiecapaciteit kan worden berekend bij het bereiken van het vloeimoment.

Uit dit onderzoek volgt dat de benodigde rotatiecapaciteit van de damwandconstructie sterk afhangt van de geometrie van de constructie en de eigenschappen van de grond. Een controle van de rotatiecapaciteit moet daarom deel uitmaken van de ontwerpberekening. De meeste geotechnische software voor het berekenen van damwanden met plastische scharnieren is echter niet geschikt om de rotatie van het plastisch scharnier berekenen. Daarom worden in dit proefschrift twee eenvoudige ontwerpmethoden gepresenteerd om de benodigde rotatiecapaciteit te bepalen. Deze worden getoetst aan een groot aantal berekeningen zowel met het verenmodel als met een eindige elementenmodel.

Scheve buiging is relevant voor dubbele U-profielen, dwz. paren van U-profielen met

277

een geknepen of gelast tussenslot. Vanwege de aparte doorsnede van een dubbele U-plank zijn de hoofdtraagheidsassen gedraaid, hetgeen gepaard gaat met een afname van de effectieve hoogte van de plank. Met andere woorden, scheve buiging gaat gepaard met een significant verlies van het effective traagheids- en weerstandsmoment van een damwand. Wanneer de gevolgen van scheve buiging onvoldoende in rekening worden gebracht in het ontwerp, dan zal de veiligheid van bouwputten met betrekking tot de stijfheid en sterkte van de damwandconstructie overschat kunnen worden.

In de bouwpraktijk kan scheve buiging worden beinvloed door andere effecten, zoals slotwrijving, detaillering van de verankering of stempeling en de wijze waarop de damwand in de grond wordt gebracht. Daarom zal in de praktijk het verlies van stijfheid en sterkte niet zo dramatisch zijn als zou volgen uit de geometrie van een plank. In de Europese ontwerppraktijk van damwandconstructies met dubbele U-profielen wordt scheve buiging niet overal erkend; de meeste landen hebben zelfs totaal geen richtlijn op dit gebied.

Enkele factoren die de mate van scheve buiging beinvloeden, worden gekwantificeerd. Het effect van verschillende soorten opleggingen op scheve buiging is onderzocht. Goede constructieve maatregelen tegen scheve buiging zijn lassen van de heisloten tijdens ontgraven en, in mindere mate, een deksloof. Verder wordt geconcludeerd dat de heimethode een belangrijke invloed heeft op scheve buiging, maar de mate waarin kon in het kader van dit onderzoek niet worden gekwantificeerd.

Op basis van deze bevindingen wordt een nieuwe ontwerpmethode gepresenteerd om scheve buiging in rekening te brengen. Tenslotte wordt de toepasbaarheid van deze methode geillustreerd met twee ontwerpvoorbeelden.

De recente ontwikkelingen met betrekking tot het ontwerpen van stalen damwandconstructies gaf inspiratie om een damwandveldproef uit te voeren. Deze veldproef richtte zich op het onderzoeken van de volgende drie aspecten:

- het gedrag van een damwand met een plastisch scharnier

- het gedrag van een damwand die bestaat uit dubbele U-profielen (scheve buiging)

- het korte- en langetermijngedrag van beide damwanden in slappe grond

Een vraag naar predicties is opgezet om de kwaliteit van de huidige rekenmodellen voor stalen damwand in slappe grond te onderzoeken, inclusief het tijdsafhankelijk gedrag.

Uit de evaluatie van de damwandveldproef kon worden geconcludeerd dat het plastisch scharnier zich volgens verwachting heeft gedragen. Dit houdt in dat de aannamen waarop de ontwerpregels in ENV 1993-5 zijn gebaseerd, geldig zijn voor een damwandconstructie in slappe grond. Verder kon de opgetreden rotatie in het plastisch scharnier worden teruggerekend met de eenvoudige ontwerpregels, hetgeen betekent dat deze methoden in een ontwerp kunnen worden toegepast.

De evaluatie van de Larssen 607K-wand heeft bewezen dat scheve buiging is opgetreden. De reductiefactoren waren per plank verschillend en lagen in de orde van $\beta_I = 0.70$ and $\beta_W = 0.75$. Deze waarden zijn ongeveer gelijk aan de waarden die worden aanbevolen door de CUR 166 richtlijn en de ontwerpregel die in dit proefschrift wordt voorgesteld.

De evalutie van de damwandproef wordt afgesloten met een aantal herberekeningen met PLASWALL en PLAXIS, waarbij de invloed van consolidatie en kruip op de lange termijngedeelte van de proef is bestudeerd. De berekeningen toonden aan dat de invloed van kruip op het gedrag van de damwanden erg belangijk was.

Curriculum vitae

Arjen Kort was born on the 10th of October 1968 in Haarlem. After attending the Stedelijk Gymnasium in Haarlem he started a Civil Engineering study at Delft University of Technology in 1988. During his study he specialised in highway, structural and geotechnical engineering. In 1993 he worked for 6 months at two different construction sites for NGT, a Dutch contractor specialised in modern foundation techniques, and later in that same year he worked a short period as a surveyor on a pile driving project. In August 1994 he graduated at the Geotechnical Laboratory under supervision of Prof. A.F. van Tol on the subject of 'Calculation methods for a single tension pile'.

After attending a short 'cours intensif de français' at the ENST in Paris he started in November 1994 as a Research Engineer at the Geotechnical Laboratory of Delft University. Until 1997 he worked on the ECSC research project 'Development of Unified European Design Rules for Steel Sheet Piles and Introduction into Part 5 of Eurocode 3' and was laterally involved in the drafting of Part 5 of Eurocode 3, ENV 1993-5:1997.

In 1997 he initiated together with Prof. A.F. van Tol and Mr. A. Jonker of the CUR the research project of the Rotterdam Sheet Pile Wall Field Test. Since 1998 he was a member of CUR committee C119 where he was responsible for the scientific part of the project, and carried out the field test in close co-operation with various consultants and contractors.

Under supervision of Prof. A.F. van Tol and Prof. A. Verruijt he started his doctoral research in 1998, which has resulted in this thesis.

In 1997 he participated in the Competition to Calculate Settlements at the Haarajoki Test Embankment, organised by the Finnish National Road Administration (FINNRA), together with Mr. W. Broere and Prof. A.F. van Tol. They were awarded a second prize for the most accurate prediction, and the first prize for the best presentation format.

During his stay at the Geotechnical Laboratory he wrote various technical reports, papers for international conferences and national journals, reviewed a scientific paper for an international journal, and supervised numerous students during their exercises and graduation work.